UNIVERSIDAD POLITECNICA DE VALENCIA

Departamento de Máquinas y Motores Térmicos

DOCTORAL THESIS:

Trends and Limits of Two-Stage Boosting Systems for Automotive Diesel Engines

---

by

Olivier Varnier

in fulfillement of the requirements for the degree of

Doctor of Philosophy
(Mechanical Engineering)

Supervisor: Prof. Dr. José Galindo Lucas

Valencia, July 2012

DOCTORAL THESIS

Trends and Limits of Two-Stage Boosting Systems for Automotive Diesel Engines

AUTHORS

Written by: Dipl. Ing. Olivier Varnier
Supervised by: Prof. Dr. José Galindo Lucas

DEFENSE COMMITTEE

Chairman: Prof. Dr. Jesús Benajes Calvo
Universidad Politécnica de Valencia

Secretary: Prof. Dr. José Ramón Serrano
Universidad Politécnica de Valencia

Members: Prof. Dr. Luis Le Moyne
ISAT Institut Supérieur de l'Automobile et des Transports

Prof. Dr. Juan José Hernández Adrover
Universidad de Castilla-La Mancha

Prof. Dr. Francisco Vera García
Universidad Politécnica de Cartagena

DISSERTATION READERS

Prof. Dr. Hans-Erik Angström
KTH Kunglia Tekniska Högskolan Stockholm

Prof. Dr. Jean-François Hetet
Ecole Centrale de Nantes

Prof. Dr. Juan José Hernández Adrover
Universidad de Castilla-La Mancha

Abstract

Internal combustion engines developments are driven by emissions reduction and energetic efficiency increase. To reach the next standards, downsized/downspeeded engines are required to reduce fuel consumption and CO2 emissions. These techniques place an important demand on the charging system and force the introduction of multistage boosting architectures. With many possible arrangements and a large number of parameters to optimize, these architectures present a higher complexity than current systems. The objective of this thesis has thus been to investigate the potential of two-stage boosting architectures to establish, for the particular case of passenger car downsized/downspeeded Diesel engines, the most efficient solutions for achieving the forthcoming CO2 emissions targets.

To respond to this objective, an exhaustive literature review of all existing solutions has first been performed to determinate the most promising two-stage boosting architectures. Then, a new matching methodology has been defined to optimize the architectures with, on the one hand the development of a new turbine characteristic maps representation allowing straight forward matching calculations and, on the other hand, the development of a complete 0D engine model able to predict, within a reduced computational time, the behavior of any boosting architecture in both steady state and transient operating conditions. Finally, a large parametric study has been carried out to analyze and compare the different architectures on the same base engines, to characterize the impacts of thermo-mechanical limits and turbocharger size on engine performance, and to quantify for different engine development options their potential improvements in terms of fuel consumption, maximum power and fun to drive.

As main contributions, the thesis provides new modeling tools for efficient matching calculations and synthesizes the main trends in advanced boosting systems to guide future passenger car Diesel engine development.

Resumen

Los desarrollos actuales en el campo de los motores de combustión interna alternativos están principalmente motivados por la reducción de las emisiones contaminantes y el aumento de la eficiencia energética. Cumplir con los nuevos estándares para automoción requiere una reducción en el consumo de combustible y en las emisiones de contaminantes, y para ello resulta imprescindible el uso de motores *downsized* and *downspeeded*. El empleo de dichas técnicas impone unos requisitos de exigencia elevados al sistema de renovación de la carga y obligan a la introducción de arquitecturas de sobrealimentación multi-etapa. Debido a la gran variedad de configuraciones posibles y al elevado número de parámetros a optimizar, esas arquitecturas presentan una mayor complejidad que los sistemas actuales. Por tanto, el objetivo principal de esta tesis ha sido investigar el potencial de las arquitecturas de sobrealimentación de doble etapa para establecer, en el caso particular de los motores *downsized* and *downspeeded*, las soluciones más eficientes que consigan cumplir con los futuros límites de emisiones de CO2.

Para alcanzar este objetivo, se ha realizado primero una exhaustiva revisión bibliográfica de todas las soluciones existentes, con objeto de determinar las arquitecturas de doble etapa más prometedoras. Luego, se ha definido una nueva metodología de *matching* que permita optimizar las arquitecturas mediante, por un lado, el desarrollo de una nueva representación de las curvas características de turbinas que permite una resolución directa de los cálculos de *matching* y, por otro lado, el desarrollo de un modelo 0D de motor capaz de predecir con reducido coste computacional el comportamiento de cualquier arquitectura de sobrealimentación en condiciones de operación tanto estacionarias como transitorias. Finalmente, se ha llevado a cabo un amplio estudio paramétrico en el que se analizan y comparan las diferentes arquitecturas sobre los mismos motores, se caracteriza el impacto del tamaño de las turbomáquinas y de los límites termo-mecánicos sobre las prestaciones del motor, y se cuantifica la mejora potencial de las distintas configuraciones en términos de consumo, potencia máxima y confort de la conducción.

Como principales contribuciones, la tesis propone nuevas herramientas de modelado más eficientes para los cálculos de matching y sintetiza las principales tendencias en sistemas avanzados de sobrealimentación para orientar los futuros desarrollos de los motores Diesel de automoción.

Résumé

Le développement des moteurs à combustion interne est aujourd'hui principalement motivé par la réduction des émissions polluantes et l'augmentation des rendements énergétiques. Pour atteindre les nouvelles normes imposées au secteur automobile, l'utilisation de moteurs *downsized* et *downspeeded* est devenue indispensable. Ces techniques qui permettent de diminuer la consommation de carburant et les rejets de CO2 sont particulièrement exigeantes en termes d'alimentation en air et obligent l'introduction de systèmes de suralimentation multi-étages. De part la grande variété de configurations possibles et du nombre élevé de paramètres à optimiser, les architectures multi-étages présentent une plus grande complexité que les systèmes actuels. L'objectif de cette thèse à donc été d'examiner le potentiel de ces architectures pour établir, dans le cas particulier des moteurs *downsized* et *downspeeded*, les solutions les plus efficaces pour respecter les futures limites d'émissions de CO2.

Afin d'atteindre cet objectif, une exhaustive révision bibliographique a premièrement été menée sur tous les systèmes de suralimentation existants pour cibler les meilleures architectures double étages. Ensuite, une nouvelle méthodologie de *matching* a été définie pour optimiser les systèmes de suralimentation avec d'un coté, le développement d'une nouvelle représentation des courbes caractéristiques de turbines permettant une résolution directe des calculs de *matching*, et d'un autre coté, le développement d'un modèle complet 0D de moteur capable de prédire dans un temps réduit le comportement de n'importe quelle configuration aussi bien en conditions stationnaires que transitoires. Finalement, une importante étude paramétrique a été réalisée pour analyser et comparer les différentes architectures sur les mêmes bases moteur, pour caractériser les impacts des limites thermomécaniques sur les performances moteur, et pour quantifier les potentiels d'amélioration en terme de consommation de carburant, puissance maximale et confort de conduite considérant différents scenarios d'évolution.

Comme principales contributions, la thèse apporte de nouveaux outils de modélisation plus efficaces pour la résolution des calculs de matching et synthétise les principales tendances des systèmes avancés de suralimentation pour orienter les développements des futurs moteurs Diesel destinés au secteur automobile.

Resum

El desenvolupament actual al camp del motors de combustió interna alternatius està principalment motivat per la reducció de les emissions contaminats i l'augment de l'eficiència energètica. El compliment del nous estàndards per a l'automoció requereix una reducció en el consum de combustible i en las emissions de contaminants i per aquesta raó resulta imprescindible l'ús de motors *downsized* i *downspeeded*. L'ús d'aquestes tècniques imposen uns requisits d'exigència elevats al sistema de renovació de la carrega i obliguen a la introducció d'arquitectures de sobrealimentació multi-etapa. Degut a la gran varietat de configuracions possibles i a l'elevat nombre de paràmetres a optimitzar, aquestes arquitectures presenten una major complexitat que els sistemes actuals. Per tant, l'objectiu principal d'aquesta tesis ha sigut investigar el potencial de les arquitectures de sobrealimentació de doble etapa per a establir, en el cas particular dels motors *downsized* i *downspeeded*, les solucions mes eficients que aconseguisquen complir amb els futurs límits d'emissions de CO2.

Per aconseguir aquest objectiu, primerament s'ha realitzat una exhaustiva revisió bibliogràfica de totes les solucions existents amb l'objectiu de determinar les arquitectures de doble etapa mes prometedores. Seguidament, s'ha definit una metodologia de *matching* que permeta optimitzar les arquitectures mitjançant, per una banda, el desenvolupament d'una nova representació de les corbes característiques de les turbines que permeta una resolució directa dels càlculs de *matching*, i per altra banda, el desenvolupament d'un model 0D de motor capaç de predir amb un reduït cost computacional el comportament de qualsevol arquitectura de sobrealimentació en condicions d'operació tant estacionaries com transitòries. Finalment, s'ha dut a terme un ampli estudi paramètric en el que s'analitzen i comparen les diferents arquitectures sobre els mateixos motors, es caracteritza l'impacte de la mida de les turbomàquines i dels límits termomecàniques sobre les prestacions del motor, i es quantifica la millora potencial de les distintes configuracions en terminis de consum, potencia màxima i confort de la conducció.

Com principals contribucions, la tesi proposa noves ferramentes de modelatge mes eficients per als càlculs de matching i sintetitiza les principals tendències en sistemes avançats de sobrealimentació per orientar els futurs desenvolupaments del motors Diesel d'automoció.

Acknowledgments

Many people have come and gone since I first arrived at CMT Motores Térmicos. Acknowledging all the people that have helped me in the course of this research is therefore quite challenging and I will almost certainly forget some of them. But the time I spent at the Universidad Politécnica de Valencia has been extremely rewarding for me and I am very grateful to all the people that put their shoulder to the wheel behind this project.

First of all, I would like to sincerely thank Dr. José Galindo Lucas, head of the air management department and advisor of this thesis, for his guidance and support throughout all these years. He brought me his technical expertise and favorable working conditions. His constant encouragement pushed me to give the best of myself.

I gratefully acknowledge Dr. Raul Payri for giving me the opportunity to carry out my PhD work at CMT Motores Térmicos and the Ministerio de Ciencia e Innovación for providing the financial support for this thesis.

I am thankful to all my colleagues of the air management department for their advice and their patience to share with me their important knowledge and experience. To some of these colleagues, I would like to particularly thank Dr. José Ramón Serrano, Dr. Hector Climent, Dr. José Manuel Luján, Dr. Vicente Dolz, Dr. Andrés Tiseira, Dr. Carlos Guardiola and Dr. Benjamín Pla.

With the innumerable hours spent in the lab, special gratitude goes to my lab-mates Oscar Garcia, Miguel Reyes and Ricardo Lang. Their constant friendship and the many activities we shared contributed to creating an excellent working atmosphere in good but also in stressful times.

This work has required knowledge in several engine fields. I am also grateful to all my colleagues of the other groups (injection, combustion, thermal management, acoustic, etc...) for their valuable help and suggestions during my doctoral thesis. Specifically, I would like to thank Dr. Jaime Martín for his advice during the development of the 0D model and Dr. Javier López for his constant support during the integration of the combustion model.

Paperwork has been sometimes quite complex and I would like to give many thanks to Teresa y Amparo for their help in the administrative tasks.

Finally, I would like to thank my family, especially my parents and my sister Coralie, for their constant support and care throughout the years. They have never stopped encouraging me and I naturally dedicate this hard work to them. I have also special thoughts for Maria, without whom life in Spain wouldn't be the same.

"Research is to see what everybody else has seen,
and to think what nobody else has thought"

Albert Szent-Gyorgyi

"Il n'y a d'homme plus complet que celui qui a beaucoup voyagé,
qui a changé vingt fois la forme de sa pensée et de sa vie"

Alphonse de Lamartine

à mes parents et à Coralie...

Contents

1 Introduction **1**
- 1.1 Background . . . 2
- 1.2 General Motivations . . . 9
- 1.3 Objectives . . . 11
- 1.4 Methodology . . . 12
- References . . . 16

2 Literature Review of Boosting Systems **17**
- 2.1 Introduction: Single Stage Turbocharging Systems . . . 18
- 2.2 Two-stage Turbocharging Systems . . . 21
  - 2.2.1 Sequential Parallel Boosting Systems . . . 21
  - 2.2.2 Serial Boosting Systems . . . 26
- 2.3 Mechanical Superchargers . . . 40
  - 2.3.1 Single Stage Mechanical Supercharging . . . 40
  - 2.3.2 Mechanical auxiliary supercharging . . . 48
- 2.4 Electric Boosting Systems . . . 54
  - 2.4.1 Electrically Assisted Turbochargers . . . 54
  - 2.4.2 Electric Boosters . . . 60
- 2.5 Centrifugal Compressor Performance Enhancement . . . 64
  - 2.5.1 Pre-Whirl Generators . . . 64
  - 2.5.2 Casing Treatments . . . 74
  - 2.5.3 Variable Geometry Diffusers . . . 78
- 2.6 Energy Recovery: Turbocompounding . . . 81
  - 2.6.1 Mechanical Turbocompounding . . . 82
  - 2.6.2 Electric Turbocompounding . . . 87
- 2.7 Concepts . . . 91
- 2.8 Conclusions . . . 94
- References . . . 113

3 Analytical study of two-stage turbocharging performance 115
3.1 Introduction . . . 116
3.2 Governing Equations . . . 116
3.2.1 Relation between Compression and Expansion Ratio . . 117
3.2.2 Model Validation . . . 125
3.3 Main Variables Influences on Two-Stage Architectures . . . 126
3.3.1 HP and LP Expansion Ratio . . . 127
3.3.2 Coolers Performance . . . 129
3.3.3 Exhaust Temperature and Turbochargers Efficiencies . . 131
3.3.4 Comparison between Single-Stage and Two-Stage Performance . . . 134
3.4 Conclusions . . . 135
References . . . 137

4 Experimental engine and turbocharger characterization 139
4.1 Introduction . . . 140
4.2 Experimental Facilities . . . 141
4.2.1 Flow Test Rig . . . 141
4.2.2 Injection Rig . . . 144
4.2.3 Turbocharger Test Bench . . . 146
4.2.4 Engine Test Bench . . . 148
4.3 Turbocharger Characteristic Maps . . . 151
4.3.1 Standard Characteristic Maps . . . 151
4.3.2 Adapted Characteristic Maps . . . 153
4.4 Conclusions . . . 163
References . . . 168

5 0D Diesel Engine Modeling 169
5.1 Introduction . . . 170
5.2 Mean Value Based Gas-Path Description . . . 174
5.2.1 Intake Line . . . 174
5.2.2 Exhaust Line . . . 180
5.3 Crank Angle Resolved Model . . . 184
5.3.1 Filling & Emptying Modeling . . . 184
5.3.2 Cylinder Model . . . 189
5.3.3 Combustion Model . . . 194
5.4 A Fully Integrated 0D Engine Model . . . 197
5.4.1 0D Engine Model Structure . . . 197
5.4.2 Algorithm Resolution and Control . . . 198

5.5 Experimental Calibration and Validation 203
5.5.1 Combustion Model 204
5.5.2 Engine Model in Steady State Operations 207
5.5.3 Engine Model in Transient Operations 212
5.6 Conclusions 215
References 224

6 Synthesis of Two-Stage Boosting Systems Performance 225
6.1 Introduction 226
6.2 Methodology 227
6.2.1 Engine Similarities 227
6.2.2 Boosting Architectures 231
6.2.3 Turbochargers Data 232
6.2.4 Engine and Intake/Exhaust Lines Constraints 235
6.3 Steady-State Results 237
6.3.1 Main-Stage Operations 238
6.3.2 Two-Stage Operations 250
6.4 Matching Analysis 258
6.4.1 Current Characteristic Maps 258
6.4.2 Future Turbocharger Maps Requirements 261
6.5 Transients Results 265
6.5.1 Turbochargers Response 265
6.5.2 Two-Stage Performance 269
6.6 Summary 278
References 280

7 Conclusions 281
7.1 Introduction 282
7.2 Boosting Technologies 282
7.3 Modeling Tools 284
7.4 Trends and Limits of Two-Stage Systems 287

Bibliography 293

Nomenclature

Acronyms

0D	Zero Dimensional.
1D	One-Dimensional.
1T	Single Stage Turbocharging.
2T	Two-Stage Turbocharging.
3D	Tri-Dimensional.
AC	Alternating Current.
ACT	Apparent Combustion Time.
AFR	Air to Fuel.
ASM	Asynchronous Machines.
BMEP	Brake Mean Effective Pressure.
BSFC	Brake Specific Fuel Consumption.
CAD	Computer-Aided Design.
CAI	Controlled Auto-Ignition.
CFD	Computational Fluid Dynamics.
CPU	Central Processing Unit.
CVT	Continuously Variable Transmission.
DPF	Diesel Particulate Filter.
DOC	Diesel Oxidation Catalyst.
EAT	Electrically Assisted Turbocharger.
ECU	Engine Control Unit.
EGR	Exhaust Gas Recirculation.
EOI	End Of Injection.
EVO	Exhaust Valve Opening.
FAMEP	Friction plus Auxiliaries Mean Effective Pressure.
FDS	Fluid Dynamic Supercharger.
FGT	Fixed Geometry Turbine.
FTP	Federal Test Procedure.
HCCI	Homogeneous Charge Compression Ignition.
HDD	Heavy-Duty Diesel.
HP	High Pressure.
HSDI	High Speed Direct Injection.
IDRCI	Injection Discharge Rate Curve Indicator.

IMEP	Indicative Mean Effective Pressure.
IVC	Inlet Valve Closing.
LP	Low Pressure.
LQG	Linear Quadratic Gaussian.
LST	Low Speed Turbocharger.
MVEM	Mean Value Engine Model.
MWE	Map Width Enhancement.
NA	Naturally Aspirated.
NEDC	New European Driving Cycle.
OEM	Original Equipment Manufacturer.
ORC	Organic Rankine Cycle.
PM	Permanent Magnet.
PMEP	Pumping Mean Effective Pressure.
POC	Point Of Combustion.
POI	Point Of Injection.
RC	Rankine Cycle.
RoHR	Rate of Heat Release.
SCR	Selective Catalytic Reduction.
SHS	Sequential Hydro-Supercharging System.
SISO	Single Input Single Output.
SOC	Start Of Combustion.
SRM	Switched Reluctance Machines.
SST	Single Stage Turbocharger.
VAIGV	Variable Axial Inlet Guide Vanes.
VGC	Variable Geometry Compressor.
VGT	Variable Geometry Turbine.

Latin symbols

A	area $[m^2]$.
a_p	instantaneous piston acceleration $[m/s^2]$.
C	completion parameter.
C_d	discharge coefficient.
C_p	specific heat at constant pressure $[J/kg.K]$.
C_w	Woschni's coefficient.
c	sound velocity $[m/s]$.
c_m	mean piston speed [m/s].
c_r	compressor compression ratio.

c_u	tangential velocity $[m/s]$.
D	diameter $[m]$.
d_{comb}	duration of the combustion phase $[cad]$.
E_{steel}	elasticity coefficient of steel $[Pa]$.
e_{cc}	piston eccentricity $[m]$.
e_r	expansion ratio.
F	absolute fuel to air ratio.
F_{rel}	relative fuel to air ratio.
H	enthalpy $[J]$.
Hc	heat of combustion $[J/kg]$.
HRT	heat release fraction.
h	heat transfer coefficient.
h_{pis}	piston height $[m]$.
k_{def}	deformation coefficient.
k_{exh}	Heat transfer coefficient.
k_{fa}	FAMEP correlation coefficient.
K_{mix}	mixing combustion model constant.
L_0	characteristic length $[m]$.
L_c	connecting rod length $[m]$.
Ope_r	optimized expansion ratio.
P	pressure $[bar]$.
MSN	mean swirl number.
m	mass $[kg]$.
$\dot{m}$	mass flow rate $[kg/s]$.
m_{alt}	mass with reciprocating motion $[kg]$.
m_i	shape parameter.
N	speed $[rpm]$.
Nu	Nusselt number.
NTU	Number of Transfer Units.
N_v	number of valves.
Pr	Prandtl number.
Q	heat transfer $[J]$.
q	heat losses $[J/kg]$.
R	ideal gas constant $[J/kg.K]$.
Re	Reynolds number.
r_c	compression ratio.
$r_{gearbox}$	supercharger transmission ratio.
S	stoke $[m]$.

SN	swirl number.
T	temperature $[K]$.
t	time $[s]$.
u	internal energy $[J]$.
V	volume $[m^3]$.
v	flow or gas velocity $[m/s]$.
W	work $[J]$.
$\dot{W}$	power $[J/s]$.
X_{EGR}	EGR rate.
Y	mass fraction.

Greek symbols

α	crank angle $[cad]$.
β	proportion of the combustion phase.
χ_{VGT}	variable geometry turbine position.
Δp	pressure drop $[Pa]$.
η	efficiency.
η_e	brake thermal efficiency.
η_{fa}	friction plus auxiliaries efficiency.
η_i	indicated thermal efficiency.
η_v	volumetric efficiency.
Γ	temperature including heat losses $[K]$.
γ	adiabatic exponent $[C_p/C_v]$.
κ	pressure loss coefficient.
λ	similarity parameter.
ω	angular speed $[rad/s]$.
$\dot{\omega}$	angular acceleration $[rad/s^2]$.
Π_c	total compression ratio.
Π_t	total expansion ratio.
ψ	crank and connecting rod lengths ratio.
ρ	gas density $[kg/m^3]$.
ε	cooler efficiency.
ϑ	mass flow distribution.

Subscripts and superscripts

$\widehat{x}$	cycle averaged value.

0	stagnation conditions.
1	LP compressor inlet conditions.
$1'$	LP compressor inlet conditions with LP EGR.
12	LP compressor outlet conditions.
$12'$	HP compressor inlet conditions.
2	HP compressor outlet conditions.
$2'$	intake manifold conditions.
3	exhaust manifold conditions.
34	HP turbine outlet conditions and LP turbine inlet conditions.
4	LP turbine outlet conditions.
a	air.
$adapt$	adapted conditions.
atm	atmospheric conditions.
b	burned product.
c	compressor.
cc	combustion chamber.
ch	IDRCI chamber.
cor	corrected conditions.
$crit$	critical conditions.
cv	control volume.
d	displaced.
em	exhaust manifold.
eng	engine.
$evap$	evaporation.
ext	external conditions.
f	fuel.
fr	friction losses.
g	gas.
H_20	cooling fluid.
im	intake manifold.
in	inlet.
$inert$	inertia.
inj	injection.
$inst$	instantaneous.
l	liquid.
mot	motoring conditions.
$nozz$	injector nozzle.
out	outlet.

p	pressure.
pp	piston pin.
ref	reference conditions.
s	isentropic process.
sc	short circuit.
st	settling tank.
TM	torque meter.
t	turbine.
th	theoretical conditions.
v	valve.
WG	Wastegate.

Groups

$K = \frac{C_{pt}}{C_{pc}}$.

$\mathbb{R}_c = (c_r)^{\frac{\gamma_c - 1}{\gamma_c}}$.

$\mathbb{R}_t = (e_r)^{\frac{1-\gamma_t}{\gamma_t}}$.

$\mathbb{Z}_c = \frac{1}{\eta_c}\left((c_r)^{\frac{\gamma_c - 1}{\gamma_c}} - 1\right)$.

$\mathbb{Z}_t = \eta_t\left(1 - (e_r)^{\frac{1-\gamma_t}{\gamma_t}}\right)$.

$\zeta = \eta_c \eta_t (1 + F) K \frac{\Gamma_{03}}{T_{01}}$.

Chapter 1

Introduction

Contents

1.1 Background **2**
1.2 General Motivations **9**
1.3 Objectives **11**
1.4 Methodology **12**
References **16**

1.1 Background

THE TRANSPORT sector with the mobility of people and freight is an important component of our economic development. During the 20^{th} century, especially after Second World War, important developments in road transportation systems and automobile manufacturing were carried out to make individual transportation available to the masses. From here, the automotive market has been continuously growing around the world, reaching more and more populations and becoming one of the bases of human societal development.

With high power-to-weight ratios and excellent fuel energy density, internal combustion engines are most commonly used for vehicle mobile propulsion. In function of their operating cycles a distinction can be made between spark ignition engines where the combustion process is ignited from a spark plug, and compression ignition engines where the heat generated from compression initiates the combustion process. These engines were respectively invented by Nicolaus Otto in 1867 and Rudolf Diesel in 1892. Since then, no fundamental changes have occurred in their thermodynamic processes but from a technological point of view they have spectacularly evolved to meet the challenging expectations of efficient mobility [145]. In the same time, lot of attention has also been paid to other technologies such as electric engines or fuel cells to compete against the domination of internal combustion engines in mobile propulsion [71, 102]. However, these technologies present still some deficiencies and are immature to be largely spread in mass production. Thus, the internal combustion engine has still a bright future ahead and its continuous development is critical to answer growing mobility needs of tomorrow.

The main factors driving the development of internal combustion engines are the emissions reduction and the energetic efficiency increase. The last being closely connected to oil availability and global warming matter.

Gas emissions are the results of combustion of fuels. Although the largest part of exhaust gases is composed by nitrogen, water vapor and carbon dioxide which are not considered as toxic, a relatively small part of combustion gases is undesirable noxious substances such as carbon monoxide from incomplete combustion, hydrocarbons from unburnt fuel, nitrogen oxides from excessive combustion temperatures and particulate matter (soot). These substances have a negative health effects on humans and cause damage to the natural en-

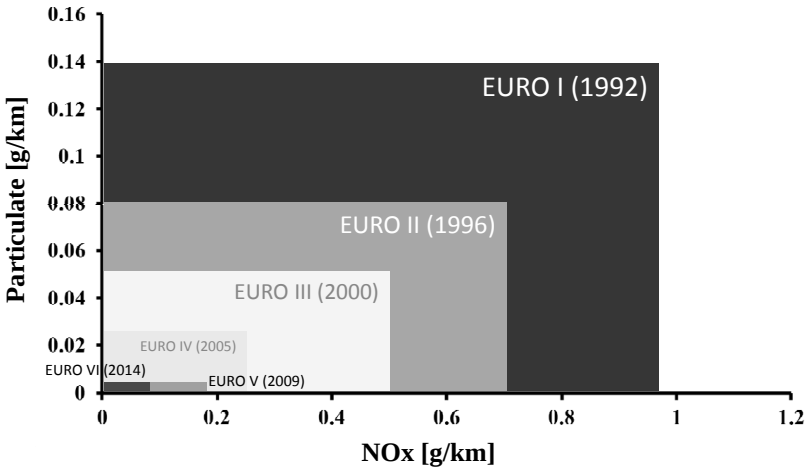

Figure 1.1: Evolution of the European emissions regulation for passenger cars and light commercial vehicles.

vironment. That is why in the last decades, different emission standards were established around the world to set specific limits for the amount of pollutants that can be released by automobiles. In Europe, these regulations are known as Euro standards and, since their introduction in 1992, their limits have been stringently reduced putting pressure on cars manufacturers to develop cleaner engines [1, 2, 6]. Figure 1.1 shows the evolution of these emissions regulations for passenger cars and light commercial vehicles. It can be observed that Euro V standard has been applied since 2009 and Euro VI represents for 2014 important challenges to meet the new ambitious NO_x emissions levels.

Energetic efficiency refers to the quantity of oil required to realize a certain work. Oil is a natural resource which has a finite availability because petroleum is formed far too slowly to be replaced at the rate at which it is being extracted. There is also some opacity and some inaccuracies about oil reserves classified as proven, many investigators [15, 40, 50] agree that the maximum rate of petroleum extraction has been reached and the rate of oil production is starting to decline as shown in figure 1.2. In fact, current oil discoveries are insignificant when compared to oil production and in the future only unconventional oils, difficult to extract and very expensive to transform, are expected to be found. With the economic development of emerging countries such as China, India, etc. . . , world demand for oil is projected to increase 21% over 2007 levels by 2030. A growing gap has therefore been initiated between the demand and the

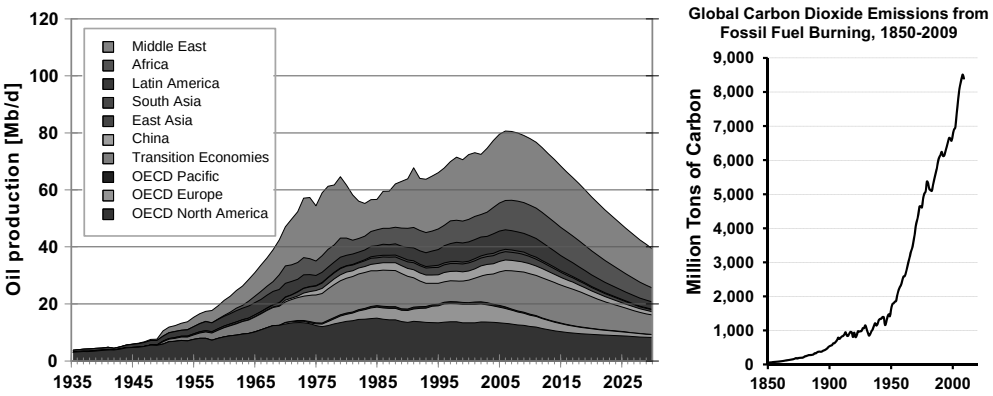

Figure 1.2: Left: evolution and prediction of worldwide oil production - Right: global carbon dioxide emissions from fossil fuel burning.

production. This demand is distributed amongst four sectors: transportation, residential, commercial and industrial but transportation is the sector that consumes more with 55% of oil use worldwide and the sector that has seen the largest growth in the last decades. Transportation is thus of particular interest to mitigate the effects of oil depletion.

Another aspect of energetic efficiency is the amount of carbon dioxide (CO_2) released into the atmosphere, which is directly proportional to the quantity of oil burnt. Being a greenhouse gas, CO_2 contributes to the negative effects of global warming (increase of the average earth's atmosphere temperature). These negative effects are sea levels rise, change in the pattern of precipitation, expansion in subtropical deserts, more frequent occurrence of extreme weather, etc... As it can be observed in figure 1.2, CO_2 emissions have exponentially increased over the last century. Improving the energetic efficiency has therefore a second objective of reducing CO_2 emissions and limiting climate change [141].

In 1998-99 through voluntary agreements with the automotive industry, a first attempt was made by the European Commission to control CO_2 emissions. These agreements were signed by the three main manufacturer associations: ACEA (European Automobile Manufacturers Association), JAMA (Japanese Automobile Manufacturers Association) and KAMA (Korean Automobile Manufacturers Association) which represent about 90% of the total European vehicle sales. The target was fleet-average CO_2 emissions under 140

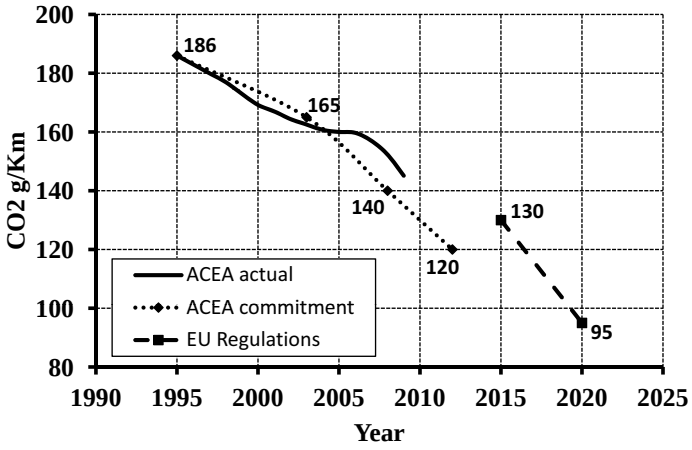

Figure 1.3: Evolution of passenger cars fleet-average CO_2 emissions.

g/km by 2008/09 for all new passenger cars. Despite significant CO_2 emission reductions were achieved in the initial years and a 5% drop was recorded in 2009 with the economic recession, none of the three associations was able to reach the 140 g/km target by 2008/09, see figure 1.3. In fact since around 2004, the manufacturers have concentrated most of their efforts to respect mandatory Euro IV and then Euro V standards. So they could no longer meet their voluntary targets. In response, the Commission developed in 2009 a mandatory CO_2 emission reduction program establishing two new fleet-average CO_2 emission targets: a mid-term one of 130 g/km to be reached by 2015 and a long-term one of 95 g/km to be reached by 2020 [5]. Important pressure is thus put on the development of new technologies which would allow to achieve these challenging targets in combination with ambitious Euro standards.

Higher efficiency and reduced operating costs have enabled the compression ignition engine taking the larger automotive market share in Europe in the last decades [289]. This leadership was possible through intensive technological developments which have changed the old heavy, smoky, noisy Diesel engine into a modern machine having the same performance as spark ignition engines and meeting strict emission regulations. Fun-to-drive character and NO_x/soot emissions were indeed the Achilles' heel of Diesel engines twenty years ago.

These technological developments have been realized in all the different engine fields. First, it can be mentioned that important progress has occurred in engine control. Since the emergence of electronic components, sensors and

modern actuators have progressively grown in number and control strategies have become considerably sophisticated [133]. Mechanically regulated systems were removed and important efforts in calibration made possible a precise control of each specific engine operating conditions. The magnitude of this change is reflected by the capacity rise suffered by the Engine Control Unit (ECU) in the last years, when in 1996 software and calibrations could be stored in 64 kBytes while today more than 2048 kBytes are required [90, 127].

Injection and combustion processes have also been largely modified. In 1991, the first High Speed Direct Injection (HSDI) Diesel engine was launched into the market. Since then, the injection pressure has been increased step-by-step reaching nowadays more than 2000 bar. These high injection pressures provide a better control of jet penetration and fuel/air mixture which are key parameters governing the combustion process. In 1997, another step forward has been achieved with the arrival of common rail systems [109]. These systems are able to realize various injections per engine stroke and present high flexibility to optimize the injection timings. Injecting a small quantity of fuel before the main injection event reduces the ignition delay and the quantity of fuel burnt during the premixed combustion. By softening the combustion explosiveness, engine noise is significantly lowered. Otherwise, injecting a small quantity of fuel after the main injection event increases exhaust temperature and fuel/air mixture at the end of the combustion. Soot emissions and after-treatment efficiency are therefore improved.

After-treatment technologies have been generalized in Diesel engines. In 2000 when Euro III came into force, Diesel Oxidation Catalysts (DOC) have been implemented to reduce the emissions of carbon monoxide, gaseous hydrocarbons and liquid hydrocarbon particles (soluble organic fraction of particulate matter) [270]. Then in 2009, Diesel Particulate Filters (DPF) have been introduced to achieve the extremely low soot emissions level required by Euro V and beyond standards [187]. In the same time, Exhaust Gas Recirculation (EGR) has been more and more employed to meet the mandatory NO_x emissions reductions. EGR works by piping back to the engine a portion of exhaust gases to lower the combustion temperature and limit NO_x production. For Euro III, EGR was only used at low speeds and loads recirculating as a maximum 30% of the total air mass flow. In Euro IV and then Euro V, EGR ranges have been progressively extended in the engine speed-torque envelope with ratings exceeding 50% [377].

Important progress has also been accomplished in terms of air management with the integration of the four-valve technology and the use of turbocharging. Four valves per cylinder improve the volumetric efficiency enabling the engine to draw in more air and eliminate exhaust gases more quickly [70]. Through wasted energy recovery in the exhaust gas stream, turbocharging increases the engine specific power forcing even more air to enter into the cylinders. With higher air densities in the combustion chamber, engine performance and specific fuel consumption have been improved. In the last years, Variable Geometry Turbine (VGT) has gradually replaced the fixed geometry turbine equipped with a wastegate. Its better regulation capacities could increase the engine operating range usable in practice and shorten transient responses [136].

Even if fuel consumption could not be significantly reduced (only 10% decrease in twelve years), all these technological developments have been particularly efficient until now to meet the strict emissions regulations requirements. However, their potential improvements to achieve the next standards (especially NO_x and CO_2) are insufficient and new technologies have to be developed.

The strong reduction of NO_x emissions will make necessary the introduction of NO_x after treatment systems [51, 169]. Two technologies will be used: the Lean NO_x Trap and the Selective Catalytic Reduction (SCR). The Lean NO_x Trap will be implemented on light-duty vehicles needing only a low NO_x reduction level while the SCR will be used on heavy duty commercial vehicles requiring a high NO_x reduction efficiency. Moreover, new combustion processes such as Controlled Auto-Ignition (CAI) and Homogeneous Charge Compression Ignition (HCCI) will be employed at low speeds and low loads [171, 189]. Their principle consists in preparing a highly diluted mixture of air, fuel and residual gases to achieve a simultaneous charge ignition in the whole space of the combustion chamber, offering in that way a strong potential to reduce the NO_x/particulate trade-off. Finally, exhaust gas recirculation will remain an important technique for NO_x control and its operating range with high EGR rates will be enlarged. For that purpose, Low Pressure (LP) EGR systems, extracting exhaust gases after the DPF to recirculate them at the compressor inlet, will arrive in complement or substitution of the conventional High Pressure (HP) EGR systems [272].

To reduce CO_2 emissions, it is a commonplace that the most promising way to achieve the 2015 and 2020 fleet average targets will be the downsized

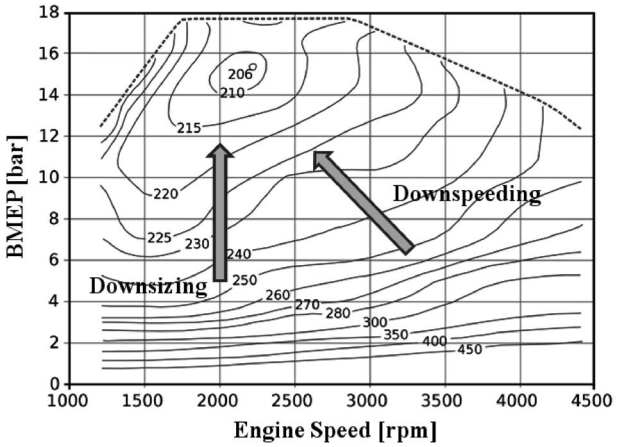

Figure 1.4: Fuel consumption enhancement through engine downsizing and downspeeding.

and downspeeded engine [100, 225]. These techniques consist in developing engines with a reduced swept volume and running at lower speeds, but with the same power output. As it can be observed in figure 1.4, fuel consumption is significantly reduced by moving the operating conditions towards areas of higher BMEP and lower speed. Nevertheless, the higher specific power required to maintain the same engine performance make these techniques quite challenging to develop.

A higher power and torque density result in a shift in the vertical direction of the steady-state power and BMEP curve. This shift generally requires an additional injection of fuel in the cylinder and thus a corresponding higher air mass flow rate, i.e. a higher charging pressure. Therefore an important demand is placed on the charging system to make a constant high pressure level available across the widest possible range of engine speeds. The high airflow required for the rated output range can only be produced by a charging device with a large design. The desire for a high charging pressure even at low engine speeds means in contrast that the compressor and turbine designs need to be relatively small. To solve this conflict, an ideal would be a charging device for the compressor and the turbine that is continuously variable on the housing and rotor sides. As this type of devices is impossible, a real possibility that is already the state of the art is the well-known method of designing the charging system with variable elements (VGT for example). But these systems

arrive now to their limits and are unable to provide the higher boost and higher operating range required by the downsized-downspeeded engine. So, optimized multistage charging systems will be introduced for further engine development.

1.2 General Motivations

In single stage arrangements, turbocharger has been the dominant technology taking almost 100% of the market share. Its high efficiency through waste energy recovery from the exhaust gases has left only little room for other systems such as mechanical supercharger. With the arrival of multistage charging systems, higher complexity is given to the boosting architecture and a large range of solutions are possible. Having various elements, the chargers can be arranged is series or parallel, working always together or sequentially. Even though the main charger is generally a turbocharger, the second one can be turbocharged, mechanically assisted (supercharger) or electrically assisted (e-booster). Variable geometry elements and additional intercooler between both stages can also be considered to enhance the architecture performance. Finally, depending on the control sophistication, more or less actuators are required to regulate the boost pressure. All these possibilities represent an important number of configurations and no standard solutions exist for all the different applications. There is therefore a need to analyze, synthesize and compare the potential of the main architectures to establish, for the particular case of the downsized-downspeeded engine, the most efficient arrangements for achieving the forthcoming CO_2 emissions targets.

These analyses have to be carried out not only under standard conditions but as well under high EGR rates. In fact, for Euro VII and beyond standards, new test cycles more stringent in terms of driving conditions are currently being developed for emissions and fuel consumption measurements [140]. These new cycles will require enlarging EGR ranges to the whole engine speed-torque envelope adding new constraints on the boosting systems. Thus the impact of high EGR rates at full load need to be characterized on the different architectures.

Downsizing and downspeeding forced to significantly increase the specific torque and power density to maintain as a minimum the same vehicle performance. This increase places a high demand on the engine components.

Conventional thermomechanical limits such as maximum cylinder pressure, exhaust manifold temperature and pressure, compressor outlet temperature, etc... become rapidly limiting factors. Modifying their levels represents major investments not only in new engine parts but as well in complete validation processes to guarantee engine reliability. So it is important to analyze how these limits restrain the downsized-downspeeded engine performance and when substantial benefits can be achieved. Another limiting factor is the small turbine size requirement to fulfill the high specific torque density at low engine speeds. Nowadays, very small turbines are not present in the automotive market as turbine efficiency significantly decreases with turbine diameter [348]. When combustion efficiency improvements through higher gas density in the cylinders are lower than pumping losses deterioration caused by the small turbine design, limitations appear in the utilization of turbocharging technologies. Reaching this point, if other solutions like mechanical or electrical assistances cannot efficiently provide the required boost pressure, downsized-downspeeded techniques cease to be efficient. These limits have therefore to be defined to quantify the maximum CO_2 benefits that can be raised by these techniques.

The right design and coupling of the boosting system to the internal combustion engine have capital importance to obtain the best overall performance. Chargers characteristics, components and control valves specifications have to be carefully optimized to match a given engine size and to fulfill as optimum as possible project objectives. Doing such optimization process experimentally would be very expensive and of little efficiency. That is why a correct combination of experimental techniques and simulation tools is required. Generally, wave action models are used for engine performance prediction [119, 134]. Through numerical methods, they solve the unsteady, non-linear and non-homentropic gas flow equations assuming one-dimensional flow in intake and exhaust piping system. Nevertheless as they predict engine performance from a specific boosting system configuration, they need a lot of iterations to perform matching calculations and are too time-consuming. With the complexity arising from multistage architectures, large parametric studies have to be carried out to optimize the large number of parameters, to understand the important interactions between systems and to check influences of particular designs. Their computational costs are therefore inappropriate to undertake these studies especially under current fast engine development process. Furthermore, when turbochargers and engine architecture are not completely defined, few intake and exhaust lines geometrical data are usually available. Without information such as intake manifold runners diameters, pipe lengths,

intercooler volume, etc... wave propagation phenomena cannot be accurately predicted and 1D model capabilities cannot be fully exploited. That is why others approaches less time consuming but sufficiently accurate to predict the correct fluid and thermodynamics behavior have to be developed.

1.3 Objectives

The general objective of this PhD-thesis is to synthesize the main criteria and trends in advanced boosting systems for future downsized-downspeeded Diesel engines. The aim is to share knowledge on promising boosting architectures giving an overview of their performance and limits to guide future developments.

To achieve this global objective, it is necessary to define at the initial stage a new methodology for efficient matching calculations. The methodological objectives can be divided in two tasks:

- Development of a new approach for the compressor and turbine characteristic maps allowing a straight forward resolution of matching calculations without any iteration.
- Development of a complete engine model to perform boosting systems matching under steady state and transient conditions within a reduced computational time.

With these new tools, the others specific objectives that are pursued in this thesis are:

- Analysis of the most efficient boosting architectures and comparison of their performance under both standard operating conditions and high EGR rates.
- Evaluation of their potential for improvements in terms of fuel consumption, maximum power and fun-to-drive for different engine development options.
- Study of the impact of thermo-mechanical limits and turbocharger size on engine performance and boosting systems operating conditions.

- Synthesis of the different interactions between the engine, EGR systems and boosting architectures.

1.4 Methodology

The correct definition of an appropriate methodology is essential to reach the objectives that have been set out for this thesis.

As every research work, the first step when subject boundaries have been defined is to perform an exhaustive literature review to assess the state of the art. Being the present work a synthesis of boosting systems, the review has been extended to all existing solutions: two-stage turbocharging systems, mechanical superchargers, electric boosting systems, compressor performance enhancement systems, turbocompounding... These solutions have been already applied on a wide range of applications and engine swept volumes for both reducing fuel consumption and increasing rated power. An analysis and synthesis of these results is thus an important starting point to understand the potential of advanced boosting systems and to select the most efficient architectures for the specific case of downsized-downspeeded Diesel engines. The results of this synthesis will be exposed in chapter 2 and only the selected architectures will be further analyzed in the frame of this work.

The complexity of multistage charging system is not only inherent in the number of elements and parameters but also in the interactions that exist between the different systems. To characterize the main factors that affect as the engine as the boosting architecture performance, a theoretical study is performed in chapter 3 with the development of an analytical model. By keeping an analytical solution, this approach is particularly interesting to check the influence of different variables independently and to understand their particular contribution to the energy balance. This model is only conceptual and cannot be applied for matching calculations. But it constitutes a first step in the behavior comprehension of complex two-stage architectures before developing more sophisticated models in the following chapters of the thesis.

As already mentioned in the motivations section, trying to reach experimentally the general objective of the thesis would results very expensive and few effective. That is why most of the work will be carried out by simulations. To be confident of the results obtained and to reduce as much as possible

the inherent uncertainties, the different models need to be calibrated and validated with experimental data. The specific installations used in this validation process will be described with their main instrumentations in chapter 4.

An effective matching methodology is required to optimize the various boosting system architectures and new modeling tools have to be developed. First, a new representation of turbine characteristic map will be described in the second part of chapter 4. This representation will be combined with a new matching procedure to directly define the turbocharger configuration as a function of intake pressure objective. In that way, iterative calculations are almost avoided and computational times are significantly reduced. Then, the turbine representation and matching procedure will be implemented in a complete 0D engine model able to predict the behavior of any boosting architectures in both steady state and transient operating conditions. Unlike 1D wave action model, this engine model resolve directly the charging system configuration as a function of engine performance objectives and matching calculations are straightforward. The development of this complete model with its resolution algorithm forms chapter 5 of the thesis.

Subsequently to the validation of all the modelling tools developed in this research framework, a large parametric study will be carried out to compare the different boosting architectures on the same base engine with various degrees of downsizing. Simulations will be realized in steady state conditions to evaluate their performance in terms of power and fuel consumption, and in transient conditions to check their acceleration capabilities under load steps at low engine speeds. Particular attention will be paid on systems interactions and benefits that can be achieved varying thermo-mechanical limits and turbocharger sizes. The results of these analyses will be exposed in chapter 6.

Finally the mains conclusions obtained by this research work will be summarized in chapter 7 with the contributions of this doctoral thesis.

References

[1] *" Council Directive 91/441/EEC of 26 June 1991 on the Approximation of the Laws of the Member States Relating to Measures to Be Taken Against Air Pollution by Emissions from Motor Vehicles".* Official Journal of the European Union, 30/08/1991, pp. 1-106, 1991. (Cit. on p. 3).

[2] *" Council Directive 98/69/EEC of 13 October 1998 on the Approximation of the Laws of the Member States Relating to Measures to be Taken Against Air Pollution by Emissions from Motor Vehicles"*. Official Journal of the European Union, 28/12/1998, pp. 1-65, 1998. (Cit. on p. 3).

[5] *" Regulation 443/2009 of the European Parliament and of the Council of 23 April 2009 Setting Emission Performance Standards for New Passenger Cars as Part of the Community's Integrated Approach to Reduce CO2 Emissions from Light-Duty Vehicles"*. Official Journal of the European Union, 05/06/2009, pp. L140/1-15, 2009. (Cit. on p. 5).

[6] *" Regulation 715/2007 of the European Parliament and of the Council of 20 June 2007 on Type Approval of Motor Vehicles with Respect to Emissions from Light Passenger and Commercial Vehicles (Euro 5 and Euro 6) and on Access to Vehicle Repair and Maintenance Information"*. Official Journal of the European Union, 29/06/2007, pp. L171/1-16, 2007. (Cit. on p. 3).

[15] K. Aleklett, M. Hook, K. Jakobsson, M. Lardelli, S. Snowden, and B. Soderbergh. *"The Peak of the Oil Age - Analyzing the World Oil Production Reference Scenario in World Energy Outlook 2008"*. Energy Policy, Vol.38, Issue 3, pp. 1398-1414, 2010. (Cit. on p. 3).

[40] R.W. Bentley. *"Global Oil and Gas Depletion: An Overview"*. Energy Policy, Vol. 30, pp. 189-205, 2002. (Cit. on p. 3).

[50] A.R. Brandt. *"Testing Hubbert"*. Energy Policy, Vol. 35, Issue 5, pp. 3074-3088, 2007. (Cit. on p. 3).

[51] S. Bremm, M. Pfeifer, J. Leyrer, W. Mueller, S. Kurze, M. Paule, B. Keppeler, and G. Vent. *"Bluetec Emissions Control System for the US Tier 2 Bin 5 Legislation"*. SAE Technical Paper 2008-01-1184, 2008. (Cit. on p. 7).

[70] B. Challen and R. Baranescu. *"Diesel Engine Reference Book"*. London: Butterworth Heinemann Ltd, Second edition, ISBN 978-0750621762, 1999. (Cit. on p. 7).

[71] C.C. Chan. *"The State of the Art of Electric and Hybrid Vehicles"*. Proceedings of the IEEE Transactions on Vehicular Technology, Vol. 90, pp. 247-275, 2002. (Cit. on p. 2).

[90] A. Dauron. *"Model-Based Powertrain Control: Many Uses, no Abuse"*. Oil & Gas Science and technology, Vol. 62, pp. 427-435, 2007. (Cit. on p. 6).

[100] H.J. Ecker, M. Schwaderlapp, and D.K. Gill. *"Downsizing of Diesel Engines: 3-Cylinder/4-Cylinder"*. SAE Technical Paper 2000-01-0990, 2000. (Cit. on p. 8).

[102] A. Emadi, K. Rajashekara, S.S. Williamson, and S.M. Lukic. *"Topological Overview of Hybrid Electric and Fuel Cell Vehicular Power System Architectures and Configurations"*. Proceedings of the IEEE Transactions on Vehicular Technology, Vol. 54, pp. 763-770, 2005. (Cit. on p. 2).

[109] U. Flaig, W. Polach, and G. Ziegler. *"Common Rail System (CR-System) for Passenger Car DI Diesel Engines - Experiences with Applications for Series Production Projects"*. SAE Technical Paper 1999-01-0191, 1999. (Cit. on p. 6).

[119] J. Galindo, J.R. Serrano, F. Arnau, and P. Piqueras. *"Description and Analysis of a One-Dimensional Gas-Dynamic Model with Independent Time Discretization"*. Proceedings of the ASME Internal Combustion Engine Division, Spring Technical Conference, Chicago, 2008. (Cit. on pp. 10, 116, 171).

[127] B. Georgi, S. Hunkert, J. Liang, and M. Willmann. *"Realizing Future Trends in Diesel Engine Development"*. SAE Technical Paper 972686, 1997. (Cit. on p. 6).

[133] O. Grondin, R. Stobart, H. Chafouk, and J. Maquet. *"Modelling the Compression Ignition Engine for Control - Review and Future Trends"*. SAE Technical Paper 2004-01-0423, 2004. (Cit. on pp. 6, 170).

[134] D. Gurney. *"The Design of Turbocharged Engines Using 1-D Simulation"*. SAE Technical Paper 2001-01-0576, 2001. (Cit. on p. 10).

[136] J. Hawley, F. Wallace, A. Cox, R. Horrocks, and G. Bird. *"Variable Geometry Turbocharging for Lower Emissions and Improved Torque Characteristics"*. Proceedings of the Institution of Mechanical Engineers Part D: Journal of Automobile Engineering, Vol. 213, pp. 145-159, 1999. (Cit. on pp. 7, 18).

[140] S. Heinz. *"Development of a Worldwide Harmonised Heavy-Duty Engine Emissions Test Cycle"*. United Nations GRPE 42$^{\text{nd}}$ session, TRANS-WP29-GRPE-2001-2, 2001. (Cit. on p. 9).

[141] A. Heinzerling. *"Global Carbon Dioxide Emissions Fall in 2009 - Past Decade Still Sees Rapid Emissions Growth"*. Earth Policy Institute, Eco-Economy Indicators, 2010. (Cit. on p. 4).

[145] J. Heywood. *"Internal Combustion Engine Fundamentals"*. New York: McGraw-Hill Inc., ISBN 978-0070286375, 1988. (Cit. on pp. 2, 191).

[169] F. Jayat, A. Reck, and K.V.R. Babu. *"SCR and SCRi as After-Treatment Systems for Low CO2 and Low NOx Vehicles"*. SAE Technical Paper 2011-26-0038, 2011. (Cit. on p. 7).

[171] N. Jeuland, X. Montagne, and P. Duret. *"New HCCI/CAI Combustion Process Development: Methodology for Determination of Relevant Fuel Parameters"*. Oil & Gas Science and Technology, Revue IFP, Vol. 59, No. 6, pp. 571-579, 2004. (Cit. on p. 7).

[187] M. Khair. *"A Review of Diesel Particulate Filter Technologies"*. SAE Technical Paper 2003-01-2303, 2003. (Cit. on p. 6).

[189] S. Kimura, O. Aoki, Y. Kitahara, and E. Aiyoshizawa. *"Ultra-Clean Combustion Technology Combining a Low-Temperature and Premixed Combustion Concept for Meeting Future Emissions Standards"*. SAE Technical Paper 2001-01-0200, 2001. (Cit. on p. 7).

[225] G. Lumsden, D. OudeNijeweme, N. Fraser, and H. Blaxil. *"Development of a Turbocharged Direct Injection Downsizing Demonstrator Engine"*. SAE Technical Paper 2009-01-1503, 2009. (Cit. on p. 8).

[270] P.R. Phillips, G.R. Chandler, D.M. Jolie, A.J.J. Wilkins, and M.V. Twigg. *"Development of Advanced Diesel Oxidation Catalysts"*. SAE Technical Paper 1999-01-3075, 1999. (Cit. on p. 6).

[272] B. Pla. *"Análisis del Proceso de la Recirculación de los Gases de Escape de Baja Presión en Motores Diesel Sobrealimentados"*. Tesis Doctoral, Universidad Politecnica de Valencia, Valencia, 2009. (Cit. on p. 7).

[289] K.P. Schindler. *"Why Do We Need the Diesel?"*. SAE Technical Paper 972684, 1997. (Cit. on p. 5).

[348] N. Watson and S. Janota. *"Turbocharging the Internal Combustion Engine"*. London: McMillan Publishers Ltd. ISBN 0-333-24290-4, 1982. (Cit. on pp. 10, 18, 55, 117, 153, 158).

[377] M. Zheng, G.T. Reader, and J.G. Hawley. *"Diesel Engine Exhaust Gas Recirculation - a Review on Advanced and Novel Concepts"*. Energy Conversion and Management, Vol. 45, pp. 883-900, 2004. (Cit. on p. 6).

Chapter 2

Literature Review of Boosting Systems

Contents

2.1 Introduction: Single Stage Turbocharging Systems **18**
2.2 Two-stage Turbocharging Systems **21**
2.3 Mechanical Superchargers **40**
2.4 Electric Boosting Systems **54**
2.5 Centrifugal Compressor Performance Enhancement **64**
2.6 Energy Recovery: Turbocompounding **81**
2.7 Concepts **91**
2.8 Conclusions **94**
References **113**

2.1 Introduction: Single Stage Turbocharging Systems

TURBOCHARGER technology history can be presented through the evolution of compressor and turbine elements over the last twenty years. The flow optimization in compressor wheel as constraints minimization obtained with new constructive arrangements have permitted the increase in compressor wheel speed and thus pressure ratio. Compressor characteristics have also been enlarged with a higher rear inclination of the compressor wheels [292]. Turbines equipped with waste gate have experimented continuous efficiency increases and inertia reduction to improve the turbocharger transient response. These evolutions can be observed in figure 2.1.

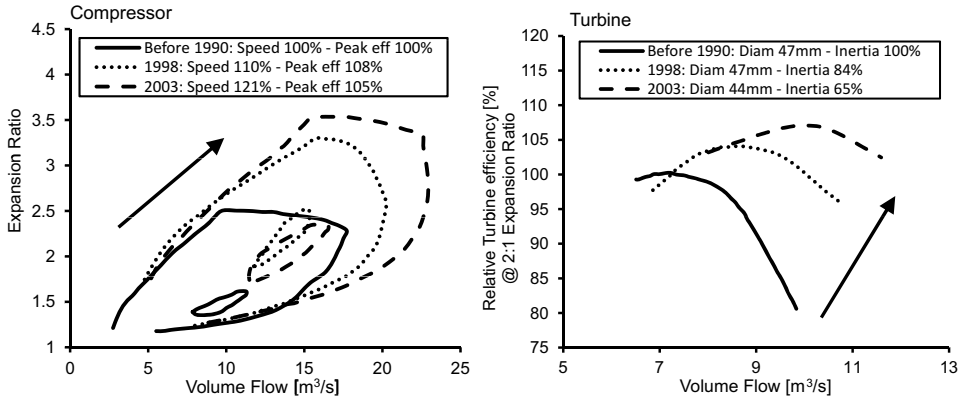

Figure 2.1: Turbocharger improvements.

The exhaust-gas turbocharger with Variable Geometry Turbine (VGT) has become established as the state of the art for Diesel engines. For this reason, an exhaustive review of single stage charging system equipped with exhaust waste gate or variable geometry nozzles is of little interest. Only a brief description is provided here to help in the understanding of multistage charging system equipped with VGT and more information can be found for example in [26, 33, 107, 136, 347, 348]. The aim of variable turbine geometry is to extend the operating range usable in practice with good efficiencies (compared to a wastegate turbocharger) [151]. For this purpose, the turbine output is controlled by varying inflow angle and inflow speed at the turbine rotor inlet. On the VGT turbocharger, this is done by guide vanes arranged upstream of the turbine rotor, as shown in figure 2.2. In the closed guide vane position, high peripheral

components of the flow velocity and a high enthalpy gradient lead to a high turbine work output and thus a high boost pressure. Whereas in the fully open position of the guide vanes, maximum turbine flow capacity is obtained with a high centripetal share of the velocity vector and a relatively lower turbine work output. The advantage of this power output control over a wastegate control relates to the fact that the full exhaust-gas mass flow is always routed via the turbine and can be converted to output. The blades are actuated by means of levers which are controlled by an adjusting sleeve accommodated in the turbine casing. This adjusting sleeve can be actuated by a number of different pneumatic or electrical actuators.

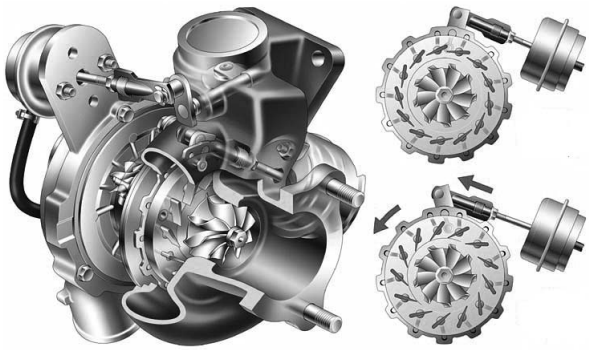

Figure 2.2: Variable geometry turbine.

A typical engine characteristic curve of a VGT application is plotted on a compressor characteristic map in figure 2.3. The conflict of goals of wishing to achieve ever-higher starting torques with lower engine speeds and, at the same time, a higher rated power output can be clearly illustrated by the compressor map. The engine characteristic curve is very near to the surge limit and the compressor efficiencies are not at the optimum at these points. In turn the rated output point is very near the compressor's maximum mass flow (choke) limit where low efficiencies lead to high boost-air temperatures. So, an increase in the starting torque is restricted by the surge limit whereas an increase in rated engine output is restricted by wheel speed limits and altitude reserve.

The requirements applicable to turbochargers with variable turbine geometry have become constantly more stringent in recent years. Just a while ago, turbocharged engines with a per-liter output of 35-40 kW/l was sufficient, but now the current state of art demands 50-58 kW/l and new advanced developments push already the turbocharger technology limits up to 65 kW/l.

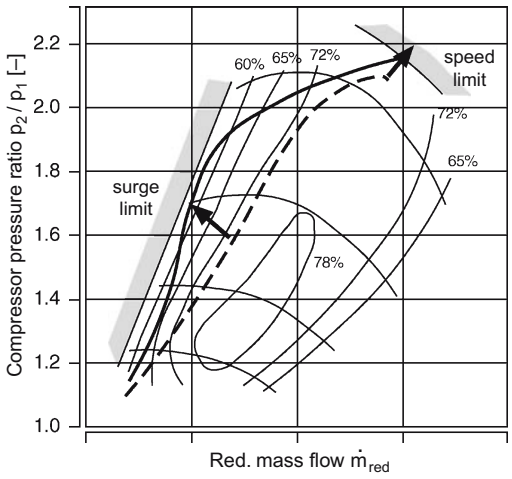

Figure 2.3: Characteristic curve of a VGT application [146].

To enhance this performance level, Schorn et al. [292] have studied on a 6-cylinder Diesel engine different single stage boosting system allowing enlarged compressor characteristics. Starting from a turbocharger with VGT, they analyzed a compressor recirculation valve, a waste gate around a smaller VGT and a variable geometry compressor as shown in figure 2.4. The recirculation valve increases the flow capacity and moves the operating conditions through higher air mass flow in the compressor map. Thus, the surge margin is improved but a higher power must be available on the turbine side. Transient response is unchanged as turbocharger inertia remains the same. The use of a smaller VGT combined with a waste gate has a lower inertia and present a better transient response, but some compromises on the rated power and fuel consumption have to be accepted due to the smaller turbine swallowing capacity. Variable Geometry Compressor (VGC) has the potential to improve overall low end performance without compromising rated power but as for the recirculation valve, does not offer advantages in terms of transient response. Futhermore, these configurations present a low potential to increase the EGR rate to respect Euro VI standards and beyond. At low loads, increasing the EGR rate decrease the mass flow passing through the turbocharger. Exhaust back-pressure regulation becomes critical because VGT is already working at its limits. At high engine speeds and loads, it is difficult to increase at the same time EGR rate and boost pressure. On one side, compressor efficiencies drop as operating conditions are shifted to the left of the compressor map,

meanwhile on the other side maximum exhaust back pressures and low efficiencies are a consequence of the VGT continuously closed. For these reasons, it seems that a per-liter rated power higher than 65 kW/l with important EGR rates is only achievable with a dual stage boosting system.

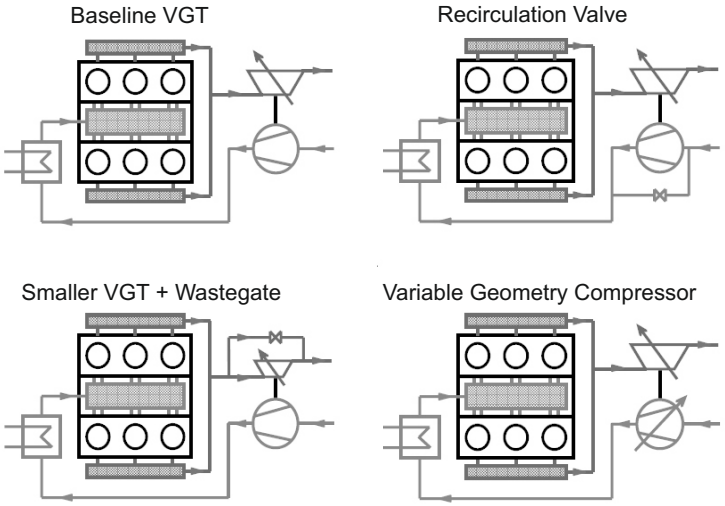

Figure 2.4: Single-stage configurations [292].

2.2 Two-stage Turbocharging Systems

2.2.1 Sequential Parallel Boosting Systems

First of all, parallel boosting systems named Twin Turbo and sequential parallel turbocharging must be differentiated. In the first case the turbocharged topologies consist in two parallel systems in which burned gases from a group of cylinder are driving one turbine. The pressurized air from both compressors is added up in a common manifold and passed through an intercooler and then fed into intake manifold [63, 226]. A typical layout of a twin turbocharger fitted on a V6 engine is shown in figure 2.5.

Boost pressure from each compressor is regulated by a waste-gate which may be built-in or separated from the turbine housing. Different manufacturers use more devices to increase performance and reliability such as electronic waste-gate regulators, two intercoolers, balance exhaust manifold and

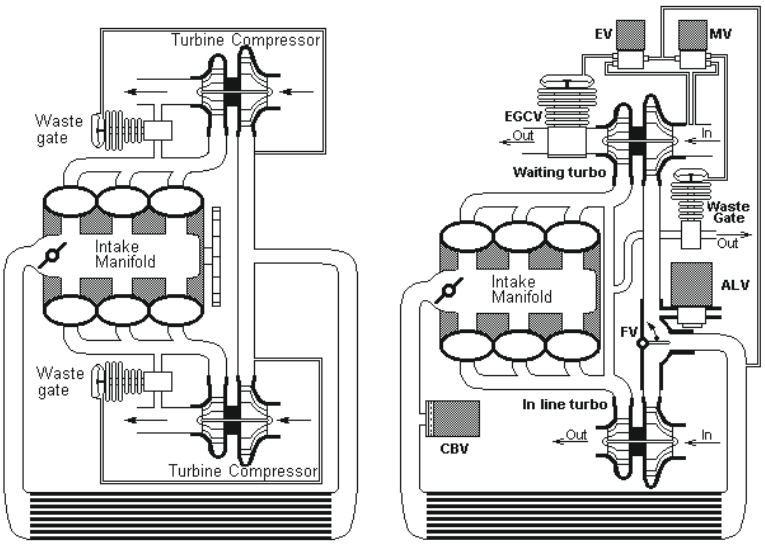

Figure 2.5: Twin turbo parallel operation (left) versus sequential turbo operation (right) [63].

many other specific equipment but the base function remains a pure parallel one. The main advantage of twin turbochargers systems when compared with single turbocharger systems is the turbo-lag phenomenon diminishes considerably. Theoretically, the turbo-lag could be reduced by 40% according to turbo-machines rules [63]. However, classical parallel connection of the two turbos does not improve the surge line and the torque at low speed operations. To compensate this, a solution is to operate only with one turbo at low engine speeds and parallel connection of compressors in the high speed operation area. This solution represents the second case called sequential parallel turbocharging as shown in figure 2.5 on the right side.

Parallel sequential turbocharging systems are able to improve diesel engine transient response since low inertia turbochargers allow faster accelerations and have advantages in terms of packaging and cost because of the lower turbo sizes. When compared to serial sequential architectures, there is an advantage in carbon monoxide (CO) and hydrocarbon emissions because of a reduced gas contact surface and only one expansion stage. This allows lower heat losses in the turbochargers and a higher temperature at catalyst entrance during the start up phase. But it has some disadvantages on rated power due to the small two turbochargers which offers a lower global efficiency

than a larger LP turbocharger, and its evolution to very small displacement engines and higher boosting pressure is limited. In addition, the sequential operation induces the need for complex transition management which has to occur without any torque impact perceptible to the driver while respecting the turbocharger limitations.

Parallel sequential turbocharging systems were introduced by Brown Boveri in 1946 and have been used in the past for marine Diesel engine [41, 78, 79, 184, 278, 320] where the running conditions are fairly constant and the transition operation are not so critical. Marine Diesel engines generally use three to five turbocharger groups with only small boost pressure drops occurring at the engine sequence transfer speed. Borila [47] showed that the equal size turbocharger solution is not optimal. Therefore turbochargers have in most case unequal sizes and, when very high BMEP are required, some turbocharger groups can be composed of two turbochargers in series due to the insufficient boost pressure obtained by a single compressor. Turbocharger activation-deactivation is realized by means of connecting-disconnecting valves. Whereas for the turbine this valve is located at its inlet section to obtain a better torque response [116, 278], the compressor connecting-disconnecting valve can be located at its inlet [184] or outlet section [47, 79, 278]. These valves are simple ON/OFF valves managed by the control system when the engine speed or the receiver pressure exceeds prefixed values. For a turbocharger switching-in procedure, the exhaust valve must be open well before the compressor switching valve, but this time lag is not necessary for a turbocharger shut down. This turbocharging system characteristics are optimized in the literature using the filling and emptying method [41, 78, 320] or one dimensional models [184].

In contrast to marine applications, engine speeds in land vehicles are subject to more variations. Thus the dynamic torque response is a key factor and transitions must be accurately managed to protect the engine components and to avoid torque oscillations. Galindo et al. [114, 115, 116, 275] applied the parallel sequential boosting system on a 2.2l modern passenger-car diesel engine to reach similar performance in terms of acceleration capability and low end torque as a 2.7l single turbo equivalent engine. The system is composed by two independent turbochargers (TC1 and TC2). TC1 is a basic charger operating throughout the complete operational range while TC2, smaller than TC1, operates only at high ranges of speed and load. A recirculation circuit with its corresponding valve was added to facilitate the transition from 1T to 2T by means of a progressive acceleration of the waiting compressor. An

important effort was devoted to the components definition and particularly the valves of the system, including new functional characteristics and specific physical definition of the different components [275]. System layout is shown in figure 2.6 where left-hand plot shows valves positions in 1T operation mode and right-hand plot shows valves positions in 2T operation mode.

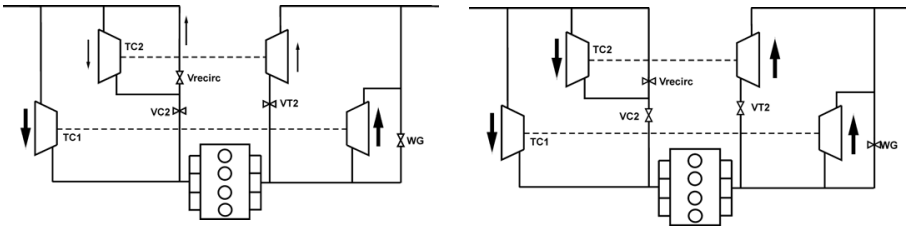

Figure 2.6: System functional architecture [116].

Turbocharger matching is a difficult task for the parallel sequential turbocharging system. In fact turbocharger surge and over-speed limits impose range limits for the different engine operating modes. In 2T operation, these limits are dependant of the flow repartition between 1T and 2T and therefore the relative area ratio between the two turbines. In addition, turbines selection are normally based on engine torque response, but a trade-off between dynamic response and transition range at full load must be considered [116].

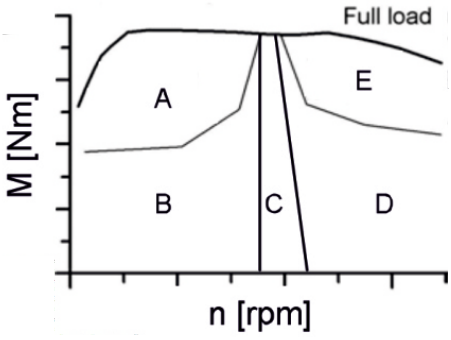

Figure 2.7: Definition of operating zones - A:2T mode is not possible (surge risk) - B:1T mode is recommended - C: switching zone - D:2T mode recommended (fuel efficiency) - E:1T mode is not possible (overspeed risk) [116].

Transition zones shown in figure 2.7 are defined respecting two critical criteria: over-speed and surge that enforce the mode transition due to risk in system damage, and two mild criteria: efficiency and system dynamics [115].

A control system decides when to operate in each one of the modes (1T or 2T), and when and how to perform the transition. This decision is taken in engine steady operation but also in transient conditions (acceleration, braking, gearbox shifts...). Control strategies are optimized on real-life driving cycles [115] for lowering the numbers of transitions and limiting over-speed and surge situations during fast engine speed variations.

The system must be able to perform the transition in a smooth way despite several dynamic processes occur as variations in both intake and exhaust manifold pressure, acceleration of the turbochargers, and thermal transients. All these phenomena interact with the combustion process and the engine pumping work, thus resulting in a non-steady evolution of engine torque during the transition. Additionally, valve management during the transition is critical, and slight variations in the timing of the closing and opening process of different involved valves can result in magnification of the torque oscillation. Controlling this was the main issue in the past for this type of engine [63].

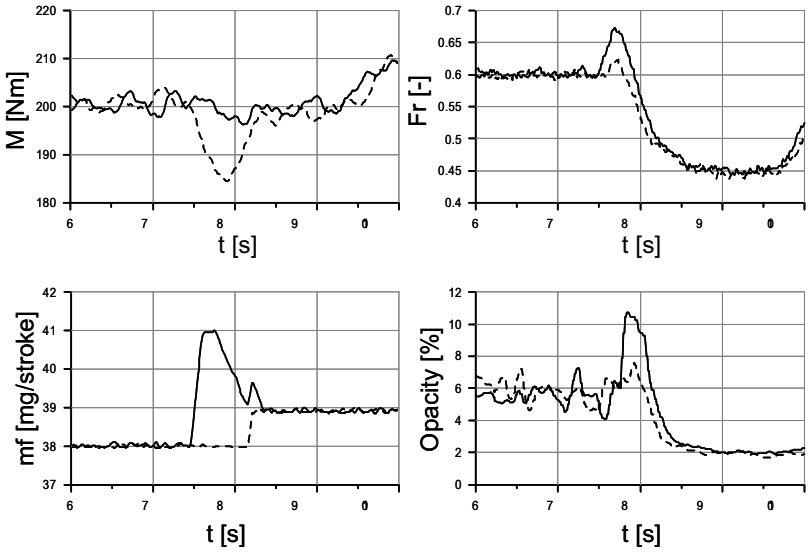

Figure 2.8: Example of a transition from 2T to 1T mode - Solid: with fuel correction strategy - Dashed: without fuel correction strategy [114].

To smooth the mode transition, Galindo et al. [114] add instantaneous corrections to injected fuel mass based on positive or negative pulses to counteract torque oscillations, steady corrections to compensate for the difference

in torque between 1T and 2T, and exhaust valve pre-lift actuation strategies. An example of resulting transitions with and without corrections can be observed in figure 2.8.

2.2.2 Serial Boosting Systems

Serial two-stage turbocharging systems were primary designed to increase the absolute boost pressure in power production and marine applications [41]. In fact, there is a limit to the boost that can be achieved by a single compressor due to efficiency decrease and map width requirements when the pressure ratio is increased. Moreover the compressor outlet temperature increases with pressure ratio and it gives way to more expensive forgings or the use of titanium for the impeller material [33]. So at higher pressure ratios, two stages of compression become more attractive and cheaper because existing turbochargers can be used and new turbocharger development is not required.

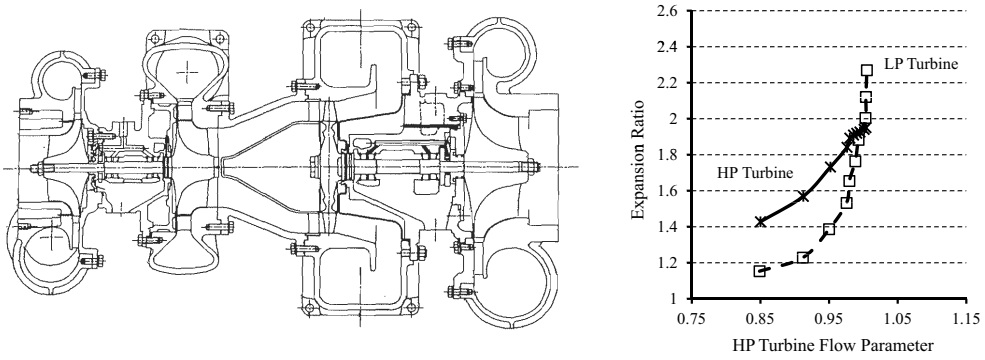

Figure 2.9: Left: cross section of two-stage turbocharger - Right: LP turbine swallowing capacity curve [322].

An example of a compact series turbocharger developed by Holset [322] comprising two single stage turbocharging is shown in figure 2.9 (left side). It comprises on the same axis a conventional turbocharger for the high pressure stage and a larger centrifugal compressor for the low pressure stage. The low pressure turbine was a custom-designed axial stage fed directly from the exhaust of the high pressure turbine. Utilizing the close coupled turbines, duct losses were kept to a minimum resulting in a high overall turbine performance. The turbocharger was designed for a high output diesel engine requiring a pressure ratio of 6:1 and operating at around 30 bar BMEP in a narrow range.

In this arrangement, flow characteristics are similar to that of a single turbine, but with significant changes in the split of expansion ratio between the stages. Once the expansion ratio has increased to the point where the turbines are nearly chocked, the HP turbine then runs at largely constant conditions. If a further increase in expansion ratio is required, for example when operating at altitude, additional expansion will only occur across the LP turbine as shown in figure 2.9 (right side).

For heavy- and light duty applications, flexibility of operation rather than absolute gain in performance is generally preferred. In 1998, Pflüger [269] was the first to introduce a regulated 2-stage turbocharging system for commercial diesel engines. These objectives were not only to increase the engine rated power but also make available a very high maximum torque at very low engine speeds and over a wide speed range. High boost pressures at low engine speeds improve the engine accelerating behavior, reduce exhaust smoke and allow relatively early high mean effective pressure. This allows, in connection with a suitably matched drive train, to reduce engine speeds (downspeeding) without compromising the drivability criteria and thus to improve fuel consumption and noise levels. On the downside, the disadvantages of regulated 2-stage turbocharging system are additional cost, complexity, packaging and poor low load performance. In fact, the lower pressure ratio per stage compared to the single-stage system combined to the low flow rate results in less efficient operations at partial loads.

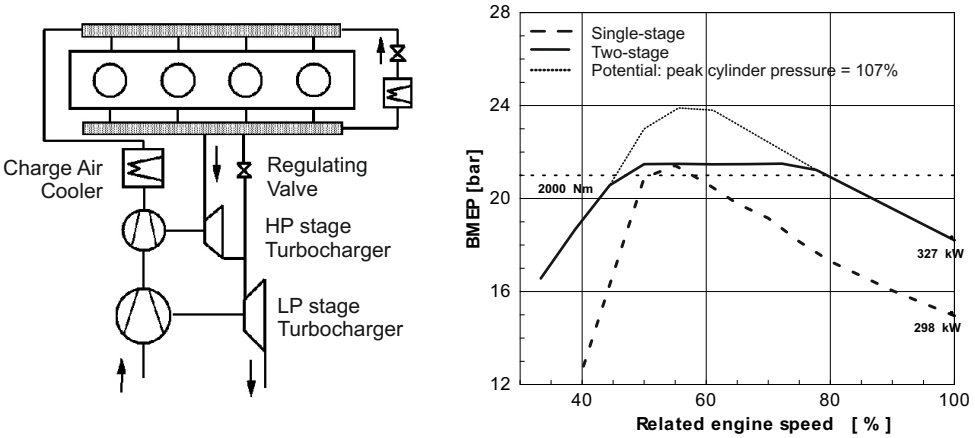

Figure 2.10: Left: diagram of a regulated 2-stage charging system for commercial application - Right: BMEP curve comparison [269].

The turbo charging system, schematized in figure 2.10, is composed of two turbochargers connected in series with a waste gate valve placed across the high pressure turbine. The larger low pressure turbine is matched to set the maximum power, while the small high pressure turbine is matched to fulfill the low end torque requirements and to decrease the turbo lag. At low engine speeds, the bypass is closed and the low exhaust gas energy is used in the high pressure stage to compress fresh air. Therefore the low pressure turbocharger is responsible for only a small part of the generated boost pressure. In the high engine speed range, as soon as the required boost pressure is reached, the bypass is regulated in a similar manner to the waste gate turbocharger diverting part of the exhaust gas energy directly in the low pressure stage. Thus, the bypass allows a continuous regulation shifting more of the expansion work to the LP turbine. In comparison to the VGT application, the engine characteristic curve with regulated 2-stage charging system runs through the center of the compressor characteristic map and achieves better efficiencies both at rated output and starting torque [290]. An example of engine characteristic curves can be observed in figure 2.11.

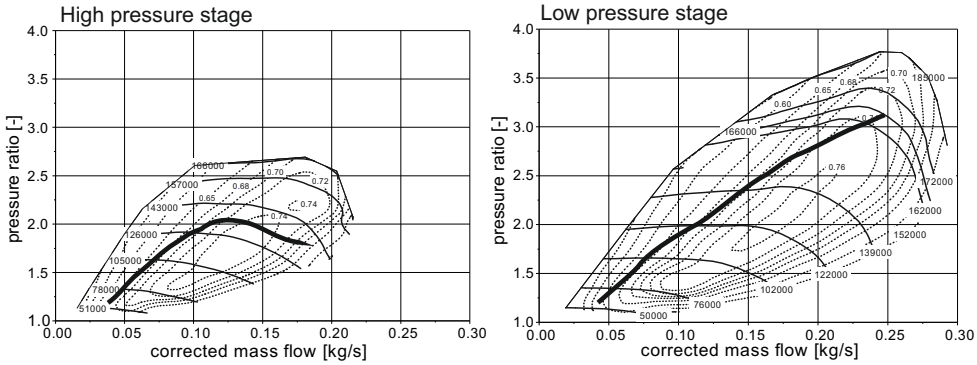

Figure 2.11: Engine characteristic curve of a regulated 2-stage charging system for commercial application.

An additional intercooler between high and low pressure compressors can be considered in function of the full load target [297, 365]. Reducing the air temperature at the HP compressor inlet reduces the compression work at constant pressure ratio and prevents an overrun of the maximum temperature tolerated by the compressor materials (around 190°C). In contrast, adding this element increases pressure losses in the air path, cost of the hardware

and packaging constraints. In view of the balance between advantages and disadvantages, this cooler is generally not implemented if the required boost pressure is maintained under 3.4-3.7 bar [132, 236, 273].

Applying this charging system on a modern 12-litre, 6-cylinder commercial diesel engine, Pflüger [269] obtained the results shown in figure 2.10. When compared with single stage turbocharging, the rated power was increased by 10%, the low end torque was significantly improved and the fuel consumption was reduced by 2 - 6.5% over a wide range. But his engine was not designed for higher ignition pressure and the full potential of the charging system could not be exploited. In fact, to ensure the permissible peak cylinder pressure, the boost pressure was limited and the start of injection was retarded limiting maximum torque and deteriorating fuel consumption. Millo et al. [236] on their 13-liter displacement HDD engine reduce simultaneously the injection advance and the engine compression ratio from 17 to 16 to fulfill their low peak firing pressure requirements (160 bar). Despite these prejudicial measures on performance enhancements, they could observe at 1500 rpm a 6% BMEP increase and an appreciable fuel economy up to 2%.

Kruithof et al. [205] used also this turbocharging system for a similar DAF engine where the high pressure turbine was replaced by a twin-entry turbine with two wastegates, one for each group of 3-cylinder. The engine was developed to operate at 30 bar BMEP with a maximum intake manifold pressure of 425 kPa to maintain an acceptable AFR. The size of the HP turbine was optimized to obtain a good compromise between steady-state and transient engine performance. Reducing the size of the HP stage improves the transient response due to lower inertia of the turbine wheel and increases the AFR which is beneficial for the fuel consumption at low engine speeds. In contrast, at higher engine speeds, a small HP turbine generates a substantial backpressure which reduces fuel efficiency. Steady-state results obtained with their engine showed a 27% increase of the rated power whereas transient response (load step 0-100%) was improved by 90%.

Variable geometry turbine can enhance even more the regulated 2-stage charging system performance. Lee et al. [216], to maximize the transient response, replaced the HP fixed geometry turbine with its waste gate by a VGT. Comparing both two-stage systems, they reported on their 4.5-liter 6-cylinder Diesel engine around 16% more low end torque, 8% more rated power and a 13% improvement of the transient response during full load acceleration from 0-60mph. While Winkler et al. [365] and Canova et al. [62] installed the

VGT on the LP stage, not for transient operation, but to optimize multiple objectives with higher control flexibility.

For passenger car applications, Saulnier et al. [288] tried at first to use a regulated 2-stage system on a highly downsized 1.5-liter diesel engine. The objective was to achieve the same performance as a similar 2.0-liter engine reaching a specific power of 70 kW/l with boost pressures higher than 3 bar. One difference with the charging system proposed by Pflüger [269] was the addition of a particulate filter between the two turbos in order to get enough enthalpy flux for regeneration purposes. Defining optimal turbochargers combination, they show the steady state performance could be reached by several turbochargers matchings, whereas transient performance needs a real optimization considering the full boost system as a whole and not stage by stage. After optimization, despite an optimal turbochargers balance in terms of turbine flow capacity, transient response targets could not be reached and "take off" problems due to low engine displacement at low RPM were observed. The HP turbine was already quite small with low efficiency and VGT technology does not yet exist for very small turbines. So at that time, it was not possible to decrease even more the turbine diameter maintaining tolerable efficiency to improve the transient response.

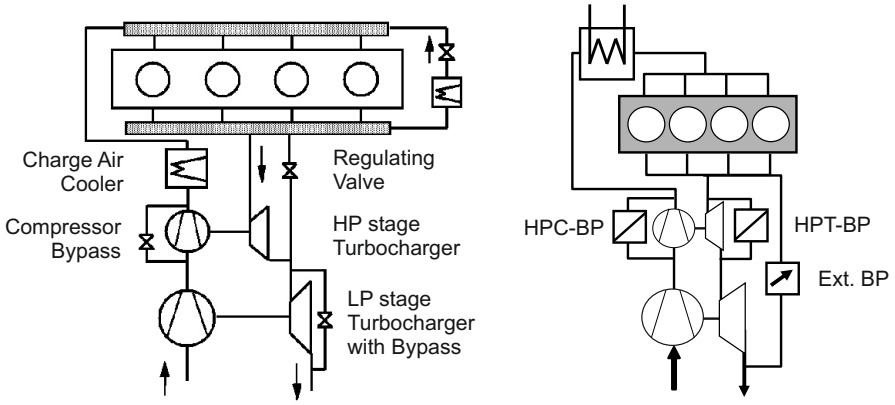

Figure 2.12: Left: diagram of a regulated 2-stage charging system for passenger application [315]- Right: FEV2 concept [352].

In 2004, Schmitt et al. [290, 315] modified the regulated 2-stage system for passenger car application paying special attention to the transient response. The system, schematized in figure 2.12, has been extended with a waste gate

across the LP turbocharger and an adequately large cross-section bypass valve across the HP compressor. The advantage of this arrangement is the flow can be fully diverted around the HP stage at high engine speeds, leaving the rotating parts to achieve just a basic speed level necessary for quick changes in load. Therefore these elements make possible the use of turbines with low absorption capacity and smaller compressors, allowing a high boost pressure to be achieved at a very early point and improving the transient response.

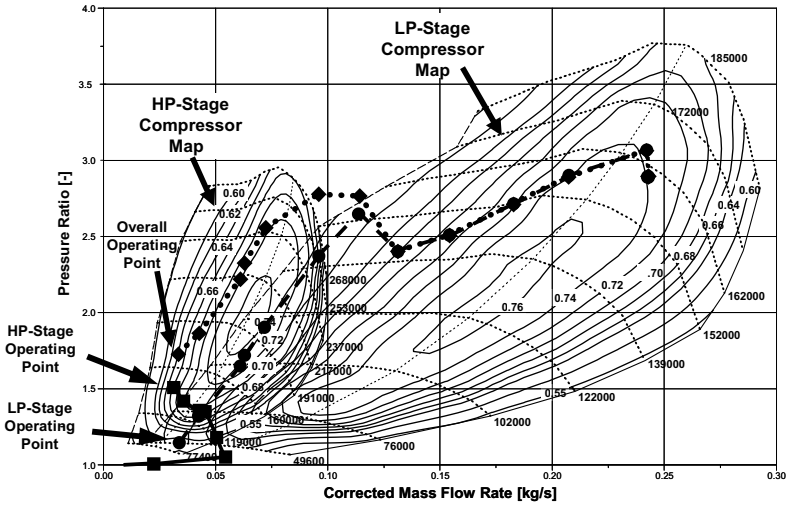

Figure 2.13: Engine characteristic curve of a regulated 2-stage charging system for passenger application [352].

As shown in figure 2.13, the matching differs from the classical regulated 2-stage charging system. The choice of the LP compressor has an immediate reflection on the HP compressor. The minimum flow rate for the LP compressor, when working alone, is the airflow corresponding to the boost pressure at medium engine speeds on the surge line. In steady conditions, this airflow is the maximum rate that the HP turbocharger must be required to deliver. Nonetheless, for optimal matching, the transient aspect has to be considered and the LP compressor must be able to support the dynamic acceleration of the high pressure compressor at the switchover point without any surge or drop in the boost pressure [54, 233, 287, 352].

Analyzing the engine characteristic curves in the compressors maps, it can be observed that they run quite far from the best efficiency areas and compressors design must be especially optimized for this charging system. As

the HP stage only contributes to the compression work at medium to high loads and under moderate engine speeds, it is only used in the lower left area of the compressor map under steady state conditions. So to optimize the HP compressor design, the area of maximum efficiency has to be shifted to lower pressure ratios and the efficiency in the lower characteristic map region has to be increased. Regarding the LP compressor, it has to provide the compressor work for the target torque and the rated output without the support of the HP stage. The operating points are shifted to higher pressure ratios in comparison to the one stage design. In consequence, the LP compressor should enable high pressure ratios and exhibit high degrees of efficiency in the upper characteristic range [287]. The optimized compressor characteristics are shown in figure 2.14. In terms of performance, these measures lead to a better transient behavior at low engine speeds, low pumping losses and therefore reduced fuel consumption.

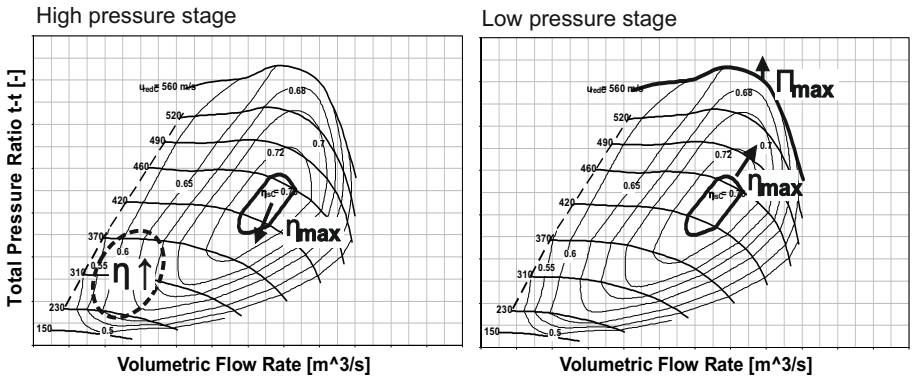

Figure 2.14: Optimized compressor map for operation in a regulated 2-stage charging system for passenger application [287].

Control system complexity also increases as 3 valves (two controlled waste gates and one ON/OFF bypass) are involved in the boost pressure regulation. To control the different valves, operating modes are defined [74, 75, 244, 352] as shown in figure 2.15. At low engine speeds and high loads, the LP waste gate and the compressor bypass are closed and the HP waste gate controls the boost pressure. At higher speeds, the HP waste gate and the compressor bypass are opened. The LP waste gate controls the exhaust energy and only the LP turbocharger provides compression works. There is an intermediate zone in which both turbochargers can operate. Since the larger LP turbocharger can provide the required boost pressure while generating less pumping losses, it is preferable to use it in steady state. Nonetheless, in transient operation, the

low HP turbine inertia allows a faster response and it is preferable to use the HP turbocharger for the compression work. In this case, the LP waste gate is opened at the start of the transient and gradually closed towards higher load [62, 352, 365].

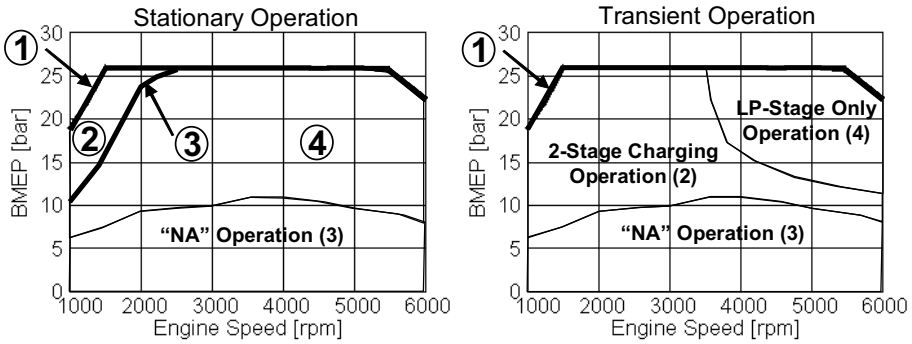

Mode	HPT-BP	HPC-BP	LPT-WG
1	closed	closed	closed
2	control	closed	closed
3	open	open	closed
4	open	open	control

Figure 2.15: Operating mode of a regulated 2-stage charging system for passenger application [352].

For control simplicity, Chasse et al. [75] keep always closed the LP waste gate when the HP turbocharger is controlled. In this way, transient response is worsened but only one actuator is regulated. Therefore, the same two cascaded controllers developed for a single stage turbocharger can be used. With this simpler strategy, an overspeed problem can arise if the HP system works near its speed limits. This is due to the low time response of the LP turbocharger in transient condition which is compensated by the faster response of the HP stage. Generally, the sensors available on the system do not give any information about the HP turbocharger speed. The HP compressor outlet pressure sensor provides a value that is the consequence of both compressions, but cannot be isolated. As for cost and liability constraints, adding new sensors between the two compressors or the two turbines are not desirable. That is why, they developed an estimator based on the turbocharger characteristic maps to estimate the turbochargers speed and the exhaust manifold pressure.

With the estimator and the corresponding SISO control strategies, the actuators could be controlled to their maximum values to reach the maximum dynamics respecting the system's safety limits.

In this boosting arrangement for passenger car application, two-stage charge compression is operated only at low to medium engine speeds. Good compressors efficiency and moderated maximum boost pressures are generally sufficient to prevent exceeding the admissible material temperature at the HP compressor outlet. Therefore, as the efficiency improvement that could be achieved by the use of an intercooler between the LP and HP stage is quite modest, such a cooler are in most cases discarded [112, 216, 233, 287, 290, 345, 352].

In terms of performance when compared with a VGT system, Schmitt et al. [290, 315] reach on a BMW 3-liter engine a high rated power output of 67 kW/l with a 40% torque increase at low engine speeds and a 22% acceleration behavior improvement. Choi et al. [81] modified a 2.2-liter diesel engine to allow an additional 15 bar of maximum peak cylinder pressure, reducing the compression ratio from 17.3 to 16.5 and optimizing the injection system. They obtained an important increase of low end torque and power with a associated 2.2% of fuel consumption reduction. Transient characteristic were also shortened by 1.2-1.8 second comparing 0%-100% load step at different constant engine speeds. Mattarelli et al. [233] on a 2.8-liter unit reported as well important performance enhancements with for example a 20% increase of low end torque.

One variant of the charging system proposed by Schmitt et al. [290, 315] is a concept suggested by Wohlberg [352] called FEV2 and shown on the right side of figure 2.12. In this system, the LP waste gate is replaced by an external bypass across both turbines and the HP waste gate is settled as an ON/OFF bypass. The boost pressure is regulated at any time by the external bypass. The LP turbine contributes less to compressor work because wastegated mass flow also bypasses the LP stage. Hence, the HP turbine delivers a larger share of power and its compressor operates at high specific work with favorable efficiency in the low speeds range. At a certain point the HP compressor and HP turbine bypasses open, the LP turbocharger speeds up, and the external bypass regulate the boost pressure. The system has advantages in compressor outlet temperature, control hardware, cost and fuel consumption at low speeds. But additional package space is required for the external bypass and sophisticated control strategies have to smooth the mode transition when HP bypasses open.

In 2009, in order to further increase the performance on the BMW 6-cylinder 3-liter passenger car diesel engine, Nefischer et al. [248] replaced in the HP stage the fixed geometry turbine with a small variable turbine geometry leaving the controlled waste gate around the VGT. The turbocharging system, in combination with improved combustion and various friction reducing measures, allows a specific power of 75 kW/l to be reached with a reduction in fuel consumption of up to 10% in the low load and speed range. The control of this architecture is more complex as the VGT actuator generates an additional degree of freedom in the boost control strategies. Canova et al. [62] have studied with a mean value model the VTG - HP turbine waste gate interactions. They showed how the VGT loses control authority approaching the behavior of a fixed geometry turbocharger as the HP turbine waste gate is progressively opened. On their system, the response to small variation of VGT and waste gate openings was very steep. A variation of 5% in the waste gate opening led to a 32% reduction of the exhaust manifold pressure. Therefore, in order to gain control, high precision was required on the waste gate actuation despite the harsh environment and the highly unsteady nature of the flow in the exhaust system. Thus, they demonstrated it is preferable to control either the VGT either the HP turbine waste gate but not both at the same time. To operate the VGT, Plianos et al. [273] developed a specific based coordinated LQG (Linear Quadratic Gaussian) controller, while Nefisher et al. [248] defined five operating modes by opening, closing or regulating the different actuators in the engine speed - torque envelope as shown in figure 2.16.

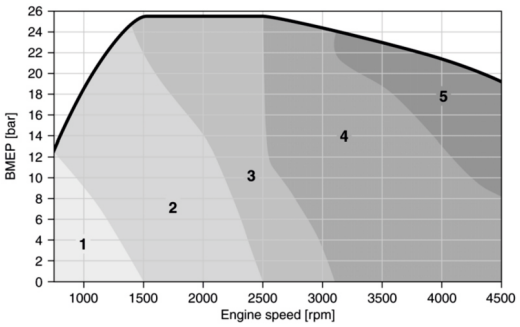

Operating mode	VTG	Turbine bypass	Compressor bypass	Wastegate
1	closed	closed	closed	closed
2	regulated	closed	closed	closed
3	open	regulated	closed	closed
4	open	open	open	closed
5	open	open	open	regulated

Figure 2.16: Extended operating modes of a regulated 2-stage charging system [248].

Adequate installation space must be available for the use of regulated 2-stage charging system. Two turbochargers with their control elements have

to fit in the engine compartment. Thus the need for compact piping is very high. Different layouts are possible but two main dispositions are generally used. On the one hand, HP stage is mounted above the exhaust manifold and LP stage below (figure 2.17 - left side) [132, 248, 290, 354]. On the other hand, the two turbochargers are positioned coaxially on the same side above the manifold in a common casting for the two turbine housings (figure 2.17 - right side) [352, 354]. In such systems, the exhaust gas is passing through at least one 90 degree bend in addition to usual layouts on single turbo units, and on the compressor side there are more than one additional bend in the piping. These additional bends give additional losses of total pressure and thus the packaging challenge leads to a tradeoff between performance and packaging.

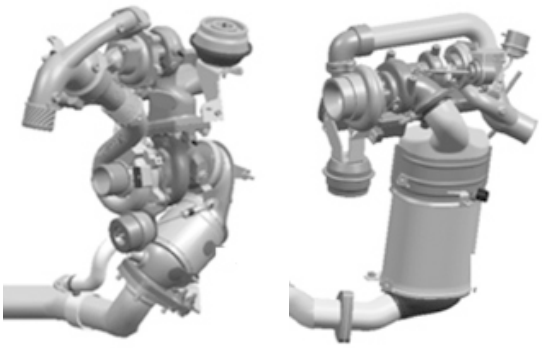

Figure 2.17: Regulated 2-stage charging system packaging solutions [354].

Because of the compact design of the turbocharging system, it is difficult and not very accurate to predict the effects of packaging two turbomachines closely together in an engine environment. Westin et al. [354] has developed a method to measure in turbocharger test rigs the loss of total pressure between the stages. He shows that a unoptimized design could lead to a two-stage total efficiency decrease of up to 8 points and a pressure ratio difference of up to 0.4. He shows also that there are influences due to the secondary flow structures (eddies, vortices, turbulence, etc...) from the upstream turbo into the downstream turbo that affect efficiency and pressure ratio. Nonetheless, these structures can lead to positive effects such as increased surge margin for the HP compressor since the LP compressor generates a co-swirl at the HP compressor inlet. Griffith et al. [132] observed on a Caterpillar on-highway truck application a fuel consumption increase of up to 4% due to an inappropriate compact design. To optimize the flow in the critical parts of the

turbocharger unit, they used computational fluid dynamics analysis. After defining air flow passages to achieve uniform axial flow into the compressor inducers, diffusing the flow out of the LP compressor as rapidly as possible without separation before entering into the HP compressor, they could mostly recover the efficiency degradation.

To reach current and future emissions goals, high rates of cooled exhaust gas recirculation (EGR) with air excess ratio at least maintained are most likely required. EGR reduces NO_x production by introducing exhaust gases in the cylinders which act as inert gases and reduce flame temperature. Further secondary effects help this mechanism like chemical dissociation, higher specific heat value for exhaust gas than air, and reduced probability of nitrogen molecules meeting and reacting with O_2 due to the presence of burnt product [209]. But reducing combustion temperature increases smoke production which can be reduced using particle traps, and the incorporation of additional inert gas in the combustion chamber reduces the quantity of oxygen available. So in general, the boost pressure must be increased to maintain the same power output. EGR may be recirculated at low pressure [54, 124, 209, 345] or at high pressure [54, 209, 297, 345, 365]. Langridge at al [209] had investigated different solutions to enhance the EGR rate maintaining high air excess ratios on their single-stage turbocharged Diesel engine originally equipped with a HP EGR circuit. The proposed EGR systems were a LP loop with an exhaust throttle, a HP loop with a pump and a HP loop with a non-return valve. They demonstrated their Euro V objectives were almost impossible to reach with such systems and two-stage turbocharging solution was the most promising way to achieve the desired EGR rates and air excess ratios with a good BSFC.

Various authors [54, 124, 345] adopted a different turbocharger matching philosophy to particularly improve the trade-off between emissions and fuel consumption instead of seeking to improve specific power. Thus, turbocharger matching is specifically optimized to minimize engine-out NO_x emissions at part load and consumption under common driving conditions. Watel et al. [345] uses two fixed geometry turbines on their downsized 1.6-liter Diesel engine, while Buchwald et al. [54] on their 2.2-liter engine was less constraint by low efficiencies imposed by small turbines and used a VGT in the LP stage. They selected the LP turbine as small as possible on the maximum output power operating point in order to maximize its capacity to recover exhaust energy at part-load, while HP turbine was matched at part-load considering EGR objectives. A very small HP turbine is normally required to recover

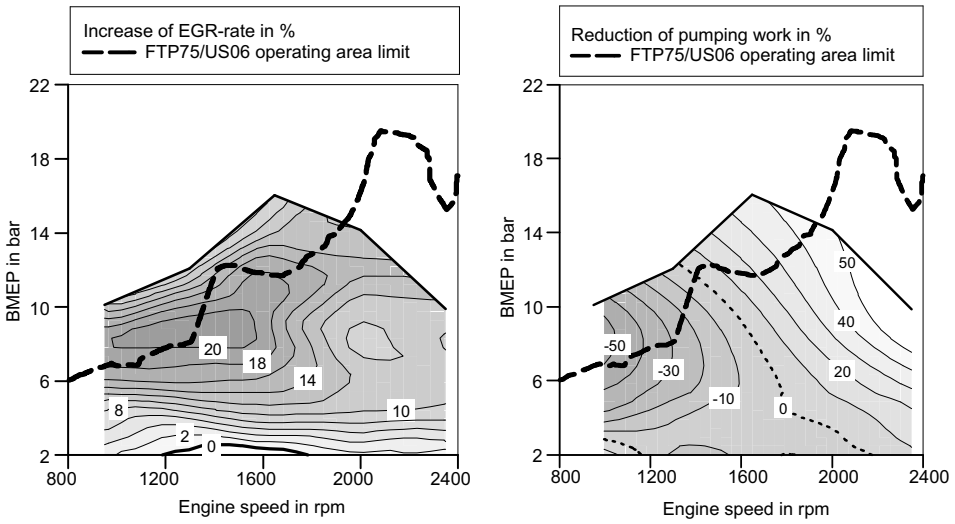

Figure 2.18: Advantages in EGR-rate and pumping work for the two-stage TC system compared to the single stage VGT system at constant air to fuel [54].

a large amount of exhaust energy but with the main drawback of substantial backpressure reducing fuel efficiency. So they matched the HP turbine as large as possible under the most restricting part-load requirements even if low end torque deteriorated. The advantages of two-stage turbocharging system associated with this type of matching in terms of HP EGR rate increase and pumping work reduction can be observed in figure 2.18. For the pumping work, a decrease of up to 60% can be seen at low engine speeds, whereas an increase is observed at medium engine speeds. In the area of higher pumping work, the HP turbine waste gate can be opened leading to a decrease of pumping work, but leading at the same time to a decrease of the EGR rate.

They had also analyzed the impact of HP EGR and LP EGR circuit in the specific case of two-stage turbocharging systems. Some results are shown in figure 2.19. The two-stage turbocharger has significant potential for increasing EGR at low engine speeds combined for slight potential for reducing fuel consumption. Conversely, at the highest engine speeds of the driving cycle, the two-stage turbocharger has substantial potential for reducing fuel consumption combined with slight potential for increasing EGR. The LP EGR circuit reaches a higher EGR rate than the HP EGR circuit but at the cost of higher fuel consumption (around 2%), due to increased gas flow in the

after-treatment system and therefore increased exhaust pressure and gas exchanges losses. Moreover the use of the LP EGR on the most loaded point can lead to a dramatically high exhaust pressure which is incompatible with the thermo-mechanical limits of the manifold. Nevertheless, the LP EGR has the advantages of reducing the intake temperature and allowing an increase in air excess through better charging capacities. So, considering a trade-off between air excess and gas exchange losses, the LP EGR may in some cases be an interesting way to reach the best compromise if the HP EGR does not permit it. Improved turbocharger efficiencies with the LP EGR also compensate, in some cases, the increase in exchange losses [345].

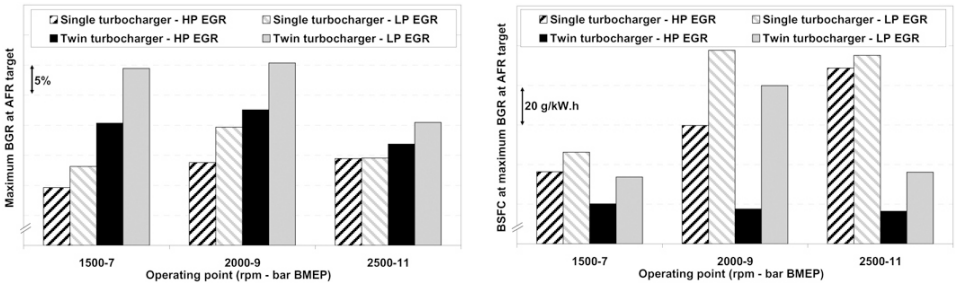

Figure 2.19: HP/LP EGR rate and fuel consumption for the two-stage TC system compared to the single stage VGT system at constant air to fuel [345].

In terms of transient processes, in addition to better engine dynamic torque, two-stage turbocharging system allows opacity and NO_x peaks to be reduced due to higher EGR capabilities [54, 297, 365]. Buchwald et al. [54] demonstrated a single stage turbocharging system is not able to produce a boost pressure high enough to keep the exhaust gas opacity low and to reach in the same time high BMEP during a load step at constant engine speed. While Serrano et al. [297] showed how a regulated 2-stage charging system associated with optimized EGR valve control strategies can improve in transient the engine performance reducing maximum opacity peaks and NO_x emissions.

Finally some authors [216, 236] have studied the potential of dual stage turbocharging combined with Miller cycle. Miller cycle consists in an early intake valve closure followed by an in-cylinder expansion of the charge during the last portion of the intake stroke. The work done by the piston to expand the air is recovered at the compression stroke as the trapped air will act as a gas spring. Miller cycle significantly reduces the peak firing pressure and the combustion temperature, whereas improves the overall thermal efficiency

as a result of better utilization of the available energy in the exhaust gas (expansion stroke longer than the effective compression stroke). Comparing the performance, Millo et al. [236] observed a 5% increase in the engine power and up to 2% increase in fuel economies with the use of a two-stage system in place of the original single stage, but in addition they observed remarkable 10% decrease of NO_x specific emissions thanks to the Miller cycle.

2.3 Mechanical Superchargers

2.3.1 Single Stage Mechanical Supercharging

Mechanical supercharging is as old as the internal combustion engine [19]. A supercharger is simple to install and in most cases does not need any complicated control. Different types of superchargers were developed for automotive applications. Even if the Lysholm compressor and the Roots blower are the most common types on the supercharger market, it exits the piston compressor, the spiral charger and the Wankel compressor.

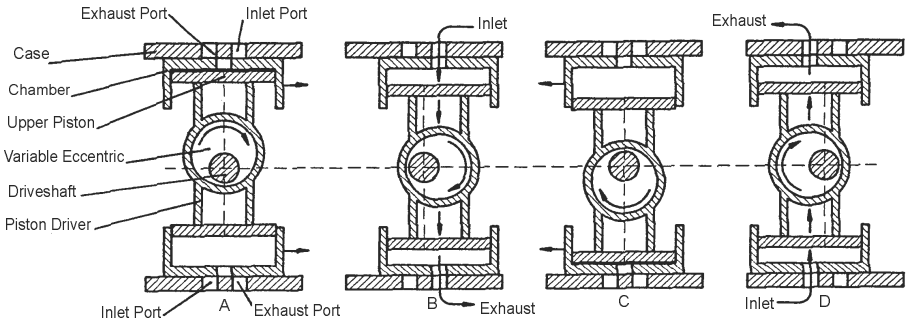

Figure 2.20: Operating description of a rotational piston charger [235].

The piston compressor is the oldest supercharger technology. It has been developed in different designs from the scavenging pump using the bottom side of the engine's piston to the so-called rotational piston charger. Rotational piston chargers are based on radially arranged pistons with pressure compensated seals. Displacement is varied by adjusting the eccentricity of the piston drive as shown in figure 2.20. Major manufacturers are Meta and Vairex. Few recent developments are present in the literature, but in 1994 Milburn [235] introduced a specific zero clearance sealing design for downsized engines.

Overall compressor efficiencies up to 85% were claimed resulting in one of the highest supercharger efficiencies observed. Nevertheless, due to the high cost and packaging limitations, this type of compressor is more appropriate to stationary applications than automotive engines [53].

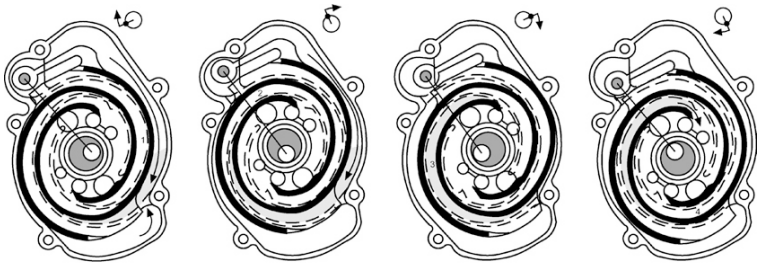

Figure 2.21: Operating description of a spiral charger [146].

Spiral chargers work according to the principle of interleaved scrolling spirals. They are composed of two identical scrolls, fixed and orbiting ones, whose axes of rotation are assembled at a relative angle of 180° to form a series of crescent-shaped chambers. As the orbiting scroll rotates, the outer chamber becomes smaller and smaller resulting in an internal compression process. A typical scroll compressor is shown in figure 2.21. The advantages of this design are its small moment of inertia, low noise emission level and low weight. Disadvantages are its complicated production and sealing problems which require important development time regarding design, manufacturing and assembly [172]. For several years, the spiral charger was in production by Volkswagen to provide high-end power for some models, but manufacturing problems such as cost and performance uniformity led to its demise [146].

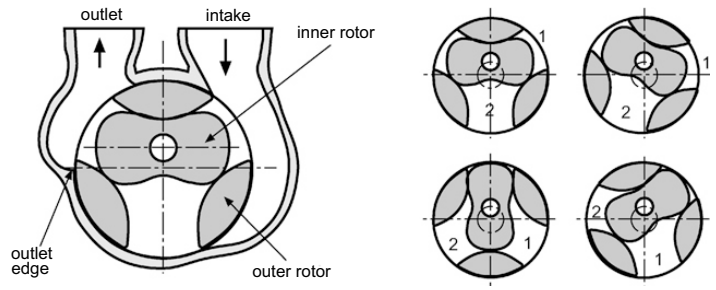

Figure 2.22: Operating description of a Wankel compressor [146].

Wankel compressors are two-concentric-shaft rotational piston chargers with three or four work plenums. As it can be observed in figure 2.22, the inner rotor dips into corresponding recesses in the outer rotor. The inner rotor is powered driving the outer rotor via a pinion and an internally geared wheel. Major manufacturers are BorgWarner, Ogura and Pierburg. Even if Schimtz et al. [291] studied the potential of a Wankel compressor to boost a Mercedes 10.9l heavy duty diesel engine, this charger type has not been used up to now in series production.

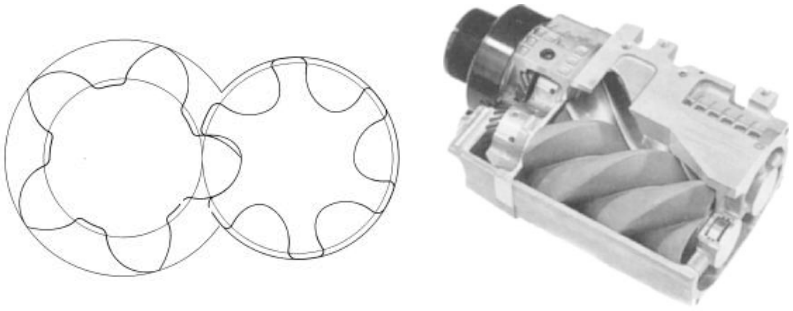

Figure 2.23: Left: example of screw compressor rotor profile [313] - Right: cutaway of screw compressor [146].

Screw compressors were first introduced in 1934 by Alf Lysholm [146]. They are composed of a pair of rotors with helical grooves separated by very small clearances, see figure 2.23. As they rotate, the space formed between them and the casing is reduced progressively, compressing in that way the gas trapped. The screw compressor works thus with internal compression, close to adiabatic conditions if friction losses and turbulences are minimized. In 1998, Takabe et al. [316] reported for the second generation Lysholm compressor adiabatic efficiencies in the 70% range. However, the real efficiency is very dependent of the engine conditions and the internal compression pressure has to match the engine inlet manifold pressure to really exploit its high efficiency. If this cannot be done, the working process will be a combination of near adiabatic compression inside the compressor and isochoric compression (or expansion) at the compressor outlet. The efficiency of this process results in an intermediate value between the adiabatic and isochoric ones. In the last decade, numerous mathematical studies based on lobe shape specification and new lobe profiles have been carried out to improve the screw compressor efficiency and reduce the cost of its manufacturing process [313, 314, 371, 372]. The results of these

studies are very interesting; however improvement cannot be evaluated due to the lack of performance data.

Major manufacturers of screw compressors are Svenska Rotor Maskiner and IHI [317]. In 2006, Mueller et al. [245] selected a Lysholm compressor to develop high specific power 4-stroke marine outboard engines. These engines work most of the time under wide open throttle operating range. Under these conditions, the Lysholm compressor benefits from its high compression ratio and relatively high adiabatic efficiencies. Before that, screw compressors were only briefly used on different AMG and Mazda series automotive applications [82, 317]. Their high cost and high momentum of inertia were limiting factors to intensively spread them in the automotive sector.

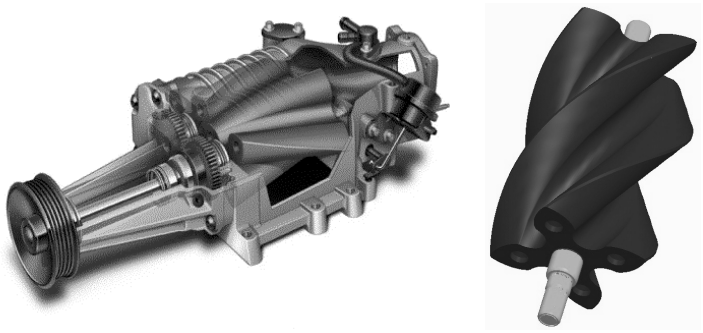

Figure 2.24: Left: cutaway of Roots blower [344] - Right: twin vortices series rotor design from Eaton [342].

The Roots blower is the most common supercharger used today. Its design consists of a pair of various lobed rotational pistons arranged on two separate shafts, see figure 2.24. The compression is not internal but takes place at isochoric conditions as the air is discharged from the blower outlet. This compression process is known to be more power consuming than the adiabatic process. Typical isentropic efficiencies for the three-lobed twisted rotor are around 60% [245, 316]. In 2006, Eaton [342] presented the twin vortices series design which consists of a four-lobed 160° twisted rotor with improved airflow handling characteristics, see figure 2.24. Isentropic efficiencies were increased up to 75%, reducing total power consumption by 13% and packaging size by 25% in comparison to the previous three-lobed 60° twisted rotor design [286]. Roots blowers have a simple design with low manufacturing cost. Its size is compact due to high possible charger speeds and its moment of inertia is lower than the screw compressor's one. Nevertheless as the air delivery occurs with

large fluctuations, high levels of tonal noise are generated from the inherent pulsations and special attention has to be paid on the inlet and outlet ports geometry [334].

Another potential noise issue, which is common to all superchargers containing timing gears, is the rattle noise [202]. Rattle noise appears with the rotational vibrations caused by cylinder firing impulses which transmit speed fluctuations to the engine crank pulley. This noise is most apparent at low engine speeds due to the lack of background noise from the engine. In the past, when the rattle noise was judged too high, costly tensional isolators were often added to the input shaft. Glover et al. [130, 344] investigated on Eaton superchargers the source and transmission path of the rattle noise. After understanding the shaft bending mode frequencies, optimum gear design was proposed and isolator needs were removed. Roots blowers as single stage charging systems are extensively used on muscle gasoline engines, like for example in the Mercedes SLK models, where dynamic response is privileged over fuel economy [45, 147, 194, 280]. They are also used on motorcycle engine as they represent a very good alternative to achieve an increase of torque without significant modifications of the naturally aspirated engine parts [311]. Formula SAE racing cars are powered with small motorcycle engines but their power are limited with an air intake restrictor. Adding Roots blowers to their engines allow sonic conditions to be maintained in the restrictor over a very large speed range. The performance is thus enhanced through a harmonious engine torque characteristic with practically constant power [31, 232].

Different investigations performed in the 80's [13, 222, 307, 334], comparing supercharging versus turbocharging, pointed out that mechanical chargers have superior dynamic response, favorable catalyst heating performance since no heat is removed from the exhaust, and good packaging capacities. However parasitic losses and lower thermal efficiencies worsen the fuel consumption. Same studies were carried out recently by Claussen et al. [85] on a 2.0l passenger car Diesel engine equipped with a twin vortices series supercharger. Results showed the absence of a turbine in the exhaust stream of the supercharged engine increased pre-DOC temperatures up to 50°C. With hotter exhaust gases flowing through the DOC, the system was able to reach during a US FTP75 test cycle the critical light-off temperature 32.5% faster than with the turbocharged engine, see figure 2.25. In terms of transient response under a 0-100% load step at 1500 rpm, the supercharged engine reached 90% of the steady-state intake manifold pressure in 0.76 seconds versus 3.34 seconds

for the turbocharged configuration. This ability to obtain rapidly the desired air flow prevented the degradation of the AFR reducing the total particulate matter production up to 14% despite the faster acceleration.

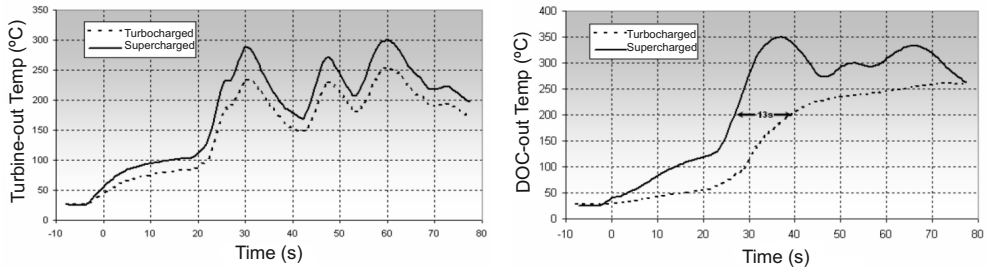

Figure 2.25: Supercharging versus turbocharging - Left: turbine out temperature - Right: DOC out temperature [85].

Parasitic losses are the main drawback of using mechanical supercharger. Miyagi at al [238] showed that 20-30% of the parasitic losses come from mechanical losses and the rest from airflow losses as a consequence of unnecessary pumping. The most obvious way of limiting these losses is to have a clutch to engage and disengage the compressor. This solution has the advantage of reducing both types of losses. However it requires a high level of torque to accelerate the compressor within a reasonable time at the working speed, which can lead to comfort problems. AC type on-off clutches are generally selected due to their simplicity and low cost. But they present important limitations as their engagement times are purely a function of the difference between the engaged and disengaged speed. At low engine speeds, engagements are too quick and too harsh whereas at high engine speeds they are slower than desired. A solution to these limitations is to use a controlled torque clutch such as electromagnetic particle clutch or plate type friction clutch [175]. With an AC type on-off clutch, Kemmler et al. [186] showed that a torque of 35 Nm can be taken of the crankshaft in very short peaks engaging the compressor in 25 ms. Using a hydraulic clutch to extend the engagement time until 0.5 seconds, they were able to reduce the torque to 15Nm. Increasing even more the engagement time to 1.2 seconds, the maximum torque did not exceed the steady state driving torque.

When a clutch is not used, a bypass valve is employed to flow the air around the supercharger. If the outlet is connected to the inlet no compression work is done. The parasitic losses come thus only from pressure losses in the

bypass valve circuit and mechanical losses as the supercharger is still turning. Controlling a bypass valve during a US FTP75 test cycle, Kociba et al. [194] showed a fuel economy improvement of approximately 1.5 mpg in comparison to a closed one (as if the bypass valve did not exist). For a screw compressor, the parasitic losses do not decrease with a bypass valve since the compression is internal. To decrease the driving power, the compression has to be punctuated. For that, Miyagi et al. [238] used a relief valve approximately in the middle of the compression process and obtained a significant reduction in the driving power. Nevertheless it would be preferable to punctuate the compression work during the entire compression process. In this way no compression work would occur and the same characteristics as the Root blower could be reached.

Another type of machine that can be used as a supercharger is the centrifugal compressor. The centrifugal compressor is not a displacement pump such as the other compressor previously described. It is a dynamic machine wherein the rotor increases density and velocity of the air. The velocity is then diffused to recover the kinetic energy as static pressure. The compression is thus realized internally. Sharing the same design as turbochargers which have been optimized over decades, isentropic efficiencies are slightly higher than the screw compressor and packaging capacities are quite low. However, very high demands are placed on the gearbox as the centrifugal compressor runs at elevated speeds well above 100000 rpm. High speeds can lead to both sound problems if gears are used and the torque needed for acceleration can be quite important even if the moment of inertia is not particularly high. An example of centrifugal compressor is the Rotrex supercharger shown in figure 2.26. It is belt driven from the crankshaft and has an internal fixed ratio epicyclic arrangement where the traction is transmitted by shearing a fluid between drive rollers. Unlike ordinary planetary gearbox, the Rotrex supercharger does not have gears which allow to obtain speed ratio of about 13 and to overcome the maximum practical limit of about 5 imposed by gear teethes of a geared epicyclic.

Up to now, centrifugal superchargers have not achieved a significant market share and were limited to enhance the performance of racing and high powered cars. In fact the flow and speed characteristics of the centrifugal compressor are not linear and a fixed gear ratio between the compressor and the crankshaft results in a poor boost pressure delivery. If the compressor is well matched at high engine speeds where maximum power is delivered, the fixed ratio drive limits boost levels available at low engine speeds as it can be observed in

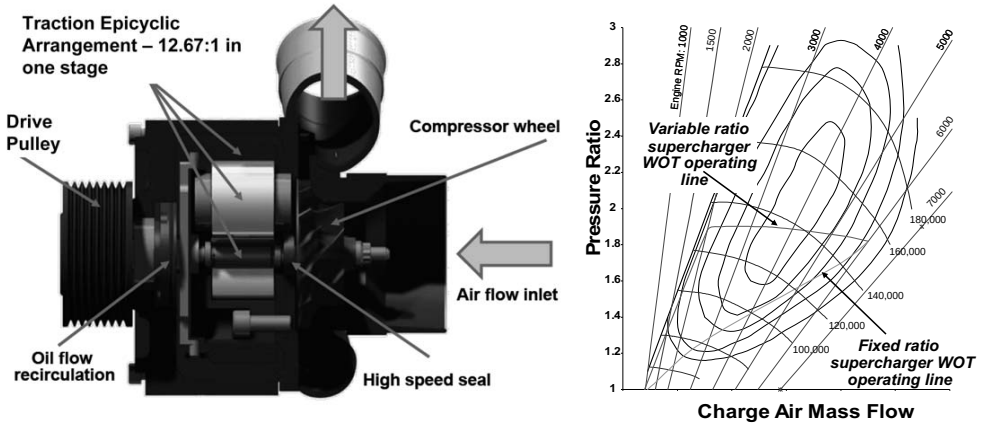

Figure 2.26: Left: view of the Rotrex supercharger - Right: fixed and variable ratio supercharger operating curve [60].

figure 2.26. To overcome this problem of under boosting in the low speed range, Burtt et al. [60] introduced in 2010 the Rotrak system which combines a Rotrex supercharger with a Torotrak Continuously Variable Transmission (CVT). The Torotrak CVT is a full toroidal traction drive variator with a wide ratio spread from an under drive of 0.4:1 to an overdrive of 2.5:1. It is torque controlled by modulating the force applied to its roller axles and has a typical mechanical efficiency of around 90% [52]. With the CVT, the boost pressure can be matched to the engine requirements as plotted in figure 2.26 speeding up the supercharger at low engine speeds and slowing it down at higher engine speeds.

An alternative arrangement presented by Brockband [52] was to connect directly a turbocharger to the engine crankshaft via a Torotrak variator extending the turbine shaft as shown in figure 2.27. By modulating the load on the variator, the system was able to control both the direction of the torque flow as well as the quantity of energy. Therefore, the turbocharger could operate as a supercharger at low exhaust gas flows, as a standard turbocharger at medium exhaust gas flow and as a compound turbine to recover energy to the crank at high exhaust energy. Using 1-D simulation, Chadwell et al. [69] with a similar system called VanDyne SuperTurbocharger (figure 2.27) showed that a modern 2.0l gasoline engine could exceed the torque curve of a 3.2l naturally aspirated gasoline engine with better part load efficiency and good transient response. The NEDC drive cycle fuel economy was simulated to be a 17%

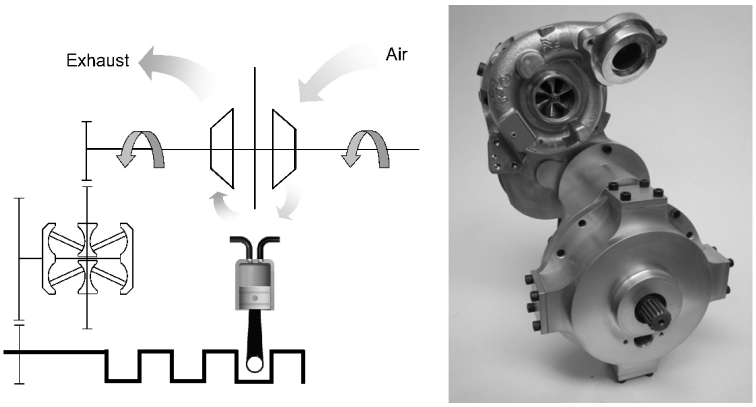

Figure 2.27: Left: variable speed turbo compound system [52] - Right: VanDyne SuperTurbocharger [69].

improvement due mainly to lower friction losses that imply a smaller swept volume engine and some exhaust energy recovery at engine speeds greater than 2000 rpm. Nevertheless, even if high speed planetary drive and CVT have been extensively developed in flywheel based mechanical hybrid system for Formula 1, their cost, weight and packaging are still challenging for midsize passenger cars.

2.3.2 Mechanical auxiliary supercharging

Mechanical auxiliary supercharging, also called hybrid system, is an arrangement that combines a mechanical charger with a turbocharger acting together to fully exploit the benefits of each type of machines. The supercharger may be of any type even if Roots blowers are generally preferred for their linearity compared to centrifugal compressors and for their low parasitic power consumption when bypassed compared to screw compressors. A typical arrangement of the hybrid system with its operating modes is presented in figure 2.28. Within the supercharger operating mode, the boosting work shifts from the supercharger to the turbocharger as engine speed increases. At very low engine speeds, the supercharger is doing the majority of the boosting whereas there is too little energy in the exhaust for the turbocharger. As engine speeds rise, the turbocharger begins to generate boost reducing directly the supercharger work. In fact being a positive displacement device, the supercharger is controlled by the downstream machine that it is pushing air into.

Then at higher speeds when the turbocharger has sufficient exhaust energy to generate all the boosting work, the supercharger is disengaged via a clutch and completely bypassed to avoid parasitic losses. Compared to the single stage mechanical supercharging system, a smaller supercharger is selected as it does not need to operate through the entire engine speed range. The bypass valve is also resized to be considerably larger to allow the whole airflow at peak power to be sucked directly from the supercharger inlet without going through the supercharger rotors which can be an air restriction.

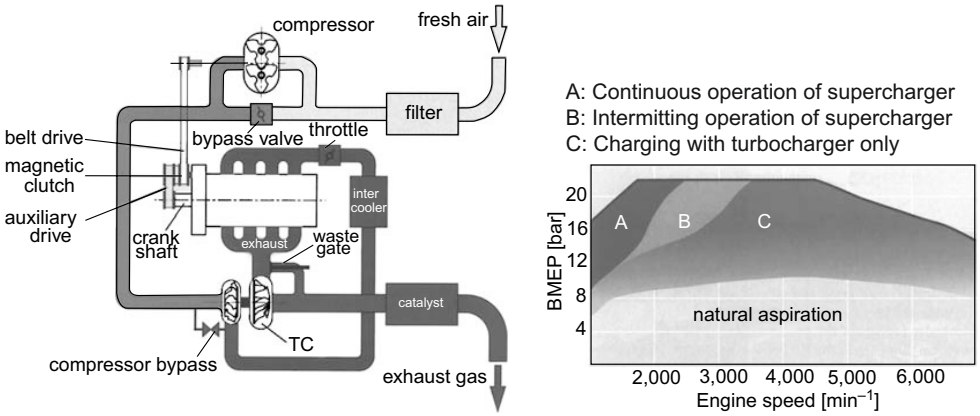

Figure 2.28: Left: sketch of mechanical auxiliary supercharging system - Right: range of the operating modes [204].

The hybrid system has been used for years in Volvo Marine and Detroit 2-stroke Diesel engines but in 1991 Tomita et al. [325] were the first to consider it for 4-stroke Diesel engines. They showed in their studies a significant low end torque increase accompanied with a reduction of particulate emissions and a 5% decrease in BSFC at low engine speeds. They also pointed out the better specific fuel consumption and power density for the mid to upper engine speed range as the turbocharger is optimally designed for these speeds, ignoring performance behavior at low air flow rates.

In 1994, Schmitz et al. [291] used a Wankel compressor as a support on a turbocharged 10.9l heavy duty Diesel engine. The supercharger was positioned upstream of the turbocharger as the inlet temperature of the supercharger is limited due to its very tight operating clearances and consequent sensitivity to thermal distortion. In addition, the fact that the turbocharger is included between two positive displacement devices (the supercharger and the engine)

makes the system relatively stable and self-limiting. Results in steady state showed that a 20% increase of low end torque can be achieved maintaining the smoke and fuel consumption levels of the standard turbocharged engine. Or in a different way, a reduction of fuel consumption up to 8% with a significant reduction in smoke level can be raised if the original torque curve was retained. The results in transient performance are presented in figure 2.29 where it can be seen that the time to obtain the desired boost pressure is reduced by 66% with the additional mechanical supercharger. Going further in the optimization of the hybrid system, Schmitz also presented the positive effect of engaging the supercharger during braking operation to contribute to the overall engine braking performance. By consuming high propulsive power and delivering boost to enable an important engine compression work, the supercharger was able to increase the engine braking performance by 140 kW i.e. 60% as shown in figure 2.29.

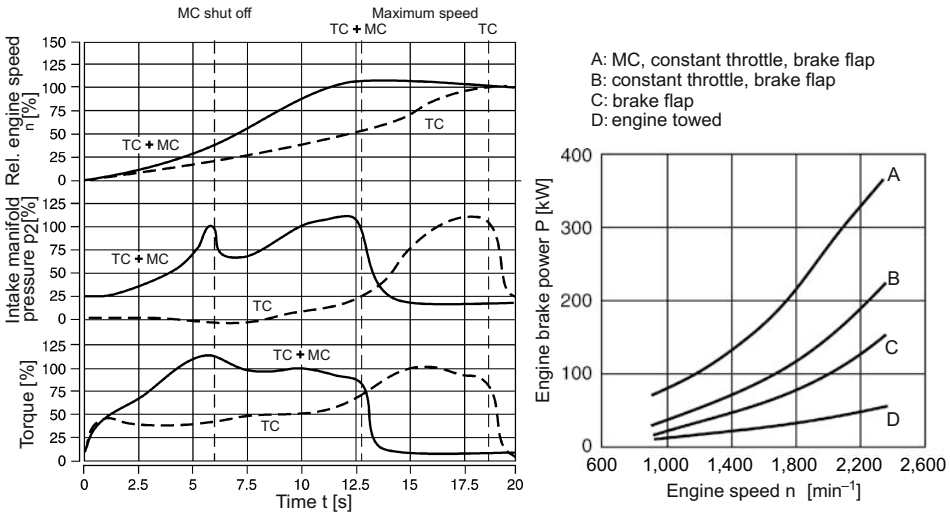

Figure 2.29: Left: transient characteristic with and without supporting supercharger - Right: engine braking performance with supercharger, decompression valve and exhaust throttle [291].

In 1998 with the development of the second generation of Lysholm compressors, Takabe et al. [157, 316] presented on an 8.8l Diesel engine some steady state performance results of their new screw compressor design in a hybrid system. In opposition to Schmitz et al. [291], they have chosen to place the compressor between the turbocharger and the engine intake man-

ifold. They reported the compressor driving power is not so different either placed in the first stage or placed in the second stage but as air density is higher in the second stage, this arrangement allows the compressor to be speeded down and its size to be reduced for better packaging capacities. On the other hand, the system requires a very sophisticated controller. The supercharger, unless controlled by the bypass, provides at each revolution the same pressure ratio regardless of its inlet pressure. Dynamics of the system are thus governed by the fact that the supercharger directly multiplies the turbocharger pressure ratio. As the engine speed increase and the turbocharger generates more compression work, it is very easy for the intake pressure ratio to spiral out of control in a very short time, resulting in a very quick reacting system but as well relatively unstable and difficult to control. A further disadvantage of this configuration is the need to install an additional intercooler between the turbocharger and the compressor. The supercharger has tight operating clearances and high thermal sensitivity. Ingesting air at high temperature from the turbocharger can result in supercharger durability and performance problems. Takabe et al. [157, 316] did not use on their engine any charge cooling between the two stages because their supercharger was disengaged at relatively low speeds when the turbocharger compression ratio was still quite low. As Schmitz [291], they observed at low engine speeds significant steady state performance improvements in terms of torque enhancement and fuel consumption reduction. Unfortunately, no transient response data was presented wherein a pressure fall during the transition mode could be expected due to the early supercharger disengagement.

Improving the Takabe's arrangement, Kanesaka et al. [177, 333] proposed a "hyperbrid" configuration with a CVT in place of the fixed gear ratio to drive the Lysholm supercharger. The hybrid philosophy was slightly changed because the supercharger was driven in the whole engine speed range under appropriate rotational speeds through the control of the CVT. Therefore, the supercharger was not only employed to increase the low end performance but also to maintain the turbocharger operating under high efficiency conditions. Very little performance data was provided with this configuration, but when compared to a standard turbocharged configuration on a 7l heavy-duty Diesel engine, 36% and 27% decreases in transient responses were reported under respectively 0-10 km/h and 0-60 km/h full load acceleration.

Cantore et al. [65] introduced in 2001 the hybrid system on passenger car Diesel engine to fully exploit the advantages of downsizing. The supercharg-

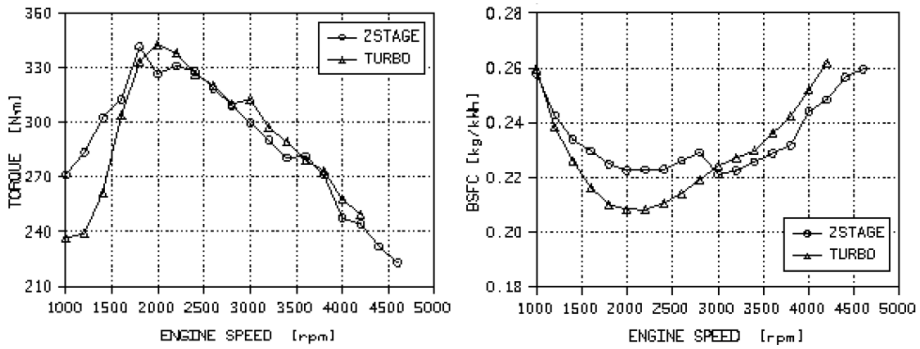

Figure 2.30: Torque and fuel consumption comparison at full load between a downsized hybrid supercharged 1.8l Diesel engine (2STAGE) and a turbocharged 2.5l Diesel engine (TURBO) [65].

ing system was applied to allow a 1.8l Diesel engine to meet the performance targets of a 2.5l turbocharged engine developed with the same technology. The configuration featured a Roots blower in the first stage and a large capacity turbocharger in the second one. It can be observed in figure 2.30 that the torque distribution between both engines was quite close at medium and high speeds while differences up to 23% appeared at low speeds in favor of the hybrid charging system. When the supercharger was engaged, the engine pumping work was positive which allowed the energy expense needed to drive the Roots blower to be reduced. In that way almost one third of the compression work was paid back by pumping. In terms of fuel consumption, results were impacted in that case by both charging system efficiencies and indicated efficiencies. Having a smaller swept volume to obtain the same brake power, indicated efficiencies were always smaller for the downsized 1.8l engine. From low to mid engine speeds with the compressor engaged, the hybrid configuration showed higher fuel consumption due to lower mechanical and indicated efficiencies. At high engine speeds, the effect of better charging system efficiencies obtained with the large capacity turbine overcame the worse indicated efficiencies allowing slightly better fuel economy. In transient operation, the hybrid system showed also an excellent behavior allowing the 1.8l unit having a better transient response than the turbocharged 2.5l engine. In fact, it was reported under a 70-120 km/h full load acceleration in fifth gear a difference of more than 1 second between both engines. From these results, various light duty downsized engines were equipped with the hybrid system. Relevant examples are the 1.4l TSI gasoline engine launched in 2005 by Volkswagen [203,

204], and the 1l 3-cylinder aggressive downsized Diesel engine presented by Howlett et al. [161] which could reach the same performance as a conventional 1.5l 4-cylinder turbocharged engine.

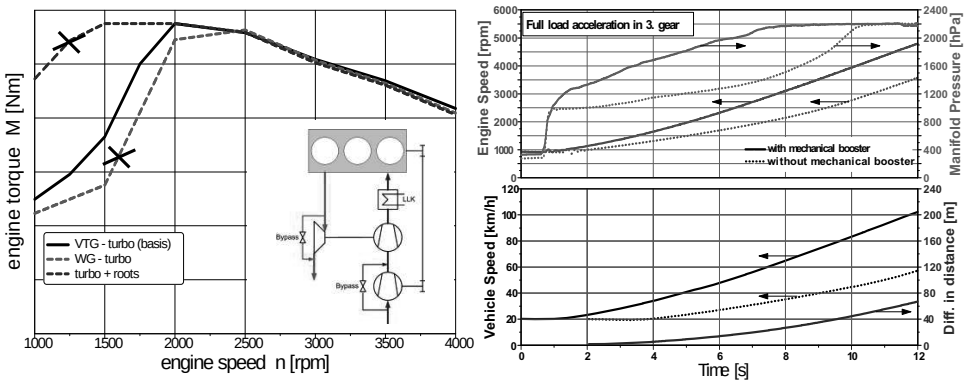

Figure 2.31: Left: turbocharging (WG or VGT) and hybrid supercharging (turbo + roots) torque characteristics [221] - Right: transient improvement with additional supercharging during vehicle acceleration [192].

Different studies comparing the performance of the hybrid system and the single stage turbocharger on the same base engine were carried out [175, 192, 221, 233]. All used a Roots-type positive displacement compressor in the first stage and pointed out important improvement in low end performance and transient response, see figure 2.31. For example, Jorgensen et al. [175] showed on a 1.8l gasoline engine how the hybrid system could generate very flat and width torque characteristics with more than 80% of peak torque produced between 1600 rpm and 7300 rpm. The reference turbocharger reached the same peak torque but maintained 80% of that peak torque only between 3000 and 7300 rpm. This corresponds to a 24.6% loss in range compared to the hybrid system due to the fact that the reference turbocharger could not fully spool until 3600 rpm. In terms of transient, the hybrid system has significantly better response than the turbocharger at all engine speeds where supercharger operation is allowed because transient characteristics are almost constant with a positive displacement compressor. Presenting results obtained under 0-100% load steps at constant engine speed, Jorgensen reported the hybrid system required between 1.0 to 1.5 second to reach at each engine speed the rated boost pressure of 200 kPa, while the reference turbocharger took nearly 4 seconds to reach 115 kPa at 1000 rpm, 150 kPa at 2000 rpm and 170 kPa at 3000 rpm.

2.4 Electric Boosting Systems

Electric boosting systems have been used in two ways, either by having the electric motor attached directly on the turbocharger shaft or by having an extra electrically driven compressor installed in series with the turbocharger. Both arrangements are described in the following subsections.

2.4.1 Electrically Assisted Turbochargers

The electrically assisted turbocharger, generally called eu-ATL or EAT, consists of a standard wastegate or variable geometry turbine turbocharger with an additional high speed electric motor. Using electrical energy, additional torque can be applied to the turbocharger shaft when there is not much exhaust gas energy available. This results in either faster acceleration of the turbocharger during transient operations or increased boost pressure under low end operating conditions. Other functions such as maintaining turbocharger speed during gearshift to reduce emissions [193], or compressing air before cranking (intake air over 100°C) to improve cold starting can also be realized with the electrical assistance.

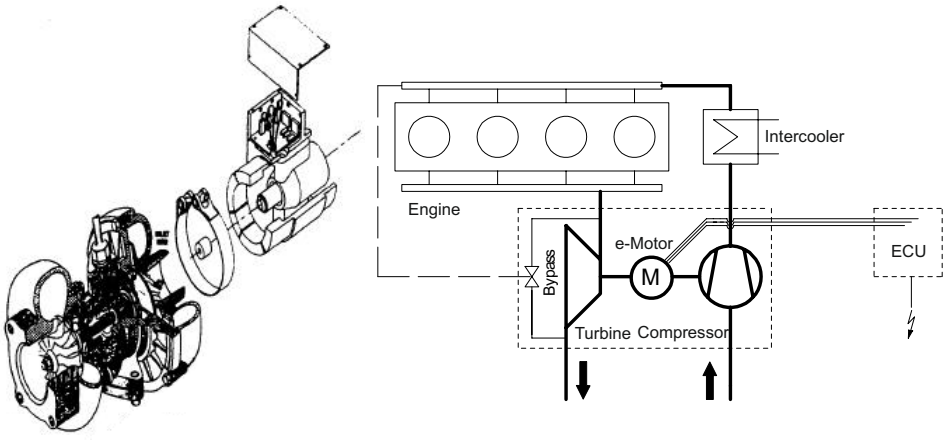

Figure 2.32: Left: the Turbostarter by Turbodyne System Inc. [253] - Right: diagram of the electrically driven turbocharger [150].

The first EAT system called Turbostarter was presented in 1995 by Turbodyne System Inc. [253]. The system was equipped with an external brush-

less electric motor coupled by a clutch to the rotor of the turbocharger, see figure 2.32. The performance of this system was quite poor. The external motor added significant volume and length to the turbocharger shaft leading to important inertia increase, high vibrations level and risk of damage when operating at high speeds. Conscious of these problems, Turbodyne System Inc. presented one year later the dynacharger [254] integrating the electric motor into the center section of the turbocharger while retaining the existing bearing housings. The length of the unit was thus limited being only a little longer (about 25mm longer) than the corresponding standard turbocharger. A diagram of this configuration is shown in Figure 2.32.

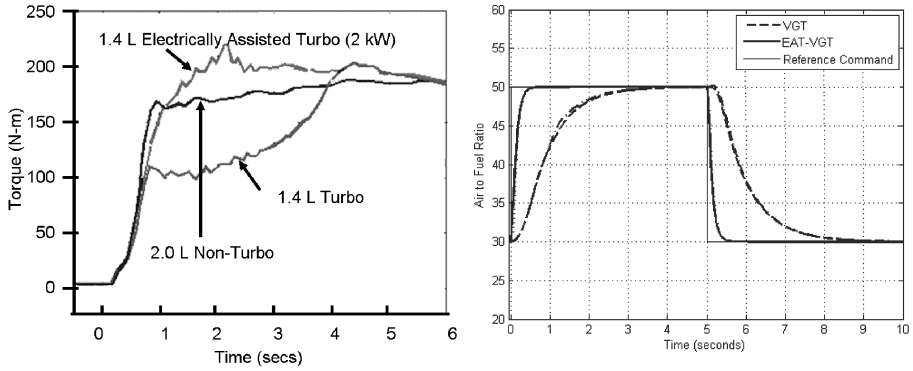

Figure 2.33: Left: vehicle acceleration performance with large non-turbo, downsized turbo and downsized EAT engines [293] - Right: steeped comparison of AFR regulation for the conventional VGT system and the EAT system [129].

During the first phase of a transient on a turbocharged engine, only a hundred watts are available on the turbocharger shaft for acceleration [348]. The transient behavior can therefore be significantly improved with addition of quite small amounts of electric power (between 1 and 3 kW) [164, 331]. Fieweger et al. [106] showed by simulation on a 6-cylinder HSDI diesel engine that vehicle acceleration from idle to 50 km/h in 2nd gear could be reduced by 0.7 second adding 2.5 kW of electric power. He assumed for the calculations 80% efficiency of the electric motor and 10% extra inertia on the shaft. Schwaderlapp et al. [293], simulating the same vehicle acceleration, reported that an 1.4l downsized EAT-turbocharged engine supplied with 2 kW could deliver the same torque response as a larger 2.0l naturally aspirated engine as it can be observed in figure 2.33. Nevertheless, being a single stage charging system, improvements in steady state boost pressure at low engine speeds

are limited by compressor surge. The EAT system has thus no appreciable potential for increasing the low end torque compared to current exhaust turbocharger, unless compressor enhancement performance devices are used in combination with the electric assistance.

When the available turbine power is higher than the power necessary to drive the compressor, the EAT system can be operated in generator mode using part of the turbine work to recover electric energy. This energy is then released in accordance with the efficiency chain into the vehicle electrical system which integrates an additional accumulator. This technique is called electric turbocompound and is of much interest for heavy duty Diesel engines to improve their specific fuel consumption. Results of different studies carried out on this technology are reported in the energy recovery section (section 2.6). In the field of conventional passenger cars, as electric power levels are limited by the 12V-based vehicle electric system, it is more challenging to technically and economically reuse this energy.

Kolmanovsky et al. [195, 196, 197] simulated on a medium-size passenger car such a system capable of bi-directional energy transfer between the turbocharger shaft and energy storage. The main objective was not to maximize the electric energy recovery to improve the fuel consumption, but during full load accelerations the EAT system should be able to regenerate its own power optimizing the transient response. Maximum power in motoring and generating mode was limited to 1.5 kW and assumed efficiencies for the motor and generator were 90% and 70% respectively. With optimal control techniques, they defined the best transient operating strategy and, under 0-40 km/h acceleration in first gear, they reported 10% improvement in takeoff performance with no deterioration in smoke emissions and essentially the same fuel consumption as a conventional turbocharged engine. Furthermore they concluded that the moment of inertia of the rotor had to increase by 250% in order to offset the acceleration improvement obtained. Extending the study to parallel hybrid configurations equipped with an electric motor attached to the drive shaft, Kolmanovsky et al. [195] found the hybrid vehicle had to deliver 10.3 kW to obtained the same acceleration time as with the 1.5 kW EAT system, while Shahed [302] required 10 kW of power on his drive-line motor assist system to reach the performance of a 2 kW EAT system. Both authors reported similar fuel consumption between both types of system when electric production is taken into consideration. This difference of power is explained by the fact the hybrid vehicle deliver directly an electric torque to the crankshaft

whereas the EAT system supplies the air which enables burning more fuel to generate the added torque. Assisted turbocharging technology has therefore a great potential to provide the same benefits (fuel consumption and transient response) as a hybrid system without the added weight and cost.

In terms of control, Glenn et al. [129] showed a precise regulation of the AFR can be achieved in transient conditions via the electrical assistance with only a small amount of power. In fact, the bidirectional capability of the electric motor allows the turbocharger to be accelerated and decelerated much faster than the conventional one overcoming undesired control saturation and inertial dynamic limitations. An example of regulation improvement obtained during an AFR step at constant fuel flow rate is shown in figure 2.33. This more precise control could result in important emissions reductions over a wide range of operating conditions, but even if load requirements over the FTP cycle were evaluated by the authors, no emissions performance data was provided.

Thermomechanical constraints are particularly important on the electric motor of the EAT system [247, 303]. The motor has to be designed for a speed range that covers the whole operating range of a standard turbocharger and for the high thermal load resulting from the turbine heat flux. The motor is very sensitive to heat and must be cooled constantly by the oil or water cooling system even when it is not in operation. The same applies to the power electronics when they are integrated to the electric motor. The mechanical stress due to centrifugal force sets an upper limit to the rotor diameter but as the turbocharger speeds are very high, the required power can be provided by a motor of relatively small size. Furthermore as power output changes with the cube of radius, small changes in radius can lead to a large change in power output.

Due to the low reliability of mechanical commutation systems at high speeds, only electronically commuted motors can be used [274] i.e. permanent magnet-excited synchronous machines (PM), switched reluctance machines (SRM) or asynchronous machines (ASM) as shown in figure 2.34. PM machines have the highest efficiencies, do not present rotor losses from the excited magnetic field and are insensitive to the gap clearance between the rotor and the stator. Since their rotor magnetic circuit does not need to be laminated, they can also have the stiffest shaft and the highest critical speed. But major challenges are the low maximum operating temperature (around 150°C) and the difficulty to retain the magnets at high speeds requiring costly

additional design measures [59]. SRM machines are interesting due to their very simple and robust construction. Their rotors generate only a few dissipation losses (low cooling level needed) and have a low mass moment of inertia due to their characteristic tooth contour. However, they require considerably reduced gap clearances which force to implement suitable roller-type or ball bearing system. They also need a device to detect the position of the rotor unless sophisticated sensorless controls are used [32]. Regarding ASM machines, they can be completely switched off and de-energized when the rotor is not driven beyond synchronous speed. They are very robust and do not need special rotor position detector [57, 58, 310]. But one disadvantage is the relatively high rotor slip under operations which generates significant losses and requires intensive cooling [308]. From these different motor technologies, none of them emerges as the favored solution for all EAT developments. Pros and cons studies have therefore to be conducted for each application to find the best compromise in function of the project objectives (power, speed, cooling, cost, manufacturing, inertia, bearing, etc...).

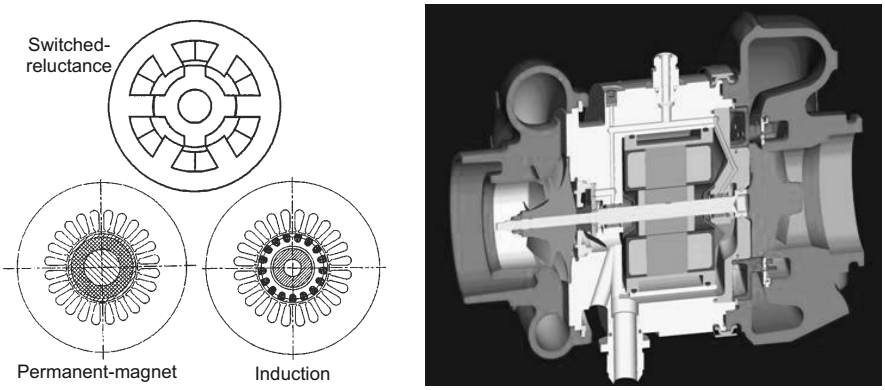

Figure 2.34: Left: electronically commuted motors types for EAT system [308] - Right: cross section of ETC turbo developed by the ELEGT consortium [237].

Important innovation in motor, battery and power electronic technologies that enable reliable operations at very high rotational speeds were obtained in the last decade. In 2000, Bailey et al. [376] presented the development of an EAT system with a PM motor for DDC heavy duty Diesel engines. The system was able to deliver 13 kW at 100000 rpm achieving 50% reduction in turbo spool-up time and 17% decrease in time response under a 0-100% load step at 1800 rpm. Following this development, Hopmann et al. [16, 17, 154, 155, 156] combined the turbocharger and turbo compound function into a large 60

kW EAT system on a Caterpillar Class 8 truck engine. They retained SRM machines in the design process for cost and performance reasons. Maximum turbocharger speed was limited to 66 000 rpm due to the high power level and important centrifugal stresses in the rotor lamination. After optimization of the motor implementation, they could reach up to 92% system efficiency over a wide range of operating conditions. Bumby et al. [56, 58, 237, 284] within the 5^{th} framework Research program of the European Commission selected ASM machines to improve transient responses and fuel economy of a 7.8l city bus Diesel engine. The motor rating was 7.6 kW at 100000 rpm. A cross section of the system can be observed in figure 2.34. Giving 1 second of electric power during a typical transient at low speeds, engine operations under smoke limitation were reduced from 7 seconds to 2 seconds corresponding to 70% improvement in turbo lag.

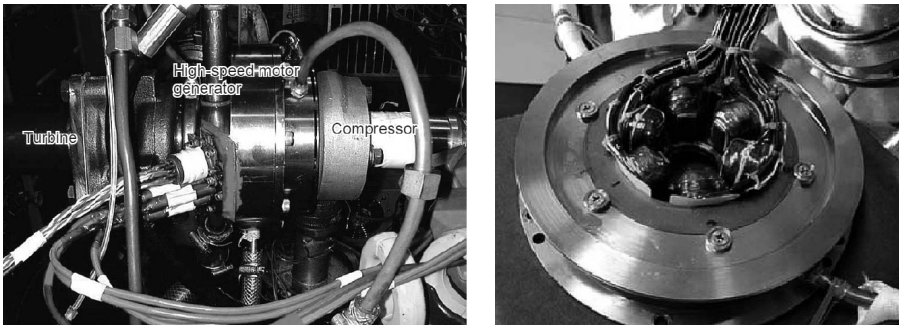

Figure 2.35: Left: Mitsubishi EAT system during engine testing - Right: external appearance of the PM motor stator [164].

Turbochargers in passenger cars can reach speeds as high as 250000 rpm. In this case, permanent magnet synchronous machines are generally chosen for their high critical speeds. In 2003, Shahed et al. [304] presented a 1.4 kW EAT system especially designed for a 2l downsized Diesel engine. The compressor was equipped with variable geometry technologies [24] to avoid surge and make full use of high boost at low engine speeds. Engine tests demonstrated that 25% and 40% torque increase could be achieved at respectively 1200 and 1500 rpm while transient response (time to 200 Nm of torque) was reduced from 6 seconds to 2.3 seconds. In 2005, Yamashita et al. [251] developed a first PM electric drive with a rating of 2.7 kW at 160000 rpm. The compressor was relatively small to overcome surge instabilities at low engine speeds. Two years later, they updated their design with a second version to increase the maximum speed up to 220000 rpm and to improve the cooling system with the use of

forced oil cooling in the stator and forced air cooling in the rotor [252], see figure 2.35. Rated power was also slightly reduced at 2 kW. Results obtained on a 1.7l turbocharged engine showed engine torque could be increased by approximately 17% at 1000 and 1200 rpm with turbo spool-up time cut down by 33% [164, 375].

2.4.2 Electric Boosters

Another way of using electric assistance is to have an extra radial flow compressor driven by an electric motor in series with the turbocharger. This electric supercharger is called eBooster. It can be placed in the intake air path before or after the turbocharger, but placing it before provides more flexibility in terms of packaging and some minor advantages in terms of power. To keep the pressure losses as low as possible, a regulated bypass valve is added around the eBooster to completely divert the air mass flow when it is switched off. Valve actuation is supervised by appropriate control strategies to avoid flow recirculation during valve opening [217]. A diagram of the serial configuration with a view of an eBooster is given in figure 2.36.

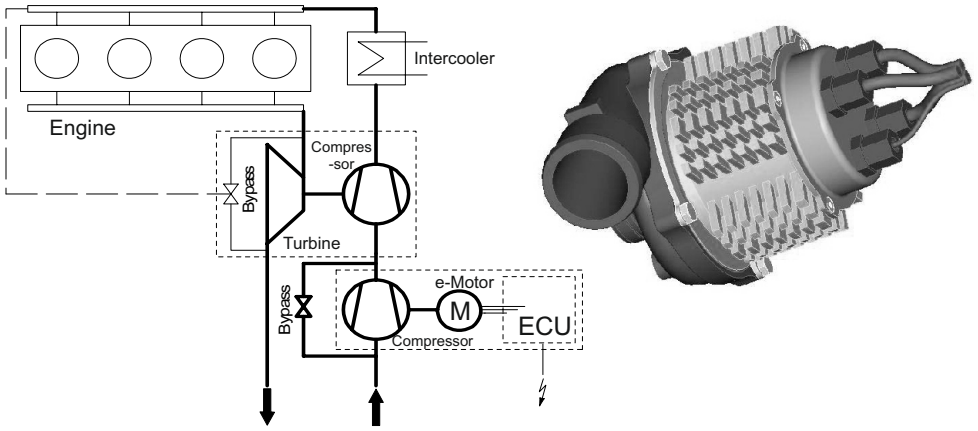

Figure 2.36: eBooster charging system [247].

The eBooster is completely independent from the turbocharger and the thermal energy of the exhaust gases. Thermomechanical loads are relatively low and there is no way to utilize an energy recovery system due to the separation of the turbine and the electric motor. Depending on the amount of

electrical energy available from the vehicle architecture, it can be used at low engine speeds as a regulated two-stage compression system to increase the steady state torque, or only in transient operating phases to reduce turbo lag effects. Due to these conditions, maximum pressure ratio is around 1.5 and maximum operating speed below 100000 rpm.

When the eBooster is inactive, no thermal loads are placed on the electric motor which is only subject to the engine compartment temperature. If the eBooster is used to improve transients, its operating time per activation is very short and the total amount of heat to be dissipated is small. Even operated various times like in city driving conditions, enough heat can be released into the air with an appropriately designed surface. In this case, ball bearings lubricated for their entire service life can withstand axial and radial loads and the connection to the oil supply is avoided. However if the eBooster is used to increase the steady state characteristics, its activation time is longer and a connection to the engine cooling system is required. In 1996, Page [254] presented the first electrical booster called "Turbopac" with a PM brushless electric motor. Motor characteristics (power, speed, etc...) were not provided but results obtained on a DDC heavy duty Diesel engine indicated the unit was capable of optimizing the AFR under low-end operating conditions, decreasing by 4-8% the specific fuel consumption and reducing by 30% particulate emissions at iso NO_x concentrations. Transient were also significantly improved with 30% reduction in turbo lag.

In 2000, Munz et al. [247] developed an eBooster rated at 2.5 kW with all power electronics integrated in. After comparing PM, SRM and ASM motors, they selected an ASM machine mainly for robustness purposes. Performing initial simulations on a gasoline engine under 60-100 km/h vehicle acceleration, they demonstrated that higher maximum electrical power gave higher acceleration as shown in figure 2.37. Nevertheless improvements were not lineal with the power level and smaller enhancement could be observed when the power exceeded 2.5 kW. In fact, a larger electric motor unproportionally increases the mass moment of inertia of the rotor. The output capacity is important but the ratio between the torque of the electric motor and the inertia of the rotor is the main factor with respect to system efficiency. Here, a small additional electric power of 1.8 kW allowed the vehicle to reach the final speed 0.6 second faster, while increasing the electrical power up to 8 kW resulted in marginal effects with only an additional gain of 0.1 second. Same conclusions were highlighted by Lefebvre et al. [217] simulating transient response of a small 3-cylinder 1l

turbocharged gasoline engine equipped with a similar eBooster to replace a naturally aspirated 1.8l engine. For their application, they considered 1.6 kW was the best compromise between power level and performance enhancement. With that power, they could obtain 32% reduction in response time and 47% improvement in low end torque. Furthermore, they showed the eBooster had also a positive effect on the main compressor behavior. By increasing the mass flow, the operating points were displaced in the main compressor map toward areas of better efficiency and higher surge margin which was beneficial for both the main compressor and engine performance.

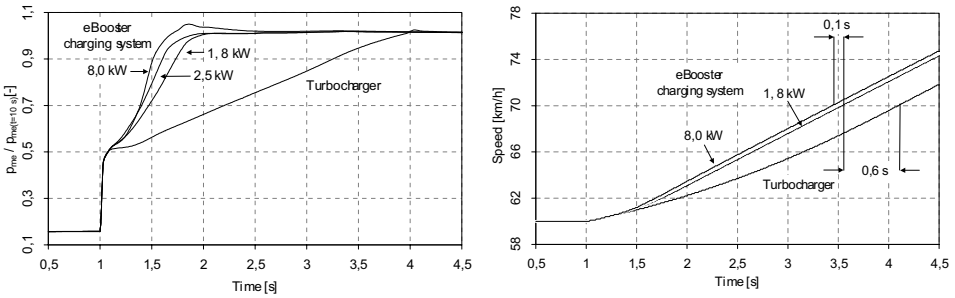

Figure 2.37: 60-100 km/h vehicle acceleration performance for different eBooster power ratings [150].

Under test bench evaluation, Munz et al. [150] reported the eBooster was able to reach a speed of 70000 rpm in 0.5 second starting from idle. Under these conditions, power consumption exceeded by 0.3 kW the rated power with maximum battery current output up to 200A. As explained by Kattwinkel et al. [182], due to these high current levels and the relatively large number of charge-discharge cycles, this energy flux cannot be fulfilled by conventional battery-generator system and high energy storage devices such as double layer capacitors (UltraCaps or SuperCaps) must be used. These devices bring additional constraints on the vehicle electrical system and power management become critical especially in small and mid passenger cars. Trying to overcome these issues, Pallotti et al. [126, 255] mounted a big alternator with a high-currents battery on a 1.4l gasoline engine equipped with an eBooster, and developed optimal strategies to limit the battery discharge at a safety point. Despite the eBooster was operated only during full load accelerations, they pointed out engine performance had to be degraded when consecutive accelerations are demanded for a long time or when important electrical loads were consumed by the other vehicle accessories (fans, air conditioning, light,

etc. . .). To provide additional electrical power and limit drops in performance, news functions like regenerative power are therefore recommended to be implemented in conjunction with. But these functions also require double layers capacitors with the respective electrical constraints that involve.

Fieweger et al. [106] compared an eBooster and an electrically assisted turbo with the same 2.5 kW electric power level on a 6-cylinder HSDI Diesel engine. They reported the eBooster response was determined in a first phase by the leakage and the closing duration of the bypass valve, and then by the power used for air compression and no longer available for compressor acceleration. The eBooster is not supported by turbine power but, during a load step at 1000 rpm when there is not much exhaust gas energy, results showed the eBooster had better performance than the EAT system due to its lower mass moment of inertia. The eBooster only needs to accelerate the compressor wheel and the electric rotor, while the EAT system had to accelerate in addition the turbine wheel with a comparatively high density and high mass moment of inertia. Munz et al. [150] evaluated a difference of 30% in power consumption to obtain the same rotor acceleration between both systems. Furthermore at 1000 rpm, the eBooster was not restricted by surging and was operating in a compressor map region of better efficiencies. At 1500 rpm, the situation was inversed with the EAT system showing more improvement potential during the load step than the eBooster. The power needed by the eBooster to compress the air to a certain pressure ratio is proportional to the mass flow and increase with engine speeds. Using a certain electric power, the acceleration process is thus limited at higher speeds by the power consumed by the air compression. The EAT system do not have this limitation as the air compression energy is provided by the turbine.

In 2011, Dynamic Boosting System Ltd. [95, 336] especially designed for electric chargers a novel low speed compressor based on the TurboClaw technology, see figure 2.38. The TurboClaw technology is a shrouded forward-swept blade profile which operates at much lower rotor tip speeds than conventional radial compressors. This design showed great potential to reduce the constraints on the electrical system reducing the electrical power needed in transients operations to accelerate the compressor. Unfortunately, no system characteristics data was provided by the authors.

Figure 2.38: TurboClaw compressor [95].

2.5 Centrifugal Compressor Performance Enhancement

Compressors require wide flow range and high efficiency to increase the performance of two-stage architectures, or in another way to avoid the complexity of multi-stage system when boosting requirements are only slightly higher than single-stage system performance. The operating range of a compressor is limited by surge at low flow rates and choke at high flow rates. In this section, different techniques are presented to enlarge the compressor operating range and to improve its matching with variable geometry turbine.

2.5.1 Pre-Whirl Generators

The first technique proposed is the introduction of pre-whirl at impeller inlet as shown in figure 2.39. In fact, there are two situations where the flow towards the compressor wheel might not be ideal. At low engine speeds, the compressor impeller speed is too high in relation to the air flow velocity, so the incidence angle of the blade tip is away from the design point. Adding pre-whirl in the rotational direction of the impeller (positive pre-whirl) can help to avoid flow separation and to increase the surge margin. At very high engine speeds and mass flow rates, the incidence angle is not optimum because the compressor wheel is spinning too slowly compared with the inlet flow speed. Negative pre-whirl (i.e. against the direction of the impeller) is then used

to improve the flow angle towards the impeller and increase the choke limit [111]. Imposing pre-rotation into the incoming air at the compressor inlet can be done aerodynamically by injecting air at some oblique angle [207, 329] but as pneumatic energy is not common in automotive applications, guide vanes are generally preferred.

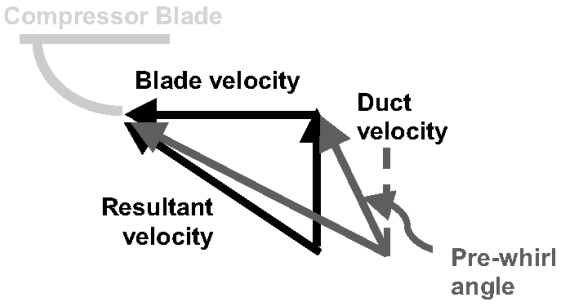

Figure 2.39: Pre-whirl effect on compressor inlet velocity and surge line [111].

In 1975, Whitefield et al. [360] investigated the application of inlet swirl for small radial turbochargers giving a theoretical and experimental comparison of different types of pre-whirl systems. The results show a significant extension of the surge and choke limits with $\pm 20°$ pre-whirl angle. The peak efficiency dropped when applying negative whirl but stayed almost constant with positive whirl. Similar studies were conducted for small gas turbines by Rodgers et al. [281, 282] and for process compressors by Simon at al [305] and Williams [363]. All the authors pointed out that the surge limit can be extended with positive pre-whirl, but a special attention had to be paid to the design of the diffuser and compressor wheel to improve even further efficiencies and operating range. To make mention of their works, Rodgers obtained a significant shift of the surge line to reduced flow rates with 40^o positive swirl angle as shown in figure 2.40, while the surge line was moved to high flow rates when negative swirl was applied. Williams reached similar beneficial shift of the surge line but, as he was working with lower compression ratios (1.7:1), had to apply swirl angles of up to $60°$.

With compressor wheel optimization in mind, Whitefield et al. [356, 357] manufactured in 1993 a special impeller to take full advantage of a positive pre-whirl of $25°$. The impeller backsweep was only $7°$and the inducer blade angle at the tip was selected as $-50°$to correspond with the minimum relative Mach number. Results showed that efficiencies were maintained quite constant up to

+20°pre-whirl angle, but dropped by 2% with +40°of pre-whirl. The extension of the surge margin was small but the pressure ratio was significantly higher for a given turbo speed. To maintain the compressor stage efficiency, different whirl devices incorporating straight or cambered vanes were used. Inlet devices with straight vanes do not generate swirl at full opening position but are inefficient to give large swirl angles. On the contrary, cambered guide vanes are designed to generate a specific swirl angle but cannot provide zero swirl at high flow rates to limit pressure losses. To resolve this conflict, Whitefield et al. [355] designed a variable geometry volute swirl generator based on a radial inflow turbine volute as it can be observed in figure 2.40. Their variable geometry concept was relatively simple with few moving parts. The volute flow could be reduced to zero as the core flow was increased but the maximum mean swirl obtained was only in the order of 15°. Despite this low pre-rotation level, they obtained a 33% surge line improvement with limited efficiency and pressure ratio decreases at low flow rates, while compressor performance was maintained at high flow rates avoiding large impeller incidence angles and flow separation.

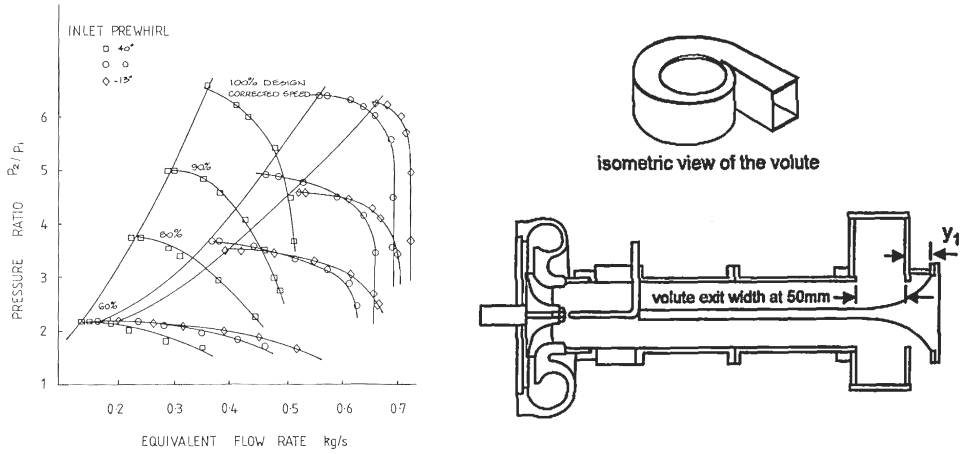

Figure 2.40: Left: pre-whirl effect on surge line [359] - Right: variable volute swirl generator [355].

These results were of particular interest because they also demonstrated the possibility to improve the surge margin and compressor efficiency despite a 90° oriented connection near the compressor inlet. In fact, due to packaging constraints dictated by crash planes, pedestrian protection areas, vehicle styling, vehicle chassis components, etc... ideal straight compressor inlet

pipe arrangements are difficult to implement in the engine compartment and 90° bends at the compressor inlet are generally imposed. As a consequence, flow non uniformity is frequently generated at the impeller inlet and compressor performances are significantly reduced [67]. Analyzing the influences of a 90°bend at the impeller inlet, Kim et al. [188] showed with experimental measurements that boundary layer separations can decrease head coefficient and efficiency up to 10%, while Kindl et al. [190] observed with CFD calculation surge line degradation of around 30%. Both attribute these results to the presence of a pressure gradient developed in curve ducts between the inner and the outer walls depending on the bend geometry and Reynolds number, and the presence of a secondary flow at the compressor tip inlet unfavorable for the compressor performance and causing the efficiency degradation. To reduce the secondary flow and lessen the degree of the pressure gradient in the radial direction, they optimized the bend curvature and inserted vanes inside the pipe as observed in figure 2.41. Their analysis showed the inner radius should be as large as possible to increase the uniformity index and there is a tradeoff for the number of vanes between pressure losses and uniformity index. With this new design, they could recover the surge behavior obtained with a straight pipe but pressure losses were still consequent, especially at high flow rates, and only part of the efficiency degradation could be recovered.

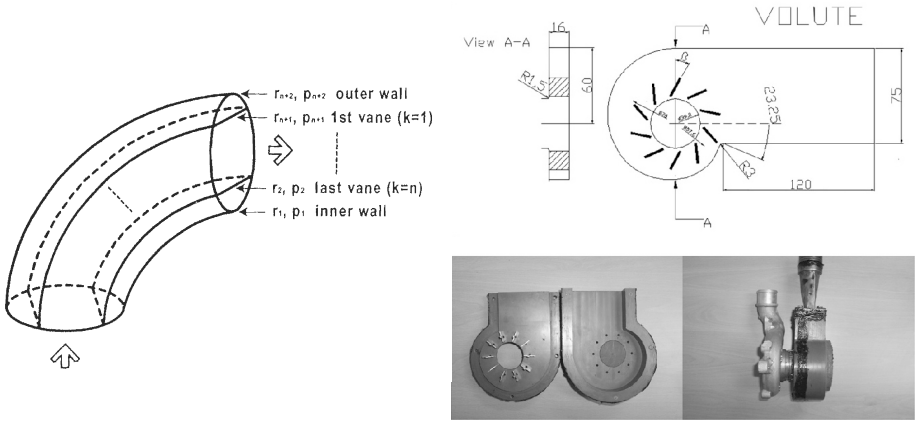

Figure 2.41: Left: 90° bend pipe with vanes [188] - Right: geometry of the swirl generator [121].

Going further with the packaging constraint previously mentioned to improve the surge line and compressor efficiency, Kindl et al. [190] and Galindo et al. [121] designed a similar device to one proposed by Whitefield et al. [355]

but with higher aerodynamic sophistication. Using CFD calculations, the volute geometry was optimized to reach the lowest pressure drop and maximum swirl level, whereas directional blades were employed as shown in figure 2.41 instead of a moving center body. The swirl level obtained with their device is practically independent of the mass flow and varies from negative values of -20° to positive values of 60°. One interesting conclusion they pointed out during their studies is the negative pre-whirl setting had higher potential to increase the surge margin than the positive pre-whirl setting. This conclusion is in contrast to the previous studies [281, 282, 305, 355, 356, 357, 360, 363] where it was demonstrated the surge limit is improved when the pre-whirl has the same direction as the compressor wheel. To explain this different behavior, the authors paid special attention to the flow distribution imposed by the radial inlet and centripetal vanes of the swirl generator, with low velocities at the center and high velocities at the periphery of the compressor inducer. Surge instabilities always start to appear at the periphery of the inducer. Increasing the axial velocity at the leading edge of the impeller with higher relative velocities allow thus to stabilize the flow in the compressor and to delay the apparition of surge phenomena. With this device, they observed a 25% surge line improvement but with still important pressure losses when the blades are relatively closed. They therefore recommend incorporating a variable actuation mechanism to get the full potential of the swirl generator for active control of the compressor performance.

Several studies are present in the literature to develop variable actuation mechanism for swirl generators. In the last example [121], despite the fact that it would be easy to design a mechanism equivalent to those used for moving the stator blades in variable centripetal turbines, most of the investigations have been centered in the development of variable axial inlet guide vanes (VAIGV) [86, 111, 144, 318, 329, 374]. VAIGV has generally a series of flat plate vanes with a cylindrical section passage as shown in figure 2.42. The vanes are pivotally mounted within the guide vane housing and setting angles can vary from -90° to +90° to induce a controlled pre-whirl by means of external linkage.

In 1999, Uchida et al. [165] presented an experimental study with VAIGV for small passenger car engines. Various VAIGV designs were investigated with in some cases the presence of a hub body. They showed that a shift by up to 15% of the surge line to smaller flow rates could be reached using positive inlet pre-swirl but a compromise had to be found for the hub body design. In fact, for small VAIGV angles, the hub body leads to decreased

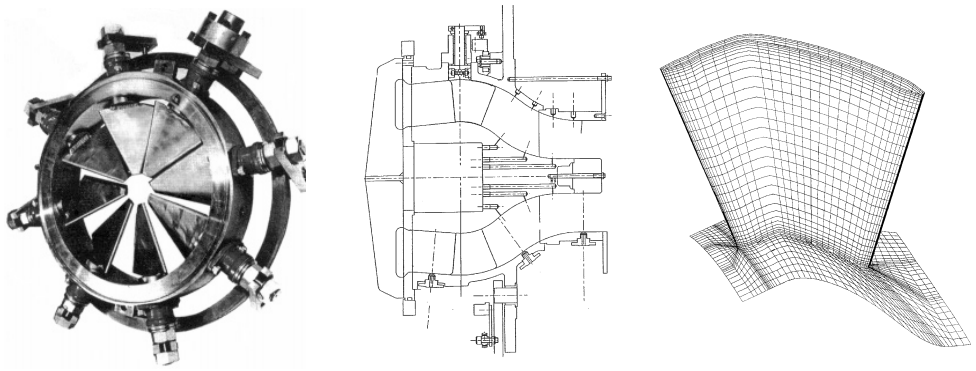

Figure 2.42: Left: VAIGV with cylindrical section passage - Middle: VAIGV with spherical section and hub body - Right: tandem vane design at setting angle of +60º [86].

stage efficiencies due to additional friction losses, while for larger VAIGV angles, a positive influence of the hub body is observed. From these results, Coppinger et al. [86] optimize the VAIGV design with a combination of numerical and experimental techniques, considering the components in isolation rather than as part of the overall centrifugal compressor. They observed the type of VAIGV proposed by Uchida et al. [165] performed more as an inlet throttle than an efficient swirl-inducing device and could be improved aerodynamically. They thus started to minimize blade clearances using a spherical surface hub and shroud profile in conjunction with circular inner and outer vane profiles as it can be seen in figure 2.42. They suggested that an ideal system would possess hub geometries with high radius ratio and low area ratio. With this design using spherical section passage, marked improvement in performance over the original cylindrical passage had been realized and the authors considered possible further increases in efficiency by focusing on the blade design. So then, they proposed the use of flat plate tandem vanes (figure 2.42) to minimize separation on the section surface of the vanes and to reduce the associated pressure losses. The advantage of this type of vanes is low incidence is achieved at all setting angles since the leading section of the vane remains in fixed alignment with the axial inlet flow, while the trailing section pivots about its leading edge. Results obtained with these tandem vanes showed a clear improvement in aerodynamic performance as separation pocket on the suction surface had almost entirely been eliminated. Nevertheless this design adds lot of complexity to the variable actuation mechanism

and its implementation is more favorable for process compressor than for small turbochargers.

To improve the VAIGV design proposed by Uchida et al. [165], more detailed analysis of the flow field behind the VAIGV was performed. Herbst et al. [144] indicated that the circumferential component of the flow velocity increases linearly with increasing radius as shown in figure 2.43, and the VAIGV setting generates a solid-body vortex. The solid-body vortex turns into a Rankine vortex caused by the high velocity at the shroud and a potential vortex is formed at a certain radius in the outer region. The vortex generation leads to an increase of the losses caused by flow separation and dissipation in the VAIGV. With CFD calculations, Xiao et al. [374] characterized flow separations in the guide vane passages under large flow conditions and located back flow regions at the front of suction surfaces of the splitter blades. Moreover, they showed that a couple of counter-rotating vortices exist in the wake of each blade within wide flow range. Mohtar et al. [239] performed measurements with Laser Doppler Anemometry to describe as well non symmetric flows and velocities distribution at different distances downstream the VAIGV. They demonstrated these flow instabilities counts for an important part of the overall system performance, and compressor pressure ratio as efficiency could be decreased by up to 3.14% and 14.5% (for respectively 30° and 60° setting angles) without a strong flow pattern optimization at the VAIGV outlet.

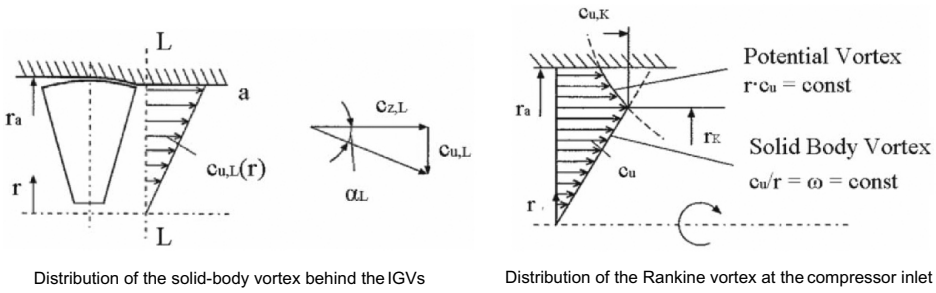

Figure 2.43: Left: velocities distribution downstream the VAIGV [144].

To simplify the variable actuation mechanism, other VAIGV design based on material resilience properties were also investigated. Fraser at al [111] developed for example a pre-whirl generator with flexible guide vanes which are adjusted actively by an external mechanism, see figure 2.44. The compensation of vane length is managed by the vane material which is stretched in

axial and radial directions when twisted. BMW has simplified even more the device by designing a swirl generator able to change its pre-rotation angle in function of the air mass flow without any actuation mechanism (figure 2.44). The swirl generator is based on the efficient tandem vane design proposed by Coppinger et al. [86] and pre-rotation angle arrangement is automatically adapted to the flow conditions through the convenient resilience of the selected material. At low mass flow rate, the supple trailing sections experiment few distortions generating a important positive whirl level, while at high flow rate, the aerodynamics forces bend the trailing sections in a straight position limiting the swirl angle and reducing the pressure losses. These devices are quite simple and more economical than the VAIGV concepts previously described but the material selection is quite challenging for this type of application. In fact, being quite close to the compressor inlet, they are exposed to hot reverse flows associated with sometimes airborne lubricating oil. In these difficult environmental conditions, most of polymers cannot reach an acceptable useful lifespan.

Figure 2.44: Left and middle: pre-whirl generator proposed by Fraser at al [111] - Right: BMW pre-whirl generator.

In terms of engine performance, Fraser et al. [111] conducted experimental tests at full load on a 1.8l turbocharged gasoline engine with their pre-whirl generator installed at the compressor inlet. Due to a relatively big turbine swallowing capacity, no significant differences were visible up to 1700 rpm. But at higher engine speeds, they could achieve a 6.4% increase of maximum torque applying 45° positive pre-whirl. At 5900 rpm and peak power, the turbo speed was reduced by approximately 6000 rpm (3.8%) when changing from 0° to 45° negative pre-whirl maintaining the boost pressure requirement. These results have a special interest when the compressor is operating close

to its maximum speed (choke line). However at the same time the compressor efficiency is reduced, increasing compressor outlet temperature and turbine energy requirement to maintain the same full load performance. This reduction in compressor efficiency could be minimized if the pressure drop across the pre-whirl device is decreased at high mass airflows and large pre-whirl angles.

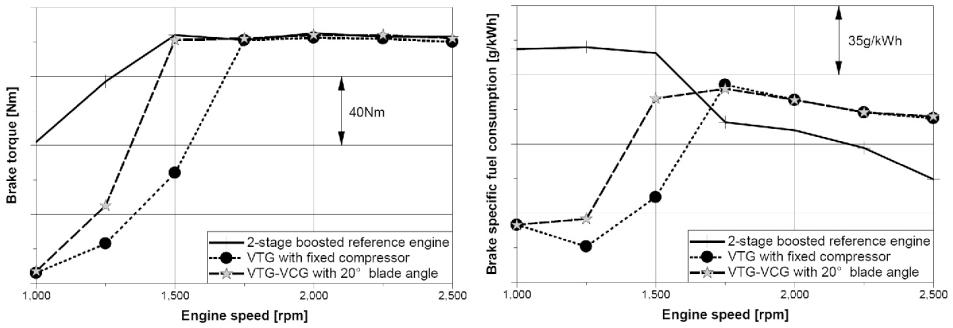

Figure 2.45: Comparison of brake torque and brake specific fuel consumption at full load [144].

Herbst et al. [144] compared, on a 1.4l direct injection gasoline engine, the low-end-performance obtained with three different boosting systems: a two-stage system consisting of a mechanical compressor and a turbocharger with wastegate, a single stage system with a variable geometry turbine, and a single stage system with pre-whirl generator and a smaller VGT equipped with an additional external wastegate. With pre-whirl generator, a smaller turbine swallowing capacity is needed to produce sufficient power at low engine speeds. Moreover, additional external wastegate can be required despite the availability of the VGT to achieve the reference nominal power, since its effective cross sectional area can be too small for the resulting exhaust gas mass flow. They obtained as a result significant low end torque improvements with the pre-whirl generator configuration, corresponding to pressure ratio increase of 20% at 1250 rpm and 48% at 1500 rpm, see figure 2.45. Compared with the two-stage system which requires more power to drive the mechanical compressor at very low speeds, a benefit in fuel consumption of 6% is observed at 1500 rpm with identical brake torque. The pre-whirl generator configuration offers therefore a great potential to improve the low end performance with single stage charging. At higher engine speeds, fuel penalties occurred with the use of VGT turbines which have more restricted exhaust temperature limits (950°C for VGT while 1050°C for FGT + wastegate) and force to lower

the AFR by higher injection rates. In transient conditions, Toussaint et al. [329] investigated the effect of pre swirl on a 2.0l gasoline engine to reduce the turbo-lag. Using different pre-whirl generators, they observed significant improvement in the acceleration time with up to 26% decrease in turbo-lag.

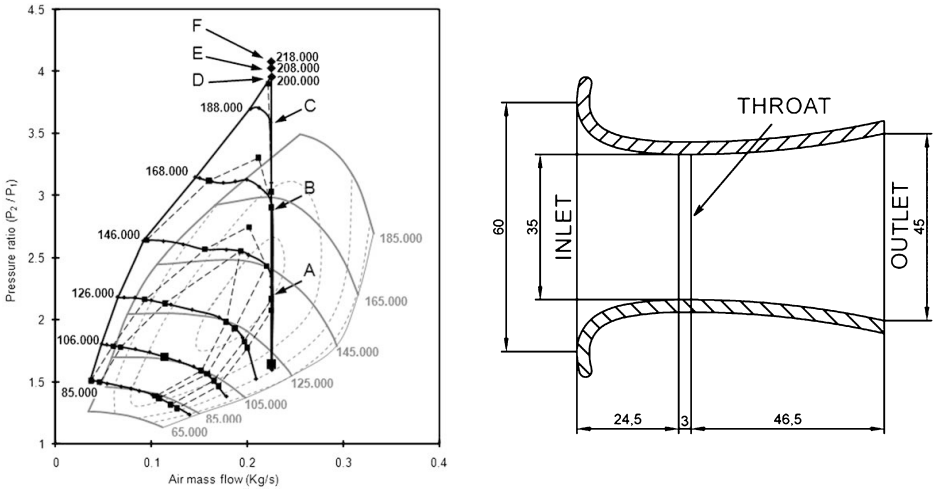

Figure 2.46: Left: effect of the nozzle on compressor map - Right: nozzle sketch [94].

Limited by racing championship regulations, Desantes et al. [94] replaced the swirl generator by a nozzle, keeping the same principle of modifying the flow pattern at the compressor inlet, to improve the performance of a racing Diesel engine. The nozzle profile shown in figure 2.46 has been designed with a convergent-divergent shape by means of Hermite polynomials to minimize the losses. Hermite polynomials describe the trajectory between two points with the lowest curvature for given initial and final direction conditions. The nozzle was thus optimized by searching the best combination between curvature and length. Using the nozzle, they obtained interesting results with a 30% improvement of the surge line associated to a significant shift of the iso-speed lines to higher pressure ratios in the region of low mass flow rates (figure 2.46). Moreover, the compressor efficiency is kept close to its original values in a wide operating range until sonic conditions are reached in the nozzle. This better compressor behavior at low flow rates enabled the engine to be highly boosted at low engine speeds, improving therefore low end torque and acceleration time. Nevertheless to get the full potential of this device, the authors recommend the incorporation of a variable effective area mechanism for active control.

2.5.2 Casing Treatments

The second technique employed to enlarge the compressor operating range is the casing treatment, also called map width enhancement system. This technique consists of an internal bleed system around the compressor shroud, which connects a zone downstream the inducer throat with the impeller inlet through slots and a secondary inlet pipe, see figure 2.47.

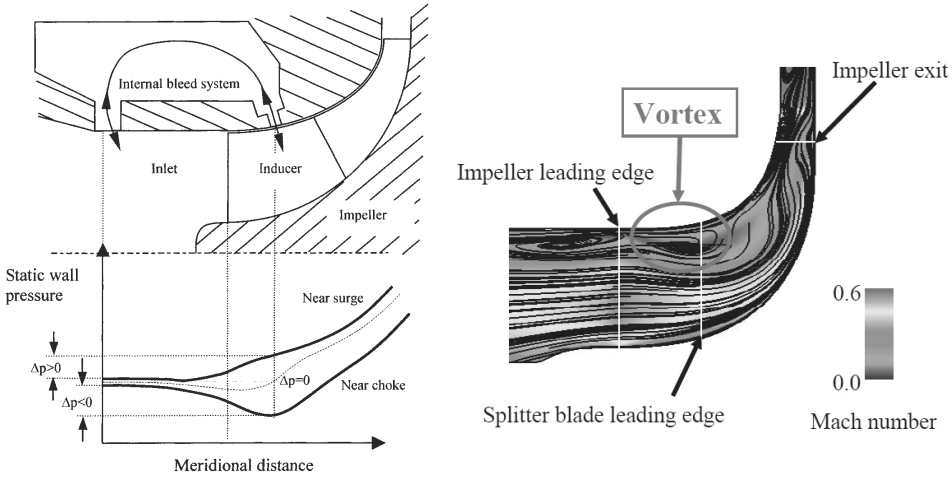

Figure 2.47: Left: casing treatment and basic force driving the recirculating flow [163] - Right: vortex in the impeller flow path at the surge flow rate [332].

In operating points near surge, a vortex is generated in the inducer. This vortex can be extended until the impeller exit and represents the flow instabilities which will initiate the surge phenomena. To improve the surge margin, the idea of the casing treatment is to suck this vortex to suppress the onset of compressor stall. The slots are therefore positioned to force some parts of the fluid entering the impeller to recirculate at the compressor inlet due to the pressure difference existing between the downstream and upstream slot. As a result, the stage characteristic is more stable and surge is delayed. At near choke operating points, on the other hand, the pressure difference between the two slots is negative and fluid is sucked into the impeller bypassing the inducer inlet. This additional air mass flow into the compressor allows to improve the choke line. Between these two operating points, conditions occur with no pressure differences between the upstream and the downstream slots. Under these conditions, stationary flows will be present in the bleed system leading to no improvement in compressor behavior.

Numbers of alternative casing treatments were proposed in the late 70's - early 80´s [73, 168, 227] for centrifugal compressors, but in 1988 Fisher et al. [108] was one of the first to presented a map width enhancement scheme for turbocharger applications. With their bleed slot concept, they experimentally showed the surge line could be moved to lower flow rates by 70% and the choke flow increased by 9%. Following the conclusions obtained by Fisher et al. [108], Hunziker et al. [163] performed CFD calculations to improve the bleed system geometry for a high performance compressor designed to deliver a pressure ratio of 4.2. Analyzing velocities pattern in the inducer, they observed the flow entering the bleed system through the downstream slot had a large circumferential component due to the work done on the fluid by the impeller blades. This generated a considerable amount of positive pre-swirl when the flow re-entered at the impeller inlet. The bleed system improved therefore the surge line combining pre-swirl and higher flow rate at the leading edge which, as previously mentioned, allow the inducer tip incidence to be reduced and flow separation downstream the inducer throat to be delayed. After various modifications of the bleed system geometry, they observed in their high pressure ratio compressor an 18% improvement of the surge line with slightly higher efficiencies.

Nikpour [250] studied both VAIGV and casing treatment to improve the surge line of heavy duty turbochargers. During these investigations, he could measure with the casing treatment system a shift of the surge line by 15% to lower mass flows maintaining the same compressor efficiencies. With the VAIGV, even more important benefits were observed for the surge line (around 25%). Nevertheless, the gain resulting from the action of the VAIGV is always accompanied by a pressure drop which can be quite significant at high pre-whirl setting. In this case with 35°vane setting angle, he noticed a drop of 15% in pressure ratio. To go further with these results and trying to get the benefits of both systems, he carried out some tests by installing the VAIGV unit in front of the map width enhancement system (MWE). This system's performance was poor because the air flowing back from the bleed slot generated lot of interactions with the in-coming main air through the VAIGV assembly. Therefore, he designed an alternative system to channel the MWE flow upstream of the VAIGV system as shown in figure 2.48. The disturbances were in that way further upstream and the flow at the impeller inlet was more uniform. Testing this arrangement, he could observe a gain in surge margin of up to 35% despite a significant drop in the pressure ratio capability due to the 45°vane setting angle. Positioning the inlet guide vane to 0°, the benefit

was reduced to 20% which still corresponds to 5% more when compared with the standard MWE system.

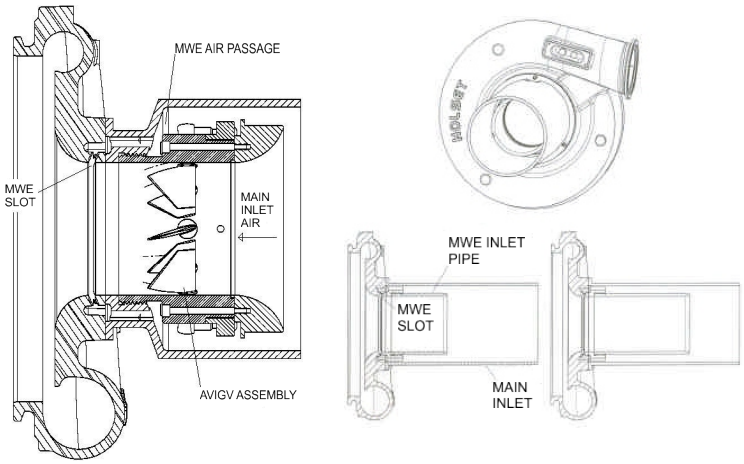

Figure 2.48: Left: combined VAIGV and MWE system at the compressor inlet - Right: MWE passage length variations [250].

A longer MWE passage length presents thus a certain potential to increase the surge line. Nikpour [250] continued his investigations removing the VAIGV and analyzing different MWE passage lengths as it can be observed in the figure 2.48. Testing theses geometries, he showed that increasing the MWE inlet pipe length resulted in proportional benefits to surge margin until reaching a 14% improvement with his compressor, after what the trend decreased for longer pipes and efficiencies dropped by around 2%. A compromise has therefore to be found between the level of surge margin improvement, package size increase and efficiency diminution. Nevertheless, he demonstrated that a moderate increase of inlet pipe length can bring a 12% shift of the surge line with only 1% drop in efficiency. Mohtar et al. [240] arrive to the same conclusions optimizing a particular casing treatment design. Their design was composed of a plurality of holes to connect the inducer to the bleed system instead of using different slots. In their first system, the flow coming back from the MWE holes and remixing with the main flow caused lot of disturbance at the compressor inlet. Surge line and efficiencies were even degraded when compared with the basic compressor characteristics. To suppress this disturbance, they mounted a long MWE passage which in combination to the bleed system showed a shift of the surge line by 40%. The efficiency was nearly conserved at low flow rates while decreased at high flow rates due to friction losses. Viewing

theses results, the authors recommended the use of a variable geometry MWE system to improve the surge margin without sacrificing compressor efficiency. The system would be able to open the bleed system at low air mass flow and close it at high flow rate to limit friction losses in the MWE passage.

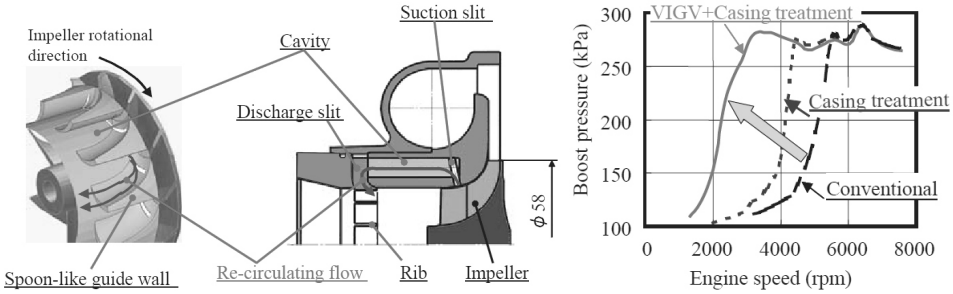

Figure 2.49: Left: casing treatment geometry [332] - Right: VAIGV and casing treatment effect on boost pressure [330].

Long MWE passage can be problematical for some applications due to strong packaging constraints. To limit the required length at the compressor inlet, Uchida et al. [166, 330, 332] proposed a sophisticated casing treatment design associated with a VAIGV. As shown in figure 2.49, the casing treatment consisted of six cavities enclosed by a spoon-like guide wall to smoothly change the velocity of the recirculating flow from the circumferential to the axial direction. Moreover, radial ribs were arranged at the discharge slit to diminish the tangential velocity component of the recirculating flow. In comparison to the Nikpour [250] design, disturbances were significantly reduced and synergy effects between casing treatment and VAIGV could be exploited. Uchida et al. [166, 330, 332] investigated first each system individually. While a 15% reduction in the surge flow rate was observed with the VAIGV alone, a 30% improvement was reported with the casing treatment. Then, combining both systems to optimize the control of the reverse flow at the tip clearance, they showed a significant 59% increase in the surge margin. At low flow rates, the pressure losses increased rapidly due to important VAIGV setting angles but thanks to the improvement in the flow caused by the pre-whirl of both systems, the compressor efficiencies could be maintained. When applied to a high power density gasoline engine, the boost pressure at low engine speeds and the corresponding low end torque were significantly improved (figure 2.49).

2.5.3 Variable Geometry Diffusers

Finally, the third technique used to widen the compressor operating range is the variable geometry diffuser. Compressor surge or choke can occur at the diffuser area. Improving the air flow downstream the impeller by diffuser design optimization is thus an effective way to extend the operating range and increase the efficiency. Vaneless diffuser is widely used in automotive turbochargers because its large capacity at choke offers a broad operating range. Whereas the vaned diffuser is used for marine or stationary power plant turbochargers due to important pressure recovery at the diffuser. This brings high efficiency around the design point but at the cost of a narrower range [319]. An example of compressor performance with the vaneless and the vaned diffuser is shown in figure 2.50.

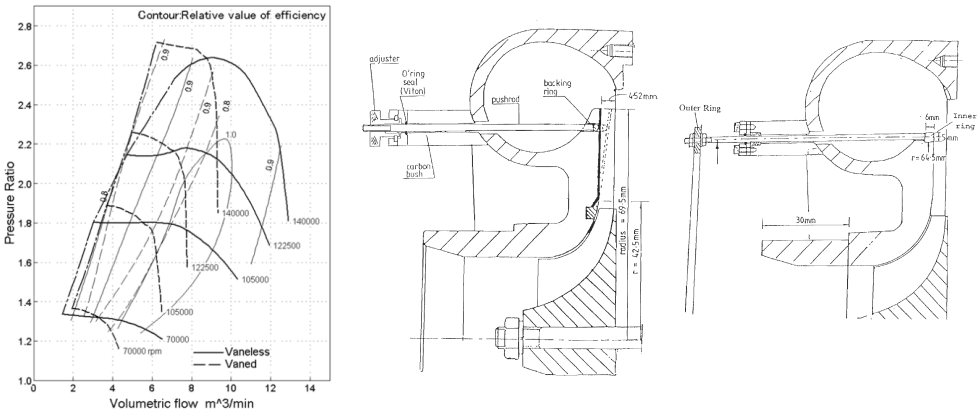

Figure 2.50: Left: performance comparison between vaneless and vaned diffuser [319] - Middle: diffuser flexing shroud wall - Right: diffuser with sliding throttle rings [359].

Whitfield et al. [361] was one of the first to simulate the application of a variable vaneless diffuser by the introduction of a series of alternative wall plates in the diffuser. In that way, he could illustrate the potential of the technique by moving the peak pressure ratio to lower flow rate and providing a large stable operating condition. This approach was then investigated by Abdel-Hamid [10, 11, 12] and Sutton et al. [358] which employed two methods to simulate the variation of the diffuser geometry: flexing shroud wall and sliding throttle rings, see figure 2.50. They showed with their experimental measurements a reduction of approximately 40% in the mass flow rate at

which the peak pressure ratio occurred, while the isentropic efficiency was maintained quite constant. Whitfield et al. [359] measured, on a 6-cylinder 11.2l truck engine, power and torque performance obtained with both methods. They reported significant improvement in BMEP in the whole engine operating range, recommending the use of the sliding rings for its mechanical simplicity and higher efficiency. Indeed, they demonstrated the flexible diffuser wall had a lower aerodynamic performance and the mechanical integrity of the polymer disc could be quite challenging.

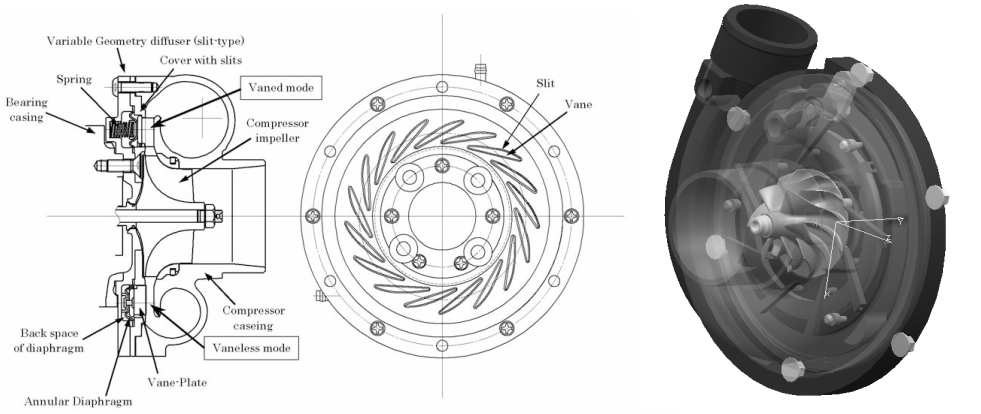

Figure 2.51: Left: variable geometry diffuser proposed by Tange et al. [319] - Right: variable geometry diffuser proposed by Arnold [24].

To obtain the good performance behavior of both vaned and vaneless diffusers, Tange et al. [319] proposed an interesting variable geometry design as it can be observed in figure 2.51. The variable geometry diffuser has two modes, the vaned and vaneless diffuser modes, by putting in and out the diffuser vanes at the diffuser passage from the hub side. The design is composed by an annular diaphragm which allows to move the vanes pneumatically. The vane-plate is tightened with the diaphragm and is driven through the cover with slits. There are some springs at the back side of the diaphragm to push the vane-plate to the shroud wall of the compressor casing.

Characterizing the compressor, they obviously noticed the vaneless mode had the same performance as the fixed geometry vaneless diffuser. Nevertheless due to slit clearances losses, the vaned mode suffered a 1.5% decrease in efficiency compared to its corresponding fixed geometry. But despite these losses, the vaned mode presented still at low flow rate advantage of 8% in efficiency and 5% in pressure ratio compared to the vaneless mode. In terms

of engine performance, simulations at full load on a 2l gasoline engine showed the vaned mode allowed an 11% higher boost pressure at low engine speeds, increasing the low end torque by 12% and decreasing the fuel consumption by 1.3%. Similar results are also showed on a 3l Diesel engine where a boost pressure increase of 4.8% and fuel benefits of 3.2% are obtained maintaining the injection fuel rate.

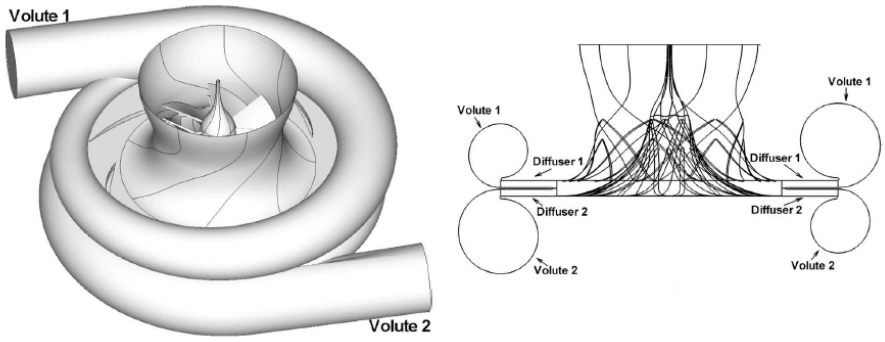

Figure 2.52: Dual volute design [174].

With the same philosophy to get benefits of both vaned and vaneless diffuser, Jiao et al. [173, 174] presented a dual volute concept for small turbocharger compressors as shown in figure 2.52. At the impeller outlet, the dual volute and the dual diffuser separates the compressor into two regions with different flow characteristics. The upper diffuser which is the closer to the shroud had vanes while the lower one (closer to the hub) was a vaneless diffuser. Analyzing the flow pattern with CFD calculations, they found the upper vaned diffuser ensures high performance at low flow rates because the guide vanes regulate the strong rotational flow. The lower vaneless diffuser ensures in the meantime large flow capacities because the radial velocity is higher at the lower section, and most of the flow passes through this diffuser at high mass flow. They thus observed the dual volute configuration provided a wider stable operating range associated with higher pressure ratio and efficiency. They also introduced the dual sequential volute concept closing one volute at low flow rate. The technique showed potential but further investigations are needed to improve the performance blocking for example the air flow at the diffuser inlet rather than at exit for reducing the loss of kinetic energy.

Variable geometry vaned diffusers were also developed in the recent year with mechanism equivalent to those used for moving the stator blades in vari-

able centripetal turbines [24, 331]. An example developed by Honeywell is shown in figure 2.51. The vane angle is adjusted for each compressor speed to control the flow separation in the diffuser and to minimize the mixing looses in the volute. This technology presents important advantages to enlarge the compressor operating range maintaining good efficiency. Nonetheless, the flow velocity at the impeller outlet is very high and changes in the flow characteristics are very sensitive to the diffuser vane angle. Moreover, as observed previously with the design proposed by Tange et al. [319], the performance of the compressor is highly dependent of the clearances between the stationary side walls and the variable diffuser vanes. As a consequence, variable geometry vaned diffusers have generally a higher efficiency at low flow rates and a lower efficiency at high flow rates than a conventional vaneless diffuser [331].

2.6 Energy Recovery: Turbocompounding

It has been shown in the last sections that downsizing techniques combined with advanced turbocharging technologies can significantly improve the overall engine performance. However in commercial applications, it exits another interesting technique to reduce fuel consumption which is the utilization of wasted exhaust energy. Modern engines still eject approximately 30-40% of fuel energy to the environment through the exhaust gas. Recovering a part of this wasted energy can therefore contribute to substantial improvement in engine efficiency. Four technologies have been developed in the last decades for exhaust heat recovery: mechanical turbocompounding, electrical turbocompounding, Rankine cycle heat recovery and thermoelectric generators. Using Peltier principles, thermoelectric generators convert directly exhaust gas heat to electric power, but their potential considering current thermoelectric material are rather limited [35, 206]. Rankine cycle systems employ steam (RC) or organic fluid (ORC) as working media to produce additional power through an expander (piston expander or turbine expander). Results reported by various investigators [96, 99, 218, 353] showed that a significant 8-12% reduction in fuel consumption could be obtained over a wide engine operating range. Nevertheless challenging issues such as complexity, size, weight, cost, durability, safety, etc... have still to be resolved to spread these systems in serial production. On the other hand, mechanical and electrical turbocompounding appear as a practical solution for heat recovery and present interesting potential, that is why both technologies will be further described in the following subsections.

2.6.1 Mechanical Turbocompounding

Mechanical turbocompounding consists of extracting energy from the exhaust gas stream by means of a mechanical link between the engine crankshaft and the exhaust-driven turbine. Different arrangements are possible. The main compounding schemes are shown in figure 2.53.

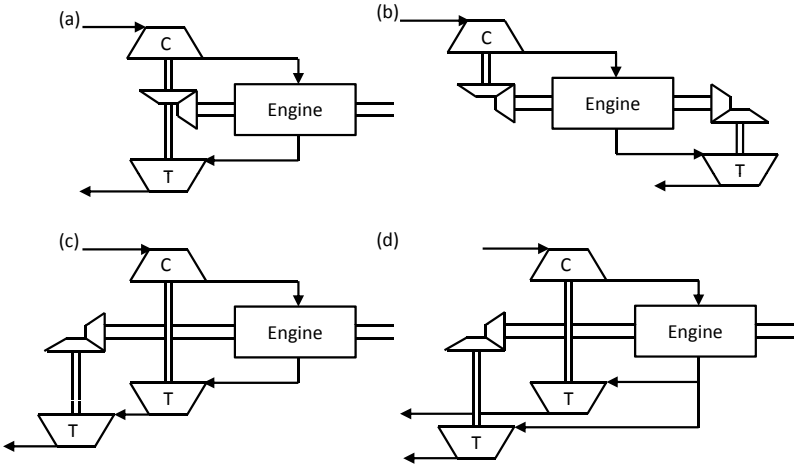

Figure 2.53: Turbocompound schemes: (a) direct coupled turbocharger - (b) separately coupled turbocharger - (c) separate power turbine with series arrangement - (d) separate power turbine with parallel arrangement.

Linking directly the engine and turbocharger shafts together offers some advantages in terms of packaging and supercharging capabilities, but requires a variable speed transmission to match the turbocharger and engine speeds over the whole engine operating range. This scheme called direct coupled turbocharger (figure 2.53a) was used in the 1950's by the Napier Nomad, one of the first compound engines designed for aircraft powerplants running long hours at constant high loads [285]. The Napier Nomad was a two-stroke 12-cylinder opposed-piston Diesel engine charged by an 8-stage axial compressor and a 3-stage axial turbine, see figure 2.54. The transmission was formed by a large and complex gear train with a Beyer continuously variable drive. The engine demonstrated excellent fuel consumption even if its design became rapidly obsolete by the intensive development of gas turbine engine for aeronautic propulsion. In 2010, Chadwell et al. [69] came back to this architecture with the last developments in efficient high speed planetary drives and CVT

[52] designing the VanDyne SuperTurbocharger. As already mentioned in the mechanical supercharger section, this system showed significant fuel consumption improvement over the NEDC cycle when mounted on a downsized 2.0l gasoline engine, but its cost and weight are still important issues for automotive series implementation.

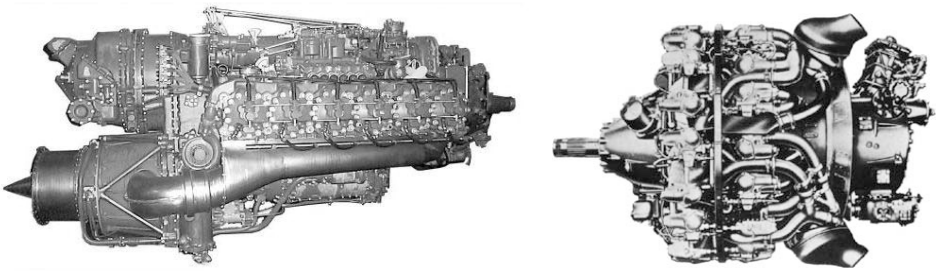

Figure 2.54: Napier Nomad (left) and Curtis Wright (right) compound aircraft engines.

The second scheme shown in figure 2.53b drives the compressor and turbine separately. This design is interesting when the compressor and turbine have different sizes and run at different speeds. In the 1950's, the Curtis Wright engine (figure 2.54), also designed for aircraft applications, used this architecture. The engine was charged by a single compressor while three turbines each one being supplied by two groups of three cylinders were connected to the crankshaft through gearing. At that time, this engine was considered as the most powerful piston engines achieving the highest power/weight ratios. Nevertheless, as the Napier Nomad engine, it was rapidly replaced by the gas turbine engine. In 1986, Klarhoefer et al. [191] studied the potential of positive displacement compressors and expanders in such arrangement. Theoretical benefits could be achieved at low speeds but high components efficiencies (well beyond what are currently available) were required.

Adding a series power turbine in the exhaust gas stream is the most common form of compound engine (figure 2.53c). The turbocharger is independent of the engine speed while the power turbine, dealing with a gas of lower density, rotates more slowly and allows a reduced transmission ratio. The power turbine adds mechanical energy to the crankshaft, but increases the engine exhaust backpressure and deteriorates the gas exchange process. The power turbine work has therefore to overcompensate for this deterioration. As power turbine output increases with engine speed and load, turbocompounding suits

better to highly-rated or high speed engines. Based on computer simulations for a compound 8l heavy duty Diesel engine, Wallace et al. [340] showed this trend reaching 6.5% improvement in engine efficiency with a 2-stage turbocharging system rated at 33 bar BMEP, while only 2.6% could be reached with a single stage turbocharging system rated at 20 bar.

For large Diesel engines, serial architectures can result in very large and expensive power turbines. In this case, parallel arrangements as shown in figure 2.53d are generally preferred. An advantage of parallel configuration is the power turbine can be shut off at low speeds and low loads reducing in that way parasitic losses. Furthermore, the proportion of mass flow that passes through the power turbine depends on the valve opening. As the power turbine mass flow and corresponding power output increase, fuel consumption decreases whereas turbine inlet pressure and temperature increase because more energy is required to drive the compressor. Pumping losses or thermomechanical limits determine thus the maximum power turbine flow [219]. For small or medium size engines, parallel architectures require small and high speed turbines which are less efficient than bigger machines. That is why, series arrangements are generally preferred in these cases.

Walsham [343] studied the effect of series turbocompounding on a typical heavy duty truck engine. As the two turbines run at different speeds and the ratio of their speeds change with engine speed, he described how the swallowing capacity of the turbocharger turbine is modified to behave as a small turbine at low mass flows and as a large one at high mass flows, see figure 2.55. In fact, at low mass flows the pressure drop across the power turbine is very small. The engine sees the true small turbocharger turbine size giving high boost pressure ratios. At higher engine speeds, the power turbine develops an appreciable expansion ratio which increases the exhaust pressure and gas density. As the pressure ratio in the turbocharger turbine stays approximately the same, the engine see now a big turbocharger turbine avoiding over boosting without any bypass or control. Comparing at full load the compound system with standard, wastegate and VGT turbochargers, Walsham reported the compound turbine could reduce the fuel consumption up to 5% over the standard turbocharger. Nevertheless in transient operations under acceleration from idle to rated speed, the compound system was less efficient than the wastegate and VGT turbochargers because its apparent turbine size increased as the airflow raised, while the others systems maintained their minimum turbine area until the required boost pressure was achieved (figure 2.55).

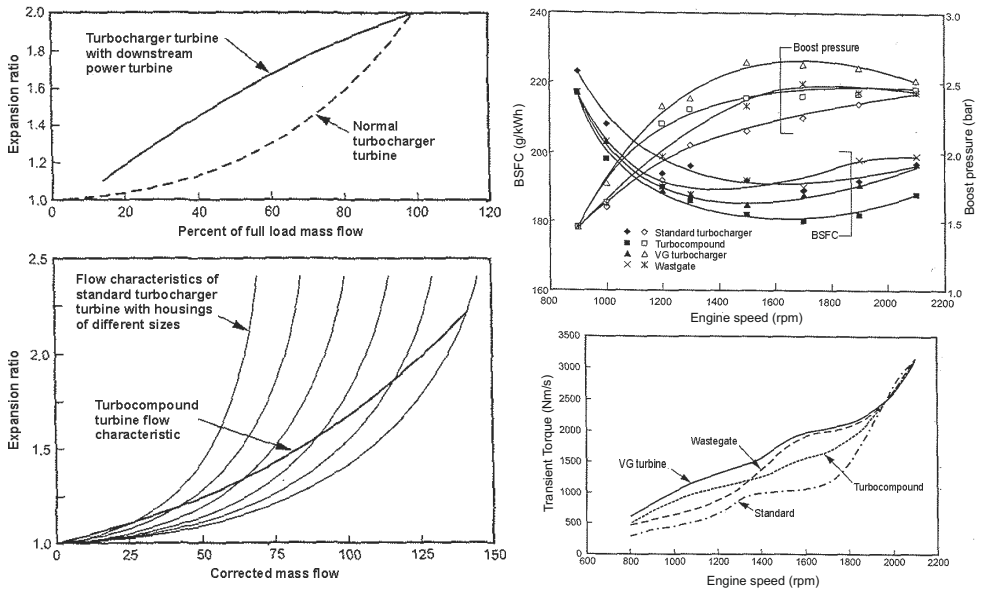

Figure 2.55: Left: effect of power turbine on flow characteristics - Right: comparison of boost pressure, fuel consumption and transient torque with various turbocharger configurations. [343].

Hountalas et al. [158, 159] arrived to the same conclusions from simulations performed on their 10.3l heavy-duty turbocompounded truck engine, obtaining at full load approximately 4.5% decrease of fuel consumption with constant turbine efficiencies (fixed at 80%). They also showed theses benefits were significantly reduced at part load operations and could even be negative under 25% load if the power turbine pressure ratio was not optimum, see figure 2.56. Considering the fuel economy obtained over the whole engine operating range, they concluded the overall optimum power turbine pressure ratio was in the range of 1.7-1.9, correlating in that way the investigations of Tennant et al. [321]. Their simulations were realized maintaining the fuelling rate. So despite turbocompounding affected in a negative way the net engine power due to higher pumping losses, they could obtain at full load up to 5% increase in total power through the work produced by the power turbine. At 25% load, the variation of total power was almost negligible. Higher pumping losses increase also the turbine inlet temperature which can be an important issue for turbocharged Diesel engine running generally close to the maximum thermomechanical limits at full load. As Wallace et al. [340], they observed

the exhaust temperature varied linearly with power turbine pressure ratio achieving an increase of around 50-70°C under the optimum pressure ratio (1.7-1.9).

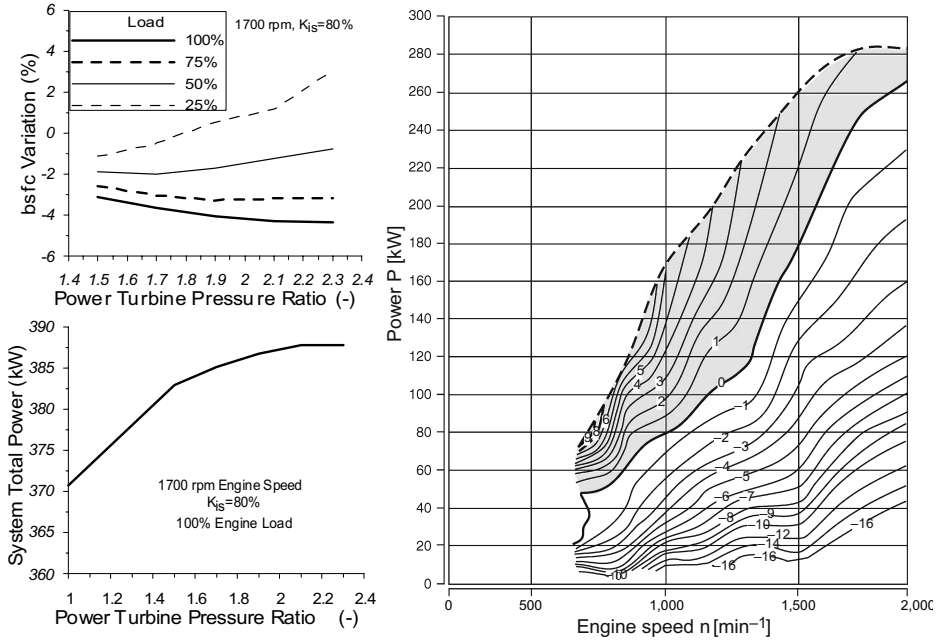

Figure 2.56: Left: fuel consumption variation and total power vs power turbine pressure ratio for various engine loads [159] - Right: fuel economy enhancement of a compound truck engine over its whole operating range [146].

The gear ratio of the power turbine is optimized to give the best performance at rated speed and load. Considering constant turbine efficiencies under part load conditions result therefore in optimistic conclusions regarding fuel economy potential. At part loads, the exhaust gas pressure and temperature are relatively small while the power turbine speed remains constant due to its connection to the engine crankshaft. The blade to speed ratio is above its optimum value and corresponding turbine efficiency is relatively low. Watson et al. [349] reported on their turbocompound truck Diesel engine mounted with a gear ratio of 30:1 that power turbine efficiency fell from 80% to 32% reducing the load from 100% to 40% at rated speed. With this efficiency, the contribution of the power turbine to the overall power output was nearly negligible and fuel consumption enhancement could only be obtained using variable gear ratio drive or variable geometry for the power turbine. These solutions add

significant cost and complexity to the compound system and are generally not justified for serial applications. Taking into account this mismatch between the power turbine and engine speeds, a typical energy balance obtained on a modern turbocompound truck Diesel engine is shown in figure 2.56 [146] where it can be seen that fuel economy improvements are only possible at high loads.

In 1981, Cummins developed one of the first compound truck engine to assess the benefits of mechanical turbocompounding [49, 176, 312]. The engine was equipped with a radial inflow power turbine, a gear box and a fluid coupling to separate the high speed gearing from the crankshaft torsional vibrations. During a 50000 miles extra-urban driving test in USA, they reported an average fuel consumption reduction of 4.7%. In 1986, Caterpillar [321, 364] selected for a 14.6l heavy-duty Diesel engine an axial power turbine for its high efficiency (up to 85%), low inertia and low duct losses since the exhaust from the radial turbocharger turbine could flow directly into the axial stage without additional turns. At full load, up to 6% fuel economy was achieved. However, the difficulties to feed the recovery energy into the powertrain via an efficient and reliable high speed gear box delayed at that time the introduction of such a system into mass production. In 1991, Scania tackled this problem and commercialized the first compounded system for heavy duty applications. The engine called DTC 1101 was an 11l 6-cylinder turbocharged Diesel engine able to provide 5% improvement of fuel consumption at full load. After this market first, Scania and Cummins worked together to release in 1995 another 12l 6-cylinder engine designed especially for mechanical turbocompounding. Since then, other OEM's have introduced this technology on their highly loaded applications, such as Volvo in 2002 with the D12-500TC [131], followed by Iveco for Case-New Holland tractors and Daimler in 2008 with the DD15 from Detroit Diesel. All these engines achieved also approximately 5% fuel economy enhancement when compared with their standard turbocharged versions.

2.6.2 Electric Turbocompounding

Electric turbocompounding recuperates part of the exhaust heat using a high speed generator directly connected to a turbine installed in the exhaust gas stream. The electricity produced is then fed back to the engine through a motor-generator mounted on the crankshaft. Some of this electric energy can also be used for other functions such as oil and water pumps, cooling

fan, air conditioning, etc..., or can be temporarily stored in high energy storage devices. As opposed to mechanical turbocompounding, the electrical system has no mechanical connection to the engine, so turbine speeds can potentially be controlled to maximize the power extracted from the exhaust gases in the whole engine operating range. Furthermore, more electric power can be recovered during vehicle braking operations via the motor-generator connected to the drive shaft.

Different electric turbocompounding configurations are possible. The first one consists of integrating the high speed motor-generator into the shaft of the turbocharger to form an EAT system. A diagram of this architecture is shown in figure 2.57. When the power produced by the turbocharger turbine exceeds the power requirement of the compressor, this surplus is converted into electrical power. The turbine speed and the corresponding boost pressure is controlled through the electric load applied to the generator, removing in that way the need of a wastegate valve or a variable geometry turbine. In addition when the power requirement of the compressor cannot be met, the electrical machine can be used as a motor to accelerate the turbo shaft reducing turbo lag effects.

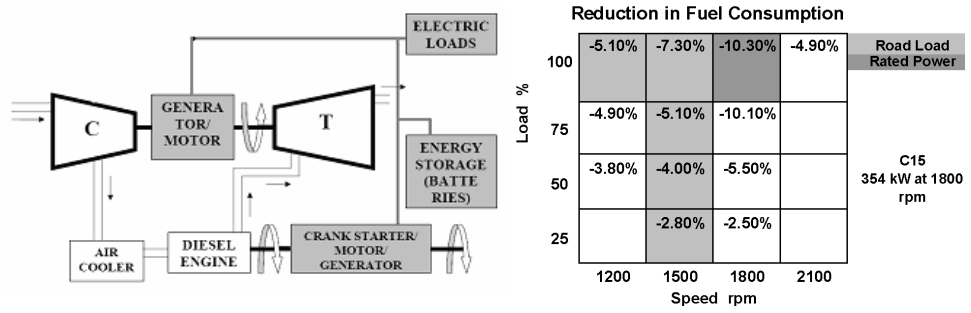

Figure 2.57: Left: diagram of a EAT electrical turbocompounding system [158] - Right: fuel economy enhancement with electric turbocompound [156].

An extensive description of the components that constitute an EAT system with a synthesis of their performance under turbocharger assistance was presented in the electric boosting system section. So only their performance as energy recovery devices will be analyzed in this subsection. Moreover, small EAT systems developed for passenger car applications are not considered as turbocompounding systems because the generated electrical power is only stored for the upcoming turbocharger needs and is not fed back to the

engine crankshaft or employed to drive accessories. In fact, even if Shahed et al. [304] reported their 1.4 kW EAT system mounted on a 2l Diesel engine could regenerate 900W at rated power, or Yamashita et al. [252] described that their 2 kW PM electric drive could recover 1.3 kW at 120000 rpm during regeneration experiments, these electric power transfers serve only to assist the turbocharger during transients and minor fuel economies when observed are purely the result of AFR variations.

Electric turbocompounding performance depends mainly on the motor rating, energy store capacity and associated power electronics which are selected as a function of the vehicle operating cycle. For a vehicle which is subject to a large number of stop/starts and operating only occasionally at high engine speeds and loads, rating the electrical system at full load would not result acceptable from a cost, size and efficiency point of view. But large energy storage can be justified to recover braking energy and help during acceleration. On the other hand, if the vehicle operates under high loads for long periods, a higher rated electrical system with smaller energy storage would be required.

In the 2000's, different EAT turbocompounding developments were carried out. For example, Hopmann et al. [16, 17, 154, 155, 156] developed such a system for a Caterpillar Class-8 truck engine (354 kW rated power at 1800 rpm). As the engine was running most of the time under motorway cruise, they rated the electrical motor at 60 kW to optimize the energy recovery at full load. With this power level, the turbocharger speed was limited to 66000 rpm due to important centrifugal stresses in the rotor lamination. The turbine was also redesigned to deliver both compressor and generator powers under efficient design conditions limiting in that way excessive pressure ratio across the turbine when high compound power was generated. Compared with the standard turbocharged engine under steady state operations, they reported significant fuel consumption improvements over the whole engine operating range (see figure 2.57) with a fuel economy of up to 10% at rated power. Considering a typical road cycle for an on-highway truck with different weighting factors for the prevailing operating speeds and loads, they calculated that an overall fuel economy of 5% could be achieved.

In an engine development program, redesigning a specific turbine for one application with its corresponding validation process can be expensive and time consuming. So to keep the same turbocharger design as the non turbocompound engine, Hountalas et al. [158, 159] limited the electric power recovery to maintain the exhaust backpressure increase below 1 bar at full load.

With this restrictive condition, simulations performed on a 10.3l heavy-duty truck engine showed that improvements in fuel consumption were reduced to respectively 1% and 3.8% at 25% and 100% load (rated speed). The maximum exhaust temperature increase which depends mainly on the exhaust backpressure was in the order of 50°C. Bumby et al. [55, 237, 284] in their EAT development for a 7.8l city bus Diesel engine maintained also the standard turbine design but reduced even more the electric motor recovery capabilities to optimize transient responses. The rating of the electric motor was 7.6 kW at 100000 rpm. This low power level was selected as the best compromise between an acceptable rotor mass moment of inertia for good acceleration and sufficient energy recovery to assist the turbocharger. A large energy storage was employed in combination with the EAT to correctly manage the power transfers. Evaluating the potential of this system for different city bus driving cycles they noticed that maximum 5% fuel savings could be achieved in extra-urban driving conditions, while the savings in urban driving conditions ranged from 0% (congested traffic) to 4% (bus lane).

Another possible configuration for electric turbocompounding consists of adding a series power turbine downstream to the main turbocharger as shown in figure 2.58. The power turbine is coupled directly to a high speed generator which converts the heat energy extracted from the exhaust gases in electric power. This configuration is less efficient than an EAT system in terms of packaging but allows thermomechanical constraints to be reduced on the generator and generator power level to be selected independently of the turbocharger design.

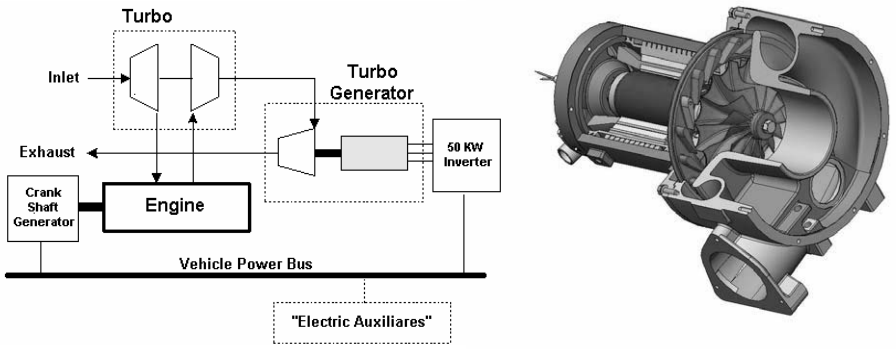

Figure 2.58: Left: diagram of a series electrical turbocompounding system - Right: cross section of the power turbine [338].

Vuk [338, 339] optimized this arrangement on a Deere 275 kW 9l large agricultural tractors engine where robustness and reliability were critical requirements. The electrical motor was rated at 50 kW. Running typical operating conditions of Tier 3 off-highway standards, they reported that fuel economy benefits of 6% were obtained at part loads while up to 10% could be achieved at full load. This configuration presents higher fuel consumption enhancements at part loads than an EAT system because the power turbine speed is completely independent of the turbocharger speed and can be controlled to optimize the energy recovery regardless of the boost pressure set point. Due to this freedom of power turbine speeds, Patterson et al. [257] showed on the same Deere tractor engine that series electrical turbocompounding was always more efficient than mechanical turbocompounding and could save approximately three times more fuel at rated power.

2.7 Concepts

Others innovative solutions presented as alternative concepts for two-stage turbocharging systems have been described in the literature.

In an effort to produce a single turbocharger with a wide operating range, Arnold et al. [24, 25, 27] had developed the Low Speed Turbocharger (LST). The LST system is a single shaft turbocharger configuration with the high and low-pressure compressor wheels mounted back-to-back in a two-stage series arrangement (figure 2.59). Its design achieved pressure ratios of up to 5:1 with a map width exceeding 3:1 choke-to-surge at 4:1 pressure ratio. To obtain these results, casing treatment technology at the LP compressor inlet was employed in combination with an innovative turbine rotor design able to maintain adequate blade to speed ratios. In fact, under identical flow and pressure ratio conditions, the LST operated at approximately 40% lower rotational speeds than a conventional single-stage design. High turbine efficiencies at low velocity ratio were therefore critical and had forced important turbine development using CFD calculations to optimize the turbine design. In the compressors side, flow between stages had been aerodynamically optimized to assure the flow entering in the second stage did not present unusual velocity profiles and losses were minimized. The single unit construction presents advantages in terms of packaging (same size as a conventional turbocharger), cost, thermal inertia and vehicle integration by eliminating the need for inter-

connection ducts, lubrication supplies and drain lines. Furthermore, compact inter-stage cooling is also possible by the oil or water turbocharger cooling system. However, turbo lag and transient responses are worsened by the additional HP compressor wheel that increases the overall mass moment of inertia, and improvements in the low end torque are limited by the relatively large LP compressor surge margin. Up to now the LST has not been used in series production.

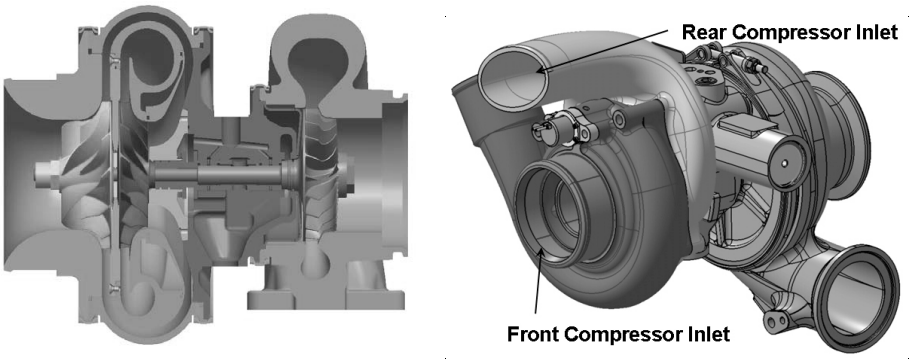

Figure 2.59: Left: Low Speed Turbocharger [25] - Right: Single Sequential Turbocharger [23].

With the same philosophy, Arnold et al. [23] had developed the Single Sequential Turbocharger (SST). The SST system is also a single shaft turbocharger configuration but in this case with a double-sided compressor (back-to-back compressor wheels in the same castings) to form a parallel arrangement. The front compressor inlet feeds the first compressor wheel while an additional inlet was created at the rear to feed the second compressor, see figure 2.59. The main objective of this design was to improve the performance of the turbine by changing the work/speed relationship of the compressor. Using a double-sided compressor increases the overall turbine speed and allows to work closer to the optimum blade to speed ratio over a wide engine operating range. A second benefit was an improved compressor flow range by stalling one compressor wheel at low mass flow rate. A toroidal piston was integrated into the compressor housing to shut off the flow at one compressor entry. Compared with a sequential parallel boosting system, the number of connecting-disconnecting valves is reduced and no complex transitions management are required as both compressors are always driven by the turbine. Moreover, a type of auto-surge control could be observed in this configuration.

When one compressor wheel is stalled, the flow in that wheel goes to essentially zero and all the flow is supplied by the opposite wheel. But since one wheel supplies the flow continuously, traditional surge phenomena with momentary complete flow reversal is not seen. The SST presents the same advantages-disadvantages as the LST system in terms of packaging, cost, thermal inertia and transient response, but in addition an aerodynamically optimized bifurcated duct had to be design to connect the air filter outlet to the turbocharger compressor inlet. In 2010, the SST system was launched in serial production on the Ford 6.7l V8 Diesel engine for light duty truck applications.

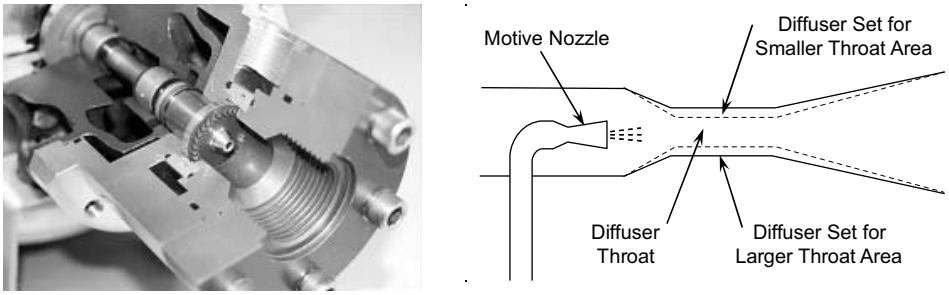

Figure 2.60: Left: hydraulic supercharger turbine drive [179] - Right: schematic diagram of Fluid-Dynamic Supercharger [335].

Another interesting concept called Sequential Hydro-Supercharging System (SHS) was presented by Kapich [179, 180, 181] to drive in a hybrid architecture a centrifugal compressor with hydraulic energy. In this configuration, the supercharger was driven by a high speed hydraulic turbine (figure 2.60) supplied by a hydraulic pump belt driven from the crankshaft and controlled via solenoid valves. In that way, the supercharger was not mechanically connected to the engine and could operate at its optimum speed without the need of costly continuously variable transmissions. Hydraulic turbine and pump efficiencies were respectively 80% and 90% and supercharger acceleration was on the order of 50000 rpm/s when connected to the oil supply. Compared to the Rotrex supercharger, the SHS system presents advantages in terms of vehicle integration because it requires only an oil supply connection and can be located practically anywhere in the engine compartment. Nevertheless, results obtained on a 7l heavy-duty Diesel engine showed mechanical powers consumed by the hydraulic pump were identical or slightly higher than ones consumed by a conventional positive displacement supercharger to obtain the same amount of boost pressure. Certainly for that reason, the SHS are still up to now unused in serial production.

Finally Fluid-Dynamic Supercharger (FDS) can employ compressed air to improve the transient performance of a turbocharged engine. One of the first attempts to use a compressed air supply as a supercharger was made by General Motors in the late 1950's integrating a supersonic nozzle with a venturi-shaped diffuser in the intake manifold. To avoid excessive pressure drop in the naturally aspirated mode, the venturi design was made larger than appropriate and FDS compression was limited to marginal values (about 14-27kPa). In the 1970's, Benson et al. [215] studied the method of injecting compressed air into the impeller of a compressor to accelerate the turbocharger during transient operations. Experiments realized in a turbocharger test rig showed that important improvements in terms of surge margin and time response could be obtained with this method, but no concrete applications were presented at that time. In 2008, Vetrovec [335] developed a FDS system based on the GM design for a gasoline passenger car engine. The system was composed of an air-operated motive nozzle, a section chamber and a diffuser duct as shown in figure 2.60. The motive nozzle discharged into the suction chamber a high velocity jet converting the potential energy of the compressed air into high kinetic energy. The air downstream of the nozzle was then pumped and entrained by the jet before being once again converted into potential pressure energy in the straight and diverging parts of the diffuser. To adjust the system to a wide range of operating conditions, the FDS was equipped with variable nozzle diameter and a variable throat area. Results based on simulations showed pressure ratios up to 1.8 with practically instant response to demand could be obtained. These performance data are favorably compared with traditional supercharging technologies. However, complex variable geometry designs and availability of air compressed supply in a vehicle are still quite challenging for FDS applications in serial production.

2.8 Conclusions

A review of a wide variety of boosting technologies which allow to increase low end torque, to improve transient response and to reduce fuel consumption has been carried out and described in this chapter. These technologies were investigated on a large variety of engines, ranging from a 1.0-liter 3-cylinder passenger car to a 13-liter 6-cylinder heavy-duty engine. It is therefore difficult to directly compare the benefits obtained by each system during their last development studies. However conclusions about their potential to im-

prove the main properties that characterize a boosting system can be made. Table 2.1 summarizes these capabilities for the main boosting architectures when compared to a conventional VGT turbocharger. For serial two-stage turbocharging, a distinction was made between architectures used in heavy-duty applications where both stages are continuously working together to provide high pressure ratios, and sequential systems used in passenger car where the HP stage is bypassed at high mass flow.

Technologies baseline : VGT turbocharger	Low end torque	Response	Max power	Range	Fuel consump-tion	Packaging	Comple-xity	EGR HP capabili-ties	Temp at catalyst entrance	Technolo-gical availabi-lity
Sequential parallel two-stage turbocharging system	++	++	0	++	-	-	--	+	0	++
Serial two-stage turbocharging system	+	+	++	+	+	--	-	++	--	++
Sequential serial two-stage turbocharging system	++	++	+	++	+	--	-	+	-	++
Single stage mechanical supercharger	++	++	0	0	--	-	0	--	++	++
Mechanical auxiliary supercharging	++	++	+	++	-	--	-	0	0	++
Electrically assisted turbocharger	0	+	0	0	0	0	--	+	0	--
Electric booster + turbocharger	++	++	+	++	+	-	-	0	0	-
Centrifugal compressor enhancement devices	+	+	0	+	0	0	-	0	0	-
Mechanical turbocompounding	0	-	+	0	++	--	-	+	-	++
Electric turbocompounding	0	-	+	0	++	--	--	+	-	--

Table 2.1: Left: Potential for improvements of the main boosting architectures.

Centrifugal compressor enhancement devices present interesting potential to increase the performance of two-stage architectures or to avoid the complexity of multi-stage system. If variable geometry turbines were able to better drive the compressor in the entire extended operating range with higher efficiency, they would certainly have stronger implication in the development of advanced boosting systems.

Development of electrically driven charging systems remains within the limits of the electrical vehicle system. Very high current levels are produced during transients operations and supercapacitors are needed to manage the power transfers. These requirements, added to an increase in the load demand by the other electricity-consuming engine accessories, are quite challenging for a conventional 12V electrical structure and higher voltage networks must be considered. Except for hybrid applications, the introduction of a 36V or 42V electrical system has been delayed in recent years for cost, complexity and

safety reasons. As these systems are still not introduced in top class vehicles production, perspectives to see a rapid spread of these advanced networks in lower class vehicles are limited. Nevertheless, electrical boosting technologies present interesting capabilities to enhance engine performance and should not be discarded due to their temporary development discrepancy with other electrical vehicle technologies.

Doing the sum of pros (+) and cons (-), it results the most promising boosting systems to increase the performance of automotive downsized-downspeeded engines are sequential serial two-stage turbocharging, mechanical auxiliary supercharging and electric booster. These architectures will thus be further analyzed within the framework of this thesis.

References

[10] A.N. Abdel Hamid. *"A New Technique for Stabilizing the Flow and Improving the Performance of Vaneless Radial Diffusers"*. ASME Journal of Turbomachinery, Vol.109, No. 1, pp.36-40, 1987. (Cit. on p. 78).

[11] A.N. Abdel Hamid. *"Control of Self-Excited Flow Oscillations in Vaneless Diffuser of Centrifugal Compression Systems"*. ASME paper 82-GT-188, 1982. (Cit. on p. 78).

[12] A.N. Abdel Hamid. *"Effects of Vaneless Diffuser Geometry on Flow Stability in Centrifugal Compression Systems"*. ASME paper 81-GT-10, 1981. (Cit. on p. 78).

[13] T.G. Adams. *"Comparison of a Turbocharger to Supercharger on a Spark Ignited Engine"*. SAE Technical Paper 841285, 1984. (Cit. on p. 44).

[16] M. Algrain. *"Controlling an Electric Turbo Compound System for Exhaust Gas Energy Recovery in a Diesel Engine"*. IEEE International Conference on Electro Information Technology, Lincoln, 2005. (Cit. on pp. 58, 89).

[17] M. Algrain and U. Hopmann. *"Diesel Engine Waste Heat Recovery Utilizing Electric Turbocompound Technology"*. Diesel Engine Emissions Reduction Conference, Newport, 2003. (Cit. on pp. 58, 89).

[19] R.F. Ansdale. *"A Reconnaissance of Supercharging Technology 1902-1980"*. SAE Technical Paper 810003, 1981. (Cit. on p. 40).

[23] S. Arnold. *"Single Sequential Turbocharger: a New Boosting Concept for Ultra-Low Emission Diesel Engines"*. SAE Technical Paper 2008-01-0298, 2008. (Cit. on p. 92).

[24] S. Arnold. *"Turbocharging Technologies to Meet Critical Performance Demands of Ultra-Low Emissions Diesel Engines"*. SAE Technical Paper 2004-01-1359, 2004. (Cit. on pp. 59, 79, 81, 91).

[25] S. Arnold, D. Calta, K. Dullack, C. Judd, and G. Thompson. *"Development of an Ultra-High Pressure Ratio Turbocharger"*. SAE Technical Paper 2005-01-1546, 2005. (Cit. on pp. 91, 92).

[26] S. Arnold, M. Groskreutz, S. Shahed, and K. Slupski. *"Advanced Variable Geometry Turbocharger for Diesel Engine Applications"*. SAE Technical Paper 2002-01-0161, 2002. (Cit. on p. 18).

[27] S. Arnold, K. Slupski, M. Groskreutz, G. Vrbas, R. Cadle, and S.M. Shahed. *"Advanced Turbocharging Technologies for Heavy-Duty Diesel Engines"*. SAE Technical Paper 2001-01-3260, 2001. (Cit. on p. 91).

[31] W. Attard, H.C. Watson, S. Konidaris, and M.A. Khan. *"Comparing the Performance and Limitations of a Downsized Formula SAE Engine in Normally Aspirated, Supercharged and Turbocharged Modes"*. SAE Technical Paper 2006-32-0072, 2006. (Cit. on p. 44).

[32] B.H. Bae, S.K. Sul, J.H. Kwon, and J.S. Byeon. *"Implementation of Sensorless Vector Control for Super-High-Speed PMSM of Turbo-Compressor"*. IEEE Transactions on Industry Applications, Vol. 39, pp. 811-818, 2003. (Cit. on p. 58).

[33] N. Baines. *"Fundamentals of Turbocharging"*. Concepts NREC. ISBN 0-933283-14-8, 2005. (Cit. on pp. 18, 26).

[35] J.C. Bass, A.S. Kushch, and N.B. Elsner. *"Thermoelectric Generator (TEG) on Heavy Diesel Trucks"*. 10^{th} International Conference on Thermoelectrics, Beijing, 2001. (Cit. on p. 81).

[41] G. Benvenuto and U. Campora. *"Dynamic Simulation of a High-Performance Sequentially Turbocharged Marine Diesel Engine"*. International Journal of Engine Research, Vol. 3, No. 3, pp. 115-125, 2001. (Cit. on pp. 23, 26).

[45] M. Bonello, D.M. Caldwell, J.A. Pigott, G.P. Prior, and T.M. Schag. *"The Supercharged Northstar DOHC 4.4L V8 Engine for Cadillac"*. SAE Technical Paper 2005-01-1854, 2005. (Cit. on p. 44).

[47] Y. Borila. *"A Sequential Turbocharging Method for Highly Rated Truck Diesel Engines"*. SAE Technical Paper 860074, 1986. (Cit. on p. 23).

[49] M.C. Brands, J.R. Werner, J.L. Hoehne, and S. Kramer. *"Vehicle Testing of Cummins Turbocompound Diesel Engine"*. SAE Technical Paper 810073, 1981. (Cit. on p. 87).

[52] C. Brockbank. *"Application of a Variable Drive to Supercharger & Turbo Compounder Applications"*. SAE Technical Paper 2009-01-1465, 2009. (Cit. on pp. 47, 48, 83).

[53] P. Brynych, J. Macek, L. Pohorelsky, P.Y. Vallaude, J.C. Ricaud, and P. Obernesser. *"Optimization of a Two-Stroke Diesel Engine Air System"*. XLII International Scientific Conference of Czech, Slovak University Departments, and Institutions Dealing with the Research of Combustion Engines, Zilina, 2011. (Cit. on p. 41).

[54] R. Buchwald, G. Lautrich, O. Maiwald, and A. Sommer. *"Boost and EGR System for the Highly Premixed Diesel Combustion"*. SAE Technical Paper 2006-01-0204, 2006. (Cit. on pp. 31, 37–39).

[55] J. Bumby, S. Crossland, and J. Carter. *"Electrically Assisted Turbochargers: their Potential for Energy Recovery"*. Hybrid Vehicle Conference, Institution of Engineering and Technology, Coventry, 2006. (Cit. on p. 90).

[56] J.R. Bumby, S. Crossland, E. Spooner, and J. Carter. *"The Development of Turbocharger Accelerator Motors and Drives and their Integration into Vehicle Electrical Systems"*. International Conference on Automotive Electronics, London, 2005. (Cit. on p. 59).

[57] J.R. Bumby, E. Spooner, and M. Jagelia. *"A Solid Rotor Induction Machine for Turbo-Assist Operations"*. International Conference on Electrical Machines, Crete, 2006. (Cit. on p. 58).

[58] J.R. Bumby, E. Spooner, and M. Jagelia. *"High Speed Solid Rotor Induction Motors"*. IEEE International Conference on Electrical Power Applications, Vol. 153, pp. 31-39, 2006. (Cit. on pp. 58, 59).

[59] J.R. Bumby, E.S. Spooner, J. Carter, H. Tennant, G. Ganio Mego, G. Dellora, H. Gstrein W.and Sutter, and J. Wagner. *"Electrical Machines for Use in Electrically Assisted Turbochargers"*. International Conference on Power Electronics, Machines and Drives, Vol. 1, pp. 344-349, 2004. (Cit. on p. 58).

[60] D.J. Burtt and A.P. Kolstrup. *"Introducing the Rotrak Variable Speed Traction Drive Centrifugal Supercharger to Fully Exploit Engine Downsizing"*. 15^{th} Supercharging conference, Dresden, 2010. (Cit. on p. 47).

[62] M. Canova, F. Chiara, G. Rizzoni, and Y.Y. Wang. *"Model-Based Characterization and Analysis of Diesel Engines with Two-Stage Turbochargers"*. SAE Technical Paper 2010-01-1220, 2010. (Cit. on pp. 29, 33, 35).

[63] C. Cantemir. *"Twin Turbo Strategy Operation"*. SAE Technical Paper 2001-01-0666, 2001. (Cit. on pp. 21, 22, 25).

[65] G. Cantore, E. Mattarelli, and S. Fontanesi. *"A New Concept of Supercharging Applied to High Speed DI Diesel Engines"*. SAE Technical Paper 2001-01-2485, 2001. (Cit. on pp. 51, 52).

[67] G. Capon and T. Morris. *"The Effect of Air Inlet System Features on Automotive Turbocharger Compressor Performance"*. Ford Motor Company Publications 2010, pp. 93-110, 2010. (Cit. on p. 67).

[69] C.J Chadwell and M. Walls. *"Analysis of a Superturbocharged Downsized Engine Using 1-D CFD Simulation"*. SAE Technical Paper 2010-01-1231, 2010. (Cit. on pp. 47, 48, 82).

[73] D.C. Chapman. *"Model 250-C30/C288 Compressor Development"*. AGARD Conference on Centrifugal Compressors, Flow Phenomenon and Performance, Vol. 282, No. 20, 1982. (Cit. on p. 75).

[74] A. Chasse, A. Albrecht, P. Moulin, A. Gautier P., L. Fontvieille, A. Guinois, and L. Doléac. *"A New Simulation Step Towards Virtual Bench Through the Challenging Case of Two-Stage Turbocharger Diesel Engine Control Design"*. SAE Technical Paper 2008-01-0355, 2008. (Cit. on pp. 32, 116).

[75] A. Chasse, P. Moulin, P. Gautier, A. Albrecht, L. Fontvieille, A. Guinois, and L. Doléac. *"Double Stage Turbocharger Control Strategies Development"*. SAE Technical Paper 2008-01-0988, 2008. (Cit. on pp. 32, 33, 127).

[78] P. Chesse, J. Hetet, X. Tauzia, and J. Frayet. *"Influence des Circuits de Liaison Moteur/Compresseur sur le Fonctionnement des Moteurs Diesel à Suralimentation Bi-Etagée"*. Revue Generale de Thermique, No. 37, pp. 801-812, 1998. (Cit. on p. 23).

[79] P. Chesse, X. Tauzia, J. Hetet, and G. Grosshans. *"Simulation des Phases de Fonctionnement Transitoires d'un Moteur Diesel Semi-Rapide à Suralimentation Séquentielle"*. Comptes Rendus de l'Académie des Sciences - Mechanics-Physics-Astronomy, Vol. 328, No 3, pp. 193-198, 2000. (Cit. on p. 23).

[81] C. Choi, S. Kwon, and S. Cho. *"Development of Fuel Consumption of Passenger Diesel Engine with 2-Stage Turbocharger"*. SAE Technical Paper 2006-01-0021, 2006. (Cit. on p. 34).

[82] M. Choshi, K. Asanomi, H. Abe, S. Okamoto, and M. Shoji. *"Development of V6 Miller Cycle Engine"*. JSAE Review, Vol. 15, pp. 195-200, 1994. (Cit. on p. 43).

[85] G. Claussen and C. Suhocki. *"Clean Diesel System Boosting Solution: TVS Supercharger"*. Eaton Corporation Publications, Engine Air Management Operations, 2010. (Cit. on pp. 44, 45).

[86] M. Coppinger and E. Swain. *"Performance Prediction of an Industrial Centrifugal Compressor Inlet Guide Vane System"*. Proceedings of the Institution of Mechanical Engineers Part A: Journal of Power and Energy, Vol. 214, pp. 153-164, 2000. (Cit. on pp. 68, 69, 71).

[94] J.M. Desantes, J.M. Lujan, B. Pla, and J.A. Soler. *"Potential of Using a Nozzle at the Compressor Inlet of a High Speed Direct Injection Diesel Engine"*. Proceedings of the Institution of Mechanical Engineers Part D: Journal of Automobile Engineering, Vol. 225, No. 2, pp. 178-189, 2011. (Cit. on p. 73).

[95] A. Dhand, J. Baekhyun C.and Villegas, K. Svencara, B. Gao, M. Wieltsch, W. Thornton, S. Etemad, J. Parra, and R. Taylor. *"Engine Downsizing Using Electrically Driven Supercharger"*. 13$^{\text{th}}$ EAEC European Automotive Congress, Valencia, 2011. (Cit. on pp. 63, 64).

[96] F.A. Dibella, L.R. Di Nanno, and M.D. Koplow. *"Laboratory and On-Highway Testing of Diesel Organic Rankine Compound Long-Haul Vehicle Engine"*. SAE Technical Paper 830122, 1983. (Cit. on p. 81).

[99] E. Doyle, L. Di Nanno, and S. Kramer. *"Installation of a Diesel-Organic Rankine Compound Engine in a Class 8 truck for a single-vehicle test"*. SAE Technical Paper 790646, 1979. (Cit. on p. 81).

[106] K. Fieweger, H. Paffrath, and N. Schorn. *"Drivability Assessment of an HSDI Diesel Engine with Electrically Assisted Boosting Systems"*. IMechE 7$^{\text{th}}$ International Conference on Turbochargers and Turbocharging, C602/009/2002, pp. 283-293, 2002. (Cit. on pp. 55, 63).

[107] Z. Filipi, Y. Wang, and D. Assanis. *"Effect of Variable Geometry Turbine (VGT) on Diesel Engine and Vehicle System Transient Response"*. SAE Technical Paper 2001-01-1247, 2001. (Cit. on p. 18).

[108] F.B. Fisher. *"Application of Map Width Enhancement Devices to Turbocharger Compressor Stages"*. SAE Technical Paper 880794, 1988. (Cit. on p. 75).

[111] N. Fraser, J. Fleischer T.and Thornton, and J. Rueckauf. *"Development of a Fully Variable Compressor Map Enhancer for Automotive Application"*. SAE Technical Paper 2007-01-1558, 2007. (Cit. on pp. 65, 68, 70, 71).

[112] V. Fsik. *"2-Stage Turbocharger Matching for a Light Duty Diesel Engine"*. Josef Bozek Research Center Publications, 2004. (Cit. on p. 34).

[114] J. Galindo, H. Climent, C. Guardiola, and J. Domenech. *"Strategies for Improving the Mode Transition in a Sequential Parallel Turbocharged Automotive Diesel Engine"*. International Journal of Automotive Technology, Vol. 10, No. 2, pp. 141-149, 2009. (Cit. on pp. 23, 25).

[115] J. Galindo, H. Climent, C. Guardiola, and A. Tisiera. *"Assessment of a Sequentially Turbocharged Diesel Engine on Real Life Driving Cycles"*. International Journal of Vehicle Design, Vol. 49, No. 1/2/3, 2009. (Cit. on pp. 23–25).

[116] J. Galindo, J. Lujan, H. Climent, and C. Guardiola. *"Turbocharging System Design of a Sequentially Turbocharged Diesel Engine by Means of a Wave Action Model"*. SAE Technical Paper 2007-01-1564, 2007. (Cit. on pp. 23, 24).

[121] J. Galindo, J.R. Serrano, X. Margot, A. Tiseira, N. Schorn, and H. Kindl. *"Potential of Flow Pre-Whirl at the Compressor Inlet of Automotive Engine Turbochargers to Enlarge Surge Margin and Overcome Packaging Limitations"*. International Journal of Heat and Fluid Flow, Vol. 28, pp. 374-387, 2007. (Cit. on pp. 67, 68).

[124] P. Gautier, A. Albrecht, A. Chasse, P. Moulin, A. Pagot, L. Fontvieille, and D. Issartel. *"A Simulation Study of the Impact of LP EGR on a Two-Stage Turbocharged Diesel Engine"*. Oil & Gas Science and Technology, Revue IFP, Vol. 64, No. 3, pp. 361-379, 2009. (Cit. on p. 37).

[126] S. George, G. Morris, J. Dixon, D. Pearce, and G. Heslop. *"Optimal Boost Control for an Electrical Supercharging Application"*. SAE Technical Paper 2004-01-0523, 2004. (Cit. on p. 62).

[129] B.C. Glenn, D. Upadhyay, and G.N. Washington. *"Control Design of Electrically Assisted Boosting Systems for Diesel Powertrain Applications"*. IEEE Transactions on Control Systems Technology, Vol. 18, pp. 769-778, 2010. (Cit. on pp. 55, 57).

[130] R. Glover, M. Pratley, and M. Marfatia. *"Gear Design for Low Whine Noise in a Supercharged Application"*. SAE Technical Paper 2007-01-2293, 2007. (Cit. on p. 44).

[131] A. Greszler. *"Diesel Turbo-Compound Technology"*. ICCT/NESCCAF workshop - Improving the fuel economy of heavy-duty fleets II, 2008. (Cit. on p. 87).

[132] R.C. Griffith. *"Series Turbocharging for the Caterpillar Heavy-Duty On-Highway Truck Engines with ACERT Technology"*. SAE Technical Paper 2007-01-1561, 2007. (Cit. on pp. 29, 36).

[136] J. Hawley, F. Wallace, A. Cox, R. Horrocks, and G. Bird. *"Variable Geometry Turbocharging for Lower Emissions and Improved Torque Characteristics"*. Proceedings of the Institution of Mechanical Engineers Part D: Journal of Automobile Engineering, Vol. 213, pp. 145-159, 1999. (Cit. on pp. 7, 18).

[144] F. Herbst, C.P. Stöber-Schmidt, P. Eilts, T. Sextro, J. Kammeyer, C. Natkaniec, J. Seume, D. Porzig, and H. Schwarze. *"The Potential of Variable Compressor Geometry for Highly Boosted Gasoline Engines"*. SAE Technical Paper 2011-01-0376, 2011. (Cit. on pp. 68, 70, 72).

[146] H. Hiereth and P. Prenninger. *"Charging the Internal Combustion Engine"*. NewYork: Springer-Verlag Wien, ISBN 978-3-211-33033-3, 2003. (Cit. on pp. 20, 41, 42, 86, 87, 275).

[147] C. Hill, D. Miller, and R. Gardner. *"2005 Ford GT Powertrain - Supercharged Supercar"*. SAE Technical Paper 2004-01-1252, 2004. (Cit. on p. 44).

[150] P. Hoecker, J.W. Jaisle, and S. Munz. *"The eBooster from BorgWarner Turbo Systems - The Key Component for a New Automobile Charging System"*. Borg Warner Turbo Systems Knowledge Library, 2000. (Cit. on pp. 54, 62, 63, 272).

[151] P. Hoecker, F. Pflüger, J. Jaisle, and S. Münz. *"Modern Turbocharging Designs for Passenger Car Diesel Engines"*. Borg Warner Turbo Systems Knowledge Library, 2000. (Cit. on p. 18).

[154] U. Hopmann. *"Diesel Engine Waste Heat Recovery Utilizing Electric Turbocompound Technology"*. Diesel Engine Emissions Reduction Conference, San Diego, 2002. (Cit. on pp. 58, 89).

[155] U. Hopmann. *"Diesel Engine Waste Heat Recovery Utilizing Electric Turbocompound Technology"*. Diesel Engine Emissions Reduction Conference, San Diego, 2004. (Cit. on pp. 58, 89).

[156] U. Hopmann and C. Algrain. *"Diesel Engine Electric Turbo Compound Technology"*. SAE Technical Paper 2003-01-2294, 2003. (Cit. on pp. 58, 88, 89).

[157] M. Hori, N. Ikeya, S. Takabe, and Y. Miyagi. *"Examinations of a Lysholm Compressor's Performance and the Engine Performance Supercharged by the Lysholm Compressor"*. IMechE 6$^{\text{th}}$ International Conference on Turbocharging and Air Management Systems, C554/019/98, London, 1998. (Cit. on pp. 50, 51).

[158] D.T. Hountalas, C.O. Katsanos, and D.A. Kouremenos. *"Study of Available Exhaust Gas Heat Recovery Technologies for HD Diesel Engine Applications"*. International Journal of Alternative Propulsion, Vol. 1, No. 2/3, 2007. (Cit. on pp. 85, 88, 89).

[159] D.T. Hountalas, C.O. Katsanos, and V.T. Lamaris. *"Recovering Energy from the Diesel Engine Exhaust Using Mechanical and Electrical Turbocompounding"*. SAE Technical Paper 2007-01-1563, 2007. (Cit. on pp. 85, 86, 89).

[161] M.F. Howlett, W. Schnider, N. Ausserhofer, M. Weissbaeck, O. Soustelle, P. Ragot, P. Mallet, and J. Rozen. *"3-Cylinder Aggressive Downsized Diesel"*. Conference Internationale et Exposition Motorisation Diesel: Face au Defi de la Competitivite. Rouen, 2010. (Cit. on pp. 53, 239).

[163] R. Hunziker, H.P. Dickmann, and R. Emmrich. *"Numerical and Experimental Investigation of a Centrifugal Compressor with an Inducer Casing Bleed System"*. Proceedings of the Institution of Mechanical Engineers Part A: Journal of Power and Energy, Vol. 215, pp 783-791, 2001. (Cit. on pp. 74, 75).

[164] S. Ibaraki, Y. Yamashita, K. Sumida, H. Ogita, and Y. Jinnai. *"Development of the Hybrid Turbo, an Electrically Assisted Turbocharger"*. Mitsubishi Heavy Industries Technical Review, Vol. 43, pp.1-5, 2006. (Cit. on pp. 55, 59, 60).

[165] M. Ishino, Y. Iwakiri, A. Bessho, and H. Uchida. *"Effects of Variable Inlet Guide Vanes on Centrifugal Compressor Performance"*. ASME paper 99-GT-157, 1999. (Cit. on pp. 68–70).

[166] Y. Iwakiri and H. Uchida. *"Numerical Fluid Analysis of a Variable Geometry Compressor for Use in a Turbocharger"*. Toyota R&D Review, Vol. 41, No. 3, pp.15-21, 2006. (Cit. on p. 77).

[168] W. Jansen, A.F. Carter, and M.C. Swarden. *"Improvements in Surge Margin for Centrifugal Compressors"*. AGARD Conference on Centrifugal Compressors, Flow Phenomenon and Performance, Vol. 282, No.19, 1980. (Cit. on p. 75).

[172] Z. Jiang, K. Cheng, and D.K. Harrison. *"A Concurrent Engineering Approach to the Development of a Scroll Compressor"*. Journal of Materials Processing Technology, Vol. 107, pp. 194-200, 2000. (Cit. on p. 41).

[173] K. Jiao, X. Li, H. Sun, T. Schram, E. Krivitzky, and L.M. Larosiliere. *"Numerical Investigation of Advanced Compressor Technologies to Meet Future Diesel Emission Regulations"*. SAE Technical Paper 2009-01-1469, 2009. (Cit. on p. 80).

[174] K. Jiao, H. Sun, X. Li, H. Wu, E. Krivitzky, T. Schram, and L.M. Larosiliere. *"Numerical Simulation of Air Flow Through Turbocharger Compressors with Dual Volute Design"*. Applied Energy, Vol. 86, pp. 2494-2506, 2009. (Cit. on p. 80).

[175] R. Jorgensen and M. Sitar. *"System Performance and Control Requirements for a Sequentially Compounded Supercharged and Turbocharged Gasoline Engine"*. Eaton Corporation Publications, Engine Air Management Operations, 2004. (Cit. on pp. 45, 53, 275).

[176] R. Kamo. *"Higher BMEP Prospects for Vehicular Diesels"*. IMechE 1th International Conference of Turbocharging and Turbochargers, C62/78, London, 1978. (Cit. on p. 87).

[177] H. Kanesaka, G. Ozawa, and H. Seiyama. *"Future Prospects for Supercharging"*. SAE Technical Paper 982045, 1998. (Cit. on p. 51).

[179] D.D. Kapich. *"High Speed Hydraulic Turbine Driven Supercharger System and Controls Optimization"*. SAE Technical Paper 972676, 1997. (Cit. on p. 93).

[180] D.D. Kapich. *"Sequential Hydro-Supercharging System for Turbodiesels"*. SAE Technical Paper 961744, 1996. (Cit. on p. 93).

[181] D.D. Kapich. *"Very High Speed, Hydraulic Turbine Driven Supercharging System"*. SAE Technical Paper 951882, 1995. (Cit. on p. 93).

[182] T. Kattwinkel, R. Weiss, and J.P. Boeschlin. *"Mechatronic Solution for Electronic Turbocharger"*. SAE Technical Paper 2003-01-0712, 2003. (Cit. on p. 62).

[184] J. Kech and H. Klotz. *"Model Based Sequential Turbocharging Optimization for Series 8000 M70/M90 Engines"*. SAE Technical Paper 2002-01-0378, 2002. (Cit. on p. 23).

[186] R. Kemmler, H.G. Lehmann, and J. Schommers. *"Trends in Development of Supercharged Gasoline Internal Combustion Engines"*. 7th Supercharging conference, Dresden, 2000. (Cit. on p. 45).

[188] Y. Kim, A. Engeda, R. Aungier, and G. Direnzi. *"The Influence of Inlet Flow Distortion on the Performance of a Centrifugal Compressor and the Development of an Improved Inlet Using Numerical Simulations"*. Proceedings of the Institution of Mechanical Engineers Part A: Journal of Power and Energy, Vol. 215, pp 323-338, 2001. (Cit. on p. 67).

[190] H. Kindl, N. Schorn, H. Schulte, J.R. Serrano, X. Margot, and J.C. Donayre. *"Influence of Various Compressor Inlet Designs on Compressor Performance"*. THIESEL Conference on Thermo- and Fluid Dynamic Processes in Diesel Engines, Valencia, 2004. (Cit. on p. 67).

[191] C. Klarhoefer and G. Winkler. *"Compounding a Passenger Car Diesel with a Positive Displacement Expander"*. IMechE 3th International Conference of Turbocharging and Turbochargers, pp. 123-127, London, 1986. (Cit. on p. 83).

[192] H. Kleeberg, D. Tomazic, O. Lang, and K. Habermann. *"Future Potential and Development Methods for High Output Turbocharged Direct Injected Gasoline Engines"*. SAE Technical Paper 2006-01-0046, 2006. (Cit. on p. 53).

[193] W. Knecht. *"Diesel Engine Development in View of Reduced Emission Standards"*. Energy, Vol. 33, pp. 264-271, 2008. (Cit. on p. 54).

[194] R. Kociba and M.D. Parr. *"The General Motors Supercharged 3800 Engine"*. SAE Technical Paper 910685, 1991. (Cit. on pp. 44, 46).

[195] I. Kolmanovsky and A.G. Stefanopoulou. *"Evaluation of Turbocharger Power Assist System Using Optimal Control Techniques"*. SAE Technical Paper 2000-01-0519, 2000. (Cit. on p. 56).

[196] I. Kolmanovsky and A.G. Stefanopoulou. *"Optimal Control Techniques for Assessing Feasibility and Defining Subsystem Level Requirements: an Automotive Case Study"*. IEEE Transactions on Control Systems Technology, Vol. 9, pp. 524-534, 2001. (Cit. on pp. 56, 116).

[197] I. Kolmanovsky, A.G. Stefanopoulou, and B.K. Powell. *"Improving Turbocharged Diesel Engine Operation with Turbo Power Assist System"*. IEEE International Conference on Control Applications, pp.454-459, Kohala Coast, 1999. (Cit. on p. 56).

[202] J.C. Koval, A.W. Fedewa, K.A Hollman, and D.G. Woolcott. *"An Automotive Supercharger Noise Test Rig Incorporating Torsional Excitation"*. SAE Technical Paper 2005-01-2440, 2005. (Cit. on p. 44).

[203] R. Krebs, H. Szengel R.and Middendorf, M. Fleib, A. Laumann, and S. Voeltz. *"The New Dual-Charged FSI Petrol Engine by Volkswagen - Part 1: Design"*. MTZ Worldwide Edition, Vol. 66, pp. 844-856, 2005. (Cit. on p. 52).

[204] R. Krebs, R. Szengel, H. Middendorf, H. Sperling, W. Siebert, J. Theobald, and K. Michels. *"The New Dual-Charged FSI Petrol Engine by Volkswagen - Part 2: Thermodynamics"*. MTZ Worldwide Edition, Vol. 66, pp. 979-986, 2005. (Cit. on pp. 49, 53).

[205] I.J. Kruithof and W.L. Sturm. *"Development of a Heavy-Duty Diesel Engine with Two-Stage Turbocharging"*. ATZ AutoTechnology, Vol. 5, 2005. (Cit. on p. 29).

[206] A.S. Kushch, J.C. Bass, S. Ghamaty, and N.B. Elsner. *"Thermoelectric Development at HI-Z Technology"*. 10^{th} International Conference on Thermoelectrics, pp. 422-430, Beijing, 2001. (Cit. on p. 81).

[207] N. Kyrtatos and N. Watson. *"Application of Aerodynamically Induced Prewhirl to Small Turbocharger Compressor"*. ASME Journal of Engineering for Power, Vol. 102, pp. 934-950, 1980. (Cit. on p. 65).

[209] S. Langridge and H. Fessier. *"Strategies for High EGR Rates in a Diesel Engine"*. SAE Technical Paper 2002-01-0961, 2002. (Cit. on p. 37).

[215] J.D. Ledger, R.S. Benson, and H. Furukawa. *"Improvement in Transient Performance of a Turbocharged Diesel Engine by Air Injection into the Compressor"*. SAE Technical Paper 730665, 1973. (Cit. on p. 94).

[216] B. Lee, Z. Filipi, D. Assanis, and D. Jung. *"Simulation-Based Assessment of Various Dual-Stage Boosting Systems in Terms of Performance and Fuel Economy Improvements"*. SAE Technical Paper 2009-01-1471, 2009. (Cit. on pp. 29, 34, 39).

[217] A. Lefebvre and S. Guilain. *"Transient Response of a Turbocharged SI Engine with an Electrical Boost Pressure Supply"*. SAE Technical Paper 2003-01-1844, 2003. (Cit. on pp. 60, 61).

[218] C.J. Leising, G.P. Purohit, S.P. DeGrey, and J.G. Finegold. *"Waste Heat Recovery"*. SAE Technical Paper 780686, 1978. (Cit. on p. 81).

[219] J.L Leroy and G. Grosshaus. *"New Development of Turbo-Compound Diesel Engines"*. IMechE 3^{th} International Conference of Turbocharging and Turbochargers, pp. 97-104, London, 1986. (Cit. on p. 84).

[221] N. Lindenkamp. *"Designing a Charging System for a Diesel Engine"*. European Users Conference, Frankfurt, 2007. (Cit. on p. 53).

[222] H. Loren, L.H. Uthoff, and J.W. Yakimow. *"Supercharger vs. Turbocharger in Vehicle Applications"*. SAE Technical Paper 870704, 1987. (Cit. on p. 44).

[226] C. Luttermann and W. Mährle. *"BMW High Precision Fuel Injection in Conjunction with Twin-Turbo Technology: a Combination for Maximum Dynamic and High Fuel Efficiency"*. SAE Technical Paper 2007-01-1560, 2007. (Cit. on p. 21).

[227] I. Macdougal and R.L. Elder. *"The Improvement of Operating Range in a Small High Speed Centrifugal Compressor Using Casing Treatment"*. IMechE 2th International Conference of Turbocharging and Turbochargers, C32/82, London, 1982. (Cit. on p. 75).

[232] E. Mattarelli, F. Perini, and A. Rinaldini. *"Optimization of a Supercharged Single Cylinder Engine for a Formula SAE Racing Car"*. SAE Technical Paper 2009-01-0309, 2009. (Cit. on p. 44).

[233] E. Mattarelli, C.A. Rinaldini, A. Mazza, and M. Oliva. *"Development of a 2-Stage Supercharging System for a HSDI Diesel Engine"*. SAE Technical Paper 2009-01-2757, 2009. (Cit. on pp. 31, 34, 53).

[235] S.M. Milburn. *"Introducing a High Efficiency Variable Positive Displacement Automotive Supercharger"*. SAE Technical Paper 940845, 1994. (Cit. on p. 40).

[236] F. Millo, F. Mallamo, and G. Ganio Mego. *"The Potential of Dual Stage Turbocharging and Miller Cycle for HD Diesel Engines"*. SAE Technical Paper 2005-01-0221, 2005. (Cit. on pp. 29, 39, 40).

[237] F. Millo, F. Mallamo, E. Pautasso, and G. Ganio Mego. *"The Potential of Electric Exhaust Gas Turbocharging for HD Diesel Engines"*. SAE Technical Paper 2006-01-0437, 2006. (Cit. on pp. 58, 59, 90).

[238] Y. Miyagi, S. Takabe, K. Miyashita, and N. Ikeya. *"Experimental Study of New Lysholm Supercharger with a Simple Unloading System"*. SAE Technical Paper 960952, 1996. (Cit. on pp. 45, 46).

[239] H. Mohtar, A. Chesse, A. Yammine, and F. Hetet. *"Variable Inlet Guide Vanes in a Turbocharger Centrifugal Compressor: Local and Global Study"*. SAE Technical Paper 2008-01-0301, 2008. (Cit. on p. 70).

[240] H. Mohtar, P. Chesse, and D. Chalet. *"Effect of a Map Width Enhancement System on Turbocharger Centrifugal Compressor Performance and Surge Margin"*. Proceedings of the Institution of Mechanical Engineers Part D: Journal of Automobile Engineering, Vol. 225, No. 3, pp. 395-405, 2011. (Cit. on p. 76).

[244] P. Moulin, O. Grondin, and L. Fontvieille. *"Control of a Two-Stage Turbocharger on a Diesel Engine"*. 48th IEEE Conference on Decision and Control, Shanghai, 2009. (Cit. on p. 32).

[245] E. Mueller, T. Kollman, and T. Reid. *"Performance Development of the Supercharged Mercury Marine Outboard Engines"*. SAE Technical Paper 2006-01-0015, 2006. (Cit. on p. 43).

[247] S. Munz, M. Schier, H.P. Schmalzl, and T. Bertolini. *"eBooster - Design and Performance of an Innovative Electrically Driven Charging System"*. Borg Warner Turbo Systems Knowledge Library, 2000. (Cit. on pp. 57, 60, 61, 272).

[248] P. Nefischer, M. Grubbauer, J. Honeder, G. Pessl, and M. Prosi. *"Diesel Engine with 2-Stage Turbocharging and Variable Turbine Geometry in Passenger Cars"*. THIESEL Conference on Thermo- and Fluid Dynamic Processes in Diesel Engines, Valencia, 2010. (Cit. on pp. 35, 36).

[250] B. Nikpour. *"Turbocharger Compressor Flow Range Improvement for Future Heavy Duty Diesel Engines"*. THIESEL Conference on Thermo- and Fluid Dynamic Processes in Diesel Engines, Valencia, 2004. (Cit. on pp. 75–77).

[251] T. Noguchi, Y. Takata, Y. Yamashita, and S. Ibaraki. *"160000-r/tr 2.7-kW Electric Drive of Supercharger for Automobiles"*. International Conference on Power Electronics and drives Systems, Kuala Lumpur, 2005. (Cit. on p. 59).

[252] T. Noguchi, Y. Takata, Y. Yamashita, Y. Komatsu, and S. Ibaraki. *"200000-r/tr 2-kW PM Motor Drive for Turbocharger"*. Electrical Engineering in Japan, Vol. 161, pp. 854-861, 2007. (Cit. on pp. 60, 89).

[253] D.L. Page. *"Emission Reductions and Improved Engine Performance with the Turbodyne System"*. Diesel Engine Emissions Reduction Conference, San Diego, 1995. (Cit. on p. 54).

[254] D.L. Page. *"Optimization of the Air/Fuel Ratio for Improved Engine Performance and Reduced Emissions"*. SAE Technical Paper 961714, 1996. (Cit. on pp. 55, 61).

[255] P. Pallotti, E. Torella, J. New, M. Criddle, and J. Brown. *"Application of an Electric Boosting System to an Small, Four-Cylinder S.I. Engine"*. SAE Technical Paper 2003-32-0039, 2003. (Cit. on p. 62).

[257] A.T.C. Patterson, R.J. Tett, and J. McGuire. *"Exhaust Heat Recovery Using Electro-Turbogenerator"*. SAE Technical Paper 2009-01-1604, 2009. (Cit. on p. 91).

[269] F. Pfluger. *"Regulated Two-Stage Turbocharging - KKK's New Charging System for Commercial Diesel Engines"*. IMechE 6$^{\text{th}}$ International Conference on Turbocharging and Air Management Systems, C554/035/98, London, 1998. (Cit. on pp. 27, 29, 30).

[273] A. Plianos and R. Stobart. *"Modeling and Control of Diesel Engines Equipped with a Two-Stage Turbo-System"*. SAE Technical Paper 2008-01-1018, 2008. (Cit. on pp. 29, 35, 127).

[274] P. Podevin and M. Toussaint. *"Techniques Avancée de Suralimentation: le Turbocompresseur"*. 5ème Cycle de Conférence Utilisation Rationnelle de l'Energie dans les Moteurs, Paris, 2004. (Cit. on p. 57).

[275] J. Portalier, J. Blanc, F. Garnier, N. Hoffmann, N. Schorn, H. Kindl, J. Galindo, D. Jeckel, P. Uhl, and J. Laissus. *"Twin Turbo Boosting System Design for the New Generation of PSA 2.2-liter HDI Diesel Engines"*. THIESEL Conference on Thermo-and Fluid Dynamic Processes in Diesel Engines, Valencia, 2006. (Cit. on pp. 23, 24).

[278] Z. Ren, T. Campbell, and J. Yang. *"Theoretical and Experimental Study on the Performance of a Sequentially Turbocharged Diesel Engine"*. IMechE 6th International Conference on Turbocharging and Air Management Systems, C554/010/98, London, 1998. (Cit. on p. 23).

[280] B.J. Roback, M.R. Holl, M.L. Eble, and D. Thornton. *"Supercharging Ford's 4.6L for Affordable Performance"*. SAE Technical Paper 2003-01-3209, 2003. (Cit. on p. 44).

[281] C. Rodgers. *"Centrifugal Compressor Inlet Guide Vanes for Increased Surge Margin"*. ASME Journal of Turbomachinery, Vol. 113, No. 4, pp. 696-702, 1991. (Cit. on pp. 65, 68).

[282] C. Rodgers. *"Impeller Stalling as Influenced by Diffusion Limitations"*. ASME Journal of Fluids Engineering, Vol. 99, No. 1, pp. 84-94, 1977. (Cit. on pp. 65, 68).

[284] O. Ryder, H. Sutter, and L. Jaeger. *"The Design and Testing of an Electrically Assisted Turbocharger for Heavy Duty Diesel Engines"*. IMechE 8th International Conference on Turbochargers and Turbocharging, pp. 157-166, London, 2006. (Cit. on pp. 59, 90).

[285] H. Sammons and E. Chatterton. *"The Napier Nomad Aircraft Diesel Engine"*. SAE Transactions, Vol. 63, No. 107, 1955. (Cit. on p. 82).

[286] M. Sandford, G. Page, and P. Crawford. *"The All New AJV8"*. SAE Technical Paper 2009-01-1060, 2009. (Cit. on p. 43).

[287] R. Sauerstein, R. Dabrowski, M. Becker, and W. Bullmer. *"Regulated Two-Stage Turbocharging for Gasoline Engines"*. Borg Warner Turbo Systems Knowledge Library, 2010. (Cit. on pp. 31, 32, 34).

[288] S. Saulnier and S. Guilain. *"Computational Study of Diesel Engine Downsizing Using Two-Stage Turbocharging"*. SAE Technical Paper 2004-01-0929, 2004. (Cit. on pp. 30, 136).

[290] F. Schmitt and B. Engels. *"Regulated 2-Stage (R2S) Charging System for High Specific Power Engines"*. Congres Le Diesel: aujourd'hui et demain, Ecole Centrale, Lyon, 2004. (Cit. on pp. 28, 30, 34, 36).

[291] T.N. Schmitz, K.D. Holloh, R. Juergens, and G. Fleckenstein. *"Potential of Additional Mechanical Supercharging for Commercial Vehicle Engines"*. SAE Technical Paper 942268, 1994. (Cit. on pp. 42, 49–51).

[292] N. Schorn, E. Karvounis, U. Späder, H. Schulte, D. Jeckel, P. Barthelet, P. Cancalon, O. Salvat, J. Portalier, and J. Minichetti. *"Boosting Systems for Next Generation Passenger Car Diesel Engines - What Systems Will Complement VNT Technology?"* Aufladetechnische Konferenz, Dresden, 2004. (Cit. on pp. 18, 20, 21).

[293] M. Schwaderlapp, K. Habermann, and K. Yapici. *"Variable Compression Ratio - A Design Solution for Fuel Economy Concepts"*. SAE Technical Paper 2002-01-1103, 2002. (Cit. on p. 55).

[297] J.R. Serrano, F.J. Arnau, V. Dolz, A. Tisiera, M. Lejeune, and N. Auffret. *"Analysis of the Capabilities of a Two-Stage Turbocharging System to Fulfill the US2007 Anti-Pollution Directive for Heavy Duty Diesel Engines"*. International Journal of Automobile Technology, Vol. 9, No. 3, pp. 227-288, 2008. (Cit. on pp. 28, 37, 39, 125).

[302] S.M. Shahed. *"An Analysis of Assisted Turbocharging with Light Hybrid Powertrain"*. SAE Technical Paper 2006-01-0019, 2006. (Cit. on p. 56).

[303] S.M. Shahed. *"Smart Boosting Systems e-Turbo and e-Charger: New Frontier?"*. Diesel Engine Emissions Reduction Conference, Pasadena, 2001. (Cit. on p. 57).

[304] S.M. Shahed, C. Middlemass, and C. Balis. *"Design & Development of e-Turbo for SUV and Light Truck Applications"*. Diesel Engine Emissions Reduction Conference, Newport, 2003. (Cit. on pp. 59, 89).

[305] H. Simon, T. Wallmann, and T. Monk. *"Improvements in Performance Characteristics of Single-Stage and Multi-Stage Centrifugal Compressors by Simultaneous Adjustments of Inlet Guide Vanes and Diffuser Vanes"*. ASME Journal of Turbomachinery, Vol. 109, No. 1, pp. 41-47, 1987. (Cit. on pp. 65, 68).

[307] D.A. Singer. *"Comparison of a Supercharger vs. a Turbocharger in a Small Displacement Gasoline Engine Application"*. SAE Technical Paper 850244, 1985. (Cit. on p. 44).

[308] W.L. Soong, G.B. Kliman, R.N. Johnson, R.A. White, and J.E. Miller. *"Novel High-Speed Induction Motor for a Commercial Centrifugal Compressor"*. IEEE Transactions on Industry Applications, Vol. 36, pp. 706-713., 2000. (Cit. on p. 58).

[310] E. Spooner and J.R. Bumby. *"Solid-Rotor Axial-Flux Motors for Very High Speed Drives"*. International Conference on Electrical Machines, Vol. 12, Cracow, 2005. (Cit. on p. 58).

[311] A. Stanciu, C. Stan, and J. Beier. *"Adaptation of a Compact High Speed SI Engine for Supercharging in Base of Numerical Simulation"*. SAE Technical Paper 2006-01-1005, 2006. (Cit. on p. 44).

[312] J.H. Stang. *"Designing Adiabatic Components for Diesel Engine"*. SAE Technical Paper 780069, 1978. (Cit. on p. 87).

[313] N. Stosic, I.K. Smith, and A. Kovacevic. *"Optimisation of Screw Compressors"*. Applied Thermal Engineering, Vol. 23, pp. 1177-1195, 2003. (Cit. on p. 42).

[314] N. Stosic, I.K. Smith, A. Kovacevic, and E. Mujic. *"Geometry of Screw Compressor Rotors and their Tools"*. Centre for Positive Displacement Compressors, City University London, 2006. (Cit. on p. 42).

[315] P. Sweetlang and F. Schmitt. *"Regulated 2-Stage (R2S) Charging Systems for Future Diesel Applications"*. Borg Warner Turbo Systems Knowledge Library, 2004. (Cit. on pp. 30, 34).

[316] S. Takabe. *"Second Generation Lysholm Compressor"*. SAE Technical Paper 980774, 1998. (Cit. on pp. 42, 43, 50, 51).

[317] S. Takabe, K. Hatamura, H. Kanesaka, H. Kurata, Y. Iguchi, and H. Matsubara. *"Development of the High Performance Lysholm Compressor for Automotive Use"*. SAE Technical Paper 940843, 1994. (Cit. on p. 43).

[318] T. Taketomi, K. Kotani, M. Aoki, Y. Ogawa, and K. Hasegawa. *"Development of High-Performance TRE Turbo-Compressor"*. IHI Engineering Review, Vol. 36, No. 3, 2003. (Cit. on p. 68).

[319] H. Tange, N. Ikeya, M. Takanashi, and T. Hokari. *"Variable Geometry Diffuser of Turbocharger Compressor for Passenger Vehicles"*. SAE Technical Paper 2003-01-0051, 2003. (Cit. on pp. 78, 79, 81).

[320] X. Tauzia, J. Hetet, P. Chesse, G. Grosshans, and L. Mouillard. *"Computer Aided Study of the Transient Performances of a Highly Rated Sequentially Turbo-Charged Marine Diesel Engine"*. Proceedings of the Institution of Mechanical Engineers Part A: Journal of Power and Energy, Vol. 212, pp. 185-196, 1998. (Cit. on p. 23).

[321] D.H.W. Tennant and B.E. Walsham. *"The Turbocompound Diesel Engine"*. SAE Technical Paper 890647, 1989. (Cit. on pp. 85, 87).

[322] D.W.H. Tennant. *"A Compact Two-Stage Turbocharger Module"*. IMechE 4^{th} International Conference on Turbocharging and Air Management Systems, C405/042/90, London, 1990. (Cit. on p. 26).

[325] T. Tomita, N. Ikeya, D. Ishihara, N. Kondoh, and A. Ohkita. *"Hybrid Charging System for Heavy Duty Diesel Engines"*. SAE Technical Paper 910419, 1991. (Cit. on p. 49).

[329] M. Toussaint and P. Podevin. *"Guide-Vanes Upstream the Impeller of Centrifugal Compressor"*. Conservatoire National des arts et Métiers, Chaire de turbomachines, 2005. (Cit. on pp. 65, 68, 73).

[330] H. Uchida. *"Transient Performance Prediction for Turbocharging Systems Incorporating Variable Geometry Turbochargers"*. Toyota R&D Review, Vol. 41, No. 3, pp. 22-28, 2006. (Cit. on p. 77).

[331] H. Uchida. *"Trend of Turbocharging Technologies"*. Toyota R&D Review, Vol. 41, No. 3, pp.1-8, 2006. (Cit. on pp. 55, 81).

[332] H. Uchida, A. Kashimoto, and Y. Iwakiri. *"Development of Wide Flow Range Compressor with Variable Inlet Guide Vane"*. Toyota R&D Review, Vol. 41, No. 3, pp. 9-14, 2006. (Cit. on pp. 74, 77).

[333] N. Ueda, N. Matsuda, M. Kamata, H. Sakai, and H. Kanesaka. *"Proposal of New Supercharging System for Heavy Duty Vehicular Diesel and Simulation Results of Transient Characteristics"*. SAE Technical Paper 2001-01-0277, 2001. (Cit. on p. 51).

[334] L.H. Uthoff and J.W. Yakimow. *"A Development of the Eaton Supercharger"*. SAE Technical Paper 870355, 1987. (Cit. on p. 44).

[335] J. Vetrovec. *"Fluid-Dynamic Supercharger"*. SAE Technical Paper 2008-01-0299, 2008. (Cit. on pp. 93, 94).

[336] J. Villegas, B. Gao, K. Svancara, W. Thornton, and J. Parra. *"Real-Time Engine Modelling for Engine Downsizing Using an Electric Supercharger"*. 13$^{\text{th}}$ EAEC European Automotive Congress, Valencia, 2011. (Cit. on p. 63).

[338] C.T. Vuk. *"Electric Turbo Compounding... A Technology Who's Time Has Come"*. Diesel Engine Emissions Reduction Conference, Chicago, 2005. (Cit. on pp. 90, 91).

[339] C.T. Vuk. *"Electric Turbo Compounding... A Technology Who's Time Has Come"*. Diesel Engine Emissions Reduction Conference, Detroit, 2006. (Cit. on p. 91).

[340] F.J. Wallace. *"The Ultimate Performance Potential of Compounded Diesel Engines for Heavy Vehicles"*. IMechE 4$^{\text{th}}$ International Conference of Turbocharging and Turbochargers, pp. 253-270, London, 1990. (Cit. on pp. 84, 85).

[342] R. Walling. *"Eaton TVS Supercharged for Downsizing"*. Engine Expo, Stuttgart, 2009. (Cit. on p. 43).

[343] B.E. Walsham. *"Alternative Turbocharger Systems for the Automotive Diesel Engine"*. IMechE 4$^{\text{th}}$ International Conference of Turbocharging and Turbochargers, pp. 39-50, London, 1990. (Cit. on pp. 84, 85).

[344] H. Wang, R. Glover, and J. Koval. *"Analytical and Experimental Study on Gear Rattle in Supercharger"*. SAE Technical Paper 2005-01-2369, 2005. (Cit. on pp. 43, 44).

[345] E. Watel, A. Pagot, P. Pacaud, and J.C. Schmitt. *"Matching and Evaluating Methods for Euro 6 and Efficient Two-Stage Turbocharging Diesel Engine"*. SAE Technical Paper 2010-01-1229, 2010. (Cit. on pp. 34, 37, 39, 253).

[347] N. Watson and K. Banisoleiman. *"Performance of the Highly Rated Diesel Engine with a Variable Geometry Turbocharger"*. IMechE 3$^{\text{th}}$ International Conference on Turbocharging and Turbochargers, C121/86, London, 1986. (Cit. on p. 18).

[348] N. Watson and S. Janota. *"Turbocharging the Internal Combustion Engine"*. London: McMillan Publishers Ltd. ISBN 0-333-24290-4, 1982. (Cit. on pp. 10, 18, 55, 117, 153, 158).

[349] N. Watson, N.P. Kyrtatos, and K. Holmes. *"The Performance Potential of Limited Cooled Diesel Engines"*. Proceedings of the Institution of Mechanical Engineers Part A: Journal of Power and Energy, Vol. 197, No.3, pp. 197-207, 1983. (Cit. on p. 86).

[352] S. Wedowski, S. Glück, R. Sauerstein, F. Schmitt, M. Westermaier, D. Oh, C. Schernus, and M. Subramaniam. *"Vehicle Demonstrator with 2-Stage Turbo SI engine - Simulation Based Layout of the GT2 Engine"*. GT-SUITE Conferences, Frankfurt, 2009. (Cit. on pp. 30–34, 36).

[353] W.M.S.R. Weerasinghe, R.K. Stobart, and S.M. Hounsham. *"Thermal Efficiency Improvement in High Output Diesel Engines a Comparison of a Rankine Cycle with Turbo-Compounding"*. Applied Thermal Engineering, Vol. 30, pp. 2253-2256, 2010. (Cit. on p. 81).

[354] F. Westin and R. Burenius. *"Measurement of Interstage Losses of a Two-Stage Turbocharger System in a Turbocharger Test Rig"*. SAE Technical Paper 2010-01-1221, 2010. (Cit. on p. 36).

[355] A. Whitfield and A.H. Abdullah. *"The Performance of a Centrifugal Compressor with High Inlet Prewhirl"*. ASME Journal of turbomachinery, Vol. 120, pp. 487-493, 1998. (Cit. on pp. 66–68).

[356] A. Whitfield, M.D.C. Doyle, and M.R. Firth. *"Design and Performance of a High Pressure Ratio Turbocharger Compressor: Part 1 Design Considerations"*. Proceedings of the Institution of Mechanical Engineers Part A: Journal of Power and Energy, Vol. 207, No. 2, pp. 115-124, 1993. (Cit. on pp. 65, 68).

[357] A. Whitfield, M.D.C. Doyle, and M.R. Firth. *"Design and Performance of a High Pressure Ratio Turbocharger Compressor: Part 2 Experimental Performance"*. Proceedings of the Institution of Mechanical Engineers Part A: Journal of Power and Energy, Vol. 207, No. 2, pp. 125-131, 1993. (Cit. on pp. 65, 68).

[358] A. Whitfield and A.J. Sutton. *"The Effect of Vaneless Diffuser Geometry on the Surge Margin of Turbocharger Compressors"*. Proceedings of the Institution of Mechanical Engineers Part D: Journal of Automobile Engineering, Vol. 203, No. 2, pp. 91-98, 1989. (Cit. on p. 78).

[359] A. Whitfield, A.J. Sutton, and H.J. Leonard. *"The Development of Turbocharger Compressors with Improved Surge Margin"*. IMechE 4^{th} International Conference on Turbocharging and Air Management Systems, C433/063/90, London, 1990. (Cit. on pp. 66, 78, 79).

[360] A. Whitfield, F.J. Wallace, and R.C. Atkey. *"Experimental and Theoretical Performance of a Radial Flow Turbocharger Compressor with Inlet Prewhirl"*. Proceedings of the Institution of Mechanical Engineers, Vol. 189, No. 1, pp. 177-186, 1975. (Cit. on pp. 65, 68).

[361] A. Whitfield, F.J. Wallace, and R.C. Atkey. *"The Effect of Variable Geometry on the Operating Range and Surge Margin of a Centrifugal Compressor"*. ASME paper 76-GT-98, 1976. (Cit. on p. 78).

[363] P.R. Williams. *"An Examination of the Methods Used to Vary the Output of Centrifugal Compressors with Particular Reference to Part-Load Efficiency"*. IMechE European Conference on Developments in Industrial Compressors, London, 1989. (Cit. on pp. 65, 68).

[364] D.E. Wilson. *"The design of a Low Specific Fuel Consumption Turbocompound Engine"*. SAE Technical Paper 860072, 1986. (Cit. on p. 87).

[365] N. Winkler and H.E. Angström. *"Simulations and Measurements of a Two-Stage Turbocharged Heavy-Duty Diesel Engine Including EGR in Transient Operation"*. SAE Technical Paper 2008-01-0539, 2008. (Cit. on pp. 28, 29, 33, 37, 39, 116).

[371] Y.R. Wu and Z.H. Fong. *"Improved Rotor Profiling Based on the Arbitrary Sealing Line for Twin Screw Compressors"*. Mechanism and Machine Theory, Vol. 43, pp. 695-711, 2008. (Cit. on p. 42).

[372] Y.R. Wu and Z.H. Fong. *"Optimization Design of an Explicitly Defined Rack for the Generation of Rotors for Twin Screw Compressors"*. Mechanism and Machine Theory, Vol. 44, pp. 66-82, 2009. (Cit. on p. 42).

[374] J. Xiao, C. Gu, X. Shu, and C. Gao. *"Performance Analysis of a Centrifugal Compressor with Variable Inlet Guide Vanes"*. Frontiers of Energy and Power Engineering in China, Vol. 1, No. 4, pp. 473-476, 2007. (Cit. on pp. 68, 70).

[375] Y. Yamashita, S. Ibaraki, and H. Ogita. *"Development of Electrically Assisted Turbocharger for Diesel Engine"*. IMechE 8^{th} International Conference on Turbochargers and Turbocharging, pp. 147-155, London, 2006. (Cit. on p. 60).

[376] H. Zhang and M. Bailey. *"Electrically Assisted Turbo-Charger Development for Performance and Emissions"*. Diesel Engine Emissions Reduction Conference, San Diego, 2000. (Cit. on p. 58).

Chapter 3

Analytical study of two-stage turbocharging performance

Contents

3.1 Introduction **116**
3.2 Governing Equations **116**
3.3 Main Variables Influences on Two-Stage Architectures . . . **126**
3.4 Conclusions **135**
References **137**

3.1 Introduction

MULTISTAGE charging systems are much more complex than conventional single-stage configurations. They present an important number of parameters and a lot of interactions exist between their different elements. The coupling of these advanced boosting architectures with an engine is therefore a difficult task that requires a good understanding of their main performance contribution factors. To study these factors and obtain clear design criteria, an analytical analysis aimed to determine optimum two-stage architectures as a function of basic engine and turbocharging system parameters has been performed in this chapter.

The analytical approach is very useful for two main reasons. First by keeping an analytical solution it is possible to check the influence of different variables independently. This cannot be undertaken with the other computer simulations approaches as wave action models [119, 337, 365] or physics-based thermodynamic zero-dimensional models [74, 196, 373]. In fact, these models predict turbocharger performance directly from manufacturer's characteristic maps which inherit relationships between turbomachines sizes and efficiencies [228, 242]. They are thus more adapted in a second stage of the development process when turbochargers and engine architectures are defined. Then by analytical models, simulations have been performed faster and with reasonable accuracy, which is important when numerous calculations are needed for having an overview of multivariable problems like two-stage systems for a given downsized engine application. Similar analytical model has also been developed in the past by Zinner [378] for single stage turbocharging.

3.2 Governing Equations

Sequential serial two-stage architectures are composed by a High-Pressure (HP) and Low Pressure (LP) turbochargers. The HP turbocharger is small with reduced inertia to achieve fast transient response at low speeds while the LP one is large and optimized for maximum power output operation. The addition of an extra intercooler between both compressors is used to reduce HP compressor inlet temperature and improve overall system efficiency. Both turbines are controlled through variable nozzle area or wastegate valves. Architecture and flow evolution through this boosting system are shown in

figure 3.1 with the corresponding nomenclature that will be used in the thesis for each characteristic points. On one hand the evolution in the LP compressor goes from 01 to 012 and the evolution in the LP turbine goes from 034 to 04, and on the other hand the evolution in the HP compressor goes from 012' to 02 and the evolution in the HP turbine goes from 03 to 034. The evolution in the intercooler between compressors goes from 012 to 012'. The objective of the analytical model is to relate the compression ratios c_r with the expansion ratios e_r for a given operating condition.

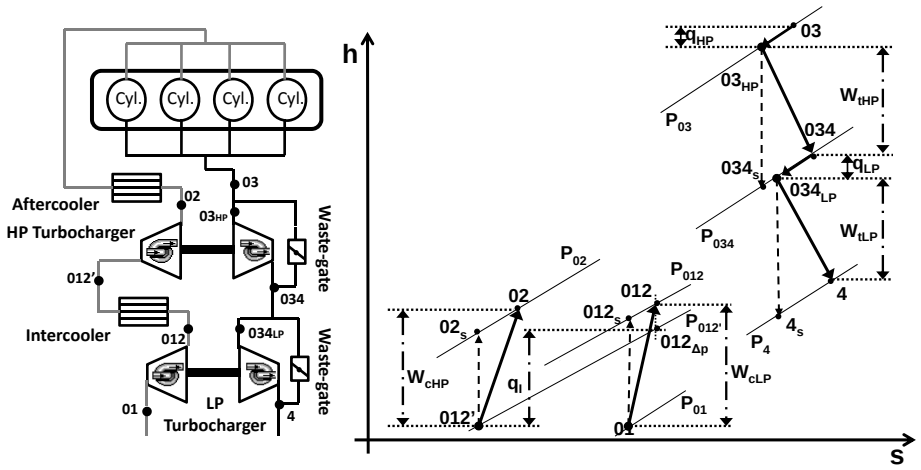

Figure 3.1: Architecture and thermodynamic evolutions of a two-stage turbochargers configuration.

3.2.1 Relation between Compression and Expansion Ratio

The compression ratio of a two-stage configuration is the product of the two elemental compression ratios developed by the HP and LP compressors, taking into account the pressure drop in the intercooler due to internal friction losses. The compression ratio is generally associated with the energy needed by the compressor to obtain a specific pressure increase. With respect to the LP (Eq.3.1) and HP (Eq.3.2) compressors, the expressions for compressors powers [348] are:

$$\dot{W}_{cLP} = \frac{\dot{m}_c C_{pc} T_{01}}{\eta_{cLP}} \left(\left(\frac{P_{012}}{P_{01}} \right)^{\frac{\gamma_c - 1}{\gamma_c}} - 1 \right) = \frac{\dot{m}_c C_{pc} T_{01}}{\eta_{cLP}} \left((c_{rLP})^{\frac{\gamma_c - 1}{\gamma_c}} - 1 \right)$$
$$= \dot{m}_c C_{pc} T_{01} \mathbb{Z}_{cLP} \tag{3.1}$$

$$\dot{W}_{cHP} = \frac{\dot{m}_c C_{pc} T_{012'}}{\eta_{cHP}} \left(\left(\frac{P_{02}}{P_{012'}} \right)^{\frac{\gamma_c - 1}{\gamma_c}} - 1 \right) = \frac{\dot{m}_c C_{pc} T_{012'}}{\eta_{cHP}} \left((c_{rHP})^{\frac{\gamma_c - 1}{\gamma_c}} - 1 \right)$$
$$= \dot{m}_c C_{pc} T_{012'} \mathbb{Z}_{cHP} \tag{3.2}$$

Assuming turbulent pressure drop in the intercooler, it can be written:

$$P_{012} - P_{012'} = \frac{1}{2} \kappa \rho_{012} v_{012}^2 = \frac{1}{2} \kappa \frac{\dot{m}_c^2}{\rho_{012} A_{012}^2} \tag{3.3}$$

Therefore $P_{012'}$ can be calculated as a function of mass flow, P_{012} and T_{012}:

$$P_{012'} = P_{012} - \dot{m}_c^2 \frac{\kappa \Re T_{012}}{2 P_{012} A_{012}^2} \tag{3.4}$$

The temperature downstream the LP compressor (T_{012}) can be expressed in terms of isentropic efficiency as:

$$\eta_{cLP} = \frac{T_{012s} - T_{01}}{T_{012} - T_{01}} \rightarrow T_{012} = T_{01} \left[1 + \frac{1}{\eta_{cLP}} \left({c_{rLP}}^{\frac{\gamma_c - 1}{\gamma_c}} - 1 \right) \right]$$
$$= T_{01} \left[1 + \mathbb{Z}_{cLP} \right] \tag{3.5}$$

The intercooler modifies the fluid thermodynamic properties upstream the HP compressor. The air mass flow is cooled and the temperature decrease depends on the intercooler efficiency (ε) and the cooling fluid temperature (T_{H_2O}).

$$\varepsilon = \frac{T_{012} - T_{012'}}{T_{012} - T_{H_2O}} \rightarrow T_{012'} = T_{012} \left(1 - \varepsilon \right) + \varepsilon \cdot T_{H_2O} \tag{3.6}$$

Rearranging Eq.3.2 with Eq.3.5 and Eq.3.6, one obtains:

$$\dot{W}_{cHP} = \dot{m}_c C_{pc} \mathbb{Z}_{cHP} T_{01} \left(\left[1 + \mathbb{Z}_{cLP} \right] \left(1 - \varepsilon \right) + \varepsilon \frac{T_{H_2O}}{T_{01}} \right) \tag{3.7}$$

By the same token, the expansion ratio of a two-stage configuration is the product of the two elemental expansion ratios developed by the HP and LP

turbines. These expansion ratios are generally the consequence of the energy required by the turbines to produce and transfer the necessary work to the compressors. With respect to HP (Eq.3.8) and LP (Eq.3.9) turbines, the expressions of turbine power are:

$$\dot{W}_{tHP} = \dot{m}_t C_{pt} \Gamma_{03_{HP}} \eta_{tHP} \left(1 - (e_{rHP})^{\frac{1-\gamma_t}{\gamma_t}}\right) = \dot{m}_t C_{pt} \Gamma_{03_{HP}} \mathbb{Z}_{tHP} \tag{3.8}$$

$$\dot{W}_{tLP} = \dot{m}_t C_{pt} \Gamma_{034_{LP}} \eta_{tLP} \left(1 - (e_{rLP})^{\frac{1-\gamma_t}{\gamma_t}}\right) = \dot{m}_t C_{pt} \Gamma_{034_{LP}} \mathbb{Z}_{tLP} \tag{3.9}$$

where e_{rHP} and e_{rLP} are the expansion ratio in the HP and LP turbine respectively defined as:

$$e_{rHP} = \frac{P_{03}}{P_{034}} \quad and \quad e_{rLP} = \frac{P_{034}}{P_4} \tag{3.10}$$

In addition, $\Gamma_{03_{HP}}$ and $\Gamma_{034_{LP}}$ are the turbine inlet temperatures considering heat losses (q) before gas expansion, as figure 3.1 shows. $\Gamma_{03_{HP}}$ and $\Gamma_{034_{LP}}$ are defined as:

$$\Gamma_{03_{HP}} = T_{03} - \frac{q_{HP}}{C_{pt}} \tag{3.11}$$

$$\Gamma_{034_{LP}} = T_{034} - \frac{q_{LP}}{C_{pt}} \tag{3.12}$$

The isentropic efficiency of the HP turbine can be expressed in terms of temperature, therefore gas temperature at its outlet can be written as:

$$\begin{aligned} \eta_{tHP} = \frac{\Gamma_{03_{HP}} - T_{034}}{\Gamma_{03_{HP}} - T_{034s}} \rightarrow T_{034} &= \Gamma_{03_{HP}} \left[1 - \eta_{tHP} \left(1 - (e_{rHP})^{\frac{1-\gamma_t}{\gamma_t}}\right)\right] \\ &= \Gamma_{03_{HP}} \left[1 - \mathbb{Z}_{tHP}\right] \end{aligned} \tag{3.13}$$

Total to total efficiency has been used since kinetic energy is further recovered by the LP turbine. Rearranging Eq.3.9 with Eq.3.13, one obtains equation

Eq.3.15 where it is clear the effect of heat losses and HP turbine expansion in the temperature upstream LP turbine ($\Gamma_{034_{LP}}$).

$$\begin{aligned}\dot{W}_{tLP} = \dot{m}_t C_{pt} \Gamma_{034_{LP}} \mathbb{Z}_{tLP} &= \dot{m}_t C_{pt} \left(T_{034} - \frac{q_{LP}}{C_{pt}} \right) \mathbb{Z}_{tLP} \\ &= \dot{m}_t C_{pt} \left(\left[T_{03} - \frac{q_{HP}}{C_{pt}} \right] \left[1 - \mathbb{Z}_{tHP} \right] - \frac{q_{LP}}{C_{pt}} \right) \mathbb{Z}_{tLP}\end{aligned} \tag{3.14}$$

In the equilibrium and considering mechanical losses included in turbine efficiencies, compressor and turbine power must be equal individually in each turbocharger. Indeed, equaling Eq.3.8 to Eq.3.7 for the HP turbocharger and Eq.3.15 to Eq.3.1 for the LP turbocharger we could write:

$$\begin{aligned}\dot{W}_{tHP} &= \dot{m}_t C_{pt} \Gamma_{03_{HP}} \mathbb{Z}_{tHP} \\ &= \dot{m}_c C_{pc} \mathbb{Z}_{cHP} T_{01} \left(\left[1 + \mathbb{Z}_{cLP} \right] (1 - \varepsilon) + \varepsilon \cdot \frac{T_{H_2O}}{T_{01}} \right) = \dot{W}_{cHP}\end{aligned} \tag{3.15}$$

$$\dot{W}_{tLP} = \dot{m}_t C_{pt} \Gamma_{03_{LP}} \left[1 - \mathbb{Z}_{tHP} \right] \mathbb{Z}_{tLP} = \dot{m}_c C_{pc} T_{01} \mathbb{Z}_{cLP} = \dot{W}_{cLP} \tag{3.16}$$

where $\Gamma_{03_{LP}}$ is defined as:

$$\Gamma_{03_{LP}} = \Gamma_{03_{HP}} \left[1 - \frac{q_{LP}}{\Gamma_{03_{HP}} C_{pt} \left[1 - \mathbb{Z}_{tHP} \right]} \right] \tag{3.17}$$

and $\Gamma_{03_{LP}}$ is equal to $\Gamma_{03_{HP}}$ when $q_{LP} = 0$.

Taking into account the fuel-to-air ratio (F) to relate the burnt gas mass flow with the air mass flow, the following expression can be obtained:

$$\frac{\dot{m}_t}{\dot{m}_c} = (1 + F) \tag{3.18}$$

We define K as the quotient between the different specific heat of burnt gas and fresh air:

$$\frac{C_{pt}}{C_{pc}} = K \tag{3.19}$$

Replacing the definitions of Eq.3.18 and Eq.3.19 in Eq.3.15 and Eq.3.16 and rearranging both equations one obtains the compression ratio groups as a function of the expansion ratio as follows:

$$\begin{aligned}\mathbb{Z}_{cLP} &= (1+F)K\frac{\Gamma_{03_{LP}}}{T_{01}}\mathbb{Z}_{tLP}\left[1-\mathbb{Z}_{tHP}\right] \\ &= (1+F)K\frac{\Gamma_{03_{HP}}}{T_{01}}\mathbb{Z}_{tLP}\left[1-\mathbb{Z}_{tHP}-\frac{q_{LP}}{\Gamma_{03_{HP}}C_{pt}}\right]\end{aligned} \tag{3.20}$$

$$\mathbb{Z}_{cHP} = (1+F)\,K\frac{\Gamma_{03_{HP}}}{T_{01}}\frac{\mathbb{Z}_{tHP}}{\left[1+\mathbb{Z}_{cLP}\right](1-\varepsilon)+\varepsilon\frac{T_{H_2O}}{T_{01}}} \tag{3.21}$$

The lower are the heat losses q_{HP} and q_{LP} the higher would be $\Gamma_{03_{HP}}$ and $\Gamma_{03_{LP}}$ respectively. As a consequence, $\mathbb{Z}_{cHP}$ and $\mathbb{Z}_{cLP}$ would increase while keeping constant HP and LP turbines expansion ratio (and the rest of parameters). From Eq.3.21, it can also be observed the effect of the inter-cooling. In fact, the lower is the cooling fluid temperature for a given intercooler efficiency the higher would be the compression ratio for a given expansion ratio. The effect of inter-cooling efficiency is clearer if we make a simple hypothesis assuming that cooling fluid temperature is equal to ambient temperature ($T_{H_2O} = T_{01}$). Then Eq.3.21 can be written as follows:

$$\mathbb{Z}_{cHP} = (1+F)\,K\frac{\Gamma_{03_{HP}}}{T_{01}}\frac{\mathbb{Z}_{tHP}}{1+\mathbb{Z}_{cLP}(1-\varepsilon)} \tag{3.22}$$

Looking at Eq.3.22, it is clear that the higher is ε the higher is $\mathbb{Z}_{cHP}$ for a given expansion ratio.

In order to make evident the effect of the turbochargers isentropic efficiency in the equations, $\mathbb{Z}$ groups can be written as a function of efficiency and the corresponding expansion or compression ratio as appear in Eq.3.23.

$$\mathbb{Z}_{cLP} = \frac{1}{\eta_{cLP}}\left(\left(c_{rLP}\right)^{\frac{\gamma_c-1}{\gamma_c}}-1\right) = \frac{1}{\eta_{cLP}}\left(\mathbb{R}_{cLP}-1\right)$$

$$\mathbb{Z}_{tLP} = \eta_{tLP}\left(1-\frac{1}{\left(e_{rLP}\right)^{\frac{\gamma_t-1}{\gamma_t}}}\right) = \eta_{tLP}\left(1-\mathbb{R}_{tLP}\right)$$

$$\mathbb{Z}_{cHP} = \frac{1}{\eta_{cHP}} \left((c_{rHP})^{\frac{\gamma_c - 1}{\gamma_c}} - 1 \right) = \frac{1}{\eta_{cHP}} \left(\mathbb{R}_{cHP} - 1 \right)$$

$$\mathbb{Z}_{tHP} = \eta_{tHP} \left(1 - \frac{1}{(e_{rHP})^{\frac{\gamma_t - 1}{\gamma_t}}} \right) = \eta_{tHP} \left(1 - \mathbb{R}_{tHP} \right) \tag{3.23}$$

In Eq.3.23 $\mathbb{R}_{cLP}$ and $\mathbb{R}_{cHP}$ groups' values increase as compression ratio grows. However $\mathbb{R}_{tLP}$ and $\mathbb{R}_{tHP}$ groups' values decrease as expansion ratio grows and the minimum value that can achieve is 0. Substituting Eq.3.23 in Eq.3.20 and Eq.3.21 and rearranging one can write:

$$\mathbb{R}_{cLP} = 1 + \eta_{cLP}\eta_{tLP}(1+F)K\frac{\Gamma_{03_{LP}}}{T_{01}} \left(1 - \mathbb{R}_{tLP} \right) \left[1 - \eta_{tHP} \left(1 - \mathbb{R}_{tHP} \right) \right] \tag{3.24}$$

$$\mathbb{R}_{cHP} = 1 + \eta_{cHP}\eta_{tHP} \left(1 + F \right) K\frac{\Gamma_{03_{HP}}}{T_{01}} \frac{\left(1 - \mathbb{R}_{tHP} \right)}{\left[1 + \eta_{tLP} \left(1 - \mathbb{R}_{tLP} \right) \right] \left(1 - \varepsilon \right) + \varepsilon \frac{T_{H_2O}}{T_{01}}} \tag{3.25}$$

Defining

$$\begin{aligned} \zeta_{LP} &= \eta_{cLP}\eta_{tLP}(1+F)K\frac{\Gamma_{03_{LP}}}{T_{01}} \quad \textit{and} \\ \zeta_{HP} &= \eta_{cHP}\eta_{tHP} \left(1 + F \right) K\frac{\Gamma_{03_{HP}}}{T_{01}} \end{aligned} \tag{3.26}$$

It can be concluded that the higher are the temperatures ratio and turbochargers efficiencies, the higher are the ζ groups. In addition, it is worth noting that $K \approx 1$ and also $(1+F) \approx 1$. Substituting Eq.3.26 in Eq.3.24 and Eq.3.25, the compression ratio for each turbocharger can be expressed as:

$$\mathbb{R}_{cLP} = 1 + \zeta_{LP} \left(1 - \mathbb{R}_{tLP} \right) \left[1 - \eta_{tHP} \left(1 - \mathbb{R}_{tHP} \right) \right] \tag{3.27}$$

$$\mathbb{R}_{cHP} = 1 + \zeta_{HP} \frac{\left(1 - \mathbb{R}_{tHP} \right)}{\left[1 + \eta_{tLP} \left(1 - \mathbb{R}_{tLP} \right) \right] \left(1 - \varepsilon \right) + \varepsilon \frac{T_{H_2O}}{T_{01}}} \tag{3.28}$$

The analysis of a two-stage turbochargers configuration can be described from two different points of view. In fact, the product of Eq.3.27 by Eq.3.28 defines the global compression ratio as a function of the different expansion ratios known in the turbines. So, it can be evaluated the maximum intake manifold pressure for a certain energy and exhaust pressure upstream the HP turbine. But, it is sometimes more convenient in the design process to evaluate the minimum back pressure cost to obtain a certain compression ratio. In the latter case, Eq.3.27 and Eq.3.28 must be rewritten to express the expansion ratio in function of compression ratio. For that, Eq.3.20 and Eq.3.21 are rearranged as follows:

$$\mathbb{Z}_{tHP} = \frac{\mathbb{Z}_{cHP}}{(1+F)\,K}\frac{T_{01}}{\Gamma_{03_{HP}}}\left(\left[1+\mathbb{Z}_{cLP}\right](1-\varepsilon)+\varepsilon\cdot\frac{T_{H_2O}}{T_{01}}\right) \tag{3.29}$$

$$\begin{aligned}\mathbb{Z}_{tLP} &= \frac{\mathbb{Z}_{cLP}T_{01}}{(1+F)K\Gamma_{03_{LP}}\left[1-\mathbb{Z}_{tHP}\right]} \\ &= \frac{\mathbb{Z}_{cLP}T_{01}}{(1+F)K\Gamma_{03_{LP}}}\cdot\frac{1}{\left[1-\frac{\mathbb{Z}_{cHP}T_{01}}{(1+F)K\Gamma_{03_{LP}}}\left(\left[1+\mathbb{Z}_{cLP}\right](1-\varepsilon)+\varepsilon\frac{T_{H_2O}}{T_{01}}\right)\right]}\end{aligned} \tag{3.30}$$

Taking into account the definition of the $\mathbb{Z}$ groups shown in Eq. 3.23 and the definitions of ζ_{LP} and ζ_{HP} from Eq.3.26, Eq.3.29 and Eq.3.31 are rearranged as:

$$\mathbb{R}_{tHP} = 1+\frac{(1-\mathbb{R}_{cHP})}{\zeta_{HP}}\left[\left(1+\frac{(\mathbb{R}_{cLP}-1)}{\eta_{cLP}}\right)(1-\varepsilon)+\varepsilon\frac{T_{H_2O}}{T_{01}}\right] \tag{3.31}$$

$$\mathbb{R}_{tLP} = 1+\frac{(1-\mathbb{R}_{cLP})}{\zeta_{LP}\left(1-\frac{\eta_{tHP}(\mathbb{R}_{cHP}-1)}{\zeta_{HP}}\left[\left(1+\frac{(\mathbb{R}_{cLP}-1)}{\eta_{cLP}}\right)(1-\varepsilon)+\varepsilon\frac{T_{H_2O}}{T_{01}}\right]\right)} \tag{3.32}$$

In this way, the relation between expansion ratios and compression ratios is more complex. The different parameters overlap themselves and their particular influences are more difficult to extract and analyze individually. But this form is more natural from a design point of view, especially when boosting system efficiency is the main constraint.

To study the performance of two-stage turbocharging architectures for a given engine and to compare different operating conditions, engine performance parameters have to be defined to easily observe and also quantify the

performance of the whole system. The first parameter used is the ratio between the global compression ratio and the global expansion ratio (Π_c/Π_t). When this term is greater than the unity, turbocharging generates a net positive work on the piston during the engine breathing process; when is lower than the unity, the engine has to produce more work to evacuate the exhaust gases of the combustion chamber than get during breathing fresh one. The second parameter, which is highly related with the previous one, is the Pumping Mean Effective Pressure (PMEP) which quantifies the engine breathing efficiency. It can be represented as the difference between the average pressure upstream the HP turbine (P_{03}) and the average pressure downstream the HP compressor (P_{02}). Using the definition of the global compression ratio by the global expansion ratio, it can be rearranged to give:

$$PMEP = P_{03} - P_{02} = P_{02}\left[\left(\frac{\Pi_t P_4}{\Pi_c P_{01}}\right) - 1\right] \tag{3.33}$$

Therefore PMEP is positive when negative net work is achieved during the gas exchange process. The third parameter used is the brake thermal efficiency (η_e). Its definition is usually based on the Brake Mean Effective Pressure (BMEP) corresponding to the energy transferred from fuel to engine output. The BMEP can be divided in three different terms: the Indicated Mean Effective Pressure (IMEP) corresponding to fuel transformation efficiency, the Pumping Mean Effective Pressure (PMEP) and the Friction plus Auxiliaries Mean Effective Pressure (FAMEP). The addition of PMEP and FAMEP is generally known as engine mechanical losses. The FAMEP corresponds to the mechanical losses generated by friction from the different engine moving parts and the energy consumed by engine auxiliaries such as water or fuel pumps. The expression of the brake thermal efficiency can be written as:

$$\eta_e = \frac{IMEP - FAMEP - PMEP}{\rho_{02} \cdot \eta_v \cdot F \cdot Hc} \tag{3.34}$$

Taking into account the definition of the indicated efficiency (η_i) and assuming for simplicity reasons the hypothesis of FAMEP $\ll \rho_{02} \cdot \eta_v \cdot F \cdot Hc$ (mainly at full load operation) to obtain results independently of engine design and engine speed, the following approximate expression is established:

$$\eta_e = \eta_i - \frac{P_{02}}{\rho_{02} \cdot \eta_v \cdot F \cdot Hc}\left[\left(\frac{\Pi_t P_4}{\Pi_c P_{01}}\right) - 1\right] \tag{3.35}$$

Engine load and speed for a given engine and specific operating conditions could then be introduced in the analysis defining the friction plus auxiliaries efficiency (η_{fa}) as:

$$\eta_{fa} = 1 - \frac{FAMEP}{\rho_{02} \cdot \eta_v \cdot F \cdot Hc} \tag{3.36}$$

3.2.2 Model Validation

A validation process was carried out to assess the analytical model accuracy and reliability. Different operating conditions, corresponding to representative steady state points of the USA anti-pollution directive US2007 [3], were tested on a two-stage turbocharging heavy duty engine. The engine used in this validation was a 12-L displacement Diesel engine and its basics characteristics are shown in table 3.1. The experimental installation as the test campaign were not specifically designed for this model validation and experimental data has only been extracted from other serial two-stage boosting system developments. That is why, a complete description of the experimental installation and measurement methodology is not given in this chapter and is only referred to the works realized by Serrano et al.[122, 297].

Table 3.1: Basic engine characteristics for model validation.

Type of engine	Double-stage turbocharged
Heavy-duty	Diesel engine
Number of cylinders	Six cylinders
Injection system	Unit pump injector
Compression ratio	16:1
Turbocharger	Wastegate HP turbine + LP turbine

A comparison between experimental and simulated results of expansion ratio versus compression ratio in the HP and LP turbines is shown in figure 3.2. Additionally, it can be observed a comparison between measured and predicted total expansion ratio through the turbines. In each case, a good agreement between computed and measured values is obtained with very small differences. These differences can be explained with the inherent experimental uncertainties that present the different sensors used. Turbines efficiencies were calculated from compressor works to include mechanical efficiencies and heat transfer effects. However, small uncertainties in measured inlet and out-

let compressor temperatures can lead to the small errors encountered in the results.

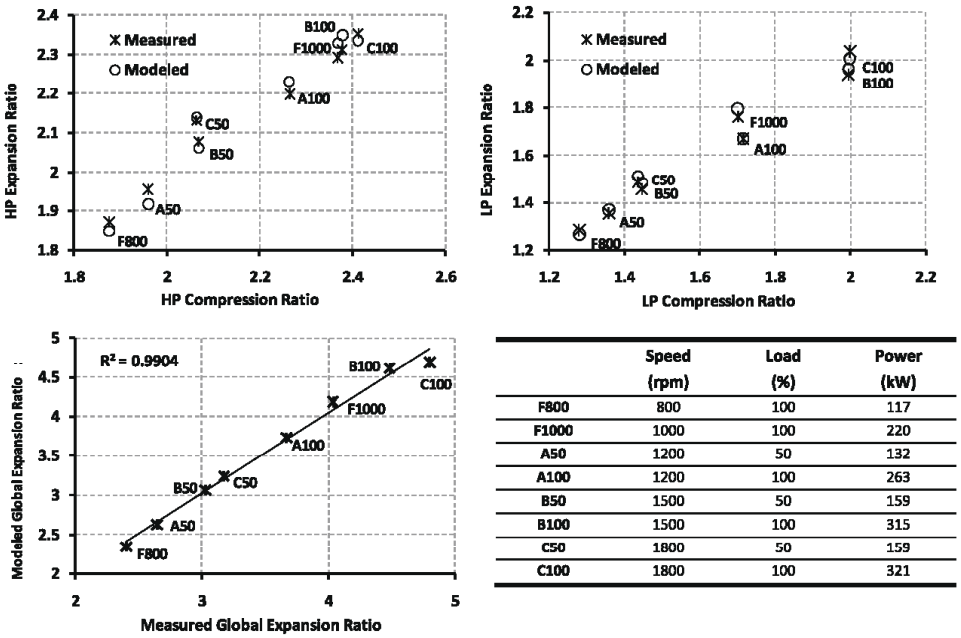

	Speed (rpm)	Load (%)	Power (kW)
F800	800	100	117
F1000	1000	100	220
A50	1200	50	132
A100	1200	100	263
B50	1500	50	159
B100	1500	100	315
C50	1800	50	159
C100	1800	100	321

Figure 3.2: Top: comparison of measured and modeled HP and LP expansion ratio as a function of HP and LP compression ratio - Bottom: comparison of measured and modeled global expansion ratio with a description of the different operating conditions.

3.3 Main Variables Influences on Two-Stage Architectures

First, the different equations were analyzed with constant parameters as shown in table 3.2. Equations were described for two different points of view. On the one hand, the compression ratio is maximized for a given expansion ratio and on the other hand, the expansion ratio is minimized for a given compression ratio. In a matching procedure, the compression ratio appears like a constraint in the engine design process and lot of optimization efforts concern the reduction of the cylinder backpressure. The following results go in the same direction. Equations were solved for different given compression

ratios and expansion ratios were optimized in the HP and LP turbines to minimize the global expansion ratio. A large range of compression ratios were analyzed to obtain general results valid for any applications and to emphasize the trends observed.

Table 3.2: Parameters used for the simulation.

C_{pt}	1209 J/kg/K	F	0.062
C_{pc}	1001 J/kg/K	κ	0
η_{cHP}	0.7 t/t	γ_c	1.402
η_{cLP}	0.7 t/t	γ_t	1.311
η_{fa}	1	q_{HP}	0 J/kg
η_i	0.4	q_{LP}	0 J/kg
η_{tHP}	0.6 t/s	H_c	42.500.000 J/kg
η_{tLP}	0.6 t/s	R	287 J/kg/K
η_v	0.8	T_{01}	298 K
ϵ	0.9	T_{03}	1000 K

3.3.1 HP and LP Expansion Ratio

Expansion ratio distribution between the HP and LP turbines is very important in terms of turbocharging performance. Figure 3.3 shows for different compression ratios the relation between the LP expansion ratio and the engine performance parameters previously described. As LP turbine outlet pressure has been fixed to atmospheric conditions, the LP expansion ratio represents the intermediate pressure between both turbines. All these performance curves have a maximum (or a minimum for the PMEP) which corresponds to the minimum cylinder backpressure for the considered operating condition. When fuel savings are the main objective, the wastegate valve or the VGT mechanism have to control the expansion ratio distribution to always maintain both stages under their best running operations [75, 273].

Here, both HP and LP turbochargers have the same efficiencies. So, the differences observed do not come from the turbomachines but only from benefits to split the compression ratio with intermediate inter-cooling. In sequential serial two-stage architecture, both turbochargers contribute to the compression work in the low to middle engine speed range. At these engine speeds, the LP turbocharger can have better or lower efficiencies than the HP one depending on how far its operating conditions are located from the area of maximum efficiency in the turbocharger characteristics maps. According to

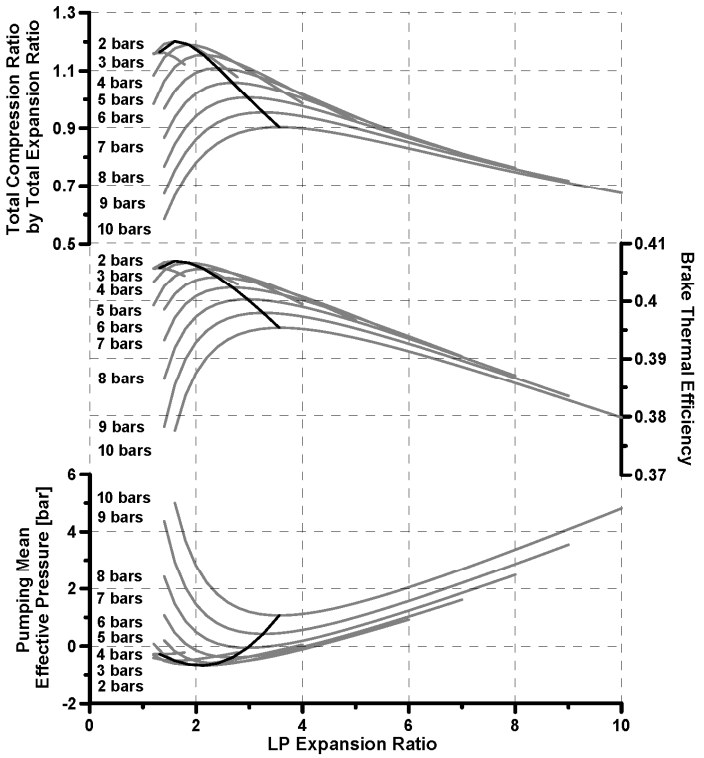

Figure 3.3: Engine performance parameters as a function of LP expansion ratio and global compression ratios.

the efficiency offset between both stages, optimized values can be significantly moved through lower or higher LP expansion ratio. With the analytical model, such optimized distribution is easy to find for a given engine operating condition and influences of turbochargers matching can thereby be rapidly checked.

The equations previously developed have been solved to minimize the cylinder backpressure and therefore to optimize the pumping losses reducing the work required for the gas exchange process. From a global engine performance point of view, they can also be solved to maximize the brake thermal efficiency to take into account the interactions between the boosting and combustion systems. When an aftercooler with a good efficiency and low cooling fluid temperature is placed at the intake manifold inlet, Optimized LP expansion ratio (Ope_{rLP}) obtained according both resolutions are similar. In that case, Ope_{rLP} can be adjusted with good agreement (R^2=99.95%) as a function of

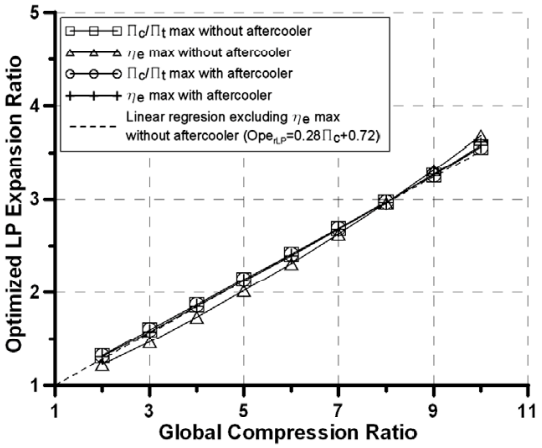

Figure 3.4: Optimized LP expansion ratio as a function of aftercooler configuration and design constraints for different global compression ratios.

the total compression ratio with lineal regression as shown in figure 3.4. But, if a system without aftercooler or with a low efficiency is considered, slight differences can be observed. These differences are generated by the IMEP calculations which take into account a constant volumetric efficiency and constant AFR. Without a good temperature control downstream the HP compressor, the air density entering to the cylinders (and so the engine indicative power) varies substantially depending on the HP compression ratio.

3.3.2 Coolers Performance

Efficiency and cooling fluid temperature have a strong impact on two-stage turbocharging efficiency and the best performance is always obtained with the highest intercooler cooling capacity. But a nonlinearity relation exits between efficiency and cooling fluid temperature. In fact, minimum cylinder backpressure is more impacted by intercooler efficiency when cooling fluid temperature is low than when is high. This nonlinear relation can be observed in figure 3.5 where the evolution of the engine performance parameters are plotted as a function of efficiency and cooling fluid temperature for different compression ratios. In each operating conditions, the work repartition between the HP and LP stage is optimized and pressure drop along the intercooler was neglected. In fact, pressure losses are strongly dependent of the running conditions, espe-

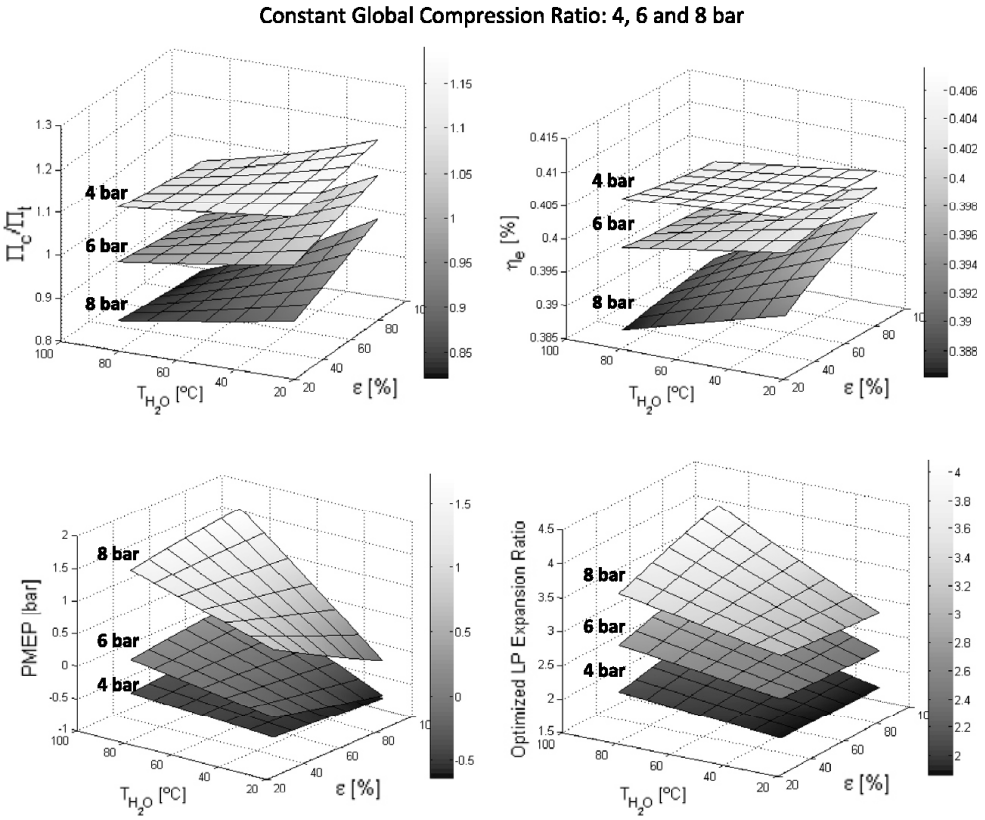

Figure 3.5: Engine performance parameters as a function of intercooler efficiencies and cooling fluid temperatures.

cially of mass flow and air density, and are generally relatively small comparing to compressors pressure ratio ($P_{012} - P_{012'} \ll P_{02} - P_{01}$). Results show also the cooling fluid temperature has higher influences on pumping mean effective pressure than intercooler efficiency. PMEP variations come from -0.6 bar to 0.3 bar modifying the cooling fluid temperature from 298K (obtained with an external air cooler) to 358K (obtained with an internal-engine-water cooler), while they only vary from -0.6 bar to -0.3 bar decreasing the intercooler efficiency from 90% to 40% and keeping the cooling fluid temperature at 298K.

When efficiency increases, the optimized expansion ratio distribution is modified increasing LP turbocharger work and decreasing HP one. In paralell, the overall system efficiency is improved and the total expansion ratio

decreases for a given compression ratio amplifying the differences between LP and HP expansion ratio. This trend is slightly different with the cooling fluid temperature. When the cooling fluid temperature decreases, the expansion ratio distribution remains practically constant. The LP turbocharger work reduction observed is only the consequence of the improved system efficiency and Π_c/Π_t increase.

3.3.3 Exhaust Temperature and Turbochargers Efficiencies

It can be observed in the compression ratio equations (Eq.3.27 and Eq.3.28) that compressor efficiencies and exhaust manifold temperature appear only in the ζ groups. However, turbine efficiencies are present not only in the terms ζ_{LP} and ζ_{HP} but appear also as factors of other terms. Being small the terms they multiply, it can be assumed as a first hypothesis their variations under these terms can be neglected. In that way, a parametric study of all turbocharger efficiencies and exhaust temperature can be performed directly with the ζ groups.

To validate this hypothesis, calculations were first performed varying compressor efficiencies and keeping turbine efficiencies constant (η_{tLP}=0.6 and η_{tHP}=0.6). Then, the same calculations were repeated keeping compressors efficiencies constant (η_{cLP}=0.7 and η_{cHP}=0.7) and varying turbines efficiencies to obtain the same values of the LP and HP groups as before. Differences between both calculations are shown in figure 3.6.

The relative differences obtained for the quotient Π_c/Π_t and the brake thermal efficiency are kept below 5% in most operating conditions. Nevertheless when turbocharger efficiencies are very small, the error increases substantially and exceeds 10%. These small turbocharger efficiencies do not reflect the typical operating conditions of sequential serial two stage architectures. Except at low loads where almost atmospheric conditions prevail in the intake manifold, at least one turbocharger is working under relatively good efficiencies. As the analysis is performed with high compression ratio objectives, this turbocharger operating range is neglected and the hypothesis can be verified for both engine performance parameters.

Concerning the optimized LP expansion ratio, the error is more important and varies from 5% to 20% in the typical engine operating range. The assumption stated before cannot be verified for this parameter and numeri-

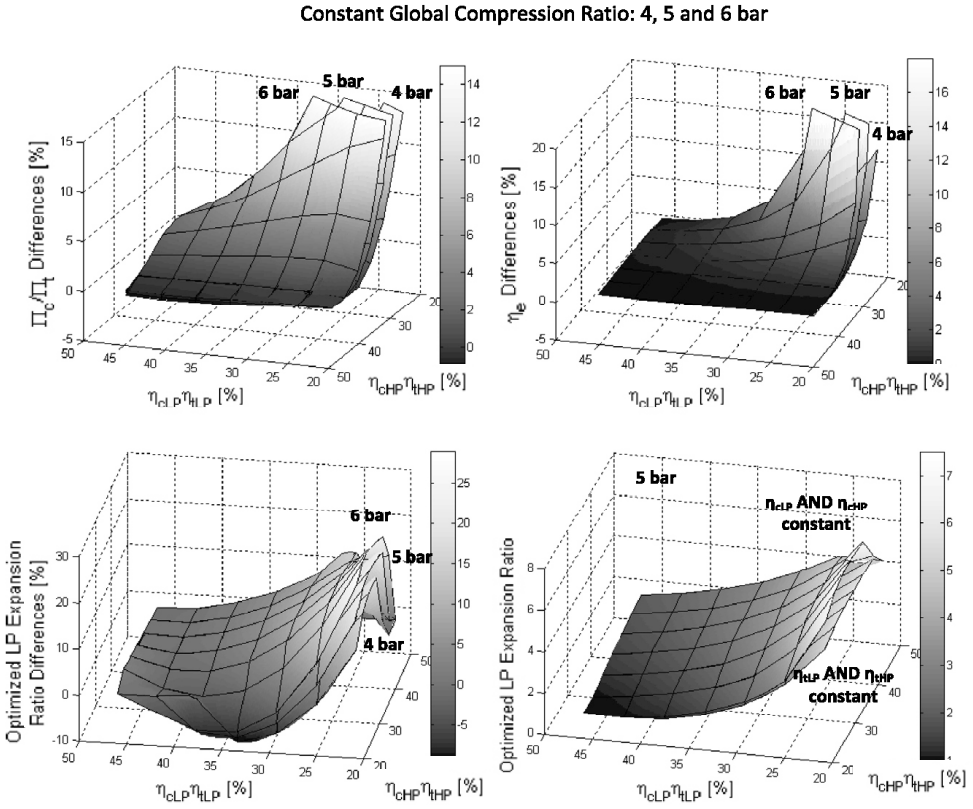

Figure 3.6: Uncertainties calculations for global compression ratio by global expansion ratio, brake thermal efficiency and optimized LP expansion ratio as a function of LP and HP stage efficiencies.

cal values cannot be directly processed. But as shown in figure 3.6 (bottom right), curves for both calculations present similar tendencies and their trends can be analyzed to estimate the influence of turbocharger efficiencies on the optimized LP expansion ratio.

The evolution of the ratio Π_c/Π_t, the brake thermal efficiency and the pumping mean effective pressure as a function of turbocharger efficiencies and exhaust temperature can be observed in figure 3.7. Results of this parametric study were obtained varying compressor efficiencies and keeping constant turbine efficiencies. To have a better representation, bottom plane scales have been reoriented for surfaces visualization optimization and the different graphs have been directly plotted as a function of LP turbocharger efficiency

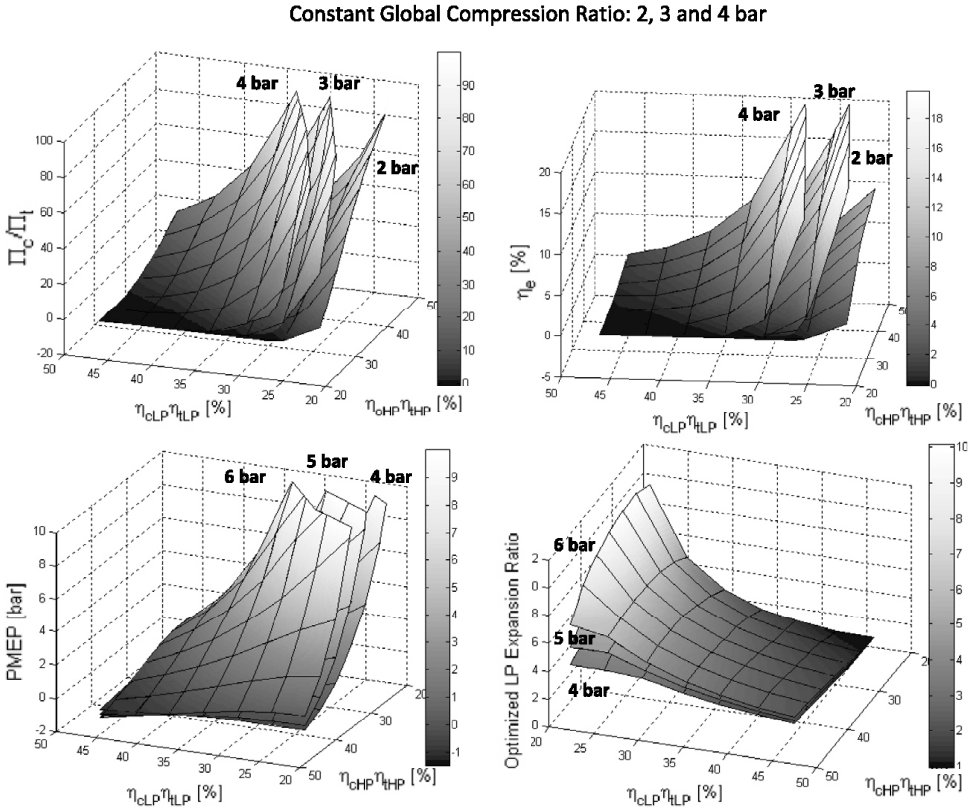

Figure 3.7: Engine performance parameters as a function of LP and HP stage efficiencies.

($\eta_{cLP} \cdot \eta_{tLP}$) and HP turbocharger efficiency ($\eta_{cHP} \cdot \eta_{tHP}$). The exhaust temperature is a proportional term in the groups, so its influence can be analyzed by the same way. T_{03}=1000K has been used as reference in the calculations and turbine adiabatic conditions have been imposed in order to simplify analyses and conclusions. A multiplication factor can be therefore applied to the graphics scales to have a visibility of the different results as a function of the exhaust temperature. Each operating conditions were calculated with an optimization process to determine the LP expansion ratio which minimizes the cylinder backpressure.

It can be noted the higher are the η parameters, the higher is the boosting architecture performance. But this relation is not linear and, when tur-

bochargers efficiencies decrease, brake thermal efficiency and pumping mean effective pressure are significantly impacted with as a consequence an important fall in overall system performance. As an example, it can be noted how the brake thermal efficiency decreases from 41% to 38% varying compressor efficiencies from 70% to 50% or exhaust temperature from 1000K to 700K.

3.3.4 Comparison between Single-Stage and Two-Stage Performance

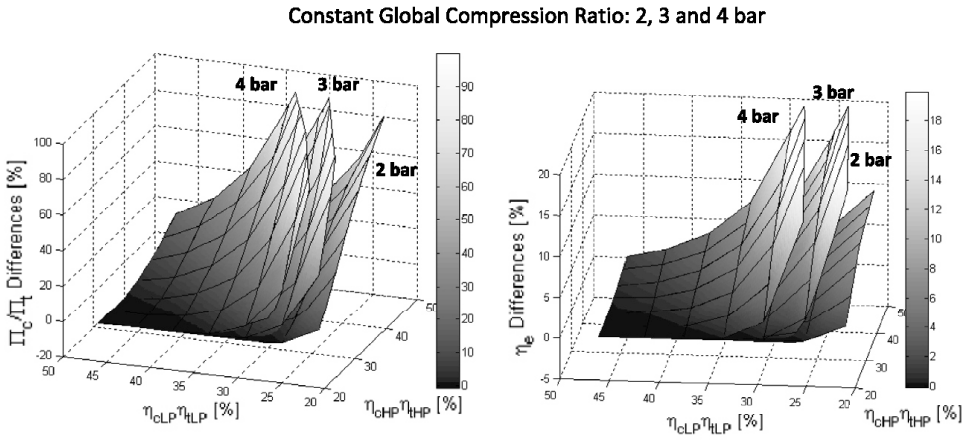

Figure 3.8: Performance comparison between single-stage and two-stage architectures as a function of turbocharger efficiencies.

Calculations were performed to compare the performance between single-stage and two-stage systems. The single-stage configuration has an aftercooler downstream the compressor and presents the same characteristics as the HP turbocharger previously described for the two-stage configuration. Global compression ratios are limited to 4:1 to keep acceptable expansion ratio in the single-stage turbocharger. Differences obtained in terms of Π_c/Π_t and brake thermal efficiency are shown in figure 3.8.

Under typical boost pressures used in passenger cars Diesel engines (2 bar), the two-stage system provide differences up to 10% in terms of brake thermal efficiency especially for operating conditions where turbocharger efficiencies are low. When boost pressures raise up to 4 bar, which is a common case for highly downsized or medium duty engines, differences can exceed 100% due to

the difficulties for single stage system to achieve high compression ratio with good efficiency. These differences become more and more important as the LP stage efficiency increases and the HP stage efficiency decreases.

3.4 Conclusions

In this chapter, an analytical pre-design model able to determine optimum two-stage architectures has been presented. Equations giving the relationship between total compression ratio and total expansion ratio as a function of basic engine parameters have been developed for two-stage systems similarly to well known existing expressions for single stage configuration. Having an analytical solution, this model can be easily resolved and contributes to understand the complex interrelations of this type of boosting architecture. By using non-dimensional or engine size reduced parameters, results can be easily used for any degree of engine downsizing and any engine power requirement.

With the developed equations, several studies have been carried out to analyze the different parameters that govern the overall system performance. Influences of the LP and HP expansion ratio on the PMEP, the ratio Π_c/Π_t and the brake thermal efficiency were characterized and optimum performance for given operating conditions has been established. As a result, a linear relation between Ope_{rLP} and Π_c has been observed. This relation allows a pre-design of wastegates or VGT's opening strategies which correspond to the main control decisions in two-stage architecture. In addition, influences of intercooler efficiency, cooling fluid temperature, turbocharger efficiencies and exhaust manifold temperature were analyzed for different global compression ratios. The main conclusions point out that it is always beneficial working with the highest intercooler cooling capacity, but cooling fluid temperature has a stronger impact on PMEP than intercooler efficiency. Moreover, best performance is achieved with the higher exhaust temperature and higher turbocharger efficiencies. Nevertheless PMEP and brake thermal efficiency are very sensitive to these parameters and overall system performance can significantly drop decreasing their values. Finally, the model was applied to compare single stage and two stage architecture. Assuming conventional turbocharger efficiencies, results highlight the real potential of two-stage architectures.

These analyses and the modeling philosophy associated could be expanded to more areas of interaction between HP and LP turbochargers. With a deeper

study for a specific application and specific operating conditions, more conclusions can be obtained and applied in the pre-design decision making process, such as components selection, valve specification etc... However, this analytical model is mainly conceptual and cannot be applied for matching calculations. In fact, to perform effective matching, advanced models are required to predict relevant parameters like volumetric efficiency, exhaust temperature, heat transfers... as a function of running conditions. Transient aspects are also fundamental in the final turbochargers size selection [288]. That is why, more sophisticated models, with special emphasis on matching problematic, will be developed in the following chapters of the thesis.

References

[3] *" Emission Standards for Model Year 2007 and Later Heavy-duty Highway Engines"*. US. Environmental Protection Agency (EPA), http://www.epa.gov, 2001. (Cit. on p. 125).

[74] A. Chasse, A. Albrecht, P. Moulin, A. Gautier P., L. Fontvieille, A. Guinois, and L. Doléac. *"A New Simulation Step Towards Virtual Bench Through the Challenging Case of Two-Stage Turbocharger Diesel Engine Control Design"*. SAE Technical Paper 2008-01-0355, 2008. (Cit. on pp. 32, 116).

[75] A. Chasse, P. Moulin, P. Gautier, A. Albrecht, L. Fontvieille, A. Guinois, and L. Doléac. *"Double Stage Turbocharger Control Strategies Development"*. SAE Technical Paper 2008-01-0988, 2008. (Cit. on pp. 32, 33, 127).

[119] J. Galindo, J.R. Serrano, F. Arnau, and P. Piqueras. *"Description and Analysis of a One-Dimensional Gas-Dynamic Model with Independent Time Discretization"*. Proceedings of the ASME Internal Combustion Engine Division, Spring Technical Conference, Chicago, 2008. (Cit. on pp. 10, 116, 171).

[122] J. Galindo, J.R. Serrano, F. Vera, C. Cervello, and M. Lejeune. *"Relevance of Valve Overlap for Meeting Euro 5 Soot Emissions Requirements during Load Transient Process in Heavy Duty Diesel Engines"*. International Journal of Vehicle Design, Vol. 41, No. 1/2/3/4, pp. 343-367, 2006. (Cit. on p. 125).

[196] I. Kolmanovsky and A.G. Stefanopoulou. *"Optimal Control Techniques for Assessing Feasibility and Defining Subsystem Level Requirements: an Automotive Case Study"*. IEEE Transactions on Control Systems Technology, Vol. 9, pp. 524-534, 2001. (Cit. on pp. 56, 116).

[228] J. Macek and O. Vitek. *"Simulation of Pulsating Flow Unsteady Operations of a Turbocharger Radial Turbine"*. SAE Technical Paper 2008-01-0295, 2008. (Cit. on pp. 116, 151).

[242] P. Moraal and I. Kolmanovsky. *"Turbocharger Modeling for Automotive Control Applications"*. SAE Technical Paper 1999-01-0908, 1999. (Cit. on pp. 116, 151, 162).

[273] A. Plianos and R. Stobart. *"Modeling and Control of Diesel Engines Equipped with a Two-Stage Turbo-System"*. SAE Technical Paper 2008-01-1018, 2008. (Cit. on pp. 29, 35, 127).

[288] S. Saulnier and S. Guilain. *"Computational Study of Diesel Engine Downsizing Using Two-Stage Turbocharging"*. SAE Technical Paper 2004-01-0929, 2004. (Cit. on pp. 30, 136).

[297] J.R. Serrano, F.J. Arnau, V. Dolz, A. Tisiera, M. Lejeune, and N. Auffret. *"Analysis of the Capabilities of a Two-Stage Turbocharging System to Fulfill the US2007 Anti-Pollution Directive for Heavy Duty Diesel Engines"*. International Journal of Automobile Technology, Vol. 9, No. 3, pp. 227-288, 2008. (Cit. on pp. 28, 37, 39, 125).

[337] O. Vitek, J. Macek, and M. Polasek. *"New Approach to Turbocharger Optimization Using 1-D Simulation Tools"*. SAE Technical Paper 2006-01-0438, 2006. (Cit. on p. 116).

[348] N. Watson and S. Janota. *"Turbocharging the Internal Combustion Engine"*. London: McMillan Publishers Ltd. ISBN 0-333-24290-4, 1982. (Cit. on pp. 10, 18, 55, 117, 153, 158).

[365] N. Winkler and H.E. Angström. *"Simulations and Measurements of a Two-Stage Turbocharged Heavy-Duty Diesel Engine Including EGR in Transient Operation"*. SAE Technical Paper 2008-01-0539, 2008. (Cit. on pp. 28, 29, 33, 37, 39, 116).

[373] J.C. Wurzenberger, P. Bartsch, and T. Katrasnik. *"Crank-Angle Resolved Real-Time Capable Engine and Vehicle Simulation - Fuel Consumption and Driving Performance"*. SAE Technical Paper 2010-01-0784, 2010. (Cit. on p. 116).

[378] K. Zinner. *"Supercharging of Internal Combustion Engines"*. Berlin, Heidelberg, New York Springer-Verlag, 1978. (Cit. on p. 116).

Chapter 4

Experimental engine and turbocharger characterization

Contents

4.1 Introduction **140**
4.2 Experimental Facilities **141**
4.3 Turbocharger Characteristic Maps **151**
4.4 Conclusions **163**
References **168**

4.1 Introduction

The matching of a boosting system to an internal combustion engine is a complicated balance of many design considerations. Appropriate turbocharger and engine components must be carefully selected to match a given engine size and to fulfill performance requirements over a wide range of operating conditions. This matching process can be carried out experimentally buying a large set of components, mounting all possible combinations on the considered base engine, and then calibrating and testing each configuration in an engine test cell. Doing such a methodology would obviously result very expensive and time consuming. That is why, a more efficient methodology based on a correct combination of experimental techniques and simulation tools has been defined to reach the objectives of this thesis.

Within this methodology, several experimental facilities such as flow test rig, injection rig, turbocharger test bench and engine test cells have been used to characterize all the different engine and charging subsystems. In this way, the information obtained constitutes the base for any matching calculations and will serve as input data for the modelling tools. A description of these installations with their main instrumentation will be presented in section 4.2. The engine test cells have also been involved in model validation. Further experimental campaigns will also be described in section 3 and in the following chapter as model developments are presented.

For the turbocharger test bench, turbine characteristic maps are generally provided in form of lookup tables giving the interrelationships between corrected mass flow, pressure ratio, efficiency, rotor speed and VGT position. This approach is not appropriate to perform matching calculations. In fact, both corrected mass flow and pressure ratio bring into play the exhaust manifold pressure which results, like the VGT position, as a consequence of the turbine behavior for a given intake pressure objective. Using these variables as input data requires therefore lots of iterations which are quite time-consuming before converging to a solution. To give an answer to this problematic, a new turbine performance representation has been developed with a specific matching procedure. This new representation avoid iterations mapping in an only plot all the different turbine positions in function of homogenous parameters relative to the natural design factors (turbocharger power and turbine mass flow). Furthermore, fitting methods and interpolations applied to this representation are more compact to implement in a turbocharger submodel

and more reliable in most operating conditions. This new representation and matching procedure will be described in section 4.3.

4.2 Experimental Facilities

4.2.1 Flow Test Rig

The flow test rig, as shown in figure 4.1, is an experimental facility able to generate by pressure or suction a continuous, steady and adjustable air mass flow through a set of pipes and volumes. It is composed of a roots blower, an electro-pneumatic valve for precise flow rate control, and a high capacity vessel to damp oscillations and to create steady air conditions for pressure measurement. The air mass flow rate is measured with a hot film anemometer, while pressures are recorded at different locations with water or mercury columns depending on their magnitudes. Atmospheric pressure and temperature are also measured with a weather station to calculate absolute pressure and air density.

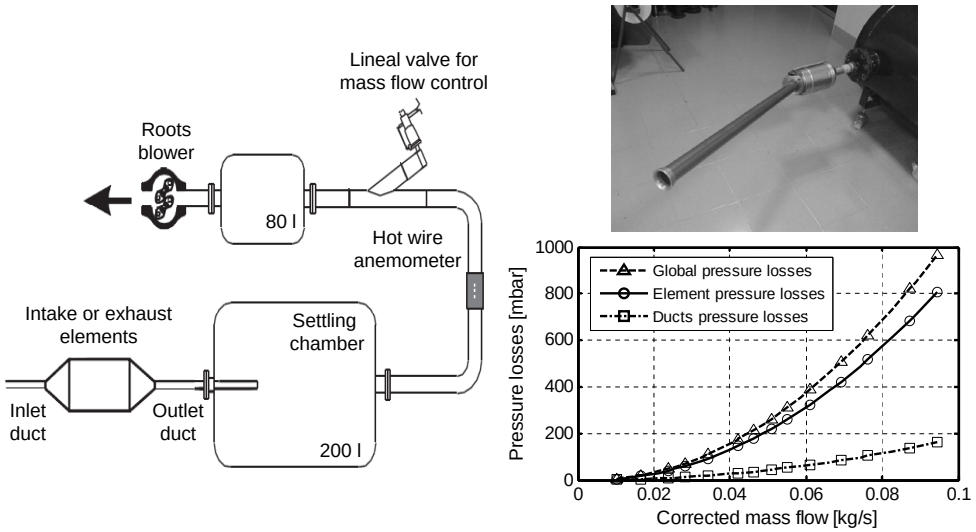

Figure 4.1: Experimental set-up and characterization of intake or exhaust line elements in the flow test rig.

In this work, the flow test rig has been used in two different characterization processes. In one hand, pressure losses were measured in the intake

and exhaust elements as a function of corrected air mass flow. These elements include air filters, intercoolers, Diesel Oxidation Catalysts (DOC), Diesel Particulate Filters (DPF), silencers and EGR coolers. Connecting pipes were considered as an integral part of their corresponding elements and were also mounted in the flow test rig to record the overall pressure losses. In the other hand, valve discharge coefficients and swirl number were measured in cylinders head as a function of valve lifts. Valve discharge coefficients represent the inherent losses suffered by the flow passing through the variable valves section, while the swirl numbers specify the intake system capacity to generate in-cylinder vorticity. Combining all these parameters, aerodynamic behavior of the intake and exhaust systems can be determined and performance between several configurations can be evaluated.

For pressure losses characterization, the considered element is mounted with specific inlet and outlet ducts in the flow test rig as indicated in figure 4.1 where the experimental setup is shown. The global pressure drop is obtained by measuring the static pressure drop Δp_0 between the ambient and the outlet settling tank when aspirating air from the ambient, ensuring that stagnation conditions hold in both measurements points. Such measurement includes the contribution of all the elements presents and global pressure drop can be decomposed as:

$$\Delta p_0 = \Delta p_0^{in} + \Delta p_0^{fr_{in}} + \Delta p_0^{element} + \Delta p_0^{out} + \Delta p_0^{fr_{out}} \tag{4.1}$$

Here, superscript ^{fr} makes reference to friction losses, whereas superscripts ^{in} and ^{out} refer to the inlet from the ambient and the discharge to the settling tank respectively. By means of an additional test in which the element is removed, it is possible to measure the contribution to the total pressure drop of the inlet mouth, the friction in the inlet and outlet ducts, and the discharge to the settling tank. Denoting the result of this measurement by $\Delta p_0'$, one has:

$$\Delta p_0' = \Delta p_0^{in} + \Delta p_0^{fr_{in}} + \Delta p_0^{out} + \Delta p_0^{fr_{out}} \tag{4.2}$$

Combining both tests, results yield therefore to the information shown in the right bottom of figure 4.1 where the pressure drop across the element is obtained as:

$$\Delta p_0^{element} = \Delta p_0 - \Delta p_0' \tag{4.3}$$

For valve discharge coefficients and swirl number characterization, a duct which represents the engine cylinder (same diameter but with a length equal to 1.75 diameters) links the cylinder head to the settling chamber. A screw connected to the valves-end adjusts the valve lifts to reproduce the engine valve timing while a micrometer records the valve opening magnitudes. To measure the solid body rotation generated by the intake ports and valve sections, a swirl meter based on the original Ricardo meter [113, 241] is installed at the cylinder outlet. Experiments are performed according to the Tippelmann methodology [324], although the swirl number calculations are based on the adaptation by Mayer [234] of the AVL Method [323].

Pressure drops between the ambient (P_{atm}) and the settling tank (P_{st}) are measured under both suction and blow induced flow for several valve lifts representative of the valve timing. With this information, valve discharge coefficients C_d are calculated for both intake and exhaust processes as:

$$C_d = \frac{\dot{m}_a}{\dot{m}_{th}} \quad with$$

$$\dot{m}_{th} = \frac{\pi D_v^2}{4} N_v \frac{P_{atm}}{(RT_{atm})^{\frac{1}{2}}} \sqrt{2\frac{\gamma}{\gamma-1}\left[\left(\frac{P_{st}}{P_{atm}}\right)^{\frac{2}{\gamma}} - \left(\frac{P_{st}}{P_{atm}}\right)^{\frac{1+\gamma}{\gamma}}\right]} \tag{4.4}$$

Here, $\dot{m}_a$ stands for the actual air mass flow passing through the valve sections whereas $\dot{m}_{th}$ correspond to the theoretical air mass flow that should be obtained for a given pressure drop in absence of losses. D_v and N_v make respectively reference to the diameter and number of valves.

Doing the same experiments in aspiration with swirl meter measurements, the instantaneous swirl number is evaluated as:

$$SN\left(\alpha\right) = \frac{\omega_{TM}\left(\alpha\right)}{\omega_{eng}} \tag{4.5}$$

where $\omega_{TM}(\alpha)$ is the vorticity speed recorded by the torque meter for a given valve timing α (corresponding to a given valve lift), and ω_{eng} is the speed that should runs the engine to blow the mass flow passing through the installation.

To take into account the whole intake process for a particular cylinder head and valve timing, a mean swirl number based on the vorticity speed at the Inlet Valve Closing (IVC) [128] is defined as:

$$MSN = \frac{\omega_{TM}\,(IVC)}{\omega_{eng}} \tag{4.6}$$

MSN will be used in the cylinder model described in the following chapter to evaluate the gas apparent speed during the compression stroke which is a fundamental factor in heat transfer calculations.

4.2.2 Injection Rig

The injection rig is an experimental facility able to determine the injection rate curve. It is composed of a high pressure common rail injection system, typically used in passenger cars, and a commercial injection rate meter called Injection Discharge Rate Curve Indicator (IDRCI) [267]. Adequate instrumentation and acquisition systems allow the injection variables such as pressure and temperature to be controlled while the IDRCI displays and records all the data describing the chronological sequence of an individual fuel injection event. A schematic of the experimental setup is shown in figure 4.2 (left side).

The measuring principle is based on the Bosch method [48] which consists of injecting fuel directly into a fuel-filled measuring tube. The injection nozzle discharges into a predetermined length of calibrated hydraulic ducts that gives rise to a pressure wave proportional to the injected fuel quantity per unit time. This pressure wave is measured by a piezoelectric pressure sensor and the injection rate is calculated as:

$$\dot{m}(t) = \frac{A}{c}\,(P(t) - P_{ref}) \tag{4.7}$$

where $\dot{m}$ is the injection rate, A the tube cross-sectional area, c the fluid sound velocity, P_{ref} the reference pressure, and $P(t)$ the dynamic pressure obtained in the measurement tube.

To determine the total injected mass quantity, a weight is placed downstream of the IDRCI. The mean quantity measured with the balance should

correspond to the integral of the mass flow rate for a recorded sequence of injections events. To improve the accuracy of the mass flow rate signal, the curve is multiplied by a factor so that the integral equals to the mass measured by the balance.

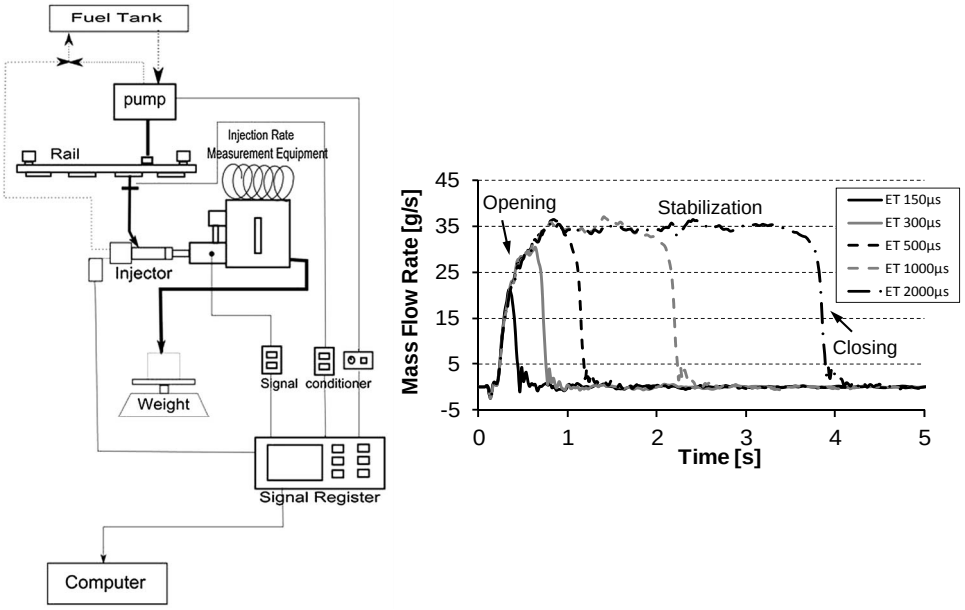

Figure 4.2: Left: Injection rig - Right: Typical injection rate curve at 160MPa.

The fuel injection rate shape has been exhaustively studied [20, 21, 229]. Figure 4.2 (right side) shows a typical injection rate signal where three different zones can be identified: the opening, stabilization, and closing zone. In general, theoretical studies have assumed that injection rate shape is perfectly rectangular. But in real cases, the mass flow rate curve is influenced by the dynamic behavior of the injector that depends on injection pressure and back pressure. This dynamic behavior generates a delay in the needle opening and closing phases [266]. Payri et al [267, 268] have described the mass flow rate in the stabilized zone (when the needle is completely lifted) as:

$$\dot{m} = C_d A \sqrt{2\rho \left(P_{inj} - P_{ch}\right)} \tag{4.8}$$

where $\dot{m}$ stands for the mass flow rate, C_d the discharge coefficient, A the nozzle orifice surface at the outlet, ρ the fluid density, P_{inj} the injection

pressure, and P_{ch} the chamber pressure during the injection time. Therefore, the mass flow rate curves at same injection pressure, back pressure conditions, and for a given injector must have the same behavior.

The injectors that equipped the different engines described in section 4.2.4 were tested in the injection rig. Measurements under several injection pressures (300, 900, 1600 bar) and several energized times (150, 300, 500, 1000, 2000μs) were performed to characterize their injection rate curves. With the in-cylinder thermodynamic conditions, the injection rate shape is one of the fundamental parameters to predict the combustion process. From these experiments, an injection rate curve for any injection pressure and any injection settings can be interpolated and imposed as input data in the combustion model. A detailed description of the combustion model will be given in the next chapter.

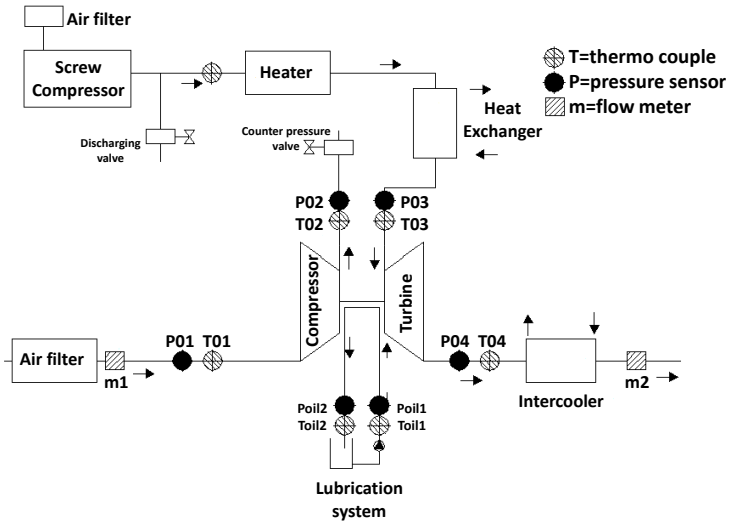

Figure 4.3: Turbocharger test bench layout.

4.2.3 Turbocharger Test Bench

Turbine and compressor characteristic maps are measured in a turbocharger test bench. This experimental facility is based on a screw compressor which provides the necessary mass flow to the system. This mass flow is heated up

by an electrical heater and then directed to the turbine inlet where temperatures can be as high as 675K at the maximum mass flow of the installation. A layout of the turbocharger test bench is shown in figure 4.3.

The amount of mass flow at the turbine inlet is controlled by changing the screw compressor speed which is handled with a PID controller. Since the screw compressor does not operate at speeds lower than its minimum design point, an electronically controlled discharge valve can reduce the amount of flow at the turbine inlet by discharging mass flow to the surrounding. In that way, the amount of energy sent to the turbine is controlled by the screw compressor, the discharging valve and the power of the heaters. Downstream the turbine, the air mass flow is cooled to allow measurements in commercial hot wire anemometers.

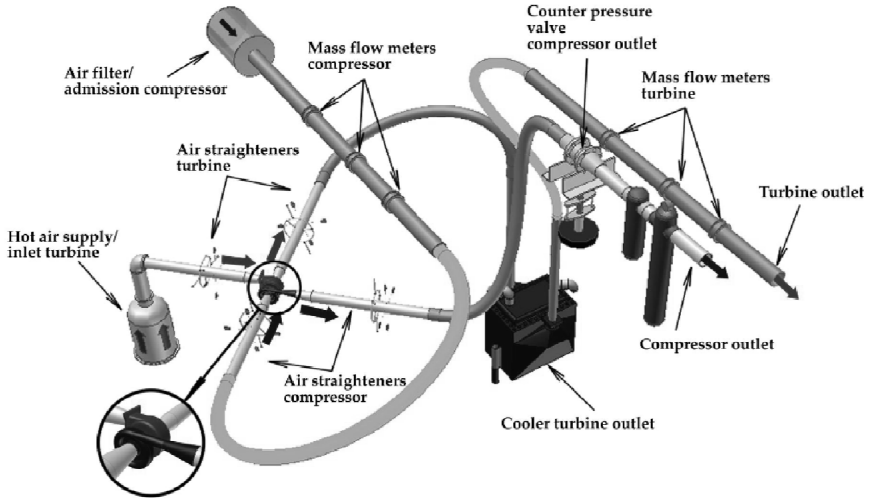

Figure 4.4: 3D distribution of the devices.

At the compressor side, the flow path begins with an air filter following with the flow measurements to finally reach the compressor inlet. Downstream the compressor, there is an electronically driven backpressure valve which helps to modify compression ratio and mass flow by changing pressure losses as required. At the exit, an oil filter is fitted to the line in order to prevent oil leakages. Additionally an independent lubrication system is used to control oil flow rate, oil pressure (by means of an oil pump and a pressure control valve) and oil temperature (by using an electrical heater and a cooler). A 3D view of the actual distribution can be observed in figure 4.4.

Temperature and pressure sensors are installed on the inlet and outlet pipes of the compressor and turbine, while a tachymeter records the turbocharger speed. The installation of these sensors regarding depth, angular and longitudinal position is made according to SAE Standards [7, 8]. The information obtained from all sensors in the different measurement points is registered with a data acquisition system, which allows also the main tests variables to be monitored and controlled.

The methodology for turbocharger testing is based on the compressor and turbine maps characterization procedure described by Cervello et al [120, 223]. Definitions proposed by the International Council on Combustion engines [9] are used for the different parameters calculations, except for the turbocharger efficiencies, where the isentropic definition proposed by Serrano et al. [299] is preferred. Several turbochargers were tested under the framework of this thesis. Information and results about their main characteristics will be described as their performances are analyzed.

4.2.4 Engine Test Bench

Three passenger car Diesel engines have been involved in the characterization and validation work. The first two engines (referred as Engine A and B) have been designed by the French manufacturer PSA under the Euro IV emissions regulations, while the third one (Engine C) has been more recently designed by Renault and respect the Euro V regulations.

Table 4.1: Basic Engines Characteristics.

	Engine A	Engine B	Engine C
Type	PSA DW10B	PSA DW12B	Renault M9R
Regulations	Euro IV	Euro IV	Euro V
Swept Volume (l)	1.998	2.179	1.995
Number of cylinders	4	4	4
Bore x Stroke (mm)	85 x 88	85 x 96	84 x 90
Number of valves	4	4	4
Compression Ratio	18:1	16.5:1	15.7:1
Injection System	Common-rail	Common-rail	Common-rail
Rated Torque (Nm)	320 Nm@1750 rpm	400 Nm@1750 rpm	340 Nm@2000 rpm
Rated Power (kW)	100 kW@4000 rpm	125 kW@4000 rpm	112 kW@4000 rpm
Boosting architecture	Single Stage	2T Sequential Parallel	Single Stage
Turbochargers	VGT GT1749	FGT GT1446/GT1241	VGT GT1752

They are all fitted with a common rail injection system, a high pressure EGR circuit and a DOC and DPF for post-treatment purposes. Their main characteristics have been summarized in table 4.1. Both Engines A and C have a 2.0l swept volume and are turbocharged by a single stage system with VGT. Whereas Engine B has a higher cylinders capacity and is equipped with a two-stage sequential parallel turbocharging system. With these differences in terms of generation, manufacturer, size and charging system, they thus offer a good representativeness of the typical diesel engines used in modern passenger cars.

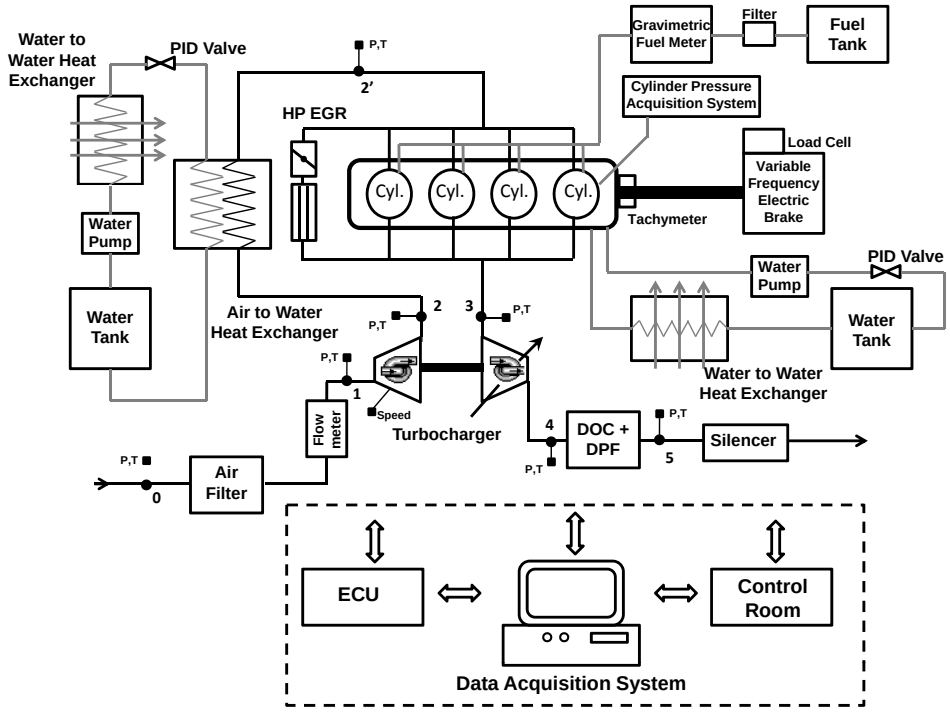

Figure 4.5: Experimental set-up of the engine test bench.

These engines have been installed in different test cells equipped with an asynchronous dynamometer Schenck Pegasus able to control engine speed and torque in both steady and transient conditions. Original Engine Control Units (ECU) have been replaced by opened ones to have a full access to the engine running parameters under the ETAS-INCA environment. In that way, engine settings could be adapted to the experiments necessities and information from the production sensors could be recorded. Engine Cooling systems and inter-

coolers have been connected to external water circuits for precise temperature control. All test cells present the same characteristics and a schematics of the different components forming the installations is shown in figure 4.5.

Table 4.2: Sensors Characteristics.

System	Variable	Sensor Type	Measuring range	Error
Air Path	Pressure	Piezoresistive	$0 - +5bar$	±100 Pa
	Temperature	Termocouple K	$-200 - +1200^{\circ}C$	±1°C
	Flow	Hot wire	$0 - 720kg/h$	±0.1%
Fuel	Pressure	Piezoresistive	$0 - +6bar$	±100 Pa
	Temperature	Termoresistence	$-200 - +650^{\circ}C$	±0.15°C
	Flow	Gravimetric	$0 - 380kg/h$	±0.1%
Oil/Water	Pressure	Piezoresistive	$0 - +6bar$	±100 Pa
	Temperature	Termoresistence	$-200 - +650^{\circ}C$	±0.15°C
	Flow	Coriolis	$0 - 100kg/h$	±0.1%
Cylinder	Pressure	Piezoelectric	$0 - +250bar$	±0.5%
Ambient	P, T, Humidity	Wheater station		
Engine	Torque	Load cell	$-600 - 600Nm$	±0.5%
	Speed	optical	$+1 - +6000rpm$	±1 rpm
Turbocharger	Speed	inductive	$+200 - +400000rpm$	±0.01%

Additionally, the engines have been instrumented with numerous sensors to measure the different variables of interest. These research-grade sensors are connected to a data acquisition system which controls and synchronize all this information with the ECU and test cell parameters under the STARS environment. In this work, the variables of interest have been: mean pressures and temperatures along the air path, ambient conditions, fuel mass flow, air mass flow, engine speed and torque and turbocharger speed. A description of the sensors used with their measuring range and errors is presented in table 4.2, while their locations can be observed in figure 4.5.

High frequency instantaneous signals such as cylinder pressure and additional pressures measurements in 2, 2', 3, 4, have been recorded using a dedicated data acquisition system. The high frequency signals are acquired using a Yokogawa DL716 oscilloscope and synchronized with the optical angular encoder with a resolution of 0.2 cad. From the cylinder pressure, the most relevant parameters related to the combustion process such as indicated mean effective pressure (IMEP), combustion phasing, maximum cylinder pressure and rate of heat release (RoHR) have been calculated by means of a combustion diagnostic thermodynamic code called CALMEC [22, 210, 211, 212, 264].

Regarding fuel flow measurements, gravimetric balances have a too low acquisition frequency to provide satisfactory results in transient operations. Information coming from the ECU has therefore been used with corrections obtained from the gravimetric balance under steady engine operations [295].

4.3 Turbocharger Characteristic Maps

4.3.1 Standard Characteristic Maps

Standard characteristic maps are generally provided in form of lookup tables where efficiency and corrected mass flow rate are given as a function of pressure ratio. Corrected rotor speed and VGT turbine position are additional inputs to characterize the turbine in a larger operating range. The representation of this data can be observed in figure 4.6.

From these maps, different approaches can be considered to model the turbocharger performance: applying a one-dimensional model (1D) derived from basic principles and calibrated with experimental data, or applying a zero-dimensional (0D) model based only on experimental data.

In the first way, a 1D approach computes in detail the energy conversion process taking into account the fluid and thermodynamic behavior of the exhaust gas. 1D turbocharger models are mainly based on the turbine geometry interrelating blade tip speed, corrected mass flow, pressure ratio and slip factor (ratio between the tangential velocity of the air leaving the impeller and the impeller tip velocity) [162, 228]. They rely on physical principles but require important computational resources and include some unavailable parameters, such as viscous drag or clearance losses, that must be previously calibrated [88, 89]. These models are interesting to study the behavior of a perfectly geometrically characterized turbine under specific thermodynamic processes but are inappropriate to perform turbocharger matching calculations. That is why, a 0D approach is in most cases preferred.

0D approaches are based on different curve fittings. In fact, even if interpolation techniques are straightforward to implement and very efficient in terms of computational time, the nonlinear nature of turbine characteristics makes unreliable direct linear interpolation from the performance lookup tables' data [170, 242, 246]. Moreover a small set of data is provided for discrete

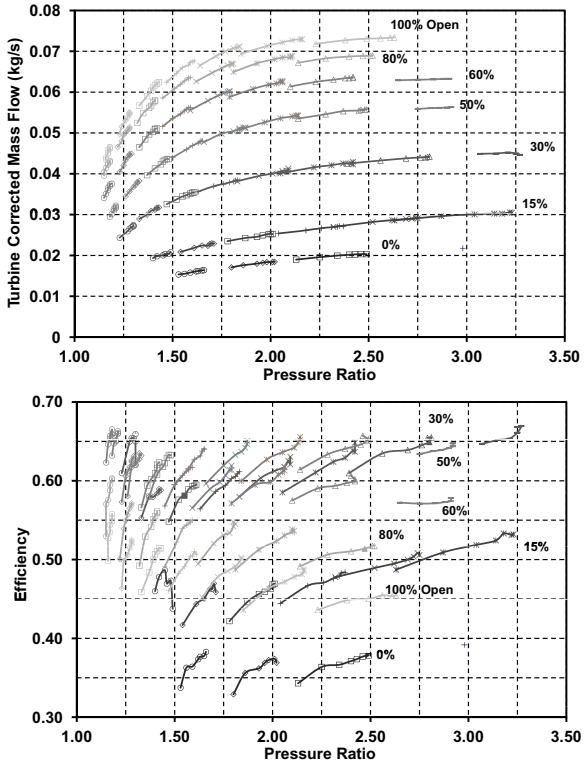

Figure 4.6: Typical turbine performance maps: mass flow rate (top) and efficiency (bottom) as a function of expansion ratio for different VGT openings and rotor speeds.

nozzle settings and the variation between different VGT positions is not linear either due to a variety of factors [39]. Hence interpolation for an arbitrary blade position is not accurate and curve fitting must be employed.

Filling and emptying models which assume that the turbine works as a quasy-steady flow device are generally used for curve fittings. In terms of mass flow, the turbine is modeled as two adiabatic nozzles in series with an intermediate volume [170, 259, 296] where the effective flows areas are calibrated as a function of blade speed ratio [300]. The reaction degree which relates the expansion ratios across the stator and rotor is set as a function of the stator blades angle, and losses through the nozzles are based on physical loss models adjusted with the performance maps. The turbine efficiency is typically modeled by a cubic polynomial in blade speed ratio with coefficient depending

on the speed parameter [348]. If turbine geometrical data such as inter-blade spacing, blade angle, blade number, etc... are provided, more physical models can also be used for turbine efficiency [231, 265].

An alternative technique for curve fittings is one proposed by Nelson et al. [249] which utilizes artificial neural network with a three neurons hidden layer to return the mass flow rate and efficiency as a function of speed parameters, pressure ratio and VGT position. As filling and emptying models, this method can give an accurate fit of the mapping points, but the previous training of the network based on the performance maps is more laborious and the mathematical resolution is not physically interpretable.

All these approaches predict turbine performance from pressure ratio and corrected mass flow which integrate the turbine inlet pressure as input data. Nonetheless, turbine inlet pressure is a consequence of turbine behavior. So, they require lots of iterations to converge first to a solution and then to a given intake pressure objective. Moreover, efficiency curve fittings are very close to each other and are strongly dependant of the turbocharger speed. Small uncertainties in the entry parameters can generate important errors during the interpolation, and turbocharger speed does not usually appear in the natural design parameters. Using these methods with standards turbine characteristics representation is therefore not adapted for matching calculations.

4.3.2 Adapted Characteristic Maps

4.3.2.1 A New Representation

Turbine characteristic map parameters are defined from the application of a dimensional analysis to compressible fluids through a turbomachine [97]. The different non-dimensional groups can be expressed as:

$$\Pi_t, \eta_t = f\left\{\frac{\dot{m}\sqrt{RT_{03}}}{D^2 P_{03}}\ , \frac{ND}{\sqrt{RT_{03}}}, \mathrm{Re}, \gamma_t\right\} \tag{4.9}$$

where Π_t stands for the total-to-static pressure ratio across the turbine, η_t the turbine total-to-static isentropic efficiency, D the impeller diameter, Re the Reynolds number, N the turbocharger speed and γ_t the exhaust gas adiabatic exponent.

For a machine of a specific size, handling a single gas and operating at high Reynolds number, it has become customary to delete D, R, γ_t and Re from Eq. 4.9. In addition, to avoid the dependence of inlet turbine temperature and pressure, corrected mass flow rate $\dot{m}_{cor}$ and corrected speed N_{cor} are employed. Under these conditions Eq. 4.9 becomes:

$$\Pi_t, \eta_t = f\left\{\dot{m}_{cor}\ , N_{cor}\right\} \tag{4.10}$$

$$\dot{m}_{cor} = \frac{\dot{m}\sqrt{\frac{T_{03}}{T_{ref}}}}{\frac{P_{03}}{P_{ref}}} \quad and \quad N_{cor} = \frac{N}{\sqrt{\frac{T_{03}}{T_{ref}}}} \tag{4.11}$$

where T_{ref} and P_{ref} represent the reference temperature and pressure chosen respectively as 298K and 101.3 kPa, T_{03} and P_{03} the turbine inlet total temperature and total pressure, and $\dot{m}$ the exhaust mass flow rate.

As mentioned before, the drawback of the corrected mass flow rate for turbocharger matching is its turbine inlet pressure dependence. This pressure is the result of the turbine behavior and appears as an unknown in the engine design. Nevertheless, the pressure downstream of the turbine, corresponding to the pressure losses of the entire exhaust line, is generally known at early development stage. Therefore the use of this pressure is more appropriate in the matching process and the adapted gas turbine flow can be introduced as:

$$\dot{m}_{adapt} = \dot{m}_{cor}\Pi_t = \frac{\dot{m}\sqrt{\frac{T_{03}}{T_{ref}}}}{\frac{P_4}{\mathrm{P}_{ref}}} \tag{4.12}$$

where P_4 is the turbine outlet pressure. This parameter has the particularity of taking into account design parameters (exhaust manifold temperature and exhaust back pressure) remaining homogeneous to the turbine behavior.

A natural design factor in turbocharger calculation is the turbocharger power. The performance maps do not normally use this parameter but, keeping with the same philosophy as for the mass flow, the turbine corrected power can be expressed as:

$$\dot{W}_{cor} = \dot{m}_{cor}C_{pt}\eta_t\left(1 - \Pi_t^{1/\gamma_t - 1}\right) = \frac{\dot{W}}{\sqrt{T_{03}T_{ref}}\frac{P_{03}}{P_{ref}}} \tag{4.13}$$

where C_{pt} is the exhaust gas specific heat at constant pressure and the turbocharger power. The adapted power is then defined as:

$$\dot{W}_{adapt} = \dot{W}_{cor}\Pi_t = \frac{\dot{W}}{\sqrt{T_{03}T_{ref}}\frac{P_4}{P_{ref}}} \tag{4.14}$$

Turbine performance expressed with turbine adapted mass flow and adapted power is entirely defined as a function of pressure ratio and VGT position by two sets of curves. The new turbine characteristics are plotted in figure 4.7 with the same lookup tables' values used in figure 4.6.

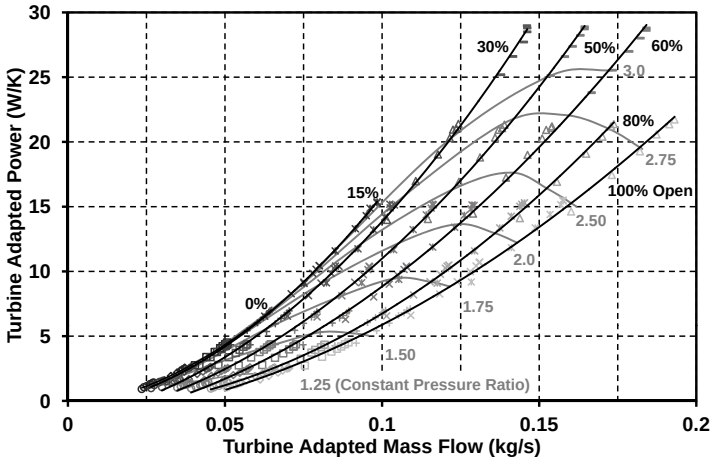

Figure 4.7: Turbine adapted characteristics map: adapted power as a function of adapted mass flow rate for different VGT openings.

Using conservative parameters which are mass and energy, these curves show a very low sensitiveness to speed variations. Thus this form is more suited for matching calculations and interpolation methods give more reliable results for a wide range of operating conditions. In addition, they present a very accurate curve fitting with quadratic polynomials functions, simple and compact interpolation routines can be employed and computational time is reduced.

4.3.2.2 Turbine Performance Simulation

For the validation of the new representation, two different turbines were characterized in the turbocharger test bench to obtain their performance data. A description of the main turbine geometrical data can be observed in table 4.3.

Table 4.3: Turbine Characteristics.

HTT turbochargers	VGT GT1749	VGT GTB1244
Compressor inducer wheel diameter	37 mm	29 mm
Compressor exducer wheel diameter	48 mm	41 mm
Compressor trim	60	50
Turbine wheel diameter	41 mm	35.5 mm
Turbine trim	72	72

Subsequently, the first turbine with the reference HTT VGT GT1749 was fitted on Engine A previously described and measurements at different engine speeds and loads corresponding to the whole engine operating range were carried out. An overview of the different operating conditions is shown in figure 4.8. In every performed test, engine running parameters were kept identical to the production calibration and all the variable of interest described in section 2.4 were recorded.

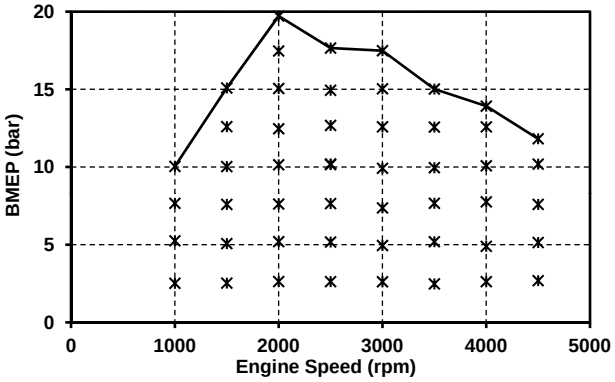

Figure 4.8: Engine performance and test operating conditions.

Turbine characteristics obtained in the turbocharger test bench for different VGT positions were plotted with the adapted representation in figure 4.9. These curves were then employed to simulate turbine performance under on-engine operations.

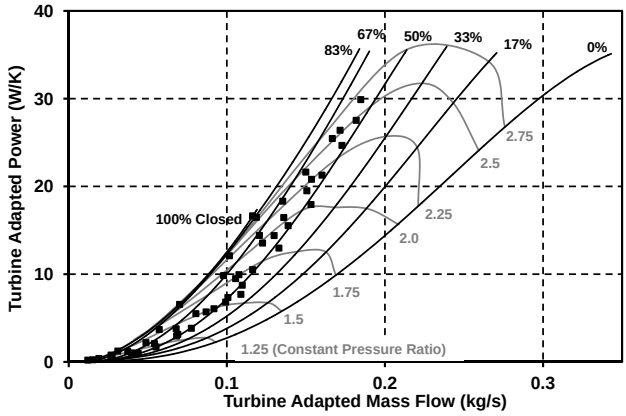

Figure 4.9: Engine operating conditions plotted in the adapted characteristics map.

For each test condition, the turbine adapted mass flow was calculated from Eq. 4.12 taking into account the air mass flow, fuel mass flow, turbine inlet temperature and turbine outlet pressure obtained from the measurements. As the different tests were performed under steady state operations, the power consumed by the compressor is equal to the power developed by the turbine including turbocharger mechanical losses. So, the adapted power was calculated from the compressor power as:

$$\dot{W}_{adapt} = \frac{\dot{W}}{\sqrt{T_{03}T_{ref}}\frac{P_4}{P_{ref}}} = \frac{\dot{m}_a C_{pc}\left(T_{02} - T_{01}\right)}{\sqrt{T_{03}T_{ref}}\frac{P_4}{\mathrm{P}_{ref}}} \tag{4.15}$$

where $\dot{m}_a$ is the air mass flow, C_{pc} the air specific heat at constant pressure, T_{01} the compressor inlet temperature and T_{02} the compressor outlet temperature. Results measured in the engine test bench were added to figure 4.9 (squared marks). It can be noted with the original engine settings, calibrated for Euro IV performance and emissions targets, stator blades are in a medium opening position in most operating conditions, which corresponds to an adequate turbine matching.

The new representation defines VGT position and pressure ratio as a function of turbine adapted mass flow and adapted power:

$$\Pi_t, \chi_{VGT} = f\left\{\dot{m}_{adapt}, \dot{W}_{adapt}\right\} \tag{4.16}$$

With simple linear interpolation methods, both parameters were interpolated from the representation for every test conditions and compared to the measurements. Results are shown in figure 4.10 where an excellent prediction is obtained.

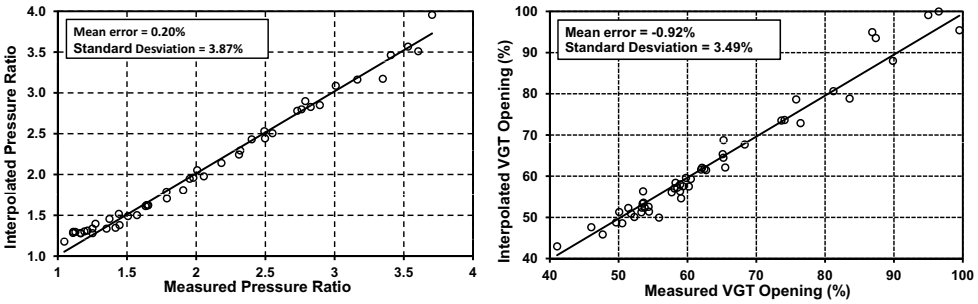

Figure 4.10: Comparison of pressure ratio and VGT turbine opening between measured data in engine test bench and interpolated data from the adapted characteristics map.

Small differences can be observed between measured and interpolated data. On the one hand, inherent sensor uncertainties exist in both type of installation. As the parameters calculated to describe the turbine performance are combinations of various measurements, results can be slightly influenced. On the other hand, some heat transfer effects [301], especially in the low speeds and low loads region, and differences between turbines behavior under steady or under pulsating flow conditions [76], affect the turbine efficiency measurement.

With the first turbine, the whole turbocharger operating range could not be tested because the interaction between the engine and the turbocharger limited certain operating conditions. That is why a second turbine, smaller than the first one and with the reference HTT VGT GTB1244, was characterized in the turbocharger rig. The main turbine specifications are presented in table 4.3. This turbine was then fitted on Engine A and tests were performed at the same engine operating conditions but changing the injection settings to maintain different constant VGT opening positions.

With this smaller turbine, the operating conditions in the engine test bench are bounded with overspeed and choked phenomena in the compressor [348]. Turbine characteristics obtained with the second turbine in turbocharger test bench and results under on-engine operations calculated as previously men-

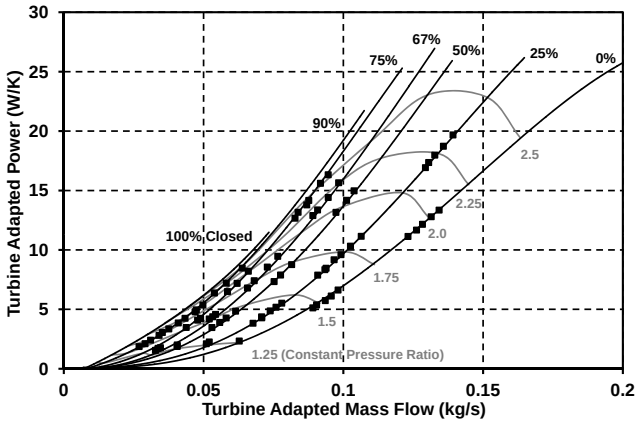

Figure 4.11: Turbocharger operating conditions plotted in the adapted characteristics map.

tioned are plotted with the adapted representation in figure 4.11.

In the same way, the exhaust manifold pressure and the VGT opening were interpolated from the representation for every test conditions and compared to measurements. Results are shown in figure 4.12. Once again, a good overall agreement is obtained. As justified before some uncertainties can be observed but they are always included in a narrow confidence interval. This comparison confirms that the new representation defined is valid to predict the turbine performance in the whole turbocharger operating range.

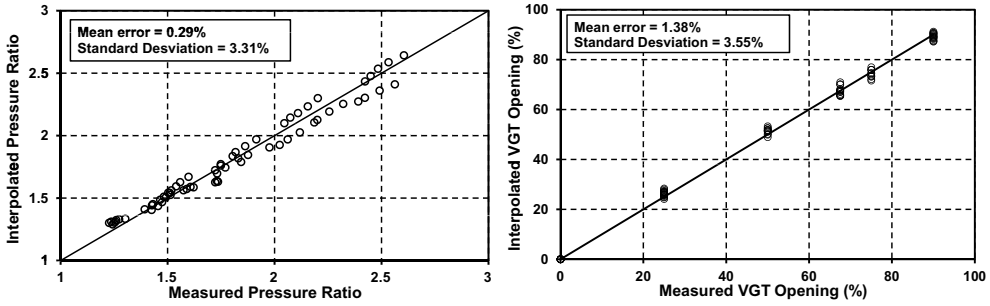

Figure 4.12: Comparison of pressure ratio and VGT turbine opening between measured data and interpolated data from the adapted characteristics map.

4.3.2.3 Engine Speed and Load Independence

Turbine performance is normally measured under steady flow conditions, but it can be observed some variations when the turbine is fitted on an engine and encounters pulsating flow conditions, heat transfers and different mechanical losses situations. A significant amount of work is present in the literature to characterize the effect of real engine flow on turbines [66, 198, 341, 366], but nowadays a simple solution does not exist to solve these problems and a correction factor based on experimental data is generaly applied to the turbine efficiency. The conventional turbine performance maps are affected by these effects but the use of conservative parameters in the definition of the adapted representation allows the turbine characteristics to be more independent of the unsteady engine behavior.

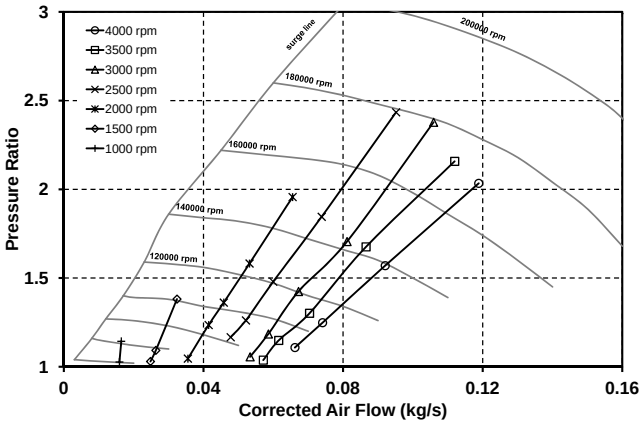

Figure 4.13: Operating conditions at constant VGT position in the compressor.

Several tests were carried out at different engine speeds and loads maintaining constant the stator blade angle in a 75% opening position. The different loads were adjusted varying fuel mass flow and injection settings to measure the same turbine adapted mass flows for each engine speed. The resulting operating conditions plotted in the compressor map are shown in figure 4.13. Adapted parameters were also calculated and represented in figure 4.14 with the corresponding turbine characteristics measured in the turbocharger rig. It can be observed how the points for each turbine adapted mass flows tested are quite centered in comparison to the flow rig measurement. Thus they validate the low dependence of this representation to the effects of pulsating flow.

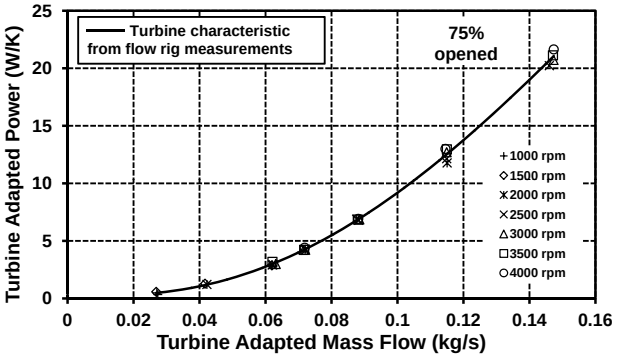

Figure 4.14: On-engine adapted turbine power for different engine speeds and loads versus turbine characteristics measured in a steady flow rig.

4.3.2.4 Turbocharger Matching

This representation can be directly implemented in an engine simulation model for carrying out an effective turbocharger matching and for predicting the performance of the whole system. To fulfill the different requirements in terms of engine power, fuel consumption and pollutant emissions, results obtained from engine models generally define the air mass flow, air-to-fuel ratio, exhaust temperature and intake pressure for each operating conditions. Taking into account constant atmospheric temperature and pressure, and estimating pressure losses along the air filter and intercooler, these air management objectives can be plotted in a compressor referential as shown in figure 4.15.

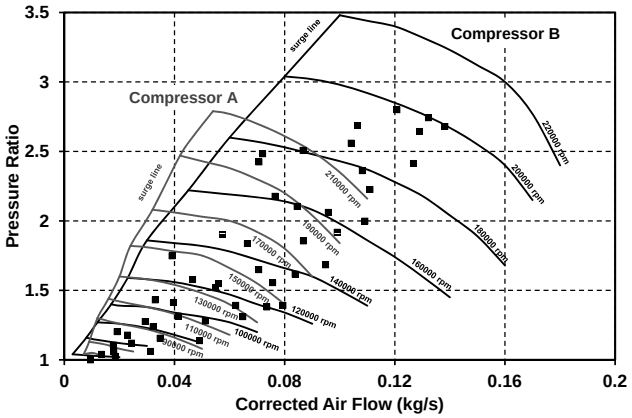

Figure 4.15: Compressor Matching.

Different curve fitting methods are present in the literature [231, 242] to interpolate efficiency and turbocharger speed from the compressor maps. With efficiency known, the power required by each candidate compressor can be calculated. The compressor choice is then a complex balance between the lower power consumed and the ability of keeping an adequate margin to the limits of stable operation in all cases.

In steady state, power and speed are equal on both compressor and turbine sides. Assuming small gas mass flow losses by blow-by and taking into account pressures losses in the exhaust line, the matching points can be directly plotted in the turbine adapted referential with the following expressions:

$$\dot{m}^c_{cor} = \frac{\dot{m}_a \sqrt{\frac{T_{01}}{T_{ref}}}}{\frac{P_{01}}{\mathrm{P}_{ref}}} \tag{4.17}$$

$$\dot{W}^c_{cor} = \frac{\dot{m}^c_{cor} C_{pc}}{\eta_c} \left(\left(\frac{P_{02}}{P_{01}} \right)^{1-1/\gamma_c} - 1 \right) \tag{4.18}$$

$$\dot{m}_{adapt} = \frac{\dot{m} \sqrt{\frac{T_{03}}{T_{ref}}}}{\frac{P_4}{\mathrm{P}_{ref}}} = \dot{m}^c_{cor} \left(1 + F\right) \sqrt{\frac{T_{03}}{T_{01}}} \frac{P_{01}}{P_4} \tag{4.19}$$

$$\dot{W}_{adapt} = \frac{\dot{W}}{\sqrt{T_{03} T_{ref}} \frac{P_4}{\mathrm{P}_{ref}}} = \dot{W}^c_{cor} \sqrt{\frac{T_{01}}{T_{03}}} \frac{P_{01}}{P_4} \tag{4.20}$$

where $\dot{m}^c_{cor}$ is the corrected air mass flow, $\dot{W}^c_{cor}$ the corrected power required by the compressor, P_{01} the compressor inlet total pressure, P_{02} the compressor outlet pressure, γ_c the air adiabatic exponent, η_c the compressor total-to-total isentropic efficiency and F the fuel-to-air ratio. Figure 4.16 shows the corresponding matching points in the new turbine characteristics representation.

Pressure ratio and VGT opening position are then directly interpolated for each candidate turbine without any iterations process, and turbine efficiency is easily deduced from Eq. 4.12 and Eq. 4.13. At the end, the turbine is chosen to fulfill all the operative conditions with the smallest pressure ratios, optimizing in that way the engine scavenging process and the overall fuel consumption.

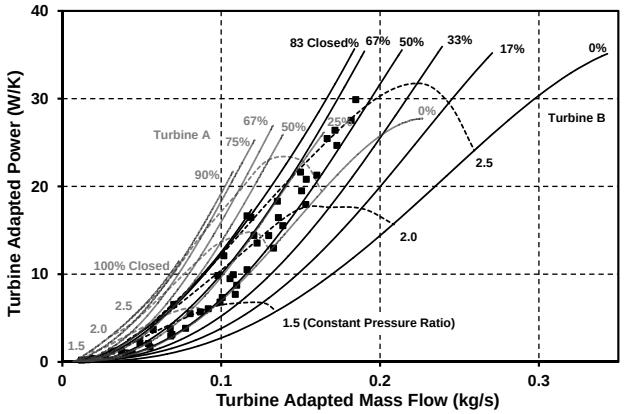

Figure 4.16: Turbine Matching.

4.4 Conclusions

The experimental facilities involved in the different engine subsystems characterization and model validations have been described with their main instrumentation. The principal variables of interest that have been measured and recorded during the experimental work have also been defined.

In addition an alternative set of parameters for characterizing the turbine behavior has been presented. These parameters are independent of the inlet turbine pressure and allow to perform direct matching calculations for given boost pressure objectives. The new turbines characteristics are more compact and allow all the turbine performance data to be plotted in a single graph as a compressor map for easier interpretation. These characteristics are accurately fitted with quadratic polynomial functions which have the particularity to be continuously differentiable and without discontinuities. When implemented in engine simulation code, standard linear interpolation routines are straightforward and computational times are reduced.

The differences between turbines behavior under steady or under pulsating flow conditions, as well as heat transfer phenomena across the turbine are still under investigation. Currently, there does not exist simple solution to solve these problems. The new representation uses conservative parameters which average these effects. So the interpolated results are more reliable and the accuracy of the whole engine simulation is improved.

Finally, a matching procedure using these new turbine characteristics has been presented. This matching procedure requires important input data such as air mass flow, exhaust temperature, etc... and possesses many variations depending on the considered boosting system architecture. That is why, both representation and procedure has been integrated in a whole engine model able to reproduce and match an important number of boosting configurations. The engine model with its resolution algorithm will be described in the next chapter.

References

[7] *" Supercharger Testing Standard SAE J1723"*. Society of Automotive Technology, issued 1995, 1995. (Cit. on p. 148).

[8] *" Turbocharger Gas Stand Test Code SAE J1826"*. Society of Automotive Technology, issued 1989, reaffirmed 1995, 1995. (Cit. on p. 148).

[9] *" Turbocharging Efficiencies - Definition and Guidelines for Measurement and Calculations"*. CIMAC Working Group, The International Council on Combustion Engines, No. 27, 2007. (Cit. on p. 148).

[20] C. Arcoumanis and M.S. Baniasad. *"Analysis of Consecutive Fuel Injection Rate Signal Obtained by the Zeus and Bosch Methods"*. SAE Technical Paper 930921, 1993. (Cit. on p. 145).

[21] C. Arcoumanis and M. Gavaises. *"Linking Nozzle Flow with Spray Characteritics in a Diesel Fuel Injection System"*. Atomization and Sprays, Vol. 8, pp. 307-347, 1998. (Cit. on p. 145).

[22] O. Armas. *"Diagnostico Experimental del Proceso de Combustion en Motores Diesel de Inyeccion Directa"*. Tesis Doctoral, Universidad Politecnica de Valencia, Valencia, 1999. (Cit. on pp. 150, 192, 193, 205).

[39] R.S. Benson. *"The Thermodynamics and Gas Dynamics of Internal Combustion Engines"*. Oxford University Press, Vol. 1, 1982. (Cit. on p. 152).

[48] W. Bosch. *"The Fuel Rate Indicator: A New Measuring Instrument for Display of the Characteristics of Individual Injection"*. SAE Technical Paper 660749, 1966. (Cit. on p. 144).

[66] M. Capobianco, A. Gambarotta, and G. Cipolla. *"Influence of the Pulsating Flow Operation on the Turbine Characteristics of a Small Internal Combustion Engine Turbocharger"*. IMechE 4^{th} International Conference on Turbochargers and Turbocharging, pp. 63-69, 1989. (Cit. on p. 160).

[76] H. Chen, I. Hakeem, and R. Martinez-Botas. *"Modelling of a Turbocharger Turbine Under Pulsating Inlet Conditions"*. Proceedings of the Institution of Mechanichal Engineers, Part A: Journal of Power and Energy, Vol. 210, No. 5, pp. 397-408, 1996. (Cit. on p. 158).

[88] R. Dambach and H.P. Hodson. *"Tip Leakage Flow - A Comparison between Small Axial and Radial Turbines"*. Micro-Turbine Generators Conference, Professional Engineering Publishing, pp. 97-108, London, 2000. (Cit. on p. 151).

[89] R. Dambach, H.P. Hodson, and I. Huntsman. *"An Experimental Study of Tip Clearence Flow in a Radial Inflow Turbine"*. ASME Journal of Turbomachinery, Vol. 121, Issue 4, pp. 644-650, 1999. (Cit. on p. 151).

[97] S.L. Dixon. *"Fluid Mechanics and Thermodynamics of Turbomachinery"*. Pergamon Press Ltd, 1998. (Cit. on pp. 153, 261).

[113] N.F. Gale. *"Accuracy of the Ricardo Steady Estate Flow Rig"*. Ricardo Engeneering Report, Vol. DP.20395, 1975. (Cit. on p. 143).

[120] J. Galindo, J.R. Serrano, C. Guardiola, and C. Cervello. *"Surge Limit Definition in a Specific Test Bench for the Characterization of Automotive Turbochargers"*. Experimental Thermal and Fluid Science, Vol. 30, pp. 449-462., 2006. (Cit. on pp. 148, 232).

[128] A. Gil. *"Caracterizacion del Flujo de Aire en el Cilindro de Motores Diesel DI Mediante Calculo Tridimensional"*. Tesis Doctoral, Universidad Politecnica de Valencia, Valencia, 2003. (Cit. on p. 144).

[162] X. Hu. *"An Advanced Turbocharger Model for the Internal Combustion Engine"*. Doctoral Thesis, Purdue University, 2000. (Cit. on p. 151).

[170] J.P. Jensen, A.F. Kristensen, S.C. Sorenson, and N. Houback. *"Mean Value Modelling of Small Turbocharged Diesel Engine"*. SAE Technical Paper 910070, 1991. (Cit. on pp. 151, 152, 172).

[198] K. Konishi, H. Yoshiki, and S. Tashiro. *"Performances of Radial Inflow Turbines for Exhaust Gas Turbochargers under Nonsteady Flow Conditions"*. International Gas Turbines Congress, pp. 157-164, Yokohama, 1991. (Cit. on p. 160).

[210] M. Lapuerta, O. Armas, and V. Bermudez. *"Sensitivity of Diesel Engine Thermodynamic Cycle Calculation to Measurement Errors and Estimated Parameters"*. Applied Thermal Engineering, Vol. 20, pp. 843-861, 2000. (Cit. on pp. 150, 204).

[211] M. Lapuerta, O. Armas, and J.J. Hernandez. *"Diagnostic of D.I. Diesel Combustion from In-Cylinder Pressure Signal by Estimation of Mean Thermodynamic Properties of the Gas"*. Applied Thermal Engineering, Vol. 19, pp. 513-529, 1999. (Cit. on pp. 150, 205).

[212] M. Lapuerta, O. Armas, and J.J. Hernandez. *"Effect to the Injection Parameters of a Common Rail Injection System on Diesel Combustion through Thermodynamic Diagnosis"*. SAE Technical Paper 1999-01-0194, 1999. (Cit. on p. 150).

[223] J.M. Lujan, V. Bermudez, J. R. Serrano, and C. Cervello. *"Test Bench for Turbocharger Groups Characterization"*. SAE Technical Paper 2002-01-0163, 2002. (Cit. on p. 148).

[228] J. Macek and O. Vitek. *"Simulation of Pulsating Flow Unsteady Operations of a Turbocharger Radial Turbine"*. SAE Technical Paper 2008-01-0295, 2008. (Cit. on pp. 116, 151).

[229] M. Marcic. *"Measuring Method for Diesel Multihole Injection Nozzles"*. Sensor and Actuators, Vol. 107, pp.152-158, 2003. (Cit. on p. 145).

[231] G. Martin, V. Talon, P. Higelin, A. Charlet, and C. Caillol. *"Implementing Turbomachinery Physics into Data Map-Based Turbocharger Models"*. SAE Technical Paper 2009-01-0310, 2009. (Cit. on pp. 153, 162, 178).

[234] K.P. Mayer. *"Swirl Measurement on the Stationary Flow Test Bench by Means of a Momentum Meter"*. AVL Report Memory No. 618, 1982. (Cit. on p. 143).

[241] M.L. Monaghan and H.F. Pettifer. *"Air Motion and its Effect on Diesel Performance and Emission"*. SAE Technical Paper 810255, 1981. (Cit. on p. 143).

[242] P. Moraal and I. Kolmanovsky. *"Turbocharger Modeling for Automotive Control Applications"*. SAE Technical Paper 1999-01-0908, 1999. (Cit. on pp. 116, 151, 162).

[246] M. Muller, E. Hendricks, and S.C. Sorenson. *"Mean Value Modelling of Turbocharged Spark Ignition Engines"*. SAE Technical Paper 980784, 1998. (Cit. on p. 151).

[249] S.A. Nelson, Z.S. Filipi, and D.N. Assanis. *"The Use of Neural Nets for Matching Fixed or Variable Geometry Compressors with Diesel Engines"*. Journal of Engineering for Gas Turbines and Power, Vol. 125, pp. 572-579, 2003. (Cit. on p. 153).

[259] F. Payri, J. Benajes, and M. Reyes. *"Modelling of Supercharger Turbines in Internal Combustion Engines"*. International Journal of Mechanical Science, Vol. 8-9, pp. 853-869, 1996. (Cit. on pp. 152, 210).

[264] F. Payri, S. Molina, J. Martin, and O. Armas. *"Influence of Measurement Errors and Estimated Parameters on Combustion Diagnostic"*. Applied Thermal Engineering, Vol. 26, pp. 226-236, 2006. (Cit. on pp. 150, 189, 192).

[265] F. Payri, J.R. Serrano, P. Fajardo, M.A. Reyes-Belmonte, and R. Gozalbo. *"A Physically Based Methodology to Extrapolate Performance Maps of Radial Turbines"*. Energy Conversion and Management, Vol. 55, pp.149-163, 2012. (Cit. on pp. 153, 210).

[266] R. Payri, V. Bermudez, F.J. Salvador, and A.H. Plazas. *"Study of the Influence of Nozzle Seat Type on Injection Rate and Spray Behavior"*. Proceedings of the Institution of Mechanical Engineers Part D: Journal of Automotive Engineering, Vol. 219, pp.667-689, 2005. (Cit. on p. 145).

[267] R Payri, J.M. Garcia, J. Salvador, and J. Gimeno. *"Using Spray Momentum Flux Measurements to Understand the Influence of Diesel Nozzle Geometry on Spray Characteristics"*. Fuel, Vol. 84, pp. 551-561, 2005. (Cit. on pp. 144, 145).

[268] R. Payri, S. Molina, F.J. Salvador, and J. Gimeno. *"A Study of the Relation Between Nozzle Geometry, Internal Flow and Sprays Characteristics in Diesel Injections Systems"*. Korean Society of Mechanical Engineers, Vol. 18, pp. 1222-1235, 2004. (Cit. on p. 145).

[295] J.R. Serrano, F.J. Arnau, V. Dolz, and P. Piqueras. *"Methodology for Characterization and Simulation of Turbocharged Diesel Engines Combustion during Transient Operation - Part 1: Data Acquisition and Post-Processing"*. Applied Thermal Engineering, Vol. 29, pp. 142-149, 2009. (Cit. on p. 151).

[296] J.R. Serrano, F.J. Arnau, V. Dolz, A. Tiseira, and C. Cervello. *"A Model of Turbocharger Radial Turbines Appropriate to be Used in Zero- and One-Dimensional Gas Dynamics Codes for Internal Combustion Engines Modelling"*. Energy Conversion and Management, Vol. 49, pp. 3729-3745, 2008. (Cit. on pp. 152, 210).

[299] J.R. Serrano, V. Dolz, A. Tiseira, and A. Paez. *"Influence of Environmental Conditions and Thermodynamic Considerations in the Calculations of Turbochargers Efficiency"*. SAE Technical Paper 2009-01-1468, 2009. (Cit. on p. 148).

[300] J.R. Serrano, B. Pla, R. Gozalbo, and D. Ospina. *"Estimation of the Extended Turbine Maps for a Radial Inflow Turbine"*. SAE Technical Paper 2010-01-1234, 2010. (Cit. on pp. 152, 210).

[301] S. Shaaban and J. Seume. *"Analysis of Turbocharger Non-Adiabatic Performance"*. IMechE 8^{th} International Conference on Turbocharging and Air Management Systems, C647/027, London, 2006. (Cit. on p. 158).

[323] G.E. Thien. *"Derivation of the Formulas for the Evaluation of Stationary Flow Measurements of Intake and Exhaust Ports"*. AVL-FA-Report, No. 463/Gen./072, 1978. (Cit. on p. 143).

[324] G. Tippelmann. *"A New Method of Investigation of Swirl Ports"*. SAE Technical Paper 770404, 1977. (Cit. on p. 143).

[341] F.J. Wallace and G.P. Blair. *"The Pulsating Flow Performance of Inward Radial Flow Turbines"*. ASME Gas Turbine Conference, Paper 65-GTP-21, Washinghton, 1965. (Cit. on p. 160).

[348] N. Watson and S. Janota. *"Turbocharging the Internal Combustion Engine"*. London: McMillan Publishers Ltd. ISBN 0-333-24290-4, 1982. (Cit. on pp. 10, 18, 55, 117, 153, 158).

[366] D.E. Winterbone and R.J. Pearson. *"Turbocharger Turbine Performance Under Unsteady Flow - A Review of Experimental Results and Proposed Models"*. IMechE 6th International Conference on Turbocharging and Air Management Systems, C554/031/98, pp.193-206, London, 1998. (Cit. on p. 160).

Chapter 5

0D Diesel Engine Modeling

Contents

5.1 Introduction **170**
5.2 Mean Value Based Gas-Path Description **174**
5.3 Crank Angle Resolved Model **184**
5.4 A Fully Integrated 0D Engine Model **197**
5.5 Experimental Calibration and Validation **203**
5.6 Conclusions **215**
References **224**

5.1 Introduction

The complexity arising from multistage boosting architectures requires an efficient matching methodology to obtain the best overall powertrain performance. With a large number of components interacting between each other, optimization processes are more and more demanding and only a correct combination of experimental techniques and simulation tools can lead to good results under suitable development time. In the last chapter, part of the proposed matching methodology has been exposed with the description of both experimental facilities and matching procedure. To complete these tools, the second part of the methodology is based on a whole engine model able to correctly match the boosting system in steady-state conditions and to reproduce its performance under transient operations.

Five types of calculation models are present in engine development. These models can be classified according to their complexity and computational cost as: three-dimensional calculation codes, 1D wave action models, 0D filling & emptying models, quasi-steady or mean value engine models and look-up tables, see figure 5.1. Each type has its pro's and con's and their selection must be adapted to the specific application with a right balance between physical description, predictive capabilities, computational speed and accuracy [14, 125]. A lot of information is present in the literature about these different modelling approaches. So only a brief description of their main characteristics will be provided here and interesting reviews of thermodynamics models applied to the Diesel engine can be found in [83, 133, 276].

2D/3D models, such as ANSYS Fluent or KIVA and also called Computational Fluid Dynamics (CFD), are the most predictive simulations. They discretize the flow domain into millions of volumes and solve for each one the full unsteady Navier Strokes equations. They provide very detailed information of internal processes but require important computational resources. That is why they are generally restricted to local studies or in-cylinder simulations where fuel spray, turbulent combustion and chemical kinetics need a very small characteristic time scale to be predicted [44].

1D approach is a reduction of CFD models assuming only one dimension in the Navier Stroke equations. Well established 1D codes such as OpenWAM, GT-Power, WAVE or AVL Boost solve the mass, momentum and energy conservation equations in piping systems with finite differential or finite volume

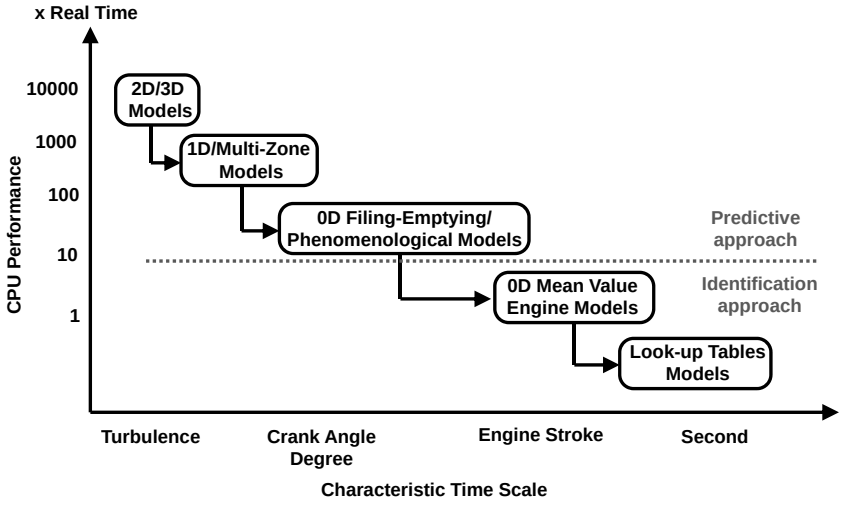

Figure 5.1: Modeling tools for engine development [125].

schemes [119, 261], and employs particular boundary conditions in the different connections. They give an accurate description of complex gas dynamic phenomena in the intake and exhaust lines (acoustics, friction, junctions, etc...) [368] but their computational time is relatively slow, in the order of 100-1000 times greater than real time. Their highly resolved gas exchange and cycle simulation are normally employed in engine development processes where inertia or wave effects are important such as air delivery ratio optimization, variable valve timing calibration, etc...

Filling & emptying models reproduce the various engine components as a series of interconnected control volumes (cylinder, manifold, intercooler, etc...) and transfer elements (valve, restrictions, etc...). They solve the mass and energy conservation equations with time steps in the order of one crank angle to obtain instantaneous state of the gas within the different volumes. They exhibit for a moderate computational cost a relatively good prediction of the engine performance in both steady and transient conditions. Nevertheless by ignoring the momentum conservation equation, they bring a further reduction to the Navier-Stokes equations which, even if engine aspiration is physically captured, make them unable to predict inertia and wave effects in the manifolds. Depending on the operating conditions, errors can be significant and must be considered. Winterbone et al. [367] and Watson et al. [346, 350] were the first in the late 1970's to introduce filling & emptying techniques

in engine development to simulate turbocharger response. Since then, these models have also been largely used in control design and fault diagnostics [178, 379].

Mean Value Engine Models (MVEM) have the same origin as filling & emptying models. They integrate transfer components and different volumes where the mass and energy conservation equations are resolved. But their resolutions are time base and predict only mean values variations [104, 135, 167]. With time step in the order of one revolution, sub-cycle processes such as combustion or flow through valves are simplified by empirical correlations or map based models. MVEM are therefore not predictive and rely mainly on data obtained from measurements or higher fidelity models. Their calibrations employ identification techniques and require a large amount of comprehensive engine data over a wide operating range, especially when nonlinearity and interaction between engine variables are significant. The main advantage of MVEM reside in their real time capabilities which make them particularly favorable for control and observer design. Hendricks et al. [142, 143, 170] were the first to develop MVEM for control supervision. Then numerous authors have integrated other empirical or semi-empirical methods (analytical derivations, radial basis functions [137, 139], Neural Networks [138, 271], etc...) to improve simulation accuracy for their specific applications.

Finally, the lowest modelling level consists to reproduce the engine behavior with look-up tables or best-fit polynomials adjusted from experimental data. This approach presents poorer accuracy but simulations are performed under very low computational times. They are generally used at a system level to run standard driving cycle with a whole vehicle model or to characterize combustion subsystems employed in higher modelling approach.

The conventional model level to perform matching calculations has been for years the 1D approach. This approach presents advantages in terms of physical description but has become extremely time-demanding with the arrival of multistage boosting systems and HP/LP EGR circuits. To face the challenge of fast engine development processes, a new approach has therefore to be defined with a more appropriate balance between model complexity and CPU performance.

Matching calculations are generally performed at an early stage of the engine development process when only little geometrical information is defined and no experimental data are available for the base engine. In these condi-

tions, lookup tables or MVEM are not appropriate to simulate combustion processes and a predictive model is required with, as a minimum, a crank angle resolution in cylinders. 1D multi zone models give a good description of in-cylinder heterogeneities involved in the local combustion and pollutant production terms [160]. However, as pollutant prediction is not essential for architecture matching, 0D phenomenological models are preferred for their sufficient physical representative capability and reasonable CPU expenses [30]. To calculate the engine scavenging behavior and the exhaust temperature, 1D wave action model are particularly accurate. Nevertheless, they require correct wave effects predictions of the design information of the intake and exhaust systems (runner diameters, pipe lengths, etc...) and a precise description of their acoustic behavior. This information which can be measured in specific impulse test rigs [327] or extracted from 3D CAD models [256], is not available at an early engine development stage. Therefore, 1D model capabilities cannot be fully exploited and the lower computational cost of 0D filling & emptying models becomes more attractive to reproduce the most important thermodynamics processes. For the different air path components such as turbochargers, intercooler, air filter, etc..., large data bases with results of characterizations performed in specific test benches are generally provided. These data are in form of characteristic maps or lookup tables over wide operating ranges. MVEM have therefore a sufficient complexity to model these different engine components.

From these considerations, it arises that the adequate trade-off between maximum physical description and minimum computational cost to perform efficient matching calculations is a combination of 0D phenomenological combustion model, with a 0D filling & emptying model for the multi-cylinders and manifolds, and a MVEM for the other air path elements. In that way, advantages of reasonable computational cost from the 0D and MVEM approaches are combined with the physical depth of detailed cycle resolved cylinder models.

In addition, matching objectives are generally defined in terms of engine performance with boost pressure targets. The variables of interest in matching calculations describe turbochargers behavior, position of turbine actuators, etc... Nonetheless, equations resolutions performed by typical matching codes such as wave action models use the actuators variables as input data to predict engine performance (actuators oriented model). In that way, control strategies for each engine actuators need to be developed and a large number of itera-

tions are required to reach given performance objectives controlling actuator positions. This approach is low efficient and time consuming for steady-state calculations. That is why a new resolution algorithm has to be defined to run the simulations in a natural sense, from engine performance objectives to charging system configuration (boost pressure oriented model). In transient operations, the gas path handle different relevant physical effects such as mass accumulation, transport of species, inertias, etc... and control strategies have an important impact on the boosting system performance. In this case, a boost pressure oriented algorithm cannot be employed and the conventional actuators oriented scheme remains the most appropriate. To reduce as much as possible CPU expenses during matching calculations, the simulation model has therefore to integrate both resolution approaches, boost pressure oriented model for steady state conditions and actuators oriented model for transient operations.

In this chapter, a 0D engine model especially developed for matching calculations will be described. First, the intake and exhaust MVEM will be presented with their different elements. Following, the crank angle resolved model that regroups the combustion and the filling & emptying models will be introduced. These models will be then interconnected to form a whole engine model and both boost pressure and actuators oriented algorithms will be described. Finally, a complete validation process has been carried out to assess the new modelling approach. Comparisons between experimental and modeled data will be discussed in the last section.

5.2 Mean Value Based Gas-Path Description

Multistage boosting architectures regroup a large number of configurations that need highly flexible simulation tools to efficiently describe different engine assemblies. The intake and exhaust line models consist thus of individual components that can be assembled arbitrary to build a complete description of the gas path. The main architectures having some similarities, based structures are also proposed here to give a better overview of possible assemblies.

5.2.1 Intake Line

The base structure and the intake boosting components library can be observed in figure 5.2. The air mass flow enters with atmospheric conditions in

the air filter to exit in 1 where it undergoes a mixing process with the LP EGR mass flow to reach conditions in 1'. The evolutions in the LP and HP intake charging systems go from 1' to 12 and 12' to 2 respectively. Between both stages, an intercooler can perform a cooling process depending on the bypass valve control. After the HP stage, the mass flow passes through an aftercooler and a throttle valve to arrive in the intake manifold. The intake throttle is only used in combination with the HP EGR system when the pressure difference between the intake and exhaust manifold is not sufficient to obtain the desired HP EGR rate. For the LP and HP intake charging systems, the component library regroups superchargers, centrifugal superchargers, eBoosters, centrifugal compressors in single or parallel configuration and connections for single boosting system.

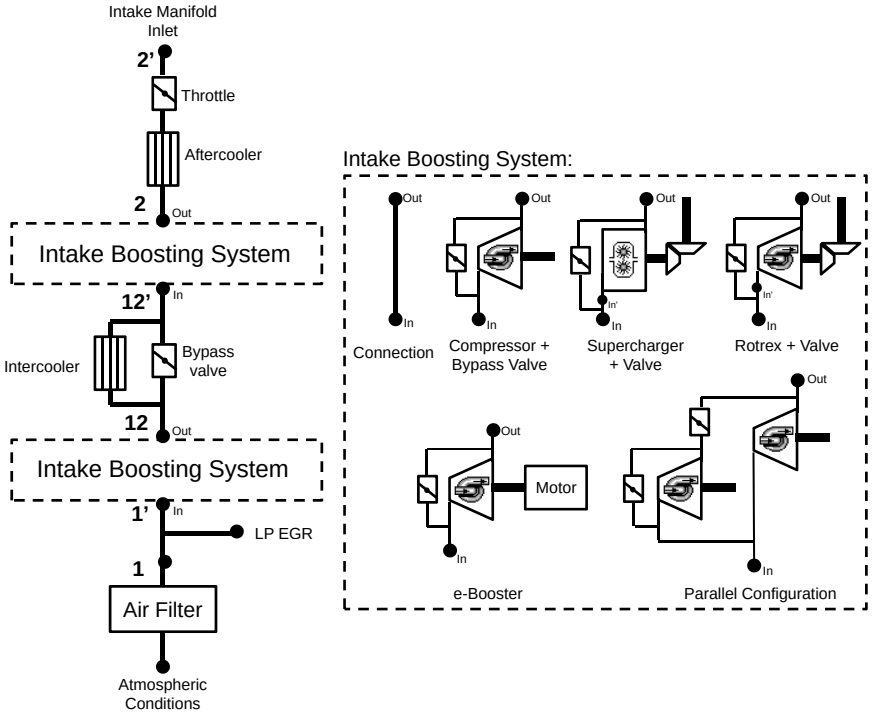

Figure 5.2: Based structure and components library of the intake line MVEM.

In steady state operations, matching calculations are based on a boost pressure oriented resolution scheme. Engine performance objectives are defined in terms of pressures in 2' and 12' corresponding to combustion and control requirements respectively. According to the boosting architectures,

variations of P12' are generally simulated to optimize cylinders backpressure and fuel consumption. Volume capacities with mass accumulation are not considered and mass flows are assumed to be constant along the whole air path. Heat transfers are discarded between the components although models like ones used for the exhaust line can be integrated if their effects are judged significant. Below are briefly described the sub-models used to calculate the different elements.

Gas properties model:

The thermodynamics properties of the gas are calculated as a function of its components and their respective mass fractions:

$$R_g = R_a Y_a + R_f Y_f + R_b Y_b \tag{5.1}$$

$$C_{p_g} = C_{p_a} Y_a + C_{p_f} Y_f + C_{p_b} Y_b \tag{5.2}$$

where subscripts $_g$, $_a$, $_f$, $_b$ refer to the mean properties of the gas, air, fuel and stoichiometric burned products respectively. A fuel with average composition $C_{10.8}H_{18.7}$ was considered. R stands for the specific constants of each species and C_p for the specific heat at constant pressure. The C_p is calculated using polynomial expressions as a function of temperature adjusted from data taken from JANAF [4] and revised by SANDIA laboratories [185]. This definition is used in the whole engine model (manifolds, cylinders, exhaust line, etc...).

Mass Balance:

Engine breathing capability is reproduced by the filling & emptying model which give to the MVEM the mass flow at the intake manifold inlet. This mass flow is imposed constant from 1' to 2'. HP and LP EGR rates (X_{EGR}) are generally defined before matching calculations as combustion objectives to respect particular emissions regulations. LP EGR mass flow and, as a consequence, air filter mass flow are defined as:

$$\dot{m}_{LPEGR} = \dot{m}_{1'} X_{LPEGR} \left(1 + \frac{X_{HPEGR}}{1 - X_{HPEGR}}\right) \tag{5.3}$$

$$\dot{m}_1 = \dot{m}_{1'} - \dot{m}_{LPEGR} \tag{5.4}$$

Fuel mass fraction is zero along the whole air path and only fresh air is considered in the air filter. The other mass fractions from 1' to 2 are calculated as:

$$Y_{b1'} = \frac{\dot{m}_{LPEGR} Y_{b_{LPEGR}}}{m_{1'}} \quad and \quad Y_{a1'} = 1 - Y_{b1'} \tag{5.5}$$

Air Filter and Coolers:

Air filters and Coolers are characterized in a flow test rig where their pressure losses are measured as a function of corrected mass flow:

$$\Delta P = f\left\{ \frac{\dot{m}_{in}\sqrt{\frac{T_{in}}{T_{ref}}}}{\frac{P_{in}}{\mathrm{P}_{ref}}} \right\} \tag{5.6}$$

Experimental data is accurately fitted with polynomials functions which are then directly integrated in the models. It is assumed that the gas flow suffers an isothermal process in the air filter, whereas heat transfer in the coolers is calculated by the effectiveness method [153] which evaluates the outlet temperature as:

$$T_{out} = T_{in} + \varepsilon\left(T_{ext} - T_{in}\right) \quad with \quad \varepsilon = f\left\{NTU, C_p\dot{m}\right\} \tag{5.7}$$

where T_{ext} stands for the external cooling fluid temperature and NTU the number of transfer units. If the coolers have not been characterized in a thermal flow rig, typical NTU values for heat exchangers can be found in [183].

Throttle and Bypass valve:

Throttle and Bypass valve are modeled as isentropic nozzle where the mass flow is expressed from the Saint Venant equation as:

$$\dot{m} = C_d A_{ref} p_{in} \sqrt{\frac{2\gamma}{R\left(\gamma-1\right)T_{in}}} \sqrt{\left(\frac{P_{out}}{P_{in}}\right)^{\frac{2}{\gamma}} - \left(\frac{P_{out}}{P_{in}}\right)^{\frac{\gamma+1}{\gamma}}} \tag{5.8}$$

C_dA_{ref} represents the effective valve section and R and γ depend on the temperature and composition of the gas. When the pressure ratio exceeds the critical value, it must be substituted in Eq. 5.8 by the corresponding value for choked flow:

$$\left(\frac{P_{crit}}{P_{in}}\right) = \left(\frac{2}{\gamma+1}\right)^{\frac{\gamma}{\gamma-1}} \tag{5.9}$$

From a control point of view C_dA_{ref} is directly proportional to the actuators position. But here, with a boost pressure oriented resolution and knowing the mass flow, the throttle is seen as a pressure drop to reach the HP EGR objectives and C_dA_{ref} is calculated as a resultant. Bypass valves are generally used in ON/OFF configurations. In this case, no pressure losses are considered across the valve.

Centrifugal Compressor and eBooster:

The compressor model is based on the characteristic maps obtained in turbocharger test bench that give corrected shaft speed and efficiency as a function of corrected mass flow rate and pressure ratio:

$$N_{cor}, \eta_c = f\left\{\dot{m}_{cor}, \frac{P_{out}}{P_{in}}\right\} \tag{5.10}$$

These maps are extrapolated in the low rpm zone with the isentropic enthalpy gain method [231] and interpolated in the model by polar basis functions. The compressor outlet temperature is derived from the isentropic efficiency as:

$$T_{out} = T_{in} + \frac{T_{in}}{\eta_c}\left(\left(\frac{P_{out}}{P_{in}}\right)^{\frac{\gamma-1}{\gamma}} - 1\right) \tag{5.11}$$

and the compressor power used as turbocharger input data in the exhaust line MVEM is expressed with the mass flow rate and enthalpy changes as:

$$\dot{W}_c = \dot{m} C_p \left(T_{out} - T_{in}\right) \tag{5.12}$$

Taking into account a motor efficiency, this power corresponds for the eBooster to the electrical demand. If limitations are imposed by the vehicle electrical network, equations are inversed and P_{out} is calculated as a function of electrical power.

Volumetric and Centrifugal superchargers:

Superchargers are connected via a transmission to the engine crankshaft. The transmission ratio is an additional variable in the matching calculations and a mechanical efficiency which depends on the running conditions is added to the compressor work. Superchargers models are also based on the measured characteristic maps but their interpolations can be performed in different ways according to the matching objectives. First, supercharger speed can be calculated as a function of corrected mass flow and pressure ratio to obtain the optimized transmission ratio:

$$N_c, \eta_c = f\left\{\dot{m}_{cor}, \frac{P_{out}}{P_{in}}\right\} \quad \rightarrow \quad r_{gearbox} = \frac{N_c}{N_{mot}} \tag{5.13}$$

Then, considering a given transmission ratio, the pressure ratio can be expressed as a function of supercharger speed and corrected mass flow to give the outlet pressure:

$$\frac{P_{out}}{P_{in}}, \eta_c = f\left\{N_c, \dot{m}_{cor}\right\} \quad \rightarrow \quad P_{out} \tag{5.14}$$

Finally, the corrected mass flow can be calculated as a function of supercharger speed and pressure ratio. In this case, a throttle valve controls the supercharger and its resultant actuator position is obtained as:

$$\dot{m}_{cor}, \eta_c = f\left\{N_c, \frac{P_{out}}{P_{in}}\right\} \quad \rightarrow \quad C_d A_{ref} = \frac{\dot{m}_c - \dot{m}}{f\left(R, \gamma, T_{in}, P_{in}, P_{out}\right)} \tag{5.15}$$

Parallel configuration:

In a parallel configuration, the mass flows passing through the compressors ($c1$ and $c2$) are defined as:

$$\dot{m}_{c1} = \vartheta_c \dot{m} \quad and \quad \dot{m}_{c2} = \dot{m} - \dot{m}_{c1} \tag{5.16}$$

where ϑ_c stands for the mass flow distribution which results from the balance between compressor and turbine performances. Under this configuration, matching calculations cannot be straightforward and an iterative process between the intake and exhaust line MVEM's must be performed to determine ϑ_c.

5.2.2 Exhaust Line

The proposed base structure of the exhaust line MVEM is shown in figure 5.3 with its boosting components library. The gas mass flow determined by the filling & emptying model enters in 3 at the HP stage inlet. The evolutions in the HP and LP exhaust charging systems go respectively from 3 to 34 and 34' to 4 while heat losses between both stages are taken into account by a heat transfer model. At the LP stage outlet, the gas flow passes through the post treatment system (DOC + DPF) and the silencer before going out to the atmosphere. A LP EGR circuit composed by a valve and a cooler connects the DPF outlet to the air filter outlet. An additional EGR valve is fitted at the silencer inlet to increase the exhaust backpressure when the pressure difference is not sufficient to reach the desired LP EGR rate. For the HP and LP exhaust boosting systems, the components library includes wastegated fixed geometry turbines in single or parallel configuration, variable geometry turbines with possibility of additional wastegate valve and connections for single charging systems, superchargers or eBoosters.

Keeping the same philosophy, volume capacities are not considered in steady state operations and mass flows as gas composition are assumed to be constant in the whole exhaust line. Eq. 5.3 and Eq. 5.8 are used to calculate the LP EGR valves position whereas a mass balance is introduced in 45 to determine the silencer mass flow as a function of the LP EGR mass flow. Pressure losses across the LP EGR cooler, post treatment system and silencer are modeled by Eq. 5.6 as defined for the air filter. Heat transfers are reproduced by the effectiveness method [153] in the EGR cooler while specific models as ones proposed by Boger et al. [43] or Konstandopoulos et al. [199, 200] can be employed for the DOC and DPF. The other sub-models used in the exhaust line MVEM are described below.

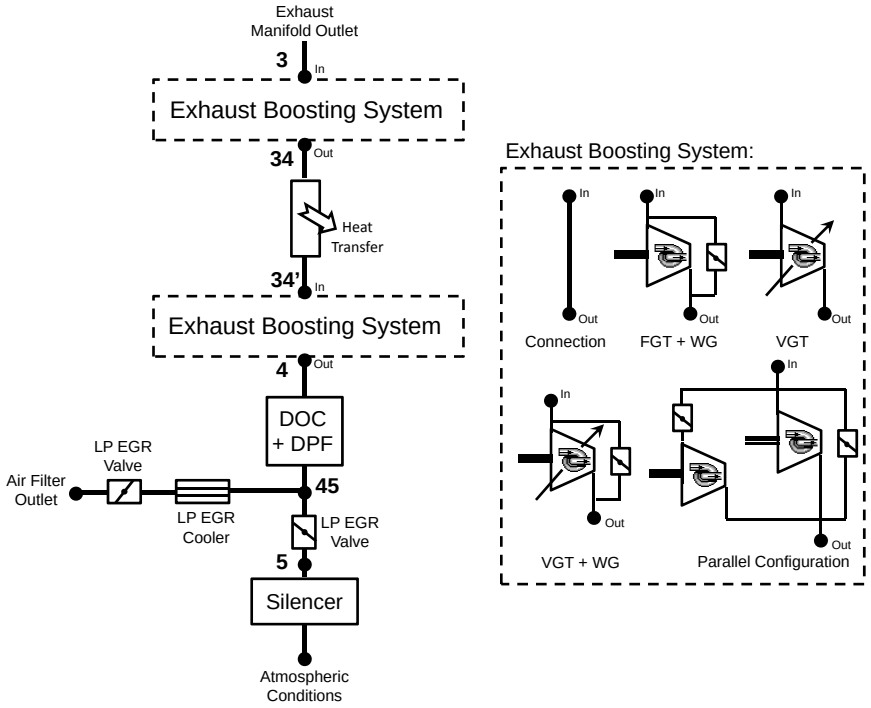

Figure 5.3: Based structure and components library of the exhaust line MVEM.

Heat transfer - 1 node model:

The heat transfer model is based on the thermal resistance scheme proposed by Dolz et al. [98, 117, 224] which computes the radial heat flux through one node at the inner side on the pipe wall, see figure 5.4. A duct with a characteristic length and diameter is defined to reproduce the considered air path geometry and equations are resolved in only one calculation point assuming constant heat transfer along the whole pipe. Convection heat transfer coefficients at the inner and outer surface are calculated by correlations presented by Depcik at al. [93] and Hilpert [148] respectively:

$$Nu_{inner} = 0.0718\,\mathrm{Re}^{\frac{3}{4}} \quad and \quad Nu_{outer} = 0.193\,\mathrm{Re}^{0.168}\,\mathrm{Pr}^{\frac{1}{3}} \tag{5.17}$$

where Nu, Re and Pr are the Nusselt, Reynolds and Prandtl number. The radiation heat transfer coefficient is derived from the Stefan-Boltzmann laws [153] and the correlations proposed by Konstantinidis [201] are employed to

estimate the emissivity of the different materials used in modern passenger cars engine design. The viscosities are obtained as a function of the temperature by the correlations proposed by Sutherland [72].

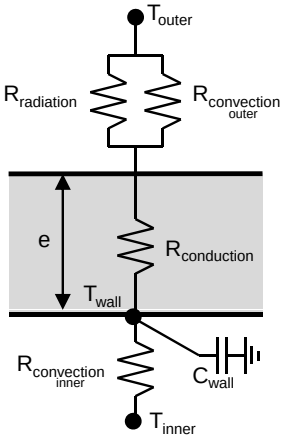

Figure 5.4: the 1 node heat transfer model.

Wastegated Fixed Geometry Turbine:

Turbine performance is modeled from the adapted characteristic maps presented in the previous chapter and measured in a turbocharger test bench. In steady state operations, turbine power is equal to the compressor power calculated by the intake line MVEM. The characteristic maps can therefore be interpolated with quadratic functions to obtain adapted mass flow and pressure ratio as a function of adapted power:

$$\dot{m}_{adapt}, \frac{P_{in}}{P_{out}} = f\left\{\dot{W}_{adapt}\right\} \quad with \quad \dot{W}_{adapt} = \frac{\dot{W}_t}{\sqrt{T_{in}T_{ref}}\frac{P_{out}}{P_{ref}}} \tag{5.18}$$

Knowing the adapted mass flow passing through the turbine, the real mass flow for both turbine (m_t) and wastegate (m_{WG}) can be calculated as:

$$\dot{m}_t = \frac{\dot{m}_{adapt}\frac{P_{out}}{P_{ref}}}{\sqrt{\frac{T_{in}}{T_{ref}}}} \qquad \dot{m}_{WG} = \dot{m} - \dot{m}_t \tag{5.19}$$

and the wastegate actuator position can be deduced from Eq. 5.8. The turbine efficiency is then derived from the isentropic power as:

$$\eta_t = \frac{W_t}{m_t C_p T_{in} \left(1 - \left(\frac{P_{in}}{P_{out}}\right)^{\frac{1-\gamma}{\gamma}}\right)} \tag{5.20}$$

Finally assuming that heat losses are small enough to be neglected in the wastegate, a temperature balance is performed at the turbine outlet as follows:

$$T_{out} = \frac{\dot{m}_t T_{t_{out}} + \dot{m}_{WG} T_{in}}{\dot{m}} \quad with \tag{5.21}$$

$$T_{t_{out}} = T_{in} - T_{in}\eta_t \left(1 - \left(\frac{P_{in}}{P_{out}}\right)^{\frac{1-\gamma}{\gamma}}\right) \tag{5.22}$$

In parallel configuration, the pressure ratio in both turbines must be identical. In this case, an iterative process is carried out with the intake line MVEM varying ϑ_c until reaching pressure equilibrium at the turbines inlet.

Variable Geometry Turbine:

In a variable geometry turbine, the full exhaust gas mass flow is routed via the turbine and its vanes position is controlled to produce the desired power. By interpolation of the turbine adapted characteristic maps, the actuator position and pressure ratio can be obtained as a function of adapted mass flow and adapted power as:

$$\chi_t, \frac{P_{in}}{P_{out}} = f\left\{\dot{m}_{adapt}, \dot{W}_{adapt}\right\} \quad with \quad \dot{m}_{adapt} = \frac{\dot{m}\sqrt{\frac{T_{in}}{T_{ref}}}}{\frac{P_{out}}{P_{ref}}} \tag{5.23}$$

If χ_t is higher than the fully open position, an additional wastegate is fitted around the VGT and equations are resolved as a FGT having the same swallowing capacity as the fully open VGT.

5.3 Crank Angle Resolved Model

Engine scavenging and in-cylinder processes experience important variations during an engine cycle. Equations describing mass transfers and thermodynamic properties evolutions must therefore be resolved with small time steps to correctly predict the effects of these variations. Here, a 0D filling & emptying model based on a variable crank angle resolution has been developed to predict the main physical phenomena taking place in the manifolds and cylinders. The cylinder model having a higher complexity, the general filling & emptying approach will be first described for the base engine architecture, manifolds and HP EGR circuit. Then, the additional submodels required in the cylinders will be presented. Finally, the combustion model to simulate the rate of heat release will be briefly introduced.

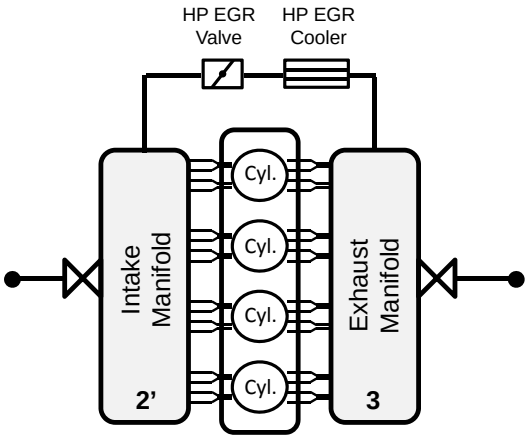

Figure 5.5: Schematic of the filling & emptying model.

5.3.1 Filling & Emptying Modeling

The filling & emptying model reproduce the physical engine scavenging processes occurring during the intake and exhaust strokes. To take into account the effects of mass transfers and accumulations, it includes a control volume for each manifold and each cylinder as shown in figure 5.5. A four cylinders engine has been represented in the figure, however the model is generic and any number of cylinders can be considered. The poppet valves

as the HP EGR valve are simulated by isentropic nozzles while the ports and the HP EGR pipes are directly included in the volume of their corresponding manifolds. The model assumes in the control volumes that the gas has a perfect behavior, is quiescent, (kinetic energy not considered), and the mixture is perfect in both temperature and composition (three species involved: air, fuel vapor and stoichiometric combustion products). These hypotheses are reasonable since negligible errors are committed as shown by Lapuerta et al. [214] for the particular case of cylinders.

To calculate the instantaneous evolution of the pressure and temperature in the control volumes (cv), the model uses the first law of thermodynamics for an open system resolving the mass and energy conservation equations in combination with the perfect gas equation. These equations can be written in their general form as:

$$\Delta \dot{m}_{cv} = \sum_i \dot{m}_i dt \tag{5.24}$$

$$d(m_{cv}u_{cv}) = dQ_{cv} + dW_{cv} + \sum \left(h_{in} + \frac{v_{in}^2}{2}\right) dm_{in} - \sum \left(h_{out} + \frac{v_{out}^2}{2}\right) dm_{out} \tag{5.25}$$

$$p_{cv}V_{cv} = m_{cv}R_{cv}T_{cv} \tag{5.26}$$

where, u is the internal energy, Q the heat transfer (combustion process and heat losses through the walls), W the work, h the enthalpy and v the gas velocity. Considering that the outgoing mass flows have the same stagnation enthalpy as the gas inside the control volume and assuming quasi-steady processes, the energy conservation equation can be rearranged between two time steps as:

$$\ln\left(\frac{V_{t+dt}}{V_t}\frac{m_{cv_t}}{m_{cv_{t+dt}}}\left(\frac{T_{cv_{t+dt}}}{T_{cv_t}}\right)^{\frac{1}{\gamma-1}}\right) = \int_t^{t+dt} \frac{dQ_{cv}}{p_{cv}V_{cv}} + \int_t^{t+dt} \frac{1}{p_{cv}V_{cv}} \sum \left(h_{in} + \frac{v_{in}^2}{2} - h_{cv}\right) dm_{in} \tag{5.27}$$

At each calculation step, the instantaneous incoming and outgoing mass flows are updated in the different restrictions from the pressure and temperature values obtained in the previous time step. With the mass variations, the energy conservation equation can then be resolved by a direct iterative method [87] to find the new temperature and therefore the new pressure applying the perfect gas equation.

By resolving only the mass and equation conservation equations, the proposed model cannot reproduce the wave effects present in the manifolds. For that, it is necessary to use a 1D wave action model which is, as already mentioned, generally impracticable for matching calculations because it requires a good knowledge of the engine geometry and it is quite time consuming. In fact, even when a simple geometry is considered, three conservation equations must be solved (mass, energy and momentum) in each calculations nodes. The number of equations is thus considerably increased and computational times become rapidly unacceptable. For this reason, a simple volume model has been adopted. It should be noticed that this hypothesis can obviously lead to important errors if the engine has some particular elements such as pulse converters. In this case the proposed model might not be suitable and hence the precise system geometry and 1D modelling would be necessary.

Mass balance:

The mass flow through each restriction is calculated with the isentropic nozzle equation (Eq. 5.8 and Eq. 5.9). For the poppet valves, the reference area (A_{ref}) corresponds to the plate section while the discharge coefficient (C_d) is interpolated from the experimental data obtained in the flow test rig as a function of valve lifts and flow direction.

$$C_d A_{ref} = f\left\{lifts, \dot{m}_{in/out}\right\} \tag{5.28}$$

For the external sections that represent the engine connections to the aftercooler outlet and HP turbine inlet, the effective areas are adjusted during the simulations according to the mean pressure calculated in the manifolds. In fact, the mean pressures in the manifolds have to coincide with the intake pressure objective and the resultant exhaust pressure calculated by the MVEM models. For that, an initial estimation of the effective section is done. Then, when an engine cycle has been calculated, the instantaneous pressures in the manifolds are averaged ($\widehat{P}$) and the effective sections are corrected as:

$$C_{\mathrm{d}_{im}}^{\alpha+720} = \frac{\sqrt{\left(\frac{P_{2'}}{P_2}\right)^{\frac{2}{\widehat{\gamma}}} - \left(\frac{P_{2'}}{P_2}\right)^{\frac{\widehat{\gamma}+1}{\widehat{\gamma}}}}}{\sqrt{\left(\frac{\widehat{P}_{im}}{P_2}\right)^{\frac{2}{\widehat{\gamma}}} - \left(\frac{\widehat{P}_{im}}{P_2}\right)^{\frac{\widehat{\gamma}+1}{\widehat{\gamma}}}}} C_{\mathrm{d}_{im}}^{\alpha} \tag{5.29}$$

$$C_{d_{em}}^{\alpha+720} = \frac{\widehat{P}_{em}\sqrt{\left(\frac{P_{em_{ext}}}{\widehat{P}_{em}}\right)^{\frac{2}{\widehat{\gamma}}} - \left(\frac{P_{em_{ext}}}{\widehat{P}_{em}}\right)^{\frac{\widehat{\gamma}+1}{\widehat{\gamma}}}}}{P_3\sqrt{\left(\frac{P_{em_{ext}}}{P_3}\right)^{\frac{2}{\widehat{\gamma}}} - \left(\frac{P_{em_{ext}}}{P_3}\right)^{\frac{\widehat{\gamma}+1}{\widehat{\gamma}}}}} C_{d_{em}}^{\alpha} \tag{5.30}$$

where the subscripts $_{im}$ and $_{em}$ stand for intake manifold and exhaust manifold respectively. It is assumed that the external intake manifold pressure is equal to the inlet aftercooler pressure (P_2) whereas the external exhaust manifold pressure ($P_{em_{ext}}$) is defined as:

$$\frac{P_3}{P_{em_{ext}}} = \sqrt{\frac{P_3}{f\left\{P_{34}, P_4\right\}}} \tag{5.31}$$

to reduce the risk of sonic conditions in the restriction. The choice between P_{34} or P_4 is realized according to the presence or not of an HP turbine in the boosting architecture.

For the EGR valve, HP EGR rates (X_{HPEGR}) appear generally as an objective in the matching calculations. The corresponding mean mass flow passing through the HP EGR circuit ($\widehat{\dot{m}}_{HPEGR}$) depends on the breathing capability and is defined as:

$$\widehat{\dot{m}}_{HPEGR} = \frac{X_{HPEGR}\left(\widehat{\dot{m}}_a + \widehat{\dot{m}}_{LPEGR}\right)}{1 - X_{HPEGR}} \tag{5.32}$$

where $\widehat{\dot{m}}_a + \widehat{\dot{m}}_{LPEGR}$ is the cycle-averaged mass flow rate entering in the intake manifold by the external section. The position of the HP EGR valve is thus

readjusted during the simulations to obtain the desired mass flow applying to the effective section the following control:

$$C_d^{\alpha+720} A_{ref} = \frac{X_{HPEGR}\left(\widehat{\dot{m}}_a + \widehat{\dot{m}}_{LPEGR}\right)}{1 - X_{HPEGR}} \frac{C_d^{\alpha} A_{ref}}{\widehat{\dot{m}}_{HPEGR}} \tag{5.33}$$

In order to calculate the thermodynamic properties of the gas in both manifolds, it is necessary to know the instantaneous gas composition. Taking into account the masses involved and assuming complete combustion (no remaining fuel vapor in the cylinders at exhaust valves opening) which is quite realistic for Diesel engines running with excess air, the instantaneous mass fractions can be expressed as:

$$Y_{b_{t+\Delta t}} = \frac{Y_{b_t} m_{cv_t} + \sum_i \left(Y_{b_i} \int_t^{t+\Delta t} \dot{m}_i dt \right)}{m_{cv_{t+\Delta t}}} \quad and \quad Y_a = 1 - Y_b \tag{5.34}$$

Heat transfers:

Heat transfer is reproduced from the effectiveness method [153] in the HP EGR cooler and by the 1 node model with thermal resistance scheme [98, 117, 224] in the ports and manifolds as previously described. Different characteristics ducts are defined to reproduce the considered geometries and the same correlations presented for the exhaust line are employed for the exhaust manifold and all outer surfaces. For the other inner surfaces, heat transfer coefficients are calculated in the intake manifold and intake ports with the correlation presented by Depcik at al. [93]:

$$Nu_{inner} = 0.0694\,\mathrm{Re}^{\frac{3}{4}} \tag{5.35}$$

while the correlations introduced by Caton [68] and modified by Reyes [279] are used in the exhaust ports. In the exhaust ports, the turbulence generated at the cylinders discharge has an important impact on the heat transfer and a distinction is made when the exhaust valves are open or closed:

$$Nu_{inner_{open}} = 0.5 \times 0.0075\,\mathrm{Re} \quad and \quad Nu_{inner_{closed}} = 0.022\widehat{Re}^{0.8} \tag{5.36}$$

When the valves are closed in addition to different correlation coefficients, a cycle-averaged Reynolds number ($\widehat{Re}$) is considered instead of an instantaneous one (Re).

5.3.2 Cylinder Model

Numerous relevant physical processes take place in the combustion chamber and have to be modeled to correctly predict engine performance and behavior. The cylinder control volume has thus a higher complexity and integrates additional submodels.

Instantaneous volume:

The instantaneous volume is calculated as the sum of the combustion chamber volume (V_{cc}), the instantaneous displaced volume ($V_{d_{inst}}$) and the deformations produced by gas pressure (ΔV_p) and inertia efforts (ΔV_{inert}).

$$V = V_{cc} + V_{d_{inst}} + \Delta V_p + \Delta V_{inert} \tag{5.37}$$

The engine deformations are normally not considered in 0D model. However in Diesel engines with pressures reaching more than 150 bar at the top dead center, these deformations can produce volume variations higher than 2% [264]. That is why a simple deformation model has been implemented and the different terms of Eq. 5.37 can be expressed as:

$$V_{cc} = \frac{V_d}{r_c - 1} \tag{5.38}$$

$$V_{d_{inst}} = \frac{\pi D^2 A}{8}\left[\sqrt{\left(1+\frac{1}{\psi}\right)^2 - e_{cc}^2} - \cos(\alpha) - \sqrt{\frac{1}{\psi^2} - (\sin(\alpha) - e_{cc})^2}\right] \tag{5.39}$$

$$\Delta V_p = k_{def}\frac{\pi D^2}{4}\frac{P}{E_{steel}}\left(\frac{D}{D_{pp}}\right)^2 L_0 \tag{5.40}$$

$$\Delta V_{inert} = k_{def} \frac{m_{alt} a_p}{E_{steel}} \left(\frac{D}{D_{pp}} \right)^2 L_0 \tag{5.41}$$

where V_d is the total displaced volume, r_c the compression ratio, D the piston diameter, ψ the crank and connecting rod lengths ratio, e_{cc} the piston eccentricity, k_{def} a calibrated deformation coefficient, E_{steel} the elasticity coefficient of steel, D_{pp} the piston pin diameter, m_{alt} the mass with reciprocating motion, a_p the instantaneous piston acceleration and L_0 a characteristic length defined as:

$$L_0 = h_{pis} + L_c + \frac{S}{2} \tag{5.42}$$

being h_{pis} the distance from the piston pin axis to the top surface of the piston, L_c the connecting rod length and S the stroke.

Heat transfer:

The calculation of the heat flux to the walls in the combustion chamber is based on the thermal resistor network proposed by Degraeuwe and Torregrosa et al. [92, 326, 328]. As it can be observed in Figure 5.6, the network consists of 4 nodes (piston, cylinder liner, cylinder head and valves) which can exchange heat with each other and with the different fluids involved (gas, coolant and oil). The thermal conductances are defined as a function of the engine geometry, operational parameters and material properties, while the heat transfer coefficient between the gas and the walls is calculated with Woschni's equation [369, 370]:

$$h = 0.012 D^{-0.2} T^{-0.53} P^{0.8} \left(C_{w1} c_m + C_{w2} c_u + 0.001 \frac{V_d T_{IVC}}{V_{IVC} p_{IVC}} (P - P_{mot}) \right)^{0.8} \tag{5.43}$$

Here c_m is the mean piston speed, c_u the instantaneous tangential velocity at the cylinder wall due to swirl, C_{w1} and C_{w2} calibration parameters, p_{mot} the motoring pressure assuming polytropic evolution and IVC refers to conditions at intake valve closing. The values of the constants and the way in which the swirl effect is considered has been specially optimized for direct injection

Diesel engines by Payri et al. [262, 263] which define from CFD calculations the instantaneous tangential velocity as:

$$c_u(\alpha) = \frac{D_{bowl}^2}{D^2\, \mathrm{e}^{\left(k_1 MSN^{k_2}\right)}} + \frac{1}{\left(\cosh\left(\frac{\alpha}{100}\right)\right)^{40} + \frac{D_{bowl}^2}{D^2\, \mathrm{e}^{\left(k_1 MSN^{k_2}\right)} - D_{bowl}^2}} \tag{5.44}$$

where D_{bowl} is the bowl diameter and MSN the mean swirl number measured in a flow test rig as described in the previous chapter.

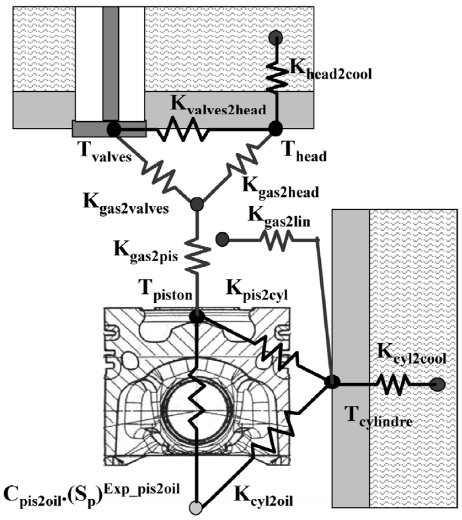

Figure 5.6: Cylinder wall thermal resistor network [326].

In the model, only convection processes are considered. This hypothesis is reasonable during the compression stroke and after the end of combustion [18]. But when combustion takes place, there is also radiation from the gas and the soot particles formed. Nowadays, there is still no agreement to characterize this radiative heat transfer. Morel et al. [243] obtained values ranging from 4% to 20% while Heywood [145] states that this fraction can be higher than 20%. With these discrepancies and the excessive complexity of soot formation models [91], it has been preferred here to omit radiative heat fluxes.

Short circuit:

The short circuit flow is defined as the mass flow which travels from one valve into the other without staying in the cylinder. This process is controlled

by the instantaneous pressure difference between the intake and exhaust manifolds and it is assumed to take place instantaneously and independently of the simultaneous in-cylinder flow evolution. The short circuit mass flow is calculated by means of Eq. 5.8 considering the flow path shown in figure 5.7 (in this case from intake to exhaust). This path is equivalent to the passage across two isentropic nozzles in series where the effective sections are defined by the angle θ and the instantaneous valve lifts [22, 38]. The reduced effective section $C_{d_{sc}}A_{sc}$ used in Eq. 5.8 is thus defined as:

$$C_{d_{sc}}A_{sc} = \sqrt{\frac{1}{\frac{1}{C_{d_1}^2 A_1^2} + \frac{1}{C_{d_2}^2 A_2^2}}} \tag{5.45}$$

Perfect displacement model:

To correctly predict the engine breathing capabilities, it is assumed the backflows during the entrance and the exit to the cylinder have no time to be cooled in the ports. As the distribution is optimized to avoid these phenomena, the backflows represent normally only a small mass quantity but their temperatures can be very different to the gas temperature in the manifolds, especially in the intake side. If a mixing process is undertaken, the temperature of these backflows will be averaged with the global manifold charge and the calculated mass flow returning to the cylinder will be overestimated [42, 110, 294]. For that, a perfect displacement model accumulates at each calculation step packets of gas with a particular mass, temperature and composition depending on the flow proceeding from the cylinder and the short circuit. When the flow returns into the cylinder, the total mass crossing the valve during that calculation step is supplied by the required number of packets being the lasts to exit the firsts to enter. Since the packet properties are known and have been unchanged, the mass flow and gas composition can be conveniently updated in the cylinder. A schematic of the perfect displacement model is shown in figure 5.7 and more details on its calculation procedure can be found in [38].

Blow by:

Blow-by mass flows are generally quite small in HSDI Diesel engines but some influences on the predicted trapped mass have been reported by Payri et al. [264] when they are not considered in the mass and energy balances.

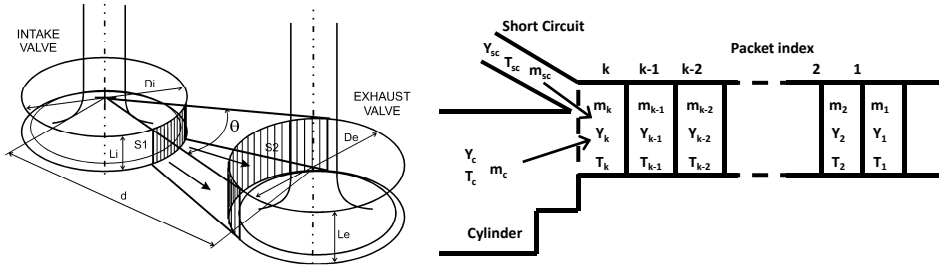

Figure 5.7: Left: short circuit effective section - Right: perfect displacement model.

The instantaneous mass flow of blow-by to the crankcase is estimated by the isentropic equation nozzle (Eq. 5.8).The discharge coefficient is adjusted from experimental measurements performed on similar base engines while the correlation proposed by Hohenberg [152] ($A_{ref} = 3.5 \cdot 10^{-6} D$) is used for the reference section.

Fuel injection:

The injection rate shape is predicted from the injection settings and the injector experimental characterizations performed in an injection rig as presented in section 4.2. Only one zone is considered in the model, so only a single gas phase is taken into account in the conservation equations assuming instantaneous fuel evaporation along the injection process. The effect of this injection process on the energy balance has positive and negative contributions that can be decomposed as:

$$\begin{aligned} h_{f,l}\left(T_{inj}\right) - u_{f,g}\left(T\right) = &\left[h_{f,l}\left(T_{inj}\right) - u_{f,l}\left(T_{inj}\right)\right] - \left[u_{f,l}\left(T_{evap}\right) - u_{f,l}\left(T_{inj}\right)\right] \\ &- \left[u_{f,g}\left(T_{evap}\right) - u_{f,l}\left(T_{evap}\right)\right] - \left[u_{f,g}\left(T\right) - u_{f,g}\left(T_{evap}\right)\right] \end{aligned} \tag{5.46}$$

where the temperature at which enthalpies and internal energies are evaluated has been indicated in brackets. The four terms in the right hand side correspond respectively to the specific flow work of the injected fuel, the liquid fuel heating from the injection temperature (T_{inj}) up to the evaporation temperature (T_{evap}), the internal energy of vaporization and finally to the gaseous fuel heating from the vaporization temperature up to the mean gas temperature (T) [22].

Mass balance:

The model calculates the instantaneous mass changes of each species (air, gaseous fuel and burned products) from the different processes that take place in the combustion chamber: intake and exhaust flows, backflows, short circuit, blow-by, fuel injection and combustion. With these mass flows, the species mass fractions can be written as:

$$Y_{b_{t+\Delta t}} = \frac{Y_{b_t} m_{cv_t} + \sum_i \left(Y_{b_i} \int_t^{t+\Delta t} \dot{m}_i dt \right) + \left(m_{f_{cycle}} + \frac{m_{f_{cycle}}}{F} \right) HRF}{m_{cv_{t+\Delta t}}} \tag{5.47}$$

$$Y_{f_{t+\Delta t}} = \frac{Y_{f_t} m_{cv_t} + \int_t^{t+\Delta t} \dot{m}_f dt - m_{f_{cycle}} HRF}{m_{cv_{t+\Delta t}}} \tag{5.48}$$

$$Y_{a_{t+\Delta t}} = 1 - Y_{b_{t+\Delta t}} - Y_{f_{t+\Delta t}} \tag{5.49}$$

being HRF the instantaneous heat release fraction and $m_{f_{cycle}}$ the fuel mass injected per cycle.

5.3.3 Combustion Model

Combustion is the most complex process to be evaluated in Diesel engine modeling. In function of the objectives, different approaches can be employed: zero-dimensional single-zone models, quasi-dimensional multi-zone models and multidimensional models. It has been shown that a single-zone approach is capable of accurately predicting the Rate of Heat Release (RoHR) with a high computational efficiency [34, 80, 105], while a multi-zone decomposition is imperative when combustion details such as emissions prediction must be accounted [101, 149, 277]. As a precise description of the combustion process is not essential to perform matching calculations, a single-zone approach has thus a sufficient complexity for the proposed 0D engine model.

Here, the predictive combustion model developed by Arregle et al. [28, 29, 30] has been used for the simulations. The model constructed around a spray-mixing model is based on the gaseous steady jets theory and on the conceptual injection and combustion models proposed by Dec [91] and Hiroyasu et al.

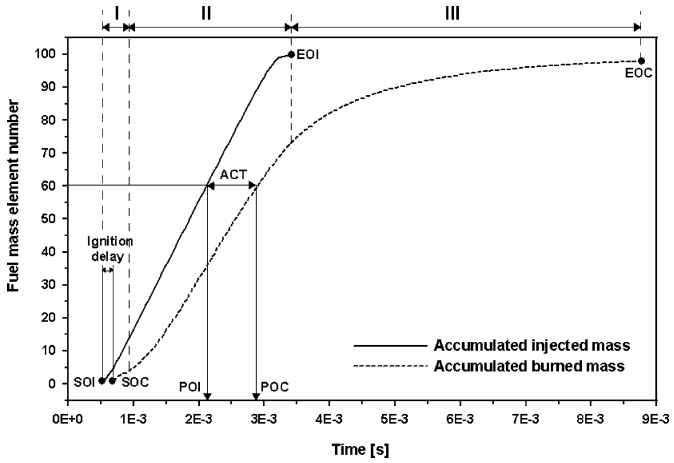

Figure 5.8: ACT parameter definition from the injection and combustion laws [28].

[149]. Through the calculation of a parameter called Apparent Combustion Time (ACT), it allows the establishment in an explicit way of the relation between the rate of heat release, the injection rate law and the instantaneous variables that control the combustion process. During the injection process, the total injected mass is divided into small chronological fuel elements, all of them with the same mass. The parameter ACT defines then the time intervals between the instant at which the fuel element is injected (Point of Injection POI) and the instant at which the fuel element is burned (Point Of Combustion POC) as shown in figure 5.8. Assuming that the diffusion combustion phase is controlled by the in-cylinder gas/fuel mixing process and the combustion process is produced in oxygen/fuel stoichiometric conditions, the ACT parameter is expressed as:

$$ACT_i = K_{mix} \left[\rho_g^{0.5} \cdot v_{inj} \cdot Y_{O_2}^{0.5} \cdot D_{nozz}^{-1} \right]_{POI_i \rightarrow POC_i}^{-1} \tag{5.50}$$

being ρ_g the in-cylinder gas density, v_{inj} the injection velocity, Y_{O_2} the oxygen concentration, D_{nozz} the nozzle diameter and K_{mix} a calibrated constant mainly related to the combustion chamber geometry and nozzle characteristics. In order to take into account the critical transient phenomena at the beginning (*) and after the end of injection (**), virtual equivalent injection velocities defined from CFD studies are added to modify the quasi-steady injection velocity in Eq. 5.50 as:

$$v^{*}_{inj} = v_{inj}\left(1 + B_1 \cdot \mathrm{e}^{\left(\frac{-t}{B_2}\right)}\right) \quad and \quad v^{**}_{inj} = v^{*}_{injEOI} \cdot e\left(\frac{-t}{M_1 \cdot e^{\left(\frac{t}{M_2}\right)}}\right) \quad (5.51)$$

B_1, B_2, M_1 and M_2 are constants adjusted by a genetic algorithm with experimental information from different engines. Through the simplification and parameterization of complex chemical kinetics and transient effects, this combustion model results valid for a wide range of operating conditions and only one fitting constant (K_{mix}) has to be adapted to the specific engine configuration.

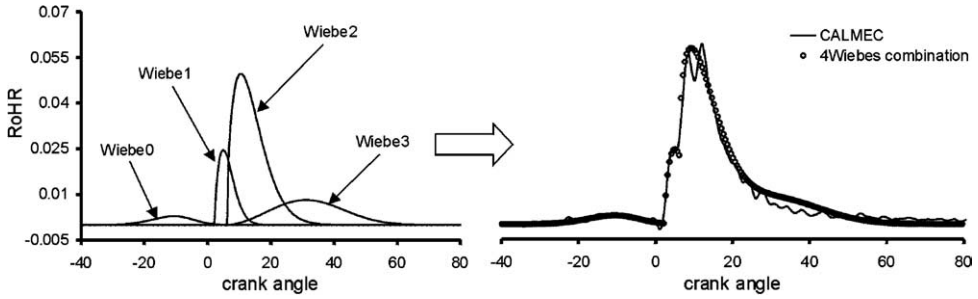

Figure 5.9: Wiebe's laws combination for RoHR determination [118].

In the engine development process, experimental RoHR's measured in mono-cylinder test benches or coming from similar base engines are sometimes available for the matching calculations. In this case, another approach based on the description of the RoHR shape by mathematical functions can also be used to reproduce the combustion process. These functions are purely empirical without direct relations to the physics of the injection-combustion process but present a very high computational efficiency which can be very interesting especially for transient calculations. These laws were proposed by Wiebe [362] and have been then adapted by Watson [351] to the specific case of HSDI Diesel engines. With this approach, the RoHR is expressed as a sum of Wiebe functions (see figure 5.9) as:

$$RoHR = \sum_i \left[\frac{C_i\,(m_i+1)}{d_{comb_i}} \left(\frac{\alpha - SOC_i}{d_{comb_i}}\right)^{m_i} \cdot e^{\left[-C_i\left(\frac{\alpha - SOC_i}{d_{comb_i}}\right)^{m_i+1}\right]} \cdot \beta_i \right] \quad (5.52)$$

where i represents the combustion phase (pilot, premixed, diffusion, late or post combustion), α the crank angle, d_{comb_i} the duration of the combustion phase, SOC_i the start of the combustion phase, β_i the proportion of the combustion phase with respect to the whole combustion, C_i is the completion parameter that is traditionally used to represent the combustion efficiency and m_i is the shape parameter that controls the gradient of the combustion phase. The values of the different parameters are fitted to the experimental RoHR with statistical methods such as Levenberg-Marquardt algorithms [220, 230] to form a complete data base. The data base is then interpolated by different techniques such as neural network [118] or weighted linear interpolation [258, 298] to predict the RoHR in other running conditions. This approach has obviously important limitations and its validity can only be guaranteed when the simulated operating conditions are relatively close to the experimental ones present in the database.

5.4 A Fully Integrated 0D Engine Model

5.4.1 0D Engine Model Structure

The different models previously described have been assembled in a Matlab environment as shown in figure 5.10 to form a whole engine model. The filling & emptying model corresponds to the central part of this engine model sharing information with both combustion and air path models. Although their submodels such as instantaneous volume, heat transfer, blow-by, fuel injection, etc... are identical, the combustion model has not been directly integrated to the cylinder model due to its relatively high computational cost and different time step (fixed 0.2cad vs. variable 0.5cad time steps). In that way, it can also be assumed that the different cylinders run under the same combustion process during one or various engine cycles to optimize the computational time.

As explained in the introduction, the air path model has been divided in two resolution approaches depending if the calculations are performed in steady state or transient conditions. In the first case, the intake and exhaust line MVEM's are resolved with a boost pressure oriented scheme to perform architecture matching. While in the second case, the filling & emptying method is extended to the intake/exhaust lines and an actuator oriented scheme allows to optimize control strategies and to evaluate architecture performance in transient operations.

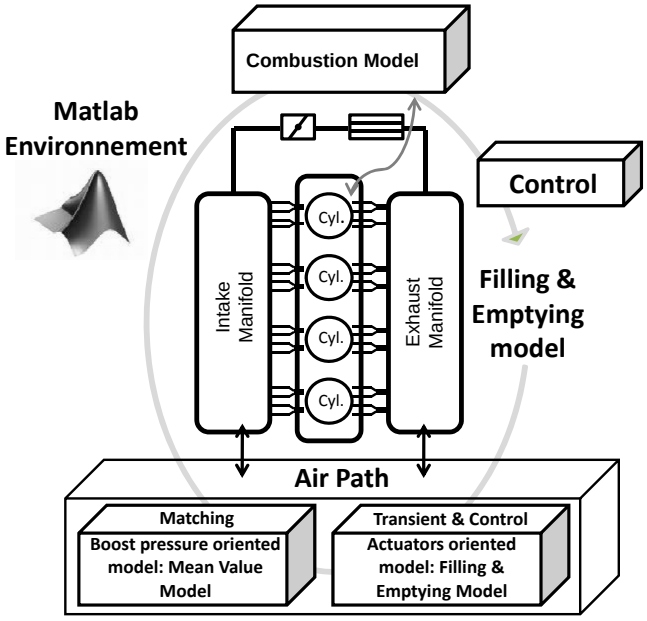

Figure 5.10: Schematic of the 0D engine model.

Finally, a control algorithm completes the structure of the engine model managing the different type of resolutions and supervising the information transfers. These information transfers regroup the exchanges between the models and the accesses to the various data bases that contain the elements characteristics (compressors, turbines, injectors, coolers, air filters, etc...), the engine geometrical data (piston diameter, crank length, compression ratio, etc...) and the test campaign data (engine speed, boost pressure, injection settings, etc...).

5.4.2 Algorithm Resolution and Control

5.4.2.1 Boost Pressure Oriented Model

The resolution methodology corresponding to the boost pressure oriented scheme is presented in figure 5.11. From initial values and test campaign data, a first air mass flow is estimated to run the intake line model. In this model, several variables are defined as a function of temperature or corrected

parameters. Although important variations of these parameters have only small consequences on the calculated variables, two or three loops are generally required to obtain the convergence of the thermodynamics properties along the whole air path. At the end, the compressors power and the aftercooler outlet temperature are respectively transferred to the exhaust MVEM and filling & emptying models.

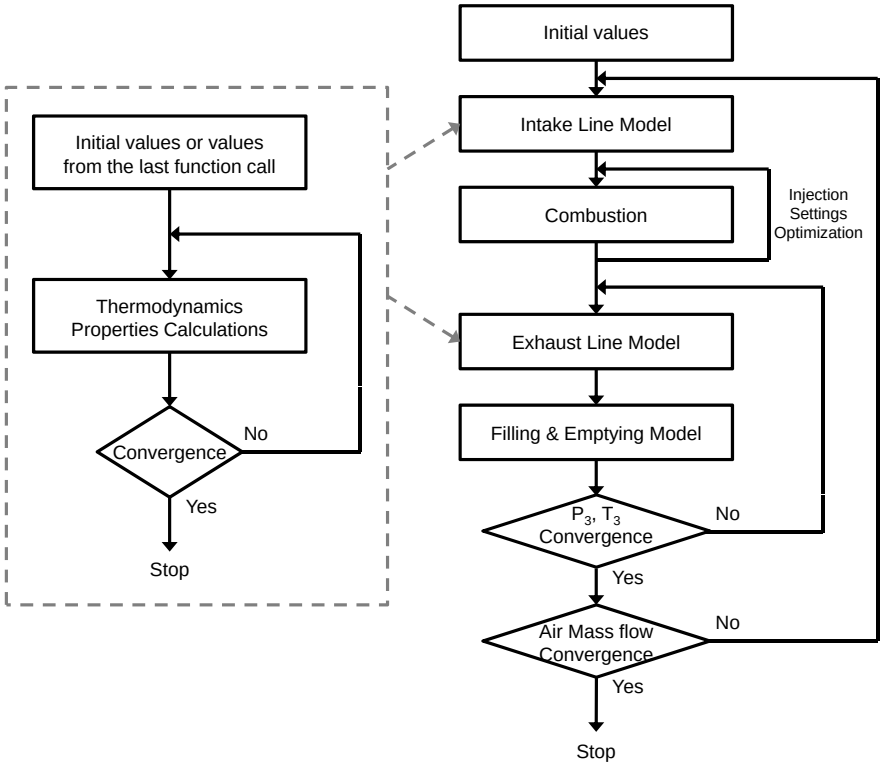

Figure 5.11: Boost pressure oriented resolution scheme.

Numerous injection strategies can be implemented with the combustion model to determine or adjust the injection settings according to specific objectives. In matching calculations, the fuel mass injected per cycle is generally defined as a function of AFR, while the injection timings are calibrated to achieve the best fuel consumption under limited maximum cylinder pressures. When the combustion model is called, an iterative process is thus performed to optimize the injection timings as a function of the combustion results obtained. The optimum injection law and the RoHR are then sent to the cylinders models.

With compressors power coming from the intake MVEM and an estimated exhaust manifold temperature, the exhaust MVEM calculates the thermodynamics properties along the exhaust line and provides the corresponding exhaust manifold pressure to the filling & emptying model. As for the intake MVEM, 2 or 3 iterations must be carried out to achieve a complete convergence of all thermodynamics properties. Knowing the RoHR and the mean pressures in manifolds, the filling & emptying model is resolved as shown in figure 5.12.

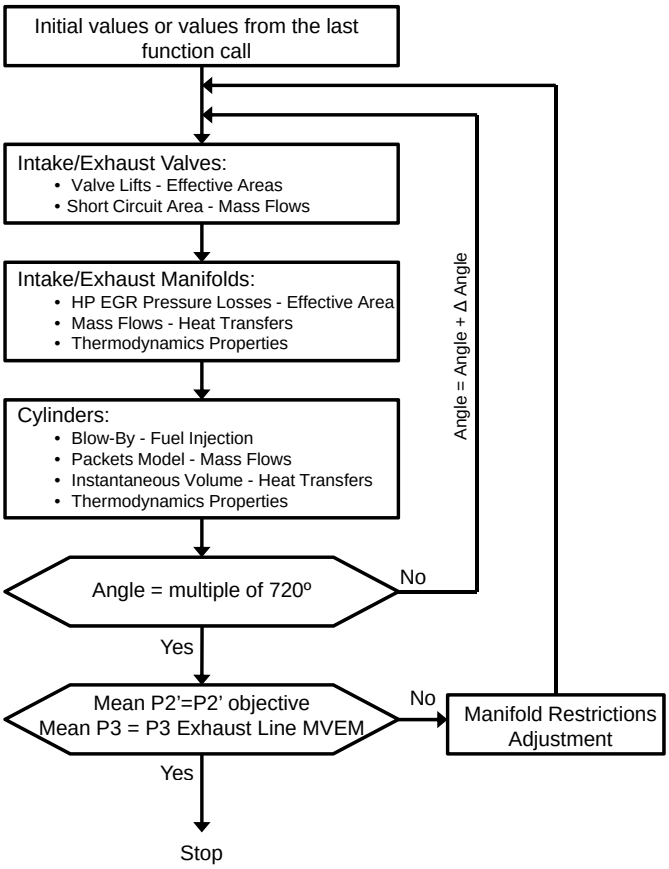

Figure 5.12: Resolution scheme of the filling & emptying model.

At each time step, the mass flows through the poppet valves, the EGR valve and the external sections are first evaluated from the pressure and temperature values obtained in the previous time step. If the new mass flows are

significantly different to the previous ones, the resolution time step is reduced from the 0.5 cad reference to a smaller one until fulfilling a calibrated stability criterion. With the new mass flows, heat transfers and thermodynamics properties are then updated in the manifolds. Finally the specific submodels such as blow-by, fuel injection, packet model, etc... are evaluated to calculate the new thermodynamics properties in the cylinders. When an engine cycle has been calculated, the instantaneous averaged manifolds pressures are compared to the mean values ones and if necessary the external sections of the manifolds are corrected before running an additional cycle. Usually, in 3 or 4 engine cycles stability is reached in the different volumes and the mean values coincide with the instantaneous averaged ones. Nevertheless under high HP EGR rates, more engine cycles are normally required due to the instabilities that create the interactions between the HP EGR valve control and the external sections corrections.

In the end, the instantaneous exhaust manifold temperature is averaged to update the exhaust MVEM and 2 or 3 iterations are realized between both models to obtain the convergence of the mean values in the exhaust manifold. Then from the filling & emptying model results, the input data of the intake MVEM and combustion models are updated and the whole resolution scheme is repeated until the mass flow passing through the intake external section corresponds to the previous calculated one. The overall model convergence is generally obtained in 2 or 3 iterations which represent about one minute of simulation in a standard computer (Intel Pentium 4 CPU 2.8GHz). This number of iterations and the computational time can obviously increase if a demanding injection setting optimization process is required or if the intake throttle has to be controlled to reach the desired HP EGR rate. Conversely, the simulation time can also be reduced as there is still some scope to further optimize the code (e.g. model simplification and solver speed up).

5.4.2.2 Actuators Oriented Model

In the actuator oriented model, the filling & emptying method is extended to the MVEM's models to take into account the effects of mass accumulation and species transport in the air path. As shown in figure 5.13, the different volumes present in the intake and exhaust lines are modeled with characteristic capacities where mass and energy conservation equations are resolved. Heat transfers are calculated using the same Nusselt-based correlations as ones de-

scribed for the manifolds while thermal capacities are added in all heat transfer models (cylinder, port, manifolds, etc...) to simulate the thermal inertia effects. During the convergence to the initial operating conditions, a strategy disables these thermal capacities to speed up the calculations. Mechanical inertial effects are also considered with inertial shafts for the turbochargers.

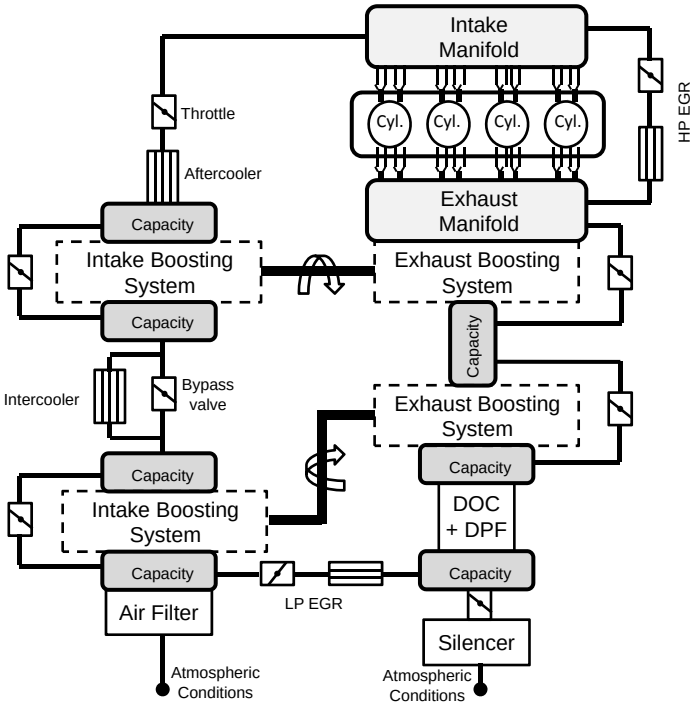

Figure 5.13: Structure of the 0D actuators oriented engine model.

The resolution of this model structure is based on actuators positions. Control strategies are therefore developed according to the transient test cycle to manage the engine dynamic and obtain the desired response. These strategies can be provided by a Simulink environment coming from ECU developments or be directly implemented in the model through Matlab functions.

The filling & emptying model corresponding to the base engine has the same resolution scheme as one described for the boost pressure oriented model (see figure 5.12). The only differences stand in the external manifold sections which are always maintained constant and in the HP EGR valve position which is determined by a control strategy (PID controller). However for the

MVEM's, most of equations are inversed. For the centrifugal compressors, corrected mass flow and efficiency are here calculated as a function of corrected shaft speed and compression ratio as:

$$\dot{m}_{cor}, \eta_c = f\left\{N_{cor}, \frac{P_{out}}{P_{in}}\right\} \tag{5.53}$$

whereas for the turbines, adapted mass flow and adapted power are determined as a function of actuator position and pressure ratio as:

$$\dot{m}_{adapt}, \dot{W}_{adapt} = f\left\{\chi_t, \frac{P_{in}}{P_{out}}\right\} \tag{5.54}$$

The relation between compressor and turbine powers is given by the shaft speed dynamic equation:

$$\dot{\omega} = \frac{W_t - W_c}{I\dot{\omega}} \tag{5.55}$$

being $\dot{\omega}$ the angular acceleration and I the inertia of the turbocharger. Valves, throttles and wastegates are directly resolved by Eq. 5.8 with effective sections defined by control strategies. Finally for the other elements such as air filter, coolers, DOC+DPF, etc... flow test rig characteristics are reversed to obtain corrected mass flows as a function of pressure drops. In that way at each time step, mass transfers are first evaluated in all air path components to then update the thermodynamics properties in the capacities. MVEM's are called each time a cylinder arrives at EVO. This fixed time step has been chosen in order to average the instantaneous manifold properties under the minimum periodic interval (at each manifold pulsation - 180cad for a 4-cylinder engine).

5.5 Experimental Calibration and Validation

Experimental data and complete engine specifications are generally not available for matching calculations. Models calibration can therefore be difficult and quite risky to carry out at this early stage of the engine development process. An advantage of 0D engine models when compared to more

sophisticated approaches such as wave action models is the reduced number of parameters they need. With only few parameters to define, there is thus a better control on the assumptions realized to estimate or extrapolate their values to a new base engine. Furthermore, sensitivity studies are straightforward to judge the consequences that would have some variations of their settings on the architecture matching.

In the following section, the adjustment process of these different parameters is described with the global model validation. This adjustment process is divided in three parts calibrating first the parameters related to the cylinders and combustion process, then those related to the whole engine behavior and finally the one related to the thermal inertia. The experimental data employed in this calibration and validation process were measured on three different modern passenger car Diesel engines. The main characteristics of these engines as a description of the installations and instrumentations used during the test campaigns can be found in section 4.2.4.

5.5.1 Combustion Model

Cylinder submodels possess three calibrated parameters which are the values of the heat transfer model constants (C_{w1} and C_{w2}) and the deformation model constant (k_{def}). These parameters are shared between the combustion and the filling & emptying models. They are fitted with experimental motoring tests performed at different speeds (from 1000 to 4000 rpm with steps of 1000 rpm) and different intake pressures (turbine actuator fully open or closed). The adjustment method is based on the sensitivity of the thermodynamic cycle to uncertainties in motoring conditions [210, 213]. In motoring conditions, the RoHR is zero and the heat transfer to the wall can be solved with the energy conservation equation. In that way, an experimental measurement of the heat transfer based on in-cylinder pressure is provided. The same analysis can be done by imposing the heat transfer of the Woschni model in the energy balance and then calculating the error in RoHR that should be zero. As the constant k_{def} has a characteristic effect on the thermodynamic cycle and the Woschni model depends on C_{w1} and C_{w2}, it is thus possible to adjust the value of the uncertainties so that the experimental heat transfer to the wall coincides with the results of the Woschni model.

In addition to these parameters, the combustion model requires the calibration of the mixing model constant (K_{mix}). K_{mix} is fitted comparing the

RoHR's calculated by the combustion model to the experimental ones obtained with the combustion diagnosis tool CALMEC [22, 211]. The calibration process was done under steady state operations distributed in the complete engine speed torque envelope as shown in figure 5.14. The experiments were realized with the original engine settings where HP EGR rates are defined to respect the Euro IV or Euro V emissions regulations. The injection settings given by the ECU were directly used as input data in the combustion code with injectors characteristics measured in an injection test rig. For each engine, ten operating conditions are employed to fit the K_{mix} constant with least squares algorithms while the other points are aimed to validate the predictive capacity of the model combustion.

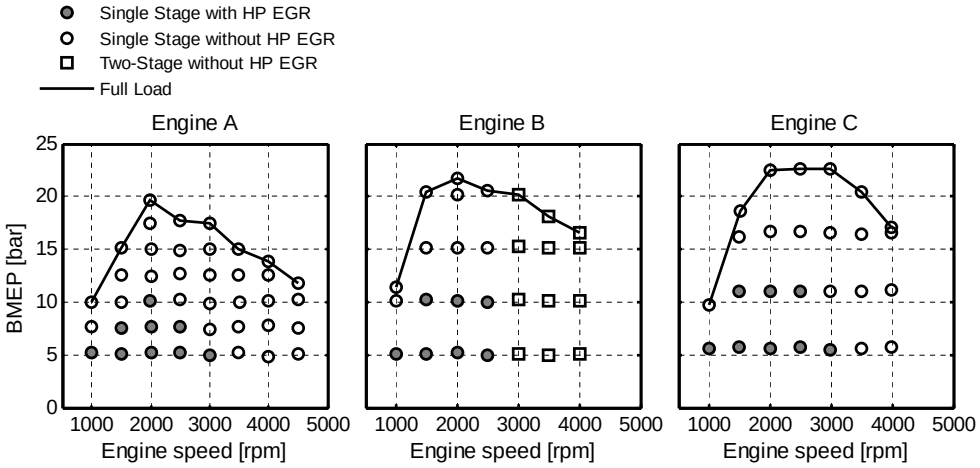

Figure 5.14: Steady-state operating conditions.

With a correct K_{mix} calibration, it can be observed in figure 5.15 how the combustion model is able to predict in-cylinder pressure and heat release rate. Here, four points measured on Engine A are shown with conditions going from 1500 to 3500 rpm, 40% to 100% load, 0% to 15% EGR and with one or two injections. These points were not used for the fitting process. Although some discrepancies exist in the prediction of the premixed combustion, especially for the pre-injections, and in the prediction of the late diffusion phase due to jet-to-jet interferences in the combustion chamber, good agreement can be seen between measured and simulated heat release laws and cylinder traces.

To further illustrate the predictive capacity of the model, figure 5.16 shows the indicated mean effective pressure and the maximum in-cylinder pressure

for all operating conditions described in figure 5.14. In general, $\pm 2\%$ of errors can be noticed for both variables. At low loads, errors can be slightly higher as the part of premixed combustion becomes significant and the hardest model hypotheses are made during that combustion phase.

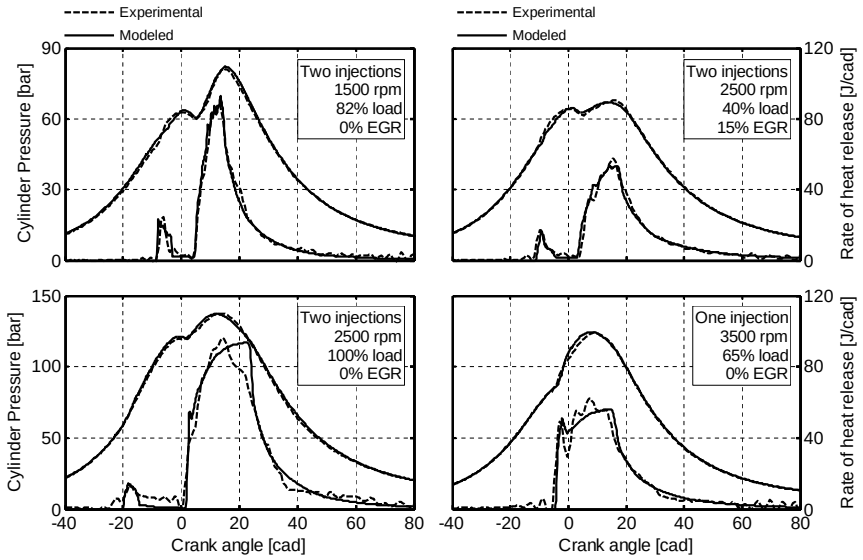

Figure 5.15: Cylinder pressure and RoHR for different operating conditions (Engine A) - Comparison between experimental and simulated evolution.

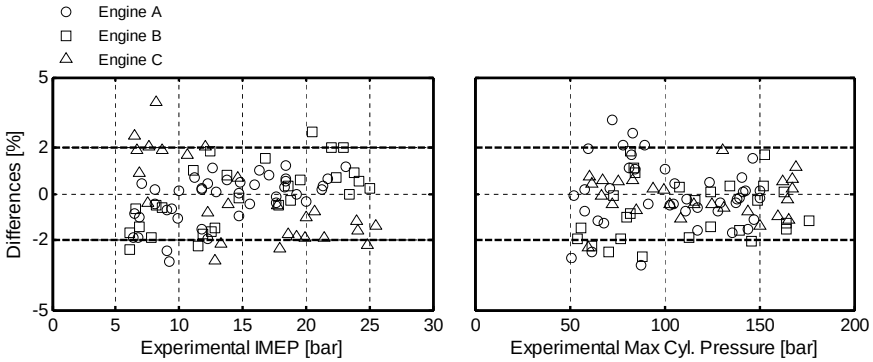

Figure 5.16: Differences between experimental and simulated IMEP and maximum in-cylinder pressures for all operating conditions.

5.5.2 Engine Model in Steady State Operations

When the whole engine is considered, Friction plus Auxiliaries Mean Effective Pressure (FAMEP) has to be evaluated to correctly predict the engine power output. Mechanical losses models are present in the literature to reproduce cylinders friction and bearing losses [77]. Nonetheless, power consumed by accessories is difficult to estimate as it depends not only on specific operating conditions but also on numerous ECU strategies. A predictive model describing the factors that affect FAMEP cannot therefore be developed and basic empirical correlations defined as a function of speed and load are generally used [258]. Here, FAMEP is modeled as:

$$\begin{aligned} FAMEP &= IMEP - PMEP - BMEP \\ &= k_{fa1} m_{f_{cycle}} + k_{fa2} N_{eng} + k_{fa3} N_{eng}^2 + k_{fa4} \end{aligned} \tag{5.56}$$

where k_{fa1}, k_{fa2}, k_{fa3} and k_{fa4} are the parameters to adjust. The experimental tests provide the BMEP while the combustion diagnosis code computes the IMEP and PMEP. These parameters were fitted with all the operating conditions described in figure 5.14 achieving correlation levels (R^2) ranged from 91.54 (Engine B) to 94.78 (Engine A).

Heat transfer effects in the exhaust line have important consequences on the turbocharger performance. The 1-node model used to reproduce these heat transfers is quite simple and a calibration process has to be performed to correctly adjust the exhaust heat fluxes. For that, a parameter k_{exh} has been added to Eq. 5.17 as:

$$Nu_{inner} = k_{exh} 0.0718 \, \mathrm{Re}^{\frac{3}{4}} \tag{5.57}$$

k_{exh} was calibrated for each engine with ten representative conditions of the entire exhaust temperatures range. k_{exh} was adjusted until the errors observed between experimental and modeled exhaust temperatures were centered on zero.

Some modern Diesel engines are equipped with a tuned intake manifold to improve breathing capabilities. In this case, gas inertia and wave action phenomena generate overboost or underboost effects depending on both engine speed and intake path length. A 0D engine model cannot predict gas dynamic

effects. So when these effects become important, significant errors are committed on the estimated gas mass flows. At an early development stage, manifold tunings are an unknown and their effects are normally omitted in matching calculations. But at a later stage when manifold designs are defined or during model validations when the base engine has a tuned manifold, empirical corrections can be used to reduce uncertainties considering some wave effects as follows:

$$P'_{2cor} = \begin{cases} (c_1 N_{eng} + c_2)\, P'_2 & N_{eng_{\min}} \leqslant N_{eng} \leqslant N_{eng_{tuned}} \\ (c_3 N_{eng} + c_4)\, P'_2 & N_{eng_{tuned}} < N_{eng} \leqslant N_{eng_{\max}} \end{cases} \tag{5.58}$$

being $N_{eng_{tuned}}$ the engine speed where maximum positive wave effects are observed, and c_1, c_2, c_3 and c_4 calibrated parameters (c_1 is positive while c_3 is negative). This correction is implemented in the connection between the intake MVEM and the filling & emptying model. In that way, the filling & emptying model estimates the gas mass flow with an averaged intake manifold pressure corresponding to P'_{2cor} instead of P'_2, while the intake MVEM keep the P'_2 objective to evaluate the thermodynamic properties and compressors powers. Having a basic formulation, this correction allows also the easily analysis of the consequences that would have some intake manifold tunings on the architecture matching. Here, the correction has only been used on Engine C which was equipped with a tuned manifold optimized at 1500 rpm.

The calibration was carried out on the seven full load operations shown in figure 5.14. After the different adjustment processes, all the operating conditions described in figure 5.14 were simulated with the 0D engine model using the combustion model to predict the RoHR's and the boost pressure oriented model for the air path. Characteristic data measured in turbocharger test bench and flow test rig were provided to the engine component models.

As it can be seen in figure 5.17, the results show a good agreement when compared to experimental data. Uncertainties are respectively around 2% and 5% for the variables in the intake and exhaust lines. In steady-state operations, the errors committed in the intake path are relatively small because the intake manifold pressure appears as an objective for model convergence. However, thermodynamics properties in the exhaust path are a result of the intake needs. The errors committed for these variables are therefore higher as their results are influenced not only by the inherent exhaust model uncertainties but as well by the intake errors. Engine breathing capacity is also correctly predicted

achieving air mass flow errors lower than 5% in the whole engine operating range. With the empirical correction for wave effects (Eq. 5.58), Engine C shows the same air mass flow uncertainties as engines not equipped with tuned manifold. For fuel consumption evaluation and boosting architecture performance, the 0D engine model is able to predict BMEP and PMEP with a maximum error of 5% and 15 mbar respectively.

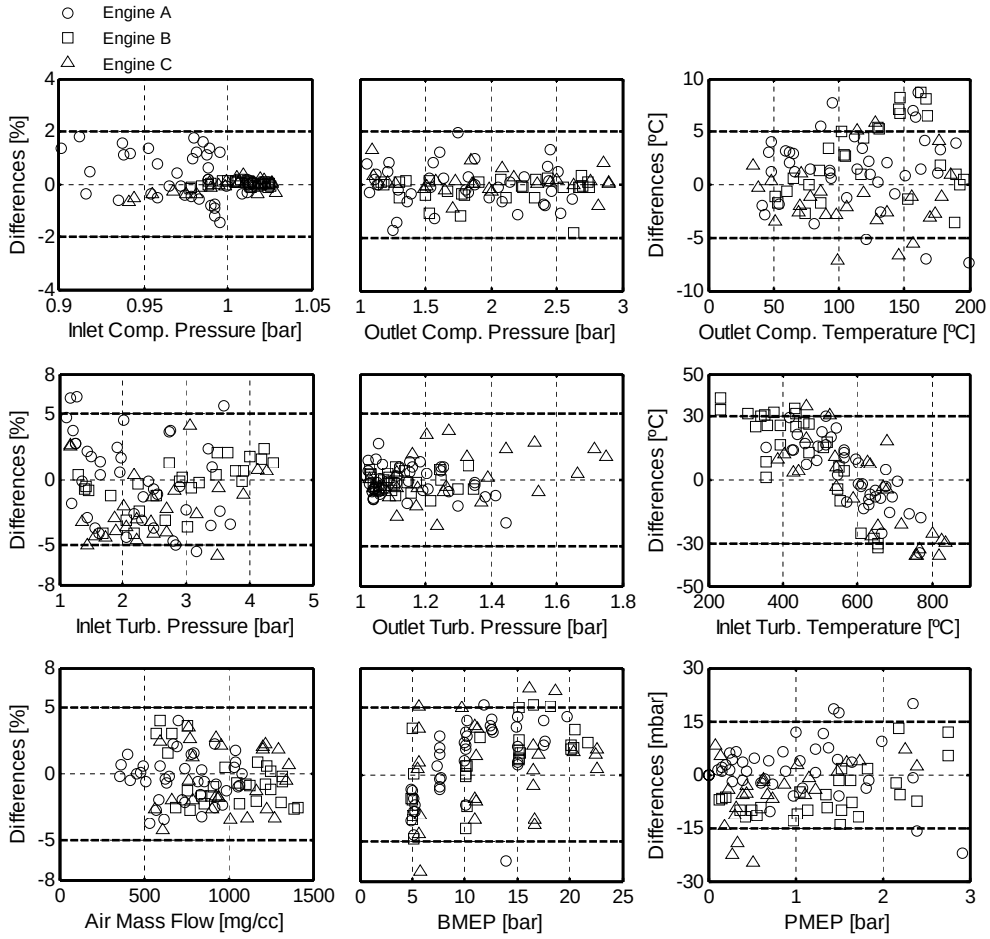

Figure 5.17: Comparison of experimental data and engine model prediction for all operating conditions.

For the exhaust manifold temperature uncertainties, it can be observed a certain trend (overestimation at low loads and underestimation at high loads).

This trend is explained by the heat transfer model which is quite simple to give a detailed heat losses description. Adding characteristic pipes to their corresponding calculation node (for example one for each manifold branch) would improve the model accuracy but at the cost of additional calibrated parameters. For both exhaust manifold temperature and pressure, uncertainties are also explained by the exhaust pulsations which significantly impact the power generated by the turbine. Turbine power is equal to compressor power. In the intake line, pulsations are small enough to consider mean compressor power calculated with mean variables. The turbine power is therefore correctly estimated. But the relation between turbine power and pressure ratio is not lineal and mean pressure ratio interpolated from mean power in the turbine adapted map does not necessary corresponds to the correct mean pressure ratio. Differences are more and more important as pulsation level increase. Using adapted characteristics maps based on conservative parameters and accurately fitted with quadratic polynomial functions allows the uncertainties to be reduced when compared to standard turbine MVEM models. But a correction factor based on experimental data is still needed. As the pressure ratio has an impact on exhaust temperature, here this correction factor is directly included in k_{exh} (equation 5.57) and only one calibration process is required to adjust heat transfer and pulsations effects. Exhaust temperature and pressure uncertainties are therefore a consequence of both phenomena.

If pulsation effects are very important (e.g. 2/3 cylinders engines, very small exhaust manifold design, etc...), the use of this correction factor is not acceptable. In this case, the filling & emptying model can be extended to the exhaust MVEM with the same crank angle resolution to reproduce pulsations in the exhaust line. Turbines are thus modeled as two adiabatic nozzles in series with an intermediate volume [259, 296] and physical based models are implemented to give turbine efficiencies as a function of blade speed ratio [265, 300]. Nonetheless, these models are generally difficult to apply in matching calculations as they require a large number of turbine geometrical data that are not available in the turbocharger maps.

In-cylinder traces (low pressure loop) and instantaneous manifold pressures are shown in figures 5.18-5.19 for different engine speeds and loads. In the low to middle engine speed range, wave effects in the air path are not so pronounced and a relatively good precision is obtained when compared to the measurements. The good agreement of cylinder pressures indicates also that gas exchange, combustion and wall heat transfer processes are correctly

simulated by the cylinder model. At higher engine speeds, wave effects become more and more pronounced and are particularly significant at the exhaust side above 4000 rpm. The missing ability of 0D approaches to predict gas dynamic effect in manifold has therefore some limitations and engine behavior cannot be properly predicted at very high speeds with this type of model.

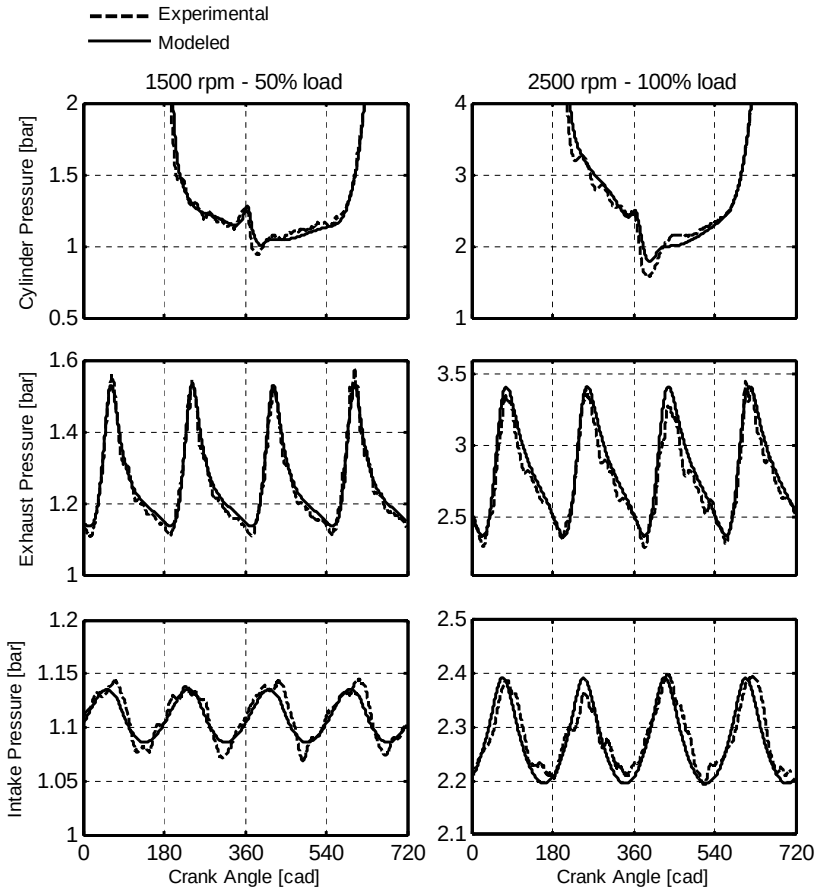

Figure 5.18: Comparison of predicted in-cylinder traces and instantaneous manifold pressures with experimental data (Engine A) - 1500 and 2500 rpm.

Modern Diesel engines run generally under moderate speeds and nowadays, with the development of downspeeded engines to respect objectives of fuel consumption reduction, maximum engine speeds are commonly limited in the 3500 to 4000 rpm range. In this case, uncertainties generated by wave

phenomena are acceptable and a 0D approach offers an overall good accuracy to reproduce the main processes taking place in the engine for matching calculations.

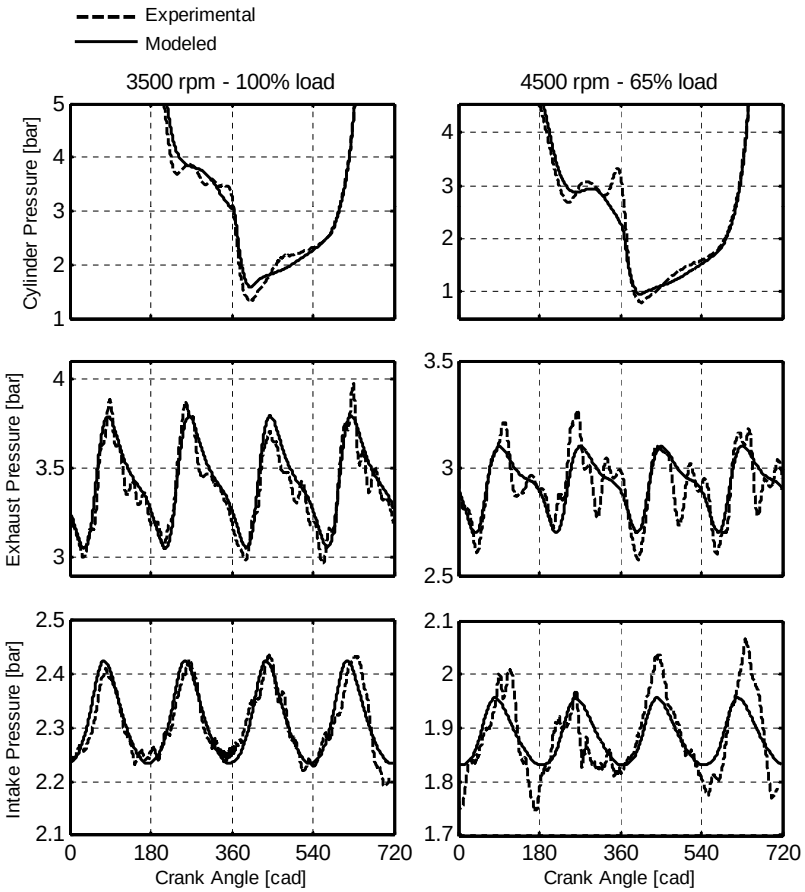

Figure 5.19: Comparison of predicted in-cylinder traces and instantaneous manifold pressures with experimental data (Engine A) - 3500 and 4500 rpm.

5.5.3 Engine Model in Transient Operations

In transient operations, characteristic volume size and thermal inertia phenomena are fundamental to accurately reproduce the engine dynamic behavior. Volumes sizes are directly obtained from the engine components, while the val-

ues of thermal capacities proposed by Romero et al. [283, 328] are employed in the different heat transfer models. As already mentioned, the heat transfer model used in the exhaust manifold is quite simple. Thus, its thermal capacity requires also an adjustment process.

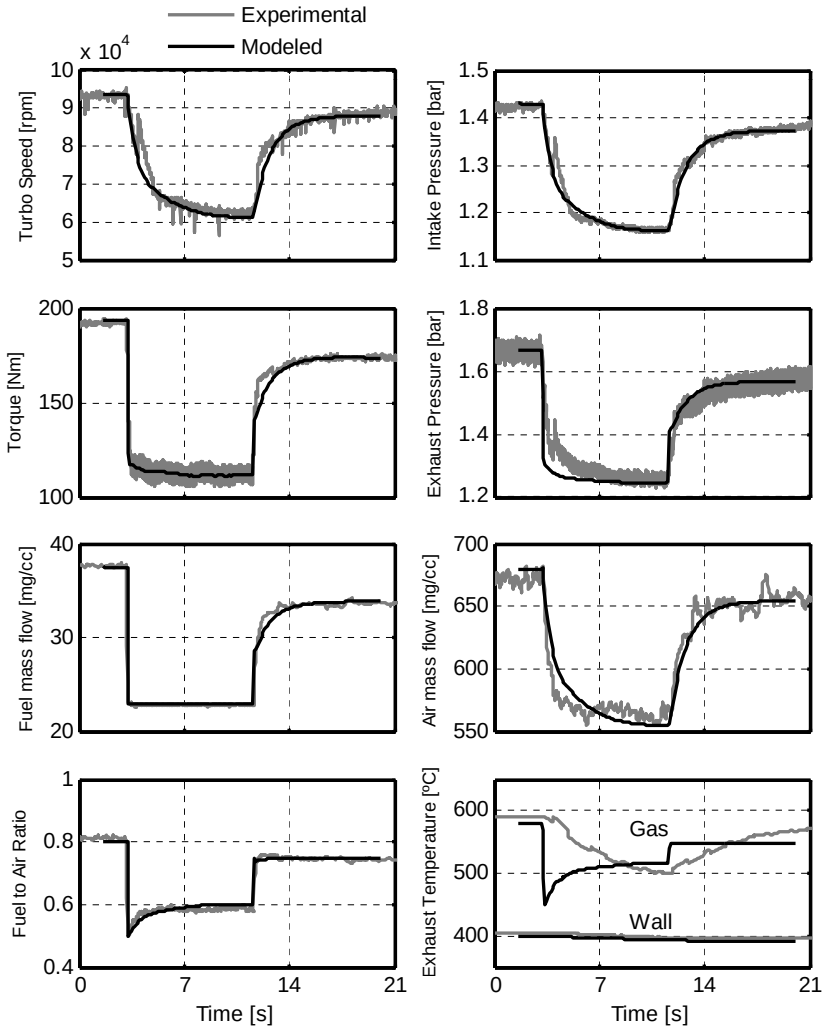

Figure 5.20: Comparison of simulation results with experimental data during a hot transient test cycle performed at 1250 rpm on Engine C.

Passenger car engines can be run in different transient conditions, but load transients performed at constant engine speeds are considered the most

representative transient cycles to evaluate engine response. Here, hot and cold transient tests were carried out at four engine speeds (1000, 1250, 1500, 2000 rpm). From wall temperature measurements, the exhaust thermal capacity was adjusted on four test cycles until reaching the best accuracy compromise between the considered transient conditions. The four other cycles are aimed to validate the predictive capacity of the engine model.

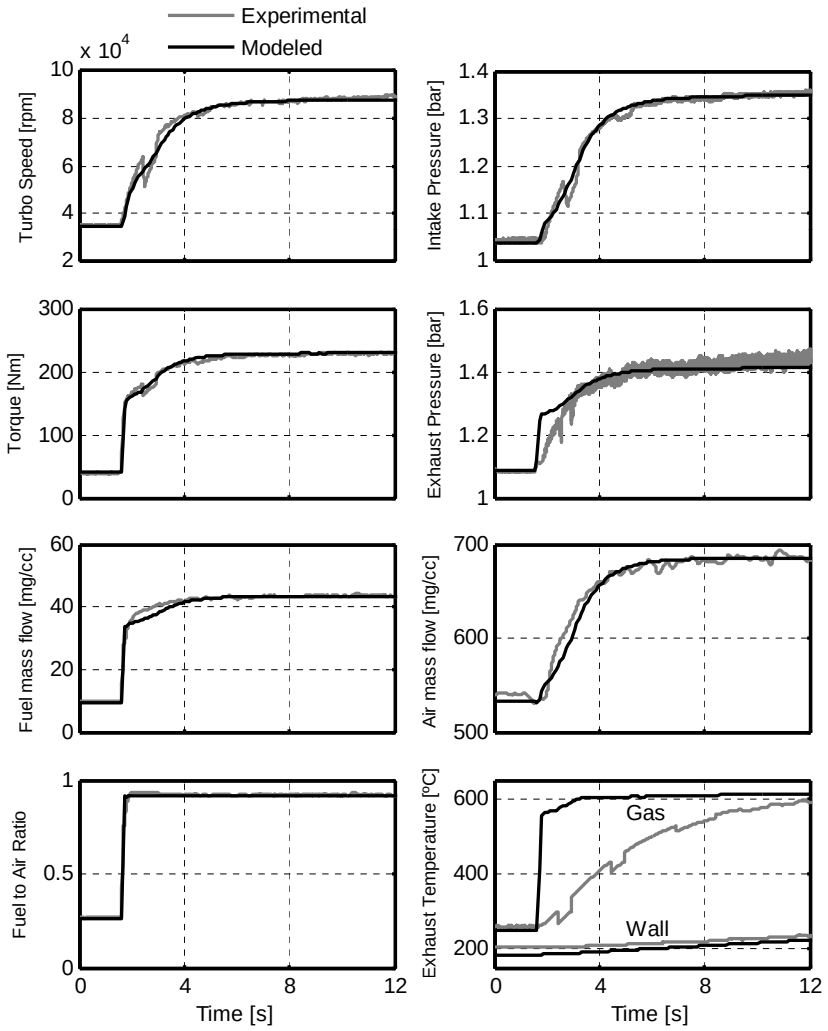

Figure 5.21: Comparison of simulation results with experimental data during a cold transient test cycle performed at 1500 rpm on Engine C.

A hot transient test is carried out stabilizing thermally the engine at full load. Next, the engine is moved to around 50% load conditions where it remains until the turbocharger achieved a stable speed. At this moment, the engine is throttled again to 100% load keeping a constant engine speed over the whole cycle. A hot transient test performed on Engine C and not used during the calibration process is shown in figure 5.20.

Looking turbocharger speed and intake pressure variations, it can be observed how both turbocharger and engine dynamic responses are well reproduced by the model. Differences observed on the exhaust gas temperature variations do not reflect errors from the model but come from the thermocouple mass inertia which filters experimental temperature variations.

Similar results are shown in figure 5.21 for a cold transient test. In this case, the transient test is carried out stabilizing the engine at low load (around 15%) and then suddenly throttle the engine to 100% load. As before, a good agreement between experimental and modeled data can be observed on the turbocharger and engine dynamic responses. These results confirm the capability of the engine model to correctly reproduce engine dynamics and boosting systems performance in transient operation.

5.6 Conclusions

A whole engine 0D model has been developed to efficiently perform matching calculations of complex multi-stage boosting architectures. The model is based on different approaches to obtain the best compromise between maximum physical description and minimum computational cost. The main physical processes involved in cylinders and manifolds are described with a crank angle resolution by a 0D filling & emptying model, while the thermodynamics properties in the air path are calculated by MVEM's with cycle mean values. Through the use of a 0D phenomenological combustion model, RoHR can be predicted over a wide range of operating conditions including the most demanding ones encountered in highly downsized-downspeeded Diesel engines. Thanks to its component based methodology, the model presents high flexibility to evaluate any multi-stage boosting architecture.

The new matching procedure based on turbine adapted representation has been implemented in the engine model and the different components sub-

models have been summarized. With this matching procedure, a new control algorithm has also been developed to reduce computational expenses by running steady-state calculations directly from engine performance objectives to charging system configuration.

The model calibration process has been presented with the different submodel constants that need to be adjusted. Compared to more sophisticated approach, the number of these constants has been significantly reduced to keep a good control on the assumptions realized when model calibrations must be extrapolated to new base engines. With few adjusted parameters, the impact of calibration process on architecture matching can also be easily analyzed through sensitivity studies.

The model has been validated on three different base engines fitted with different charging systems. Comparing measured and simulated data in the whole engines speed torque envelope, the predictive capabilities of the engine model have been demonstrated and the overall model accuracy has been judged more than sufficient to carry out matching calculations. In fact, it has been shown that combustion model uncertainties generate errors on both IMEP and maximum cylinder pressure lower than 2%, while engine model uncertainties do not exceed 2% in the intake path, 5% in the exhaust line, 5% for the BMEP and 15 mbar for the PMEP. In transient operations, a good agreement has also been obtained between experimental and modeled variables through correct predictions of turbocharger and engine dynamic responses.

Based on a 0D approach, the engine model presents important limitations to reproduce gas dynamics phenomena in the manifolds. However, it has been justified that uncertainties generated by gas dynamic phenomena in the exhaust are generally acceptable in the low to middle engine speed range (up to 3500 - 4000 rpm), and some basic empirical correlations are sufficient to correct air mass flow estimations in the case of engines equipped with tuned intake line. As nowadays maximum engine speeds are commonly limited in the 3500 to 4000 rpm range, the engine model is thus valid to perform calculations in the whole engine operating range.

References

[4] *" JANAF Thermodynamical Tables".* DOW Chemical Company, 1962, Addendum, 1966. (Cit. on p. 176).

[14] A. Albrecht, O. Grondin, F. Le Berr, and G. Le Soliec. *"Towards a Stronger Simulation Support for Engine Control Design: a Methodological Point of View"*. Oil & Gas Science and Technology, Revue IFP, Vol. 62, No. 4, pp. 437-456, 2007. (Cit. on p. 170).

[18] W.J.D. Annand. *"Heat Transfer in the Cylinders of Reciprocating Internal Combustion Engines"*. Proceedings of the Institution of Mechanical Engineers, Vol. 177, pp. 973-990, 1963. (Cit. on p. 191).

[22] O. Armas. *"Diagnostico Experimental del Proceso de Combustion en Motores Diesel de Inyeccion Directa"*. Tesis Doctoral, Universidad Politecnica de Valencia, Valencia, 1999. (Cit. on pp. 150, 192, 193, 205).

[28] J. Arregle, J.J. Lopez, J.M. Garcia, and C. Fenollosa. *"Development of a Zero-Dimensional Diesel Combustion Model - Part 1 Analysis of the Quasi-Steady Diffusion Combustion Phase"*. Applied Thermal Engineering, Vol. 23, pp. 1301-1317, 2003. (Cit. on pp. 194, 195).

[29] J. Arregle, J.J. Lopez, J.M. Garcia, and C. Fenollosa. *"Development of a Zero-Dimensional Diesel Combustion Model - Part 2 Analysis of the Transient Initial and Final Diffusion Combustion Phases"*. Applied Thermal Engineering, Vol. 23, pp. 1319-1331, 2003. (Cit. on p. 194).

[30] J. Arregle, J.J. Lopez, J. Martin, and E. Mocholi. *"Development of a Mixing and Combustion Zero-Dimensional Model for Diesel Engines"*. SAE Technical Paper 2006-01-1382, 2006. (Cit. on pp. 173, 194).

[34] C. Barba, C. Burkhardt, K. Boulouchos, and M.A. Bargende. *"A Phenomenological Combustion Model for Heat Release Rate Prediction in High-Speed Di Diesel Engines with Common Rail Injection"*. SAE Technical Paper 2001-01-2933, 2001. (Cit. on p. 194).

[38] J. Benajes, E. Reyes, and J.M. Lujan. *"Modelling Study of the Scavenging Process in a Turbocharged Diesel Engine with Modified Valve Operation"*. Proceedings of the Institution of Mechanical Engineers Part C: Journal of Mechanical Engineering Science, Vol. 210, pp. 383-393, 1996. (Cit. on p. 192).

[42] P.N. Blumberg, Lavoie G.A., and R.J. Tabaczynski. *"Phenomenological Models for Reciprocating Internal Combustion Engines"*. Progress in Energy and Combustion Science, Vol. 5, pp. 123-167, 1979. (Cit. on p. 192).

[43] T. Boger and A.K. Heibel. *"Heat Transfer in Conductive Monolith Structures"*. Chemical Engineering Science, Vol. 60, pp. 1823-1835, 2005. (Cit. on p. 180).

[44] J. Bohbot, A. Lafossas, A. Albrecht, M. Miche, M. Chraibi, and A. Menegazzi. *"A New Coupling Approach Using a 1D System Simulation Software and a 3D Combustion Code Applied to Transient Engine Operation"*. SAE Technical Paper 2004-01-3002, 2004. (Cit. on p. 170).

[68] J.A. Caton and J.B. Heywood. *"An Experimental and Analytical Study of Heat Transfer in an Engine Exhaust Port"*. International Journal of Heat and Mass Transfer, Vol. 24, pp. 581-895, 1981. (Cit. on p. 188).

[72] A.J. Chapman. *"Heat Transfer"*. Macmillan Publishing Company, New York, 1960. (Cit. on p. 182).

[77] S.K. Chen and P. Flynn. *"Development of a Compression Ignition Research Engine"*. SAE Technical Paper 650733, 1965. (Cit. on p. 207).

[80] F. Chmela and G. Orthaber. *"Rate of Heat Release Prediction for Direct Injection Diesel Engines Based on Purely Mixing Controlled Combustion"*. SAE Technical Paper 1999-01-0186, 1999. (Cit. on p. 194).

[83] A. Chow and M.L. Wyszynski. *"Thermodynamic Modelling of Complete Engine Systems - A Review"*. Proceedings of the Institution of Mechanical Engineers, Part D: Journal of Automobile Engineering, Vol. 213, No. 4, pp. 403-415, 1999. (Cit. on p. 170).

[87] J.M. Corberan. *"Contribucion al Modelado del Proceso de Renovacion de la Carga en MCIA"*. Tesis Doctoral, Universidad Politecnica de Valencia, Valencia, 1984. (Cit. on p. 186).

[91] J.E. Dec. *"A Conceptual Model of DI Diesel Combustion Based on Lasersheet Imaging"*. SAE Technical Paper 970873, 1997. (Cit. on pp. 191, 194).

[92] B. Degraeuwe. *"Contribution to the Thermal Management of DI Diesel Engines"*. Tesis Doctoral, Universidad Politecnica de Valencia, Valencia, 2007. (Cit. on p. 190).

[93] C. Depcik and D. Assanis. *"A Universal Heat Transfer Correlation for Intake and Exhaust Flows in a Spark-Ignition Internal Combustion Engine"*. SAE Technical Paper 2002-01-0372, 2002. (Cit. on pp. 181, 188).

[98] V. Dolz. *"Contribucion al Modelado de la Transmision de Calor en los MCIA y su Aplicacion en el Aprovechamiento Energetico de los Gases de Escape Durante los Transitorios de Carga"*. Tesis Doctoral, Universidad Politecnica de Valencia, Valencia, 2006. (Cit. on pp. 181, 188).

[101] R. Egnell. *"Combustion Diagnostics by Means of Multizone Heat Release Analysis and NO Calculation"*. SAE Technical Paper 981424, 1998. (Cit. on p. 194).

[104] L. Eriksson. *"Modeling and Control of Turbocharged SI and DI Engines"*. Oil & Gas Science and Technology - Revue IFP, Vol. 62, No. 4, pp. 523-538, 2007. (Cit. on p. 172).

[105] C. Fenollosa. *"Aportacion a la Descripcion Fenomenologica del Proceso de Combustion por Difusion Diesel"*. Tesis Doctoral, Universidad Politecnica de Valencia, Valencia, 2003. (Cit. on p. 194).

[110] J.W. Fox, W.K. Cheng, and J.B. Heywood. *"A Model for Predicting the Residual Gas Fraction in Spark-Ignition Engines"*. SAE Technical Paper 931025, 1993. (Cit. on p. 192).

[117] J. Galindo, J.M. Lujan, J.R. Serrano, V. Dolz, and S. Guilain. *"Description of a Heat Transfer Model Suitable to Calculate Transient Processes of Turbocharged Diesel Engines with One-Dimensional Gas-Dynamic Codes"*. Applied Thermal Engineering, Vol. 26, pp.66-76, 2006. (Cit. on pp. 181, 188).

[118] J. Galindo, J.M. Lujan, J.R. Serrano, and L. Hernandez. *"Combustion Simulation of Turbocharged HSDI Diesel Engines During Transient Operation Using Neural Networks"*. Applied Thermal Engineering, Vol. 25, pp. 877-898, 2005. (Cit. on pp. 196, 197).

[119] J. Galindo, J.R. Serrano, F. Arnau, and P. Piqueras. *"Description and Analysis of a One-Dimensional Gas-Dynamic Model with Independent Time Discretization"*. Proceedings of the ASME Internal Combustion Engine Division, Spring Technical Conference, Chicago, 2008. (Cit. on pp. 10, 116, 171).

[125] P. Gautier, A. Albrecht, P. Moulin, A. Chasse, L. Fontvieille, A. Guinois, and L. Doleac. *"A New Simulation Step Towards Virtual Bench Through the Challenging Case of Two-Stage Turbocharger Diesel Engine Control Design"*. SAE Technical Paper 2008-01-0355, 2008. (Cit. on pp. 170, 171).

[133] O. Grondin, R. Stobart, H. Chafouk, and J. Maquet. *"Modelling the Compression Ignition Engine for Control - Review and Future Trends"*. SAE Technical Paper 2004-01-0423, 2004. (Cit. on pp. 6, 170).

[135] L. Guzzella and C.H. Onder. *"Introduction to Modeling and Control of Internal Combustion Engine Systems"*. Springer-Verlag Berlin Heidelberg, ISBN 970-3-642-10774-0, 2010. (Cit. on p. 172).

[137] Y. He and C.C. Lin. *"Development and Validation of a Mean Value Engine Model for Integrated Engine and Control System Simulation"*. SAE Technical Paper 2007-01-1304, 2007. (Cit. on p. 172).

[138] Y. He and C. Rutland. *"Application of Artificial Neural Networks for Integration of Advanced Engine Simulation Methods"*. ASME ICE Division Fall 2000 Technical Meeting, Peoria, Illinois, 2000. (Cit. on p. 172).

[139] Y. He and C.J. Rutland. *"Application of Artificial Neural Networks in Engine Modeling"*. International of Engine Research, Vol. 5, No. 4, pp. 281-296, 2004. (Cit. on p. 172).

[142] E. Hendricks. *"The Analysis of Mean Value Engine Models"*. SAE Technical Paper 890563, 1989. (Cit. on p. 172).

[143] E. Hendricks, A. Chevalier, M. Jensen, S.C. Sorenson, D. Trumpy, and J. Asik. *"Modelling of the Intake Manifold Filling Dynamics"*. SAE Technical Paper 960037, 1996. (Cit. on p. 172).

[145] J. Heywood. *"Internal Combustion Engine Fundamentals"*. New York: McGraw-Hill Inc., ISBN 978-0070286375, 1988. (Cit. on pp. 2, 191).

[148] R. Hilpert. *"Experimental Study of Heat Dissipation of Heated Wire and Pipe in Air Current"*. Forschungsarbeiten auf dem Gebiete des Ingenieur - Wesens - Ausgabe A, Vol.4, No.5, pp.215-224, 1933. (Cit. on p. 181).

[149] H. Hiroyasu, T. Kadota, and M. Arai. *"Development and Use of a Spray Combustion Modeling to Predict Diesel Engine Efficiency and Pollutant Emissions - Part 1 Combustion Modeling"*. Bulletin of the Japan Society Mechanical Engineering, Vol. 26, pp. 569-575, 1983. (Cit. on pp. 194, 195).

[152] G. Hohenberg. *"Definition und Eigenschaften des Thermodynamischen Verlustwinkels von Kolbenmaschinen"*. Automobil-Industrie, Vol. 4, pp. 15-21, 1976. (Cit. on p. 193).

[153] J.P. Holman. *"Heat Transfer"*. McGraw Hill Book Company, Sixth Edition, New York, 1986. (Cit. on pp. 177, 180, 181, 188).

[160] D.T. Hountalas, D.A. Kouremenos, G.C. Mavropoulos, K.B. Binder, and Schwarz V. *"Multi-Zone Combustion Modelling as a Tool for DI Diesel Engine Development - Application for the Effect of Injection Pressure"*. SAE Technical Paper 2004-01-0115, 2004. (Cit. on p. 173).

[167] M. Jankovic, M. Jankovik, and I. Kolmanovsky. *"Constructive Lyapunov Control Design for Turbocharged Diesel Engines"*. IEEE Transactions on Control Systems Technology, Vol. 8, No.2, pp.288-299, 2000. (Cit. on p. 172).

[170] J.P. Jensen, A.F. Kristensen, S.C. Sorenson, and N. Houback. *"Mean Value Modelling of Small Turbocharged Diesel Engine"*. SAE Technical Paper 910070, 1991. (Cit. on pp. 151, 152, 172).

[178] M. Kao and J.J. Moskwa. *"Nonlinear Cylinder and Intake Manifold Pressure Observer for Engine Control and Diagnostics"*. SAE Technical Paper 940375, 1994. (Cit. on p. 172).

[183] W.M. Kays and A.L. London. *"Compact Heat Exchangers"*. McGraw Hill Book Company, Second Edition, New York, 1964. (Cit. on p. 177).

[185] R.J. Kee, F.M. Rupley, and J.A. Miller. *"The Chemkin Thermodynamic Data Base"*. Sandia Report, SAND87-8215B, 1991. (Cit. on p. 176).

[199] A.G. Konstandopoulos, E.A. Kladopoulou, S.L. Yang, J.H. Johnson, and G.G. Parker. *"A Study Describing the Performance of Diesel Particulate Filters During Loading and Regeneration - A Lumped Parameter Model for Control Applications"*. SAE Technical Paper 2003-01-0842, 2003. (Cit. on p. 180).

[200] A.G. Konstandopoulos, M. Kostoglou, E. Skaperdas, E. Papaioannou, D. Zarvalis, and E. Kladopoulou. *"Fundamental Studies of Diesel Particulate Filters - Transient Loading, Regeneration and Aging"*. SAE Technical Paper 2000-01-1016, 2000. (Cit. on p. 180).

[201] P.A. Konstantinidis, G.C. Koltsakis, and A.M. Stamatelos. *"Transient Heat Transfer Modelling in Automotive Exhaust Systems"*. Proceedings of the Institution of Mechanical Engineers Part C: Journal of Mechanical Engineering Science, Vol. 211, No.1, pp. 1-15, 1997. (Cit. on p. 181).

[210] M. Lapuerta, O. Armas, and V. Bermudez. *"Sensitivity of Diesel Engine Thermodynamic Cycle Calculation to Measurement Errors and Estimated Parameters"*. Applied Thermal Engineering, Vol. 20, pp. 843-861, 2000. (Cit. on pp. 150, 204).

[211] M. Lapuerta, O. Armas, and J.J. Hernandez. *"Diagnostic of D.I. Diesel Combustion from In-Cylinder Pressure Signal by Estimation of Mean Thermodynamic Properties of the Gas"*. Applied Thermal Engineering, Vol. 19, pp. 513-529, 1999. (Cit. on pp. 150, 205).

[213] M. Lapuerta, O. Armas, and S. Molina. *"Study of the Compression Cycle of a Reciprocating Engine Through the Polytropic Coefficient"*. Applied Thermal Engineering, Vol. 23, No. 3, pp. 313-323, 2003. (Cit. on p. 204).

[214] M. Lapuerta, R. Ballesteros, and J.R. Agudelo. *"Effect of the Gas State Equation on the Thermodynamic Diagnostic of Diesel Combustion"*. Applied Thermal Engineering, Vol. 26, pp. 1492-1499, 2006. (Cit. on p. 185).

[220] K. Levenberg. *"A Method for the Solution of Certain Non-Linear Problems in Least Squares"*. The Quarterly of Applied Mathematics, Vol. 2, pp. 164-168, 1944. (Cit. on p. 197).

[224] J.M. Lujan, J.R. Serrano, F. Arnau, and V. Dolz. *"Heat Transfer Model to Calculate Turbocharged HSDI Diesel Engines Performance"*. SAE Technical Paper 2003-01-1066, 2003. (Cit. on pp. 181, 188).

[230] D. Marquardt. *"An Algorithm for Least-Squares Estimation of Non-Linear Parameters"*. SIAM Journal of Applied Mathematics, Vol. 11, pp.431-441, 1963. (Cit. on p. 197).

[231] G. Martin, V. Talon, P. Higelin, A. Charlet, and C. Caillol. *"Implementing Turbomachinery Physics into Data Map-Based Turbocharger Models"*. SAE Technical Paper 2009-01-0310, 2009. (Cit. on pp. 153, 162, 178).

[243] T. Morel and R. Keribar. *"Heat Radiation in DI Diesel Engines"*. SAE Technical Paper 860445, 1986. (Cit. on p. 191).

[256] J. Park, K.S. Lee, S. Song, and K.M. Chun. *"Numerical Study of a Light-Duty Diesel Engine with a Dual-Loop EGR System Under Frequent Engine Operating Conditions Using the DOE Method"*. International Journal of Automotive Technology, Vol. 11, No. 5, pp. 616-623, 2010. (Cit. on p. 173).

[258] F. Payri, J. Benajes, J. Galindo, and J.R. Serrano. *"Modelling of Turbocharged Diesel Engines in Transient Operation - Part 2 Wave Action Models for Calculating the Transient Operation in a High Speed Direct Injection Engine"*. Proceedings of the Institution of Mechanical Engineers Part D: Journal of Automobile Engineering, Vol. 216, No. 6, pp. 479-493, 2002. (Cit. on pp. 197, 207).

[259] F. Payri, J. Benajes, and M. Reyes. *"Modelling of Supercharger Turbines in Internal Combustion Engines"*. International Journal of Mechanical Science, Vol. 8-9, pp. 853-869, 1996. (Cit. on pp. 152, 210).

[261] F. Payri, J. Galindo, J.R. Serrano, and F.J. Arnau. *"Analysis of Numerical Methods to Solve One Dimensional Fluid-Dynamic Governing Equations Under Impulsive Flow in Tapered Ducts"*. International Journal of Mechanical Science, Vol. 46, pp. 981-1004, 2004. (Cit. on p. 171).

[262] F. Payri, X Margot, A. Gil, and J. Martin. *"Computational Study of the Heat Transfer to the Walls of a DI Diesel Engine"*. SAE Technical Paper 2005-01-0210, 2005. (Cit. on p. 191).

[263] F. Payri, X. Margot, A. Gil, and J. Martin. *"Prediction of Heat Transfer to the Walls in DI Diesel Engines"*. Proceedings of the 2nd EACC International European Automotive CFD Conference, Frankfurt, 2005. (Cit. on p. 191).

[264] F. Payri, S. Molina, J. Martin, and O. Armas. *"Influence of Measurement Errors and Estimated Parameters on Combustion Diagnostic"*. Applied Thermal Engineering, Vol. 26, pp. 226-236, 2006. (Cit. on pp. 150, 189, 192).

[265] F. Payri, J.R. Serrano, P. Fajardo, M.A. Reyes-Belmonte, and R. Gozalbo. *"A Physically Based Methodology to Extrapolate Performance Maps of Radial Turbines"*. Energy Conversion and Management, Vol. 55, pp.149-163, 2012. (Cit. on pp. 153, 210).

[271] S. Pischinger, S. Schernus, G. Lutkenmeyer, H.J. Theuerkauf, T. Winsel, and M. Ayeb. *"Investigation of Predictive Models for Application in Engine Cold-Start Behavior"*. SAE Technical Paper 2004-01-0994, 2004. (Cit. on p. 172).

[276] C.D. Rakopoulos and E.G. Giakoumis. *"Review of Thermodynamic Diesel Engine Simulations under Transient Operating Conditions"*. SAE Technical Paper 2006-01-0884, 2006. (Cit. on p. 170).

[277] C.D. Rakopoulos, D.C. Rakopoulos, E.G. Giacoumis, and D.C. Kyritsis. *"Validation and Sensitivity Analysis of a Two Zone Diesel Engine Model for Combustion and Emissions Prediction"*. Energy Conversion and Management, Vol. 45, pp. 1471-1495, 2004. (Cit. on p. 194).

[279] M. Reyes. *"Modelo de Transferencia de Calor Para Colectores de Escape de Motores Alternativos"*. Tesis Doctoral, Universidad Politecnica de Valencia, Valencia, 1994. (Cit. on p. 188).

[283] C. Romero. *"Contribucion al Conocimiento del Comportamiento Termico y la Gestion Termica de los Motores de Combustion Interna Alternativos"*. Tesis Doctoral, Universidad Politecnica de Valencia, Valencia, 2009. (Cit. on p. 213).

[294] P.K. Senecal, J. Xin, and R.D. Reitz. *"Predictions of Residual Gas Fraction in IC Engines"*. SAE Technical Paper 962052, 1996. (Cit. on p. 192).

[296] J.R. Serrano, F.J. Arnau, V. Dolz, A. Tiseira, and C. Cervello. *"A Model of Turbocharger Radial Turbines Appropriate to be Used in Zero- and One-Dimensional Gas Dynamics Codes for Internal Combustion Engines Modelling"*. Energy Conversion and Management, Vol. 49, pp. 3729-3745, 2008. (Cit. on pp. 152, 210).

[298] J.R. Serrano, H. Climent, C. Guardiola, and P. Piqueras. *"Methodology for Characterisation and Simulation of Turbocharged Diesel Engines Combustion During Transient Operation - Part 2: Phenomenological Combustion Simulation"*. Applied Thermal Engineering, Vol. 29, pp. 150-158, 2009. (Cit. on p. 197).

[300] J.R. Serrano, B. Pla, R. Gozalbo, and D. Ospina. *"Estimation of the Extended Turbine Maps for a Radial Inflow Turbine"*. SAE Technical Paper 2010-01-1234, 2010. (Cit. on pp. 152, 210).

[326] A. Torregrosa, P. Olmeda, B. Degraeuwe, and M. Reyes. *"A Concise Wall Temperature Model for DI Diesel Engines"*. Applied Thermal Engineering, Vol. 26, pp.1320-1327, 2006. (Cit. on pp. 190, 191).

[327] A.J. Torregrosa, J. Galindo, C. Guardiola, and O. Varnier. *"Combined Experimental and Modeling Methodology for Intake Line Evaluation in Turbocharged Diesel Engines"*. International Journal of Automotive Technology, Vol. 12, No. 3, pp. 359-367, 2011. (Cit. on p. 173).

[328] A.J. Torregrosa, P. Olmeda, J. Martin, and C. Romero. *"A Tool for Predicting the Thermal Performance of a Diesel Engine"*. Heat Transfer Engineering, Vol. 32, pp. 891-904, 2011. (Cit. on pp. 190, 213).

[346] N. Watson. *"Transient Performance Simulation and Analysis of Turbocharged Diesel Engines"*. SAE Technical Paper 810338, 1981. (Cit. on p. 171).

[350] N. Watson and M. Marzouk. *"A Non-Linear Digital Simulation and Analysis of Turbocharged Diesel Engines under Transient Conditions"*. SAE Technical Paper 770123, 1977. (Cit. on p. 171).

[351] N. Watson, A.D. Pilley, and M.A. Marzouk. *"Combustion Correlation for Diesel Engine Simulation"*. SAE Technical Paper 800029, 1980. (Cit. on p. 196).

[362] I. Wiebe. *"Halbempirische Formel fur die Verbrennungs-Geschwindigkeit"*. Verlag der Akadimie der Wissenschaften der Vd SSR, Moscow, 1956. (Cit. on p. 196).

[367] D.E. Winterbone, C. Thiruarooran, and A. Wellstead. *"A Wholly Dynamical Model of a Turbocharged Diesel Engine for Transfer Function Evaluation"*. SAE Technical Paper 770124, 1977. (Cit. on p. 171).

[368] D.E. Winterbone and M. Yoshitomi. *"The Accuracy of Calculating Wave Action in Engine Intake Manifolds"*. SAE Technical Paper 900677, 1990. (Cit. on p. 171).

[369] G. Woschni. *"A Universally Applicable Equation for the Instanatenous Heat Transfer Coefficient in the Internal Combustion Engine"*. SAE Technical Paper 670931, 1967. (Cit. on p. 190).

[370] G. Woschni. *"Die Berechnung der Wandverluste und der Thermischen Belastung der Bauteile von Dieselmotoren"*. MTZ 31/12, pp. 491-499, 1970. (Cit. on p. 190).

[379] Y.H. Zweiri, J.F. Winterbone, and L.D. Seneviratne. *"Detailed Analytical Model of a Single-Cylinder Diesel Engine in the Crank-Angle Domain"*. Proceedings of the Institution of Mechanical Engineers Part D: Journal of Automobile Engineering, Vol. 215, pp. 1197-1216, 2001. (Cit. on p. 172).

Chapter 6

Synthesis of Two-Stage Boosting Systems Performance

Contents

6.1 Introduction **226**
6.2 Methodology **227**
6.3 Steady-State Results **237**
6.4 Matching Analysis **258**
6.5 Transients Results **265**
6.6 Summary **278**
References **280**

6.1 Introduction

THERE is nowadays a need to analyze the potential of the most efficient boosting architectures to enhance the performance of downsized and downspeeded engines. With the arrival of new emissions test cycles much more demanding in terms of driving conditions, these analyses must be carried out not only under standard conditions but with high EGR rates as well. Thermomechanical limits have also important consequences on engine performance and their impact have to be characterized to quantify possible benefits modifying their values. Finally, turbocharger size is a critical factor for further engine development and new turbocharger requirements must be defined to satisfy fast transient responses with high low-end torque demands. Following the development and validation of all modeling tools, a comprehensive study has been performed with the 0D engine model to respond to these specific objectives.

An analytical model was first investigated in chapter 3 to reproduce the engine and boosting system performance. Although this model showed interesting features to define pre-design criteria from a charging system point of view, it presents important limitations to analyze the different interactions that exist between the engine, the EGR system and the boosting architecture. That is why, a more sophisticated model that includes a 0D phenomenological combustion model (combustion process) and a 0D filling & emptying model (multi-cylinders and manifolds) was then developed to achieve the model complexity required by this study.

With an important number of parameters coming into the picture, an energetic approach has been employed in a first instance to analyze the engine and boosting systems performance under steady-state operations. The description of this approach with the hypotheses that have been assumed will be presented in the second section. As the considered boosting architectures work most of the time with the main turbocharger, using the second stage only in the low engine speed range, a distinction has been made between both running modes. In the third section, the results obtained with the main turbocharger will thus be reported before those obtained in two-stage operations. Then in the fourth section, to estimate the future needs in charger development, the operating ranges required by downsized-downspeeded engines will be confronted to state-of-art supercharger, compressor and turbines characteristics maps. Finally in the last section, the transient aspects will be considered with an analysis of

the boosting architectures performance on different downsized engines during cold transient test cycles.

6.2 Methodology

The main difficulty when it comes to multi-stage boosting architectures analysis is the correct formulation of parametric studies to obtain clear design criteria limiting the interactions of variables. With these architectures, there are too many parameters to carry out direct sensitivity studies on each one of them and some hypotheses have to be assumed to reduce the number of input data.

Here, several degrees of engine downsizing have been considered. So before describing the selected boosting architectures, the engine scaling process based on a similarity approach will be first introduced. Then, the energetic approach defined to avoid particular turbocharger design influences in steady-state calculations will be reported. Finally, the other hypotheses made on the input data relating to the gas path elements, injections settings and EGR systems will be exposed in the last part of this section.

6.2.1 Engine Similarities

Three engine displacements (2.3l, 1.6l and 1.2l) have been selected for the simulations. 1.6l and 2.3l displacements correspond to the typical swept volume range of modern passenger car Diesel engines. Considering downsizing, they also represent different degrees of swept volume reduction substituting bigger engines in the 2.0l to 3.0l displacement range. 1.2l displacement is relatively small and represents directly a moderate or strong degree of downsizing replacing actual engines in the 1.6l to 2.0l range. For small engine displacements, 3-cylinder arrangements can also be considered. But here 4-cylinder configurations have been preferred to limit pulsations uncertainties in 0D engine model calculations.

The 2.3l engine is defined with the same geometrical data and model calibration as Engine C described in chapter 4. Only the connecting rod length has been increased to reach the desired swept volume and the compression ratio has been reduced to take into account the last trends in combustion

chamber development [37, 84]. For the 1.6l and 1.2l engines, the similarity method [46, 64, 260] has been used to obtain scaled replicas of the 2.3l engine. All geometrical elements have been sized with the similarity parameter λ to maintain the proportions of the reference engine. The main engine geometrical data are shown in table 6.1. In that way, simulations results are only influenced by scaling effects and direct comparisons can be made between the different engines.

Table 6.1: Main engine geometrical data.

Swept volume [l]	2.3	1.6	1.2
Number of cylinders	4	4	4
Similarity parameter λ	-	0.886	0.805
Compression ratio	16	16	16
Piston diameter [m]	0.0840	0.0745	0.0676
Connecting rod length [m]	0.143	0.127	0.115
Crank radius [m]	0.0518	0.0459	0.0417
Piston pin diameter [m]	0.0210	0.0186	0.0169
Fire ring height from the top [m]	0.0378	0.0335	0.0304
Bowl volume [l]	0.0240	0.0167	0.0125
Connecting rod weight [kg]	1.49	1.32	1.20
Piston set weight [kg]	1.192	0.830	0.622
Number of intake valves	2	2	2
Number of exhaust valves	2	2	2
Intake valve diameter [m]	0.0277	0.0245	0.0223
Exhaust valve diameter [m]	0.0260	0.0230	0.0209
Intake Manifold Volume [l]	0.9	0.63	0.47
Exhaust Manifold Volume [l]	1.3	0.83	0.68
Number of injector holes	7	7	7
Injector hole diameter [μm]	131	116	105

To complete the geometrical data and model calibration, several hypothesis of conservation have been assumed. For the valve system, although valve lifts have been scaled with the similarity parameter, valve timing and valve discharge coefficients have been kept unchanged for the different engines. For the combustion chamber, the unchanged parameters have been the mean swirl number, Woschni coefficients, mixing model constant and deformation model constant; and for the exhaust manifold, the heat transfer constant. Details of these conservative parameters can be observed in table 6.2. For the FAMEP correlation, the same relative mechanical losses have been assumed between the different engines. k_{fa1} (Eq. 5.56) has thus been scaled with λ while the other parameters (k_{fa2}, k_{fa3}, k_{fa4}) have been kept constant.

Table 6.2: Parameters assumed constant for the different engine displacements.

Intake valve opening [cad]	353
Intake valve closing [cad]	602
Exhaust valve opening [cad]	114
Exhaust valve closing [cad]	402
Mean swirl number MSN	2.3
Mixing model constant K_{mix}	0.354
Woschni coefficient C_{w1}	1.69
Woschni coefficient C_{w2}	0.99
Deformation model constant k_{def}	0.8
Heat transfer constant k_{exh}	1.4

In this study, two degrees of downspeeding have also been considered. A moderate one with a rated power reached at 3500 rpm and a strong one with a rated power achieved at 3000 rpm. The similarity theory is based on constant Mach number through the valves that involves identical linear piston velocity between the different engines. But here, engine and boosting architecture performance are compared at the same engine speeds. So the similarity theory cannot be purely respected and some engine settings have been adapted to correct the consequences of different linear piston velocities. These differences mainly impact the volumetric efficiency and combustion heat release pattern.

Table 6.3: Injection pressure calibration for similarity theory adaptation.

	Swept volume		
Engine speed	2.3l	1.6l	1.2l
1000 rpm	800 bar	660 bar	570 bar
1250 rpm	800 bar	660 bar	570 bar
2250 rpm	1300 bar	1100 bar	960 bar
3000 rpm	1800 bar	1540 bar	1370 bar
3500 rpm	1800 bar	1540 bar	1370 bar

For the volumetric efficiency, the variations have been offset by modifying the empirical wave effect corrections defined in the previous chapter. When engine displacements are reduced at iso-engine speeds, linear piston velocities decrease lowering pressure losses through the valves and increasing volumetric efficiency. This increase has thus been corrected reducing the overboost effect generated by the empirical wave effect corrections (Eq. 5.58). For the combustion, the rate of heat release is predicted by the combustion model as a

function of injection rate and in-cylinder thermodynamic conditions. The injector diameters have been sized with λ to scale the flame lift-off length to the combustion chamber, while injection timings have been maintained constant to control the start of combustion. Working with constant fuel-to-air ratio, the last degree of freedom is therefore the injection pressure which has been calibrated to obtain the same injection duration. With identical injection timings and injection durations, similar heat release pattern are predicted by the combustion model. The values of this calibration process are shown in table 6.3 while an example of corresponding rates of heat release and in-cylinder pressures are plotted in figure 6.1.

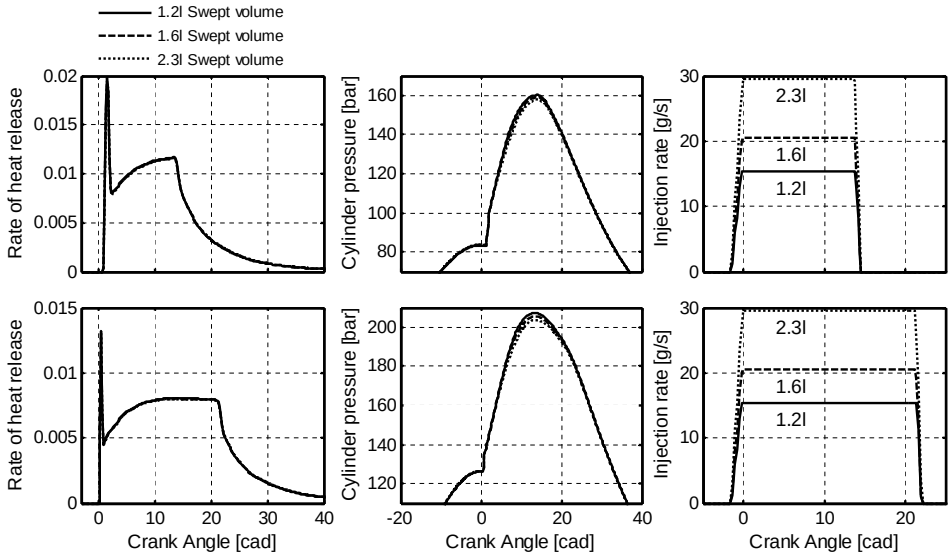

Figure 6.1: Rates of heat release, in-cylinder pressures and injection rates after injection pressure calibration (1000 rpm - F_{rel}=0.9 - intake pressure top: 2 bar, bottom: 3 bar.

As it can be observed in figure 6.1, a good concordance is obtained between the different engine displacements and only slight differences appear on in-cylinder pressures. These differences are explained not only by the combustion process but also by heat transfer phenomena. In fact, a reduction of swept volume leads to an increase of the relative surface area in contact with the gas making the engine less adiabatic. But on the other hand, the lower linear piston velocities decrease heat losses making the engine more adiabatic. Analyzing the IMEP to evaluate the overall uncertainties, it is shown in figure

6.2 that the first phenomena nearly offset the second one and global IMEP differences result insignificant in the whole engine operating range. Similar performance can thus be considered between the different engine displacements.

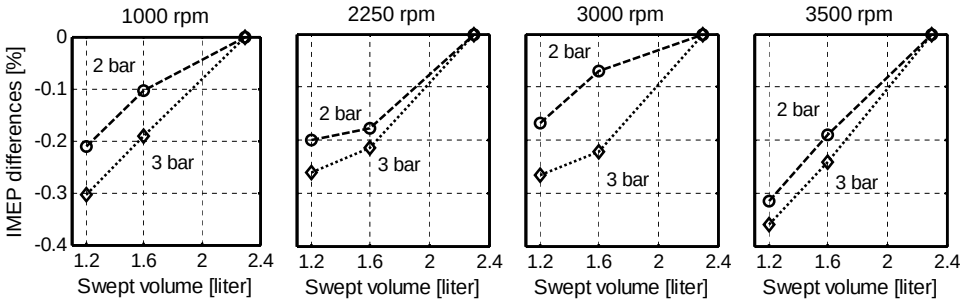

Figure 6.2: uncertainties as a function of engine speed and intake pressure (F_{rel}=0.9).

6.2.2 Boosting Architectures

From the literature review in chapter 2, it has been highlighted the most promising boosting systems to increase the performance of automotive downsized-downspeeded engines are sequential serial two-stage turbocharging, mechanical auxiliary supercharging and electric booster. These architectures have thus been analyzed in this chapter and a schematic of each one of them can be observed in figure 6.3.

All architectures are composed by a main turbocharger fitted with a variable geometry turbine, a HP and LP EGR circuit equipped with their corresponding valves and cooler, an intake throttle to forced HP EGR mass flows when necessary, an air filter, an aftertreatment system and a muffler. To cool the intake gas, an aftercooler is positioned before the intake manifold. An additional intercooler can also be employed between both stages to perform an extra cooling through the control of a bypass valve. In the serial two-stage turbocharging system, the second turbocharger is fitted in the HP stage with a fixed geometry turbine while in the other systems, the mechanical supercharger and the eBooster are placed in the LP stage. Finally in each configuration a bypass valve is arranged around the second charger to avoid parasitic losses in single-stage operations (sequential mode). These architectures have been

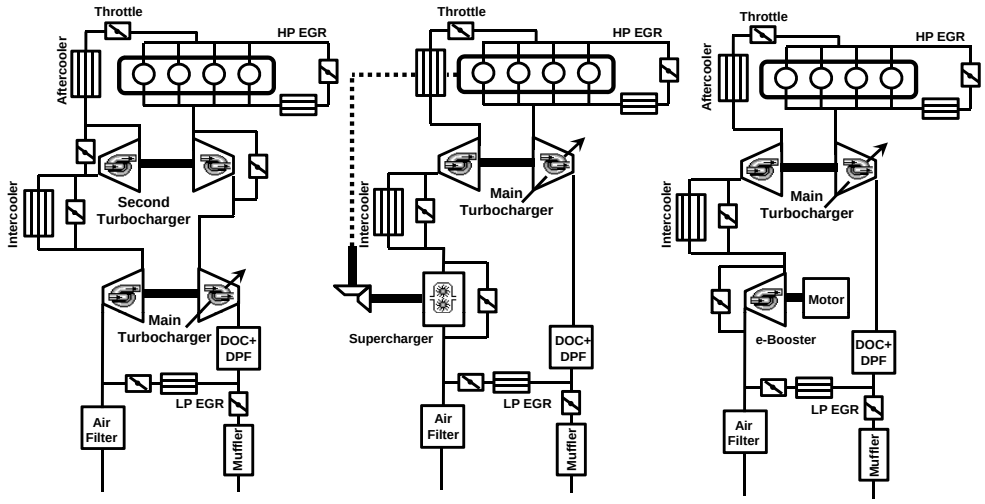

Figure 6.3: Two-Stage boosting architectures.

largely described and justified in the literature review, that is why only a brief picture is given here and more information about their features, operating modes, etc. . . can be found in chapter 2.

6.2.3 Turbochargers Data

The information relating to the turbochargers comes from characteristic maps measured in turbocharger test benches similar to those described in chapter 4. These data correspond to specific compressor and turbine designs which can be optimized for each application to achieve particular objectives. In the automotive market, a wide range of turbocharger designs are present and no map generalization can be made to perform global parametric studies. As shown in figure 6.4 where compressors and superchargers operating ranges have been plotted, the maps from an entire turbocharger family can give information about the actual technological limits. But both surge line and overspeed limits (respectively right limit and left limit of the compressor maps) are too dependent of the installation and measuring methods [120, 123, 208] to be assumed as strict limiting factor in the calculations. Efficiencies are also strongly dependent of wheels designs and important variations can be observed between different turbochargers with similar operating ranges. That is why in this study, particular characteristic maps have not been used

in the steady-state calculations and an energetic approach has been preferred. This energetic approach avoids design influences assuming infinitely large turbocharger operating ranges and making some hypotheses on the efficiencies.

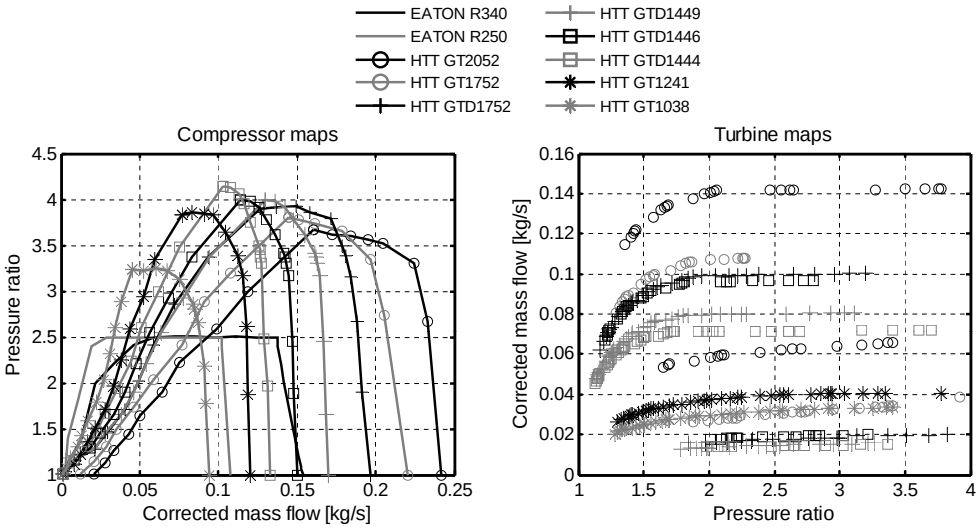

Figure 6.4: HTT turbocharger family and small Eaton superchargers maps.

Analyzing a wide turbocharger data base, interrelations between wheel diameter and peak efficiency can be stated for both compressors and turbines, see figure 6.5. Typical wheel diameters for single-stage turbocharged 2.3l engines are around 52mm for the compressor and 50mm for the turbine, while the smaller turbochargers currently available in the automotive market have wheel diameters of around 38mm and 34mm respectively. Between the bigger and smaller considered turbochargers, a decrease of 3 points and 5 points can thus be observed in compressor and turbine peak efficiencies (points expresssed in %).

In the following section, the boosting architectures will be analyzed under full load operations at 1000 rpm, 1250 rpm, 3000 rpm and 3500 rpm to characterize low-end torque and rated power performance. As explained in sections 2.1 and 2.2.2, a correct main turbocharger matching involves operations very close to the surge line at low engine speeds and near the overspeed limit at rated speeds (see figure 2.3 and 2.13). On the turbine side, it involves running operations in the closest guide vane positions at low speeds and in a wide open position at rated speeds. Under these conditions, compressor and

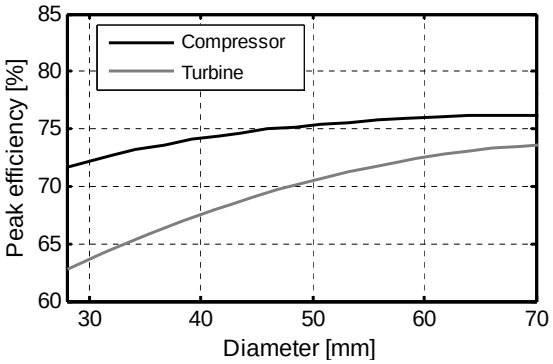

Figure 6.5: Compressor and turbine state-of-art peak efficiencies as a function of wheel diameter.

turbine efficiencies are not optimum and an efficiency decrease of roughly 5 points has been generally observed in the characteristics maps when compared to peak efficiencies. For the second charger, this efficiency decrease has also been noticed in the compressor which is matched near the surge line at 1000 rpm and 1250 rpm to enlarge the two-stage operation mode. While in the turbine, peak efficiencies are nearly achieved as its small swallowing capacity is especially optimized for these low speed operations.

Table 6.4: Charger efficiencies [%] used in steady-state calculations.

		Main Turbocharger		Second Stage	
		Compressor	Turbine	Compressor	Turbine
Single-Stage	State-of-art	70	65	-	-
	Hypothesis	80	75	-	-
Two-Stage Turbocharger	State-of-art	70	65	67	65
	Hypothesis	80	75	77	75
Two-Stage Supercharger	State-of-art	70	65	65	-
	Hypothesis	80	75	75	-
Two-Stage eBooster	State-of-art	70	65	67	-
	Hypothesis	80	75	77	-

From these considerations, constant charger efficiencies have thus been assumed in the steady-state calculations retaining the values shown in table 6.4. For the main turbocharger, peak efficiencies of 75% and 70% have been selected for the compressor and turbine respectively. Taking into account the

5 points decrease in single stage operations (3000-3500 rpm) as in two-stage operations (1000-1250 rpm), the remaining efficiencies are 70% and 65% respectively. For the second stage, the smallest turbochargers available in the automotive market have been considered with peak efficiencies of 72% and 65%. As explained above, these efficiencies remain then at 67% and 65% under working conditions. For the eBooster, the same compressor hypothesis has been assumed with additional electric motor efficiencies of 95%. Whereas for the supercharger, peak efficiencies of small Eaton four lobed 160°twisted rotors are around 70% and efficiencies of 65% have been retained with mechanical transmission efficiencies of 95%. Finally, to evaluate the sensitivity of these hypotheses and to determine the impact of future wheel design development, variations of 10 points have been considered on each value. These variations are relatively important and represent the maximum improvements in turbocharger designs that could be expected in the near future.

6.2.4 Engine and Intake/Exhaust Lines Constraints

Gas Path Elements:

Pressure losses in the intake and exhaust lines elements have important impacts on engine and boosting architecture performance. Their characteristics are mainly dependent of mass flow rate and component design. The selection of the engine elements is specific to each application and responds to a delicate balance between pressure drops, packaging constraint, efficiency to fulfill the component function, cost, etc... So, an energetic approach has also been considered for the engine components to generalize their pressure losses characteristics to the different engine displacements and rated power levels (maximum mass flow).

Table 6.5: Pressure losses [mbar] in gas path elements under full load conditions.

Engine speed	Air filter	Aftercooler	Muffler	DOC+DPF reference	DOC+DPF large capacity
1000 rpm	11	10	10	38	19
1250 rpm	13	16	18	74	37
3000 rpm	73	72	117	468	234
3500 rpm	98	101	160	644	322

Pressure losses measured under full load conditions in the air filter, aftercooler, muffler and aftertreatment system of Engine C are shown in table 6.5. As similar drops have also been measured on the engines A and B, especially for the aftercooler and muffler, the same data have been considered independently of the mass flow rate. This hypothesis amounts to scaling the pressure losses characteristics for each application in order to maintain the same component influences in the simulations. A picture of this hypothesis is given in figure 6.6 where it can be seen how the reference pressure losses characteristic is adapted to the considered maximum gas mass flow.

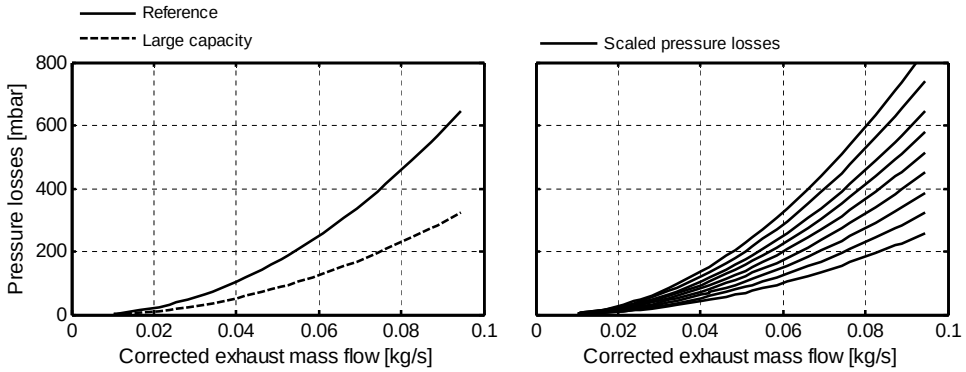

Figure 6.6: Scaled pressure losses characteristics in the aftertreatment system.

The aftertreatment system is the engine component that involves the higher pressure drops. To analyze the performance sensitivity of its design, a large capacity system producing only half losses has also been considered. For the charge air coolers, the same pressure losses characteristics have been employed for the intercooler and aftercooler and NTU models have been replaced by ideal cooling efficiencies (external cooling fluid temperatures of 35°C).

Injection Settings:

To limit the number of parameters, the injection process has been reduced to a unique main injection without any pre- or post injections. The injection timings have been optimized to maximize the IMEP (minimum specific fuel consumption) or to respect the maximum allowable cylinder pressure. At 1000 rpm and 1250 rpm, the relative fuel-to-air ratio has been fixed to 0.9. This value represents a typical maximum fuel-to-air ratio allowed by smoke limiters. While at 3000 rpm and 3500 rpm, a fuel-to-air ratio of 0.7 has been

retained to limit exhaust manifold temperatures. This lower fuel-to-air ratio obviously imposes a higher demand on the boosting system. That is why its value has been progressively increased up to 0.9 when turbine inlet pressure or compressor outlet temperature becomes a limiting factor.

EGR Systems:

Low Pressure and High Pressure EGR systems have been analyzed under three different EGR rates: 0% (without EGR), 15% (Euro VII objectives) and 30% (strong EGR constraint). In the coolers, ideal efficiencies have been employed with external cooling fluid temperatures of 90°C. Their pressure losses have been fixed in the calculations at 3 mbar at 1250 rpm, 18 mbar at 3000 rpm and 25 mbar at 3500 rpm. EGR performance has not been considered at 1000 rpm as no emissions test cycle requires EGR under full load at that speed.

For the other gas path components, two hypotheses have been assumed on their pressure losses characteristics. On the one hand, the same pressure drops have been used between the three different EGR rates scaling the element characteristics for each running operation. In that way, as LP EGR involves higher gas mass flows in the intake/exhaust lines, bigger charge air coolers and aftertreatment system effective sections are considered for LP EGR operations. On the other hand, the same pressure losses characteristics have been employed under LP and HP EGR rates scaling the characteristics for the LP EGR mode. In that case, the same elements are considered between both modes and pressure drops in charge air coolers as aftertreatment system result lower in the HP EGR mode. In the following section, this second hypothesis is labeled *HP EGR low dP*.

6.3 Steady-State Results

Simulations have been carried out with the 0D engine model to analyze the engine and boosting architecture performance under steady-state full load operations. The main objective of these simulations has been to characterize how the boosting system and the thermomechanical limits affect the maximum reachable brake power. The operating conditions have thus been defined as a function of brake power objectives increasing for each configuration the

brake power level until reaching one of the thermomechanical limits. With the energetic approach, the different engine components are directly matched to the considered brake power level. The obtained results correspond therefore to the behavior of optimized configurations.

To compare the different architectures and to analyze the influences of the considered design factors, the Brake Specific Fuel Consumption (BSFC) has been retained. Generally under full load conditions, BSFC is not so important because the current passenger cars emission test cycles don't include these running conditions. But this parameter becomes relevant for future engine development as the new emission test cycles integrate more and more highly loaded operations. Furthermore here, BSFC has been selected to quantify in each study the overall system efficiency taking into account not only the engine or the boosting architecture performance but also all the systems interactions. The BSFC allows therefore to evaluate the impact of each parameter from a global point of view such as the brake thermal efficiency.

For the thermomechanical limits, two levels of maximum compressor outlet temperature have been defined, one at 190°C and one at 210°C. The first level corresponds to the current state-of-art in turbocharger and intake line development, while the second represents the maximum allowable working temperature for cast aluminum alloy compressor wheels. This second level does not involve major modifications in compressor wheel design but requires advanced plastic materials for the intake piping. Although turbine inlet pressures have also been limited at 4.5 bar, maximum compressor outlet temperatures have always been a more restrictive factor in the calculations. Here, exhaust temperatures have not been constrained in order to define new maximum temperature requirements.

6.3.1 Main-Stage Operations

Using an energetic approach, limits and performance of single stage turbocharging system can be evaluated in the whole engine operating range. Simulations have thus been performed not only at 3000 rpm and 3500 rpm (rated speeds) where the boosting architecture works exclusively with the main turbocharger, but also at 1000 rpm and 1250 rpm to characterize from a general point of view system interactions and turbocharger requirements at low speeds. Depending of the main turbocharger matching (i.e. its ability to produce compression work at low speeds) theses requirements can be directly applied to the

second stage turbocharger or to both LP and HP turbochargers considering the two-stage architecture as a global system.

In this subsection, sensitivity studies will be first conducted without EGR to evaluate the influence of maximum in-cylinder pressure, engine component characteristics and turbocharger efficiency. Then additional analyses will be performed with EGR to characterize the impact of EGR rate and EGR system technology on maximum engine performance.

Effect of maximum allowed in-cylinder pressure:

For maximum in-cylinder pressures, two levels have been analyzed: one corresponding to the state-of-art in engine development and one considering future thermomechanical limits evolutions [36, 161]. These limits, which depend on engine speed, are defined to ensure that oscillating gas force loads do not exceed the material fatigue strength in bearing and cylinder head top desk areas. The considered values are shown in table 6.6 while the performance results are plotted in figure 6.7.

Table 6.6: Maximum in-cylinder pressures used in simulations.

Engine speed	State-of-art	Hypothesis
1000 rpm	130 bar	150 bar
1250 rpm	150 bar	180 bar
3000 rpm	170 bar	190 bar
3500 rpm	170 bar	190 bar

As it can be observed in figure 6.7, the BSFC presents a trend that firstly decreases and then increases as a function of brake power level. This trend is explained by both combustion velocity and injection timings. In fact, increasing the brake power level increases the charge density in the combustion chamber accelerating the RoHR and improving the combustion efficiency. However, when the maximum in-cylinder pressure is reached, injection timings are retarded and combustion efficiency decreases. A higher maximum in-cylinder pressure moves therefore the point of minimum BSFC to higher BMEP and reduces the BSFC at high BMEP. At low speeds with moderate BMEP objectives (around 20 bar), there are no benefits to increase the actual state-of-art limits. But for strong BMEP objectives (around 30 bar), fuel savings up to 7 g/kWh can be obtained. Exhaust temperatures rise more or less linearly with the brake power level. Increasing the maximum in-cylinder pressure allows

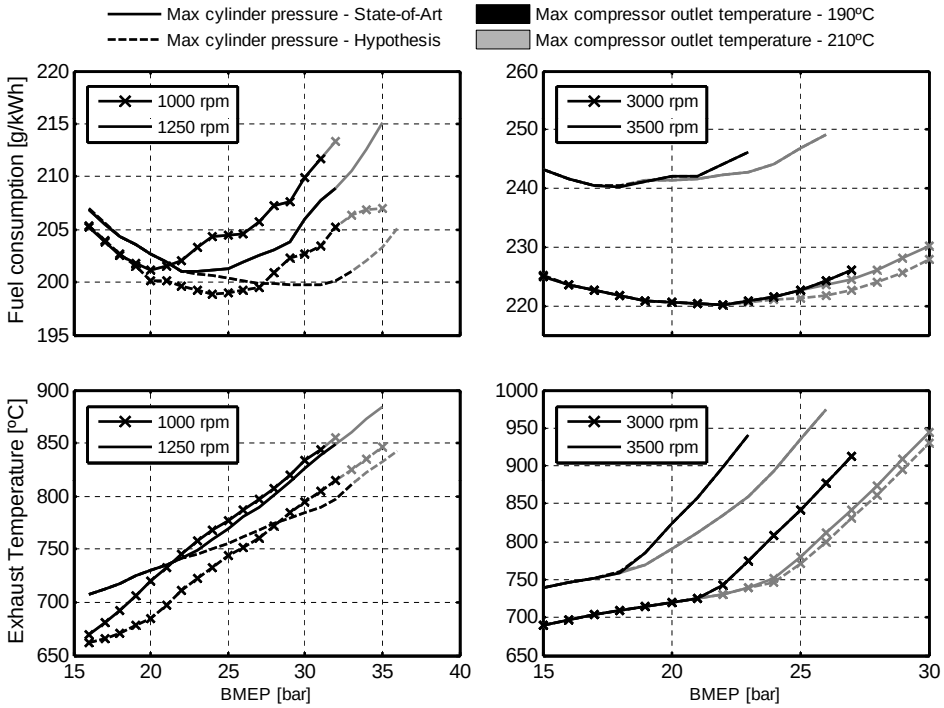

Figure 6.7: Impact of maximum in-cylinder pressure and maximum compressor outlet temperature on engine performance as a function of brake power levels.

also the reduction of the temperature constraints at high BMEP limiting the need to retard injection timings.

At 3000 rpm and 3500 rpm, the variation of fuel-to-air ratio is an additional factor affecting the BSFC. The change of trend noticed on the exhaust temperature shows how the fuel-to-air ratio is gradually increased to respect the maximum compressor outlet temperatures. A relatively low fuel-to-air ratio requires a higher compression work but reduces the thermal constraint in the exhaust. It also increases the charge density and oxygen concentration in the combustion chamber. As already explained a higher charge density can improve or deteriorate the BSFC, while a higher oxygen concentration always increases the combustion velocity and the corresponding combustion efficiency. The impact of lower fuel-to-air ratio on BSFC is therefore a balance between boosting systems losses and combustion benefits which mainly depends on the in-cylinder pressure limit. This balance is generally positive until the injec-

tion timings need to be delayed. At 3500 rpm, the in-cylinder pressures do not reach the state-of-art pressure limits. So, the fuel consumption increases from the moment when fuel-to-air ratio rises. The same effect is observed at 3000 rpm with the 190°C limit at the compressor outlet. With the 210°C limit, the fuel consumption increases before modifying the fuel-to-air ratio as the higher charge density requires some injection timings delays. Nonetheless, these injection timings delays are relatively small and generate only resultant fuel penalties of 2 g/kWh. From these considerations, at 3000 rpm and 3500 rpm the differences in BSFC are therefore mainly explained by fuel-to-air ratio variations and the small benefits observed at 3000 rpm do not justify an increase of the current state-of-art in-cylinder pressure limits at rated speeds.

In terms of maximum BMEP, the maximum allowable compressor outlet temperature always limits cylinder charge densities before exceeding the maximum in-cylinder pressure at the end of the compression stroke. Extending the thermal limit from 190°C to 210°C allows to increase the maximum BMEP of around 3 bar at rated speeds and between 1 bar and 3 bar at low speeds. At low speeds, similar benefits are also obtained increasing the maximum in-cylinder pressures due to higher combustion efficiencies (more centered injection timings). Maximum in-cylinder pressures appear therefore as indirect limiting factors.

These results are obviously dependant of the cylinder compression ratio. If a higher value is retained, the impacts observed on the BSFC will be more marked but the main trends will remain and the curves will be only shifted to lower BMEP. Finally comparing running operations performed at 3000 rpm and 3500 rpm, the effectiveness of the downspeeding technique to reduce fuel consumption can be noticed with differences up to 20 g/kWh between both considered rated speeds. Exhaust temperature constraints stay as for them relatively constant.

Effect of exhaust backpressure:

The influences of engine components pressure losses characteristics on engine and boosting system performance are shown in figure 6.8. Having higher pressure drops, a sensitivity study has been performed on the aftertreatment system considering a reference and a large capacity design as previously described. With both designs, it can be observed that elements pressure characteristics have minor impacts at 1000 rpm and 1250 rpm because gas mass flows

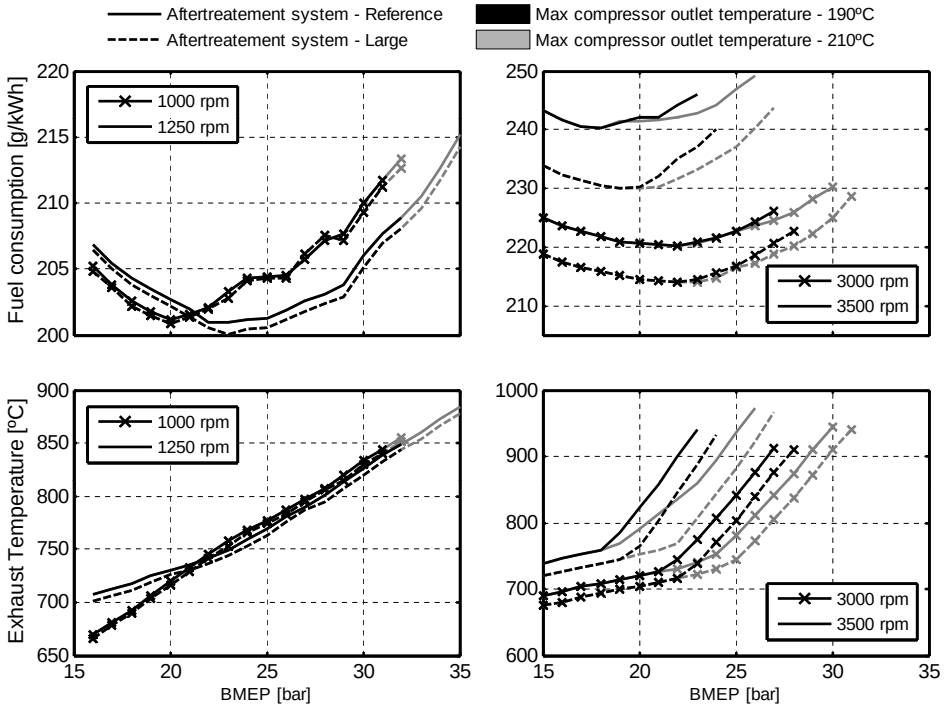

Figure 6.8: Impact of pressure drops across the aftertreatment system and maximum compressor outlet temperature on engine performance as a function of brake power levels.

as pressure drops are relatively small at these speeds. However at high engine speeds, their impacts have important consequences on the BSFC. In fact here it can be noticed how pressure losses differences of 234 mbar and 322 mbar between both designs at 3000 rpm and 3500 rpm offset the BSFC of around 5 g/kWh and 10 g/kWh respectively. In addition, the large capacity design increases the maximum reachable BMEP of 1 bar decreasing the exhaust thermal constraints of around 30°C at both rated speeds. The optimization of elements pressure characteristics is therefore fundamental to improve in the medium to high speed range the fuel consumption of downsized-downspeeded engines.

Effect of turbocharger efficiency:

For the influences of turbocharger efficiencies on engine and boosting system performance, different hypotheses have been assumed to fix state-of-art

levels before considering variations of 10 points on both compressor and turbine efficiencies. As it can be observed in figure 6.9, these important efficiency variations have limited consequences on the BSFC at low speeds reaching fuel savings of only 2-3 g/kWh at 1000 rpm and 1250 rpm. However at rated speeds, their impacts are much more significant achieving BSFC reductions of around 5 g/kWh and 10 g/kWh at 3000 rpm and 3500 rpm respectively. These reductions are similar to those obtained with the large capacity aftertreatment system. That means, optimizing the elements pressure characteristics can bring the same BSFC benefits as increasing by 10 points the turbocharger efficiencies. In terms of maximum BMEP, compressor outlet temperatures are highly dependent of turbocharger efficiencies and variations of 10 points allow to increase the maximum BMEP of around 3-4 bar in the whole engine speed range.

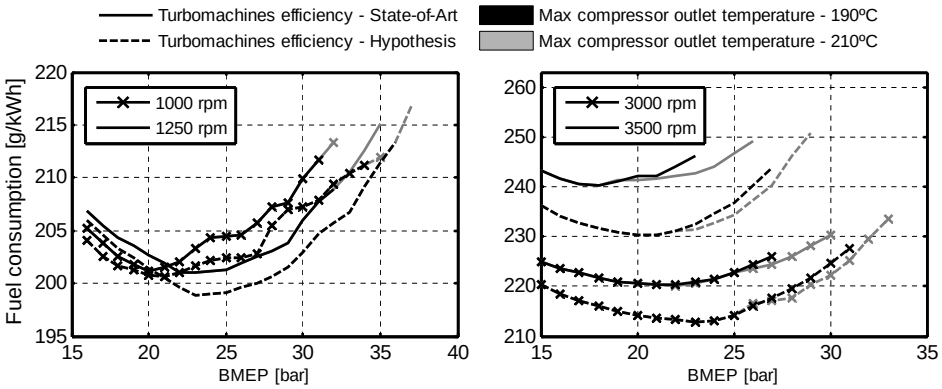

Figure 6.9: Impact of turbocharger efficiencies and maximum compressor outlet temperature on engine performance as a function of brake power levels.

These results also demonstrate that the conclusions obtained with this energetic approach can be generalized to similar downsized-downspeeded engines. In fact, efficiency hypotheses have been established with a turbocharger size corresponding to a 2.3l engine. But it has been shown maximum efficiency variations do not exceed 3 points for the compressor and 5 points for the turbine when smaller turbochargers and smaller engine displacements are considered (1.2l-1.6l engines). These efficiency variations are relatively limited when compared to the variations performed in the sensitivity study. As efficiency variations mainly offset the performance results keeping identical trends, the same conclusions can be easily extrapolated to other turbocharger efficiencies and to other engine displacements.

Synthesis of the thermal constraints:

In order to analyze how the thermal constraints limit the engine performance, the maximum reachable BMEP obtained in the previous sensitivity studies have been plotted in figure 6.10 with several levels of maximum exhaust temperature. As the simulations are not limited by turbocharger operating ranges, it can be noticed that maximum BMEP are higher at low speeds than at rated speeds. This is mainly explained by lower gas path pressure losses and lower friction plus auxiliaries' mechanical losses suffered at reduced speeds. Between both considered rated speeds, the higher losses suffered at 3500 rpm offset the brake power benefits implied by a higher speed and both downspeeding levels achieve similar maximum engine powers. Regarding the different component optimization scenarios, turbocharger efficiencies and maximum in-cylinder pressures involve the major BMEP variations at low speeds. While at high speeds, the major BMEP variations are produced by turbocharger efficiencies and element pressure characteristics.

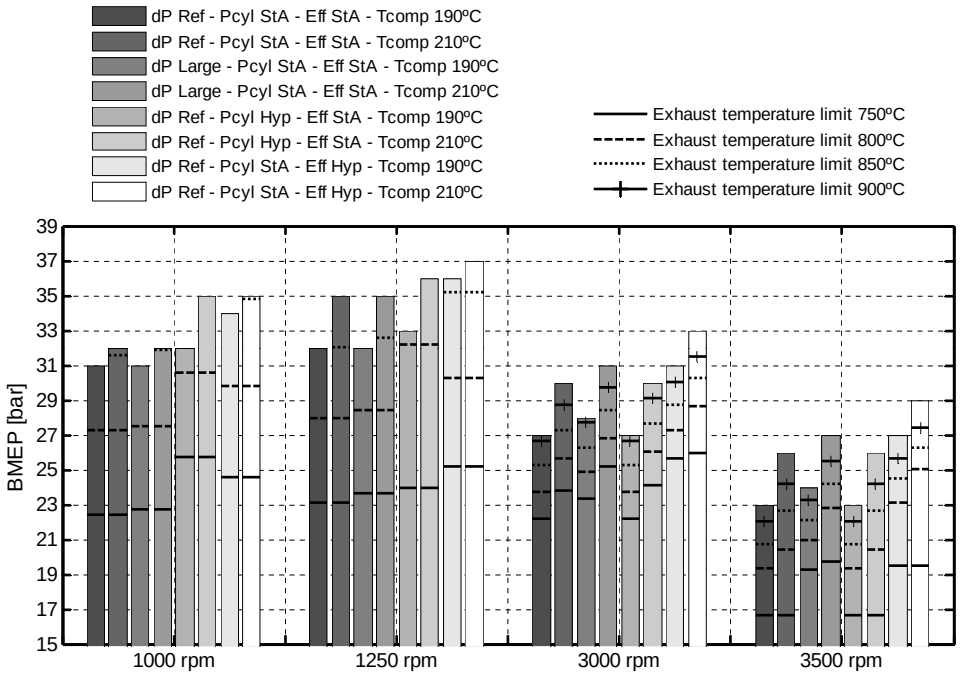

Figure 6.10: Influences of thermal constraints on maximum reachable BMEP for different component optimization scenarios.

These results have been obtained limiting directly the maximum outlet compressor temperature in the calculations. Taking into consideration the exhaust thermal constraints, it can be seen the maximum exhaust temperature is much more restrictive than the maximum outlet compressor temperature. In fact, the allowable exhaust temperature must be higher than 850°C at low speeds and higher than 950°C at rated speeds so that the maximum outlet compressor temperature becomes the limiting factor. A high exhaust temperature limit is therefore a fundamental requirement to increase the performance of downsized-downspeeded engines. Due to torque limitations in vehicle transmission, maximum BMEP objectives are generally constant between 1250 rpm and rated speed. Analyzing the results at iso-BMEP objectives, it can be noticed the exhaust temperatures are higher at rated speeds than at 1250 rpm despite the lower fuel-to-air ratio. The rated power represents thus the most critical running operation and exhaust temperature limitations must be rated at that point. Nowadays, exhaust temperature limitations vary between 750°C and 850°C according to the load duty cycle of each application. But exhaust manifolds and turbochargers able to withstand temperatures higher than 1050°C have already been developed for passenger car gasoline engines [306]. Considering the exhaust constraints shown in figure 6.10, materials and turbocharger technologies used on gasoline engines are thus necessary to develop highly-rated Diesel downsized-downspeeded engines.

Effect of EGR level:

EGR requirements imposed by new emission test cycles have important consequences on the engine and boosting system performance. To analyze these consequences, a first sensitivity study has been performed on the EGR rate provided by the LP EGR circuit. The previous parameters (engine components pressure characteristics, turbocharger efficiencies and maximum in-cylinder pressure) have been maintained at their state-of-art or reference values.

Low Pressure EGR has an impact on the combustion process, the turbocharger work and the gas path pressure drops. Here, with the hypotheses assumed on the pressure losses characteristics, the engine components are directly matched to the different LP EGR rates and gas mass flows. So the components pressures losses do not have any influence in this first EGR sensitivity study. Besides with the pressure drops retained for the air filter and muffler, the use of the second LP EGR valve placed at the muffler inlet has not

been required in the calculations. For the combustion process, EGR increases the density in the combustion chamber but reduces significantly the oxygen concentration and the resultant combustion velocity. Combustion efficiency and fuel consumption are thus deteriorated with EGR. However, a slower combustion velocity decreases the in-cylinder pressure and requires lower injection delays to respect the in-cylinder pressure limitations. In that case, the more centered combustion obtained with EGR can improve the fuel consumption. This effect depends obviously on the hypotheses assumed for the injection settings and can be avoided using multi-injection strategies or defining other objectives for the injection timings optimization process. For the turbocharger, LP EGR increases the compressor gas mass flow and the required turbocharger work to provide a given boost. LP EGR increases also the gas mass flow passing through the turbine but this higher flow does not offset the higher compression work and turbine expansion ratio increases. Introducing EGR in the cylinders lowers gas temperature during the combustion process and reduces the available energy at the turbine inlet which further increases the turbine expansion ratio. LP EGR deteriorates therefore the fuel consumption due to higher engine pressure losses.

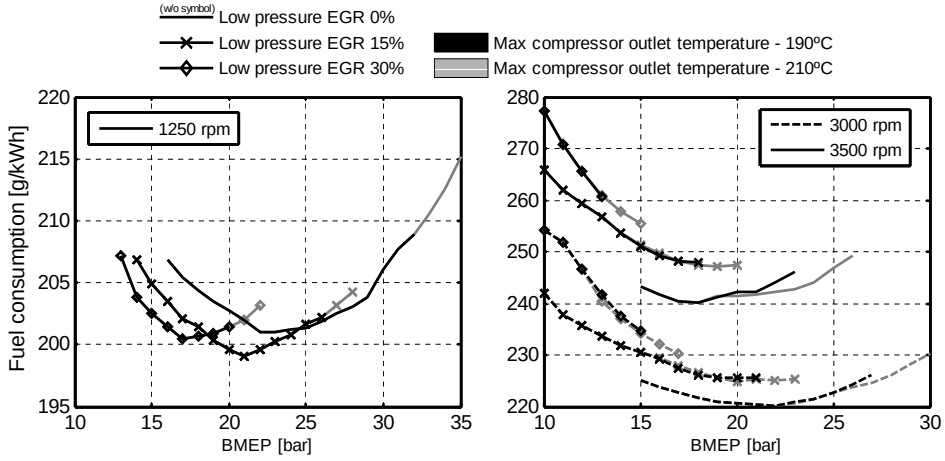

Figure 6.11: Impact of LP EGR rates and maximum compressor outlet temperature on engine performance as a function of brake power levels.

In figure 6.11, the balance of theses different impacts can be observed for various LP EGR rates (0%, 15% and 30%). At 1250 rpm, the higher cylinder charge densities move the BSFC curves and the point of minimum fuel consumption to lower BMEP. With a LP EGR rate of 15%, the lower injec-

tion delays allow fuel benefits that largely compensate for the losses involved by higher turbine expansion ratios and BSFC are improved. With 30%, the combustion benefits just offset the backpressure losses and BSFC are relatively closed to ones obtained without EGR. In terms of maximum BMEP, even employing an ideal EGR cooler which corresponds to the most optimistic situation, the maximum compressor outlet temperature strongly limits the engine performance with decreases of 7 bar and 13 bar under LP EGR rates of 15% and 30% respectively. In two-stage architectures, these performance falls can be minimized dividing the compression work between the HP and LP stages and using an intermediate intercooler. But at low speeds, the main turbocharger has generally no ability to produce significant compression works forcing the boosting architecture operating only with the second charger. In these conditions, an intermediate intercooler does not present any potential to maintain or increase the engine performance.

At 3000 rpm and 3500 rpm, increasing by 15% the LP EGR rates generates fuel consumption penalties from 5 g/kWh to 10 g/kWh. In fact, the in-cylinder pressure limitations have lower influences on the injection timings and the injection strategy does not bring any fuel benefits when working with EGR. The gas mass flows are also relatively important and the backpressure losses generated by higher turbine expansion ratios become significant. For the maximum BMEP, performance reductions from 5 bar to 7 bar can be noticed between the different EGR rates. These performance reductions cannot be minimized by an intermediate intercooler because the second charger is generally too small to provide boost at theses speeds.

Effect of EGR architecture:

With these results, a second sensitivity study has been carried out to analyze the impacts of the EGR circuit (High Pressure and Low Pressure) to provide different EGR rates (15% and 30%). The main differences between both EGR circuits lie in turbocharger works and intake temperatures. Under LP EGR, turbocharger works are more important due to higher gas mass flows passing through the intake/exhaust lines and intake temperatures are lower thanks to the aftercooler cooling process. Considering ideal aftercooler and EGR coolers, the intake temperature variations reach 8°C and 16°C under 15% and 30% EGR respectively. These temperature variations deteriorate the engine breathing process. Higher boosts are therefore necessary under HP EGR to admit the desired gas mass flows into the cylinders. As previously

described for the pressure losses characteristics, two hypotheses have been assumed; one considering the same pressure drops between both systems (HP EGR) and one considering the same elements effective sections (HP EGR Low dP). The results of this analysis are shown in figure 6.12. Having the same trends, the 3500 rpm rated speed operations have not been represented here for the sake of clarity.

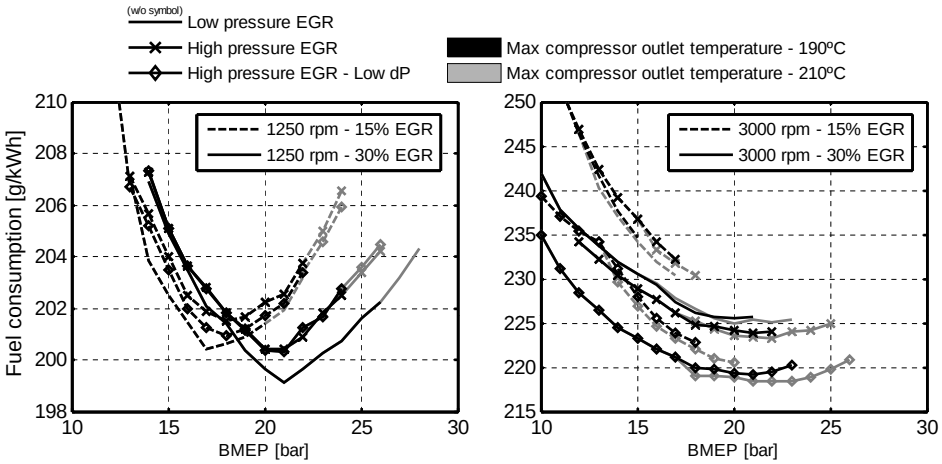

Figure 6.12: Impact of EGR rates, EGR systems and maximum compressor outlet temperature on engine performance as a function of brake power levels.

At 1250 rpm, the different hypotheses assumed on turbocharger efficiencies and element pressure losses forced to use the intake throttle to provide the 15% HP EGR rate. The pressure losses required in the intake line to increase the engine backpressures range from 50 mbar at 15 bar BMEP to 300 mbar at 25 bar BMEP. These losses imply higher compression ratios which increase fuel consumption and reduce maximum reachable BMEP by 2 bar. BSFC are thus higher with the HP EGR circuit. At 30% EGR, the intake throttle is no more required due to higher turbocharger works involved. But volumetric efficiency differences still imply higher boost demands for the HP EGR. As the benefits of lower turbocharger gas mass flows do not offset these higher boost demands, the HP EGR circuit stays less efficient. Nonetheless, with its lower compressor inlet temperatures, it allows to reach at this EGR rate 2 bar higher maximum BMEP. Regarding the HP EGR Low dP configuration, no significant differences are noticed at 1250 rpm between both HP EGR systems because the elements pressure losses are relatively small at that speed.

At 3000 rpm, with identical turbocharger efficiencies and pressure losses, similar fuel consumptions are obtained between both LP and HP circuits. The impacts of different volumetric efficiencies are more or less offset by the influences involved by the different turbocharger gas mass flows. Slight benefits can thus be observed for the LP system at 15% EGR while at 30% EGR these benefits are reported for the HP system. However, when the same engine components are used in both circuits, fuel savings of up to 7 g/kWh can be noticed with the HP EGR low dP system. That means the elements pressure drops are the most influential factors when both circuits are compared and pressure losses characteristics are critical for the LP EGR system. Unless large capacity components are employed, the HP circuit presents therefore significant benefits at rated speeds. In terms of maximum BMEP, variations from 1 bar to 3 bar give additional advantages to the HP systems.

Hypotheses of identical turbocharger efficiencies between both EGR systems are obviously unexpected in practice because the different gas mass flows move the running operations to different places in the compressor and turbine maps. At low speeds, turbocharger efficiencies are greater with LP EGR because the higher gas mass flows center the operating conditions in the characteristics maps, while at high speeds this effect is produced with HP EGR. These efficiency variations which strongly depend on the turbocharger maps can therefore positively or negatively influence the results previously found. Nevertheless, these variations are relatively small and generally go in the same directions as the trends observed. Their impacts have thus limited consequences on the obtained conclusions.

Synthesis of the thermals constraints with EGR:

To synthesize how the EGR rates and thermal constraints limit the engine performance, the maximum reachable BMEP obtained with the different EGR configurations have been plotted in figure 6.13. With EGR requirements at full load, it can be seen that the maximum allowable compressor outlet temperature is now more restrictive than the maximum allowable exhaust temperature. In fact, engine performances are limited by compressor outlet temperatures before exhaust constraints exceed 800°C. As an intermediate intercooler presents limited potential to reduce the compressor thermal constraints, advanced materials for both compressor wheel and intake piping are thus necessary for the further development of highly-rated downsized-downspeeded engines running at full load with EGR. Titanium compressor impellers able to withstand higher

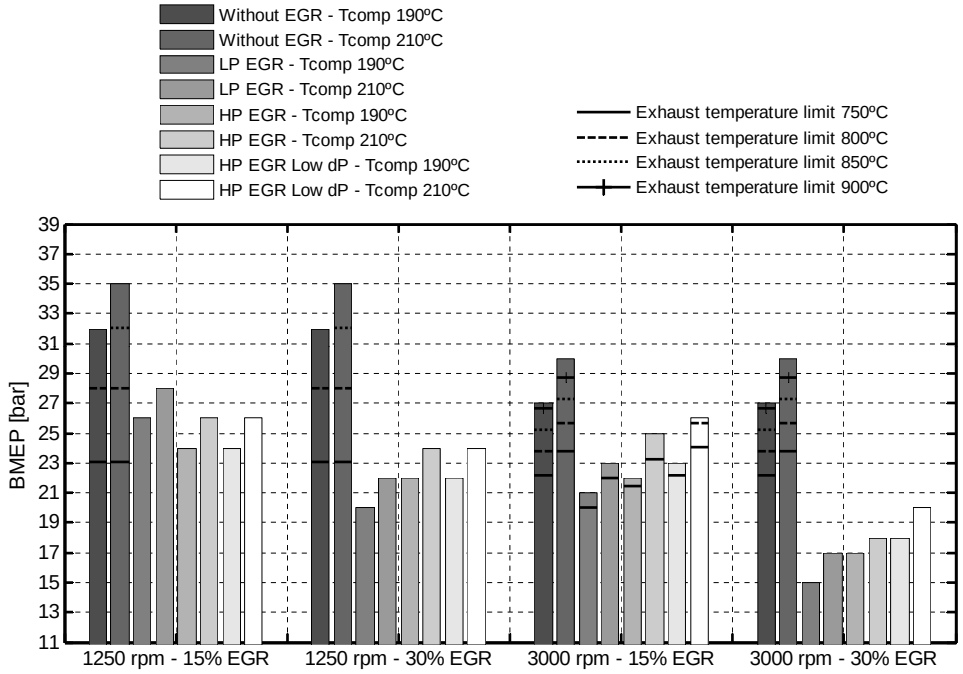

Figure 6.13: Synthesis of maximum reachable BMEP under LP and HP EGR rates.

temperatures and higher cyclical loads are already present in the market for special applications [103], but their costs are still challenging to see their rapid spread in low to medium class vehicles.

6.3.2 Two-Stage Operations

In this subsection, the energetic approach has been extended to the two-stage operations. Simulations have been performed at full load at 1000 rpm and 1250 rpm which represent the most critical two-stage running conditions for the considered boosting architectures. As already mentioned, the ability of the main turbocharger to produce boost at these speeds is generally very limited and mainly depends on the turbocharger matching. That is why the results have been divided in two representations. On the one hand, the desired boost is entirely provided by the second charger and the engine performances are analyzed as a function of brake power levels. On the other hand, as calculations are not limited by turbocharger operating ranges, the required boost

is provided by a combination of both chargers and the engine performances are analyzed as a function of compression ratio distribution for a given brake power level. 0% compression ratio distribution corresponds to a boost demand entirely produced by the main turbocharger while 100% represents one completely supplied by the second charger.

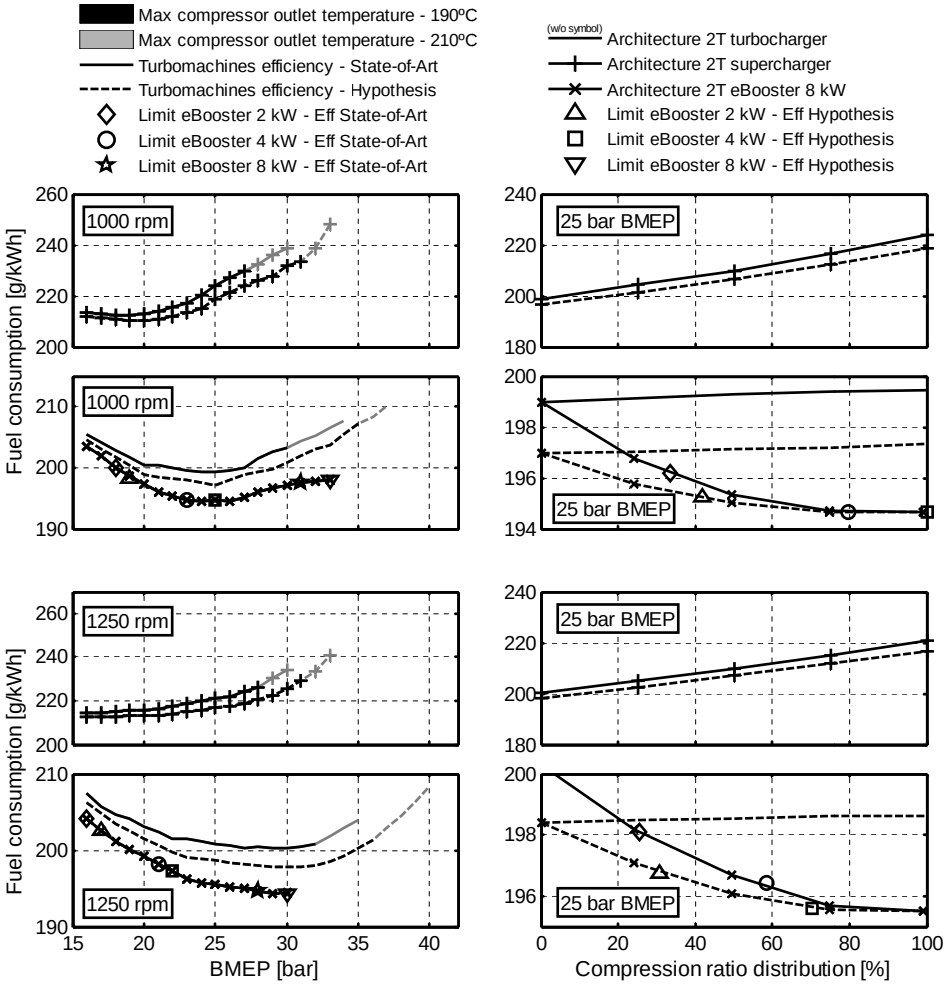

Figure 6.14: Engine and boosting architecture performance under two-stage operations.

Comparing the boosting architectures, a good energetic representativeness is obtained with the different second charger technologies, In fact, the su-

percharger uses net mechanical power from the crankshaft, the turbocharger recovers waste energy from the exhaust gases and the eBooster consumes electricity supplied by an external source. For the eBooster, the electric consumption is not taken into account in the calculations (free driving energy). It is assumed recovery systems such as regenerative brakes [61, 309] can produce enough electricity to respond to the eBooster demands through energy storages (i.e. supercapacitors). According to the last eBooster developments described in chapter 2, three electric power levels have been retained for the simulations: 2 kW, 4 kW and 8 kW.

To analyze the engine and boosting architecture performance under two-stage operations, a first sensitivity study has been performed on the charger efficiencies with the values presented in table 6.4. The calculations have been carried out without EGR, without intermediate intercooler and using the hypotheses of maximum in-cylinder pressures corresponding to future engine developments (see table 6.6). These hypotheses have been selected to reduce the influences of in-cylinder pressures limitations and to increase the maximum brake power level range for systems comparisons. Since pressure losses characteristics have limited impacts at these speeds, the reference engine components described in table 6.5 have been retained. The results of this sensitivity study are plotted in figure 6.14.

As expected, the supercharger presents the highest fuel consumptions. When compared to the turbocharger, the supercharger fuel penalties reach 15 g/kWh at 20 bar BMEP and more than 35 g/kWh at 35 bar BMEP. Between the turbocharger and eBooster, the differences are relatively small with values around 5 g/kWh. As the eBooster driving energy has no impact on fuel consumption, these small differences show the efficiency of the turbocharger to fulfill the desired boost demands through waste energy recovery from the exhaust gas.

Regarding the efficiency variations, the same conclusions as those obtained in the previous subsection can be noticed for the turbocharger (fuel savings of around 2-3 g/kWh and maximum BMEP increase of around 3-4 bar). For the supercharger, an efficiency variation of 10 points does not reduce in a significant way the required mechanical power. In fact, BSFC are only decreased from 2 g/kWh to 5 g/kWh according to the brake power level. That means efforts in supercharger design optimization do not show important potential to diminish fuel penalties generated by mechanical chargers. The efficiency variation also increases the maximum BMEP by 2-3 bar but, as part of the

brake power is employed to drive the supercharger, the maximum BMEP stays around 4-5 bar lower than those reached with the turbocharger.

For the eBooster, the maximum reachable BMEP strongly depends on the electric power limitations. For example at 1250 rpm with state-of-art efficiencies, maximum powers of 2 kW, 4 kW and 8 kW restrain the engine performance to 16 bar, 21 bar and 28 bar BMEP respectively. Without these limits, the engine performance could be increased until reaching the maximum allowable compressor outlet temperatures and the corresponding maximum BMEP would be slightly greater than the turbocharger ones. Increasing the eBooster efficiency by 10 points reduces the electric power needs allowing for a given electric power level to increase the maximum BMEP by 1-2 bar. The electric power results are shown here for the 2.3l engine. Although BSFC results can be generalized to similar downsized-downspeeded engines, the electric power results rely on gas mass flows and are specific to a given swept volume. They cannot therefore be assumed for other engine displacements. For that reason, the specific power limitations obtained on the 1.2l and 1.6l engine will be presented at the end of this subsection with the synthesis of the maximum performance results.

Thanks to the energetic approach, the impact of the compression ratio distribution between both stages can be analyzed without turbocharger operating range limitations. Considering a representative brake power level (25 bar BMEP), it can be seen how the fuel consumption is progressively reduced in the 2T supercharger and 2T turbocharger configurations as the proportion of boost provided by the main turbocharger increases. In the 2T eBooster configuration, this trend is reversed as the electric power is supplied by an external source. At this brake power level, modifying the compression ratio distribution from 100% to 0% brings for the 2T supercharger configuration fuel benefits of up to 20 g/kWh. This is mainly explained by the reduction of brake power needs. For the 2T turbocharger configuration, these fuel benefits are much smaller reaching only 2 g/kWh due to the limited efficiencies differences between both turbochargers. These small fuel savings give thus certain flexibility to the boosting architecture to optimize other objectives such as engine control, mode transition, EGR abilities at part loads [345], etc... without significantly deteriorating the fuel consumption. For the 2T eBooster configuration, using the main turbocharger can increase the BSFC up to 3-4 g/kWh. However in this architecture the selection of the optimum compression ratio distribution depends not only on the main turbocharger boost abilities but

also on the electric power limitations which can make unachievable a 100% distribution. For example here with state-of-art efficiencies, the 2 kW and 4 kW maximum electric powers limit the compression ratio distribution at 25% and 58% respectively.

Effect of inter-stage cooling:

With the same approach, the fuel benefits obtained using an intermediate intercooler have also been analyzed for two brake power levels (20 bar and 30 bar BMEP). With this cooler, the maximum reachable BMEP have not been considered due to the extremely high values that could theoretically be achieved. After a first compression in the LP stage, an intermediate intercooler allows to reduce the HP compression work increasing the gas density at the HP charger inlet. Nonetheless, adding an intermediate intercooler increases the pressure losses in the intake line. Fuel savings are thus a balance between both effects. The intermediate intercooler operates only at low speeds during two-stage operations. Its design is generally smaller than that of the aftercooler. However here to analyze an optimistic situation, the same pressure losses characteristics have been retain in both coolers.

The results of this study are shown in figure 6.15 as a function of compression ratio distribution. At 0% and 100% compression ratio distribution, there is obviously no fuel benefit from compression work reductions and the results reflect fuel penalties generated by higher pressure losses. The differences observed at 0% between the different architectures mainly lie in the intercooler relative position. In fact in the 2T turbocharger configuration, the intercooler is fitted downstream the main turbocharger while in the 2T supercharger and 2T eBooster configurations it is placed upstream. At 100%, the differences are higher with the supercharger as the pressure losses must be offset using mechanical power, while they are null with the eBooster as its electric consumption is not considered. For the 2T configuration, at 25% the HP compression work is relatively small. So, a reduction of this work has limited consequences on the fuel consumption. At 75%, the HP charger work is much more important but the temperature rise in the LP charger is relatively small. So, an intermediate cooling process has also little effect and the maximum benefits are obtained around 50%. For the other configurations, the same effects are noticed but the maximum benefits are rather observed around 75% due to the different costs that represent offsetting the pressure losses with the second charger (any impact with the eBooster while important fuel penalties

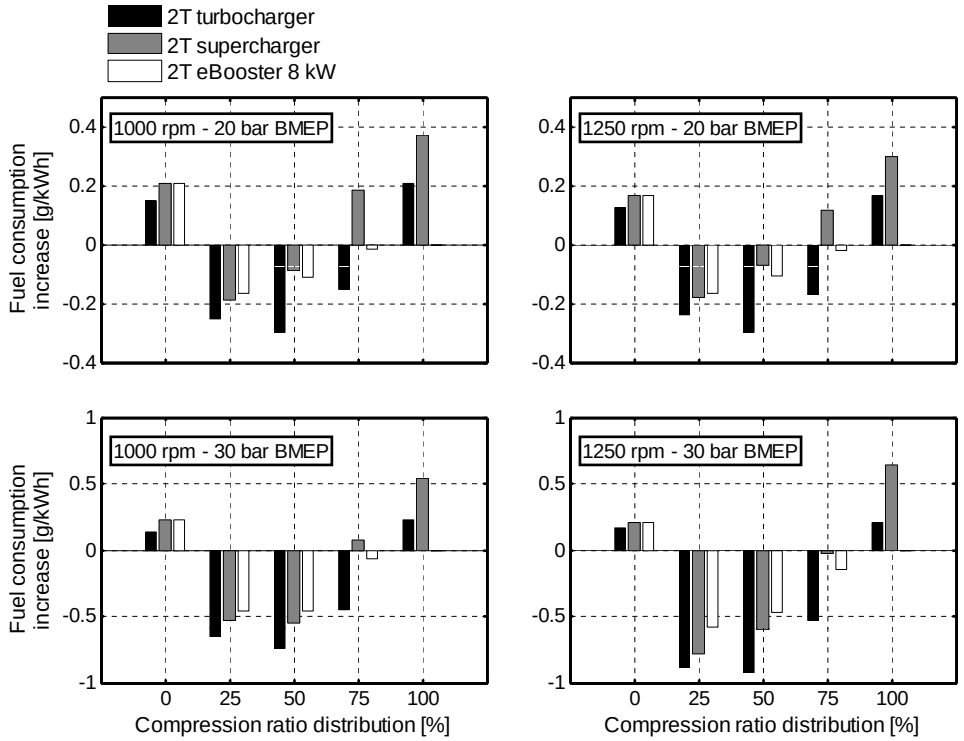

Figure 6.15: Impact of inter-stage cooling on engine fuel consumption as a function of compression ratio distribution.

with the supercharger). At the end, the fuel benefits are generally very small with maximum values of around 0.2 g/kWh at 20 bar BMEP and 0.9 g/kWh at 30 bar BMEP. So, even though the main turbocharger has the ability to produce boost at low speeds, these small fuel savings do not justify the cost and packaging constraints that involve the implementation of an intermediate intercooler.

Effect of EGR level in 2T operation:

To complete the results obtained under two-stage operations, a second sensitivity study has been performed on EGR rates provided by the LP EGR circuit (0%, 15% and 30%). Here the HP circuit has not been considered because, on the one hand, the supercharger and eBooster do not have any ability to produce the required engine backpressures, and on the other hand,

the main conclusions regarding the differences between HP and LP systems working with a turbocharging architecture have already been given in the last subsection. The calculations have been carried out with state-of-art efficiencies and without intermediate intercooler. The results are plotted in figure 6.16 using the representations previously defined.

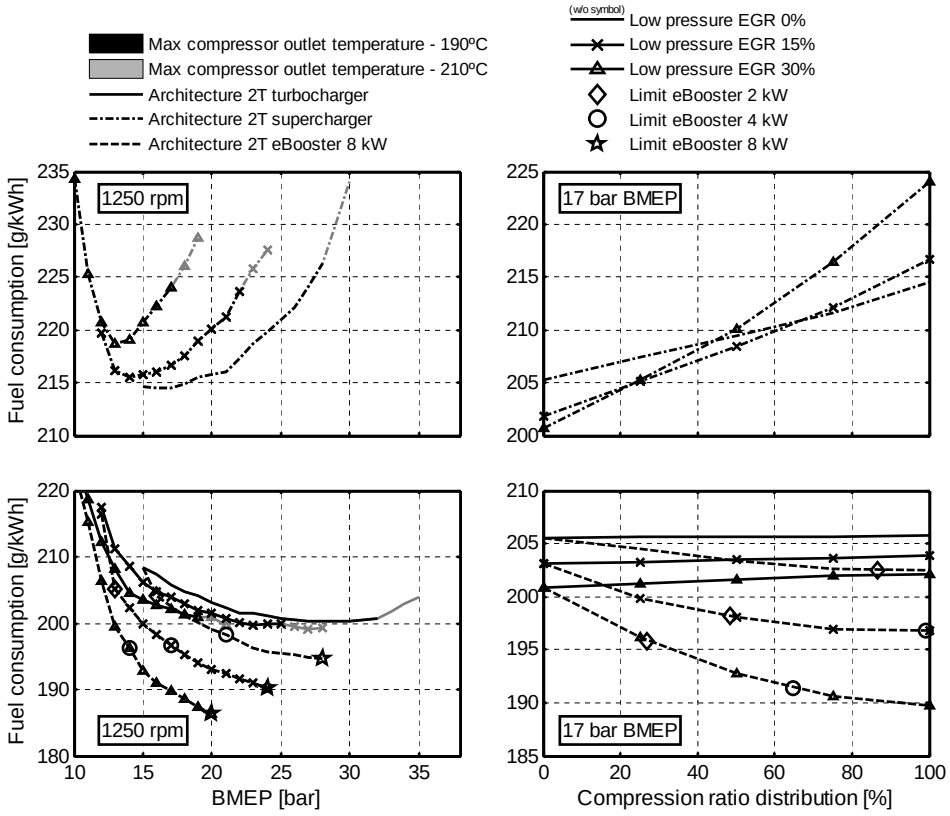

Figure 6.16: Impact of LP EGR rates, electrical power limitations and maximum compressor outlet temperature on engine and boosting architecture performance under two-stage operations.

With the hypotheses assumed on the elements pressure losses characteristics, LP EGR has an impact on the combustion process and chargers work. For the eBooster, the compressor work is produced with electricity coming from an external source. The fuel benefits of around 5 g/kWh that can be observed between the different EGR rates correspond therefore to the combustion efficiency improvements generated by the injection timings strategy.

For the turbocharger, the higher compression works increase the turbine expansion ratios and the resultant engine backpressure losses. Comparing the eBooster and turbocharger results, the fuel penalties involved by these losses can thus be estimated to around 8 g/kWh and 13 g/kWh at 15% and 30% LP EGR respectively. However here, the combustion improvements offset theses looses and BSFC are maintained almost constant between the different EGR rates. For the supercharger, the fuel penalties involved by higher brake power demands are too important to be offset by the combustion improvements and fuel consumptions are deteriorated under LP EGR. In terms of maximum engine performance, increasing by 15% the LP EGR rate reduces the maximum BMEP by 5-7 bar in the case of the turbocharger and supercharger due to the maximum compressor outlet temperatures, while this reduction is around 2-4 bar with the eBooster due to limited electric power levels. Regarding the compression ratio distribution influences, it can be noticed the same trends as those previously described for the two-stage operations running without EGR.

Synthesis of the thermal constaints in 2T operation:

Finally, to synthesize how the thermal constraints, the EGR rates and the electric power levels limit the engine performance, the maximum reachable BMEP obtained under two-stage operations have been plotted in figure 6.17. As it can be observed, when the electric power is not restrained, the 2T eBooster architecture allows to reach 1-2 bar higher maximum BMEP than the 2T turbocharger configuration due to free exhaust gas mass flows. Whereas, the 2T supercharger architecture reaches 2-5 bar lower maximum BMEP due to brake power consumption.

For the thermal constraints, if the exhaust temperature limitations are lower than 850°C, the maximum exhaust temperature stays the limiting factor in the 2T turbocharger configuration running without EGR. Otherwise, with higher exhaust temperature limitations or under EGR, the maximum compressor outlet temperature becomes more restrictive. In the 2T eBooster and 2T supercharger configurations, the exhaust temperature limitations are not so critical because the engine backpressures are significantly lower. In these architectures, the maximum compressor outlet temperature is therefore always the limiting factor. Modifying the thermal resistance of the intake piping system from 190°C to 210°C presents thus important benefits in most cases to improve by 2-3 bar the maximum reachable BMEP.

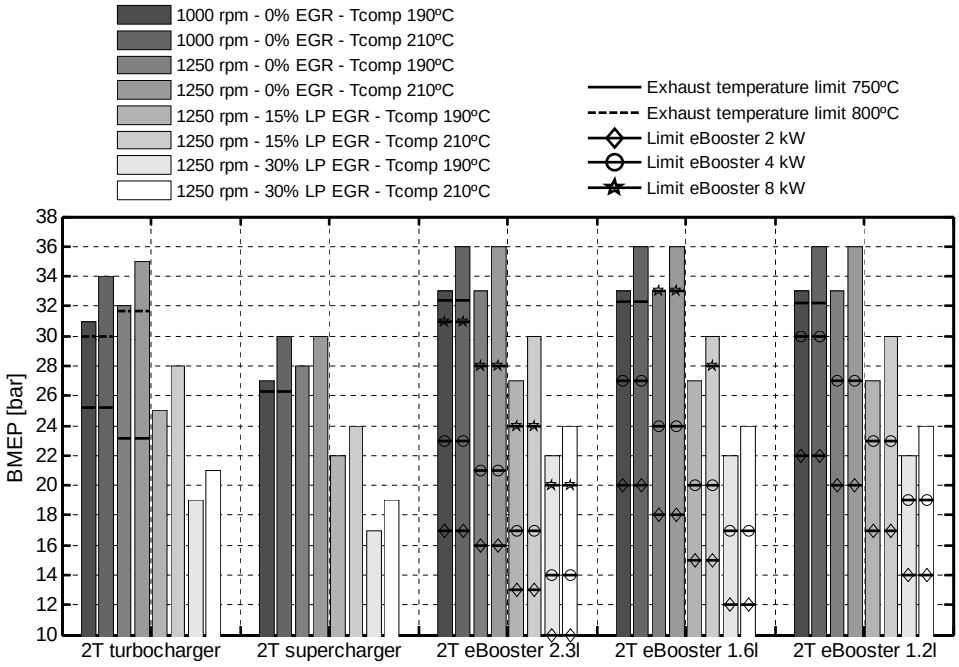

Figure 6.17: Synthesis of maximum reachable BMEP in two-stage operation.

Regarding the electric constraints, the electric power level requirements are proportional to the gas mass flows which mainly depend on the engine displacement. Here, it can be noticed how the 2 kW, 4 kW and 8 kW electric power limitations restrain the maximum reachable BMEP for the different engine displacements. To achieve the maximum compressor outlet temperatures, the electric power levels must approximately exceed 10 kW, 8 kW and 6 kW for the 2.3l, 1.6l and 1.2l engines respectively. The maximum electric power level defined by the eBooster motor or by the electric vehicle network is therefore in most cases the limiting factor to reach high low-end torques with the 2T eBooster configuration.

6.4 Matching Analysis

6.4.1 Current Characteristic Maps

From the results obtained with the energetic analysis, the charger operating ranges required by downsized-downspeeded engines can be compared

to current characteristics maps, see figure 6.18. The compressor and turbine maps have been selected from a typical HTT turbocharger family.

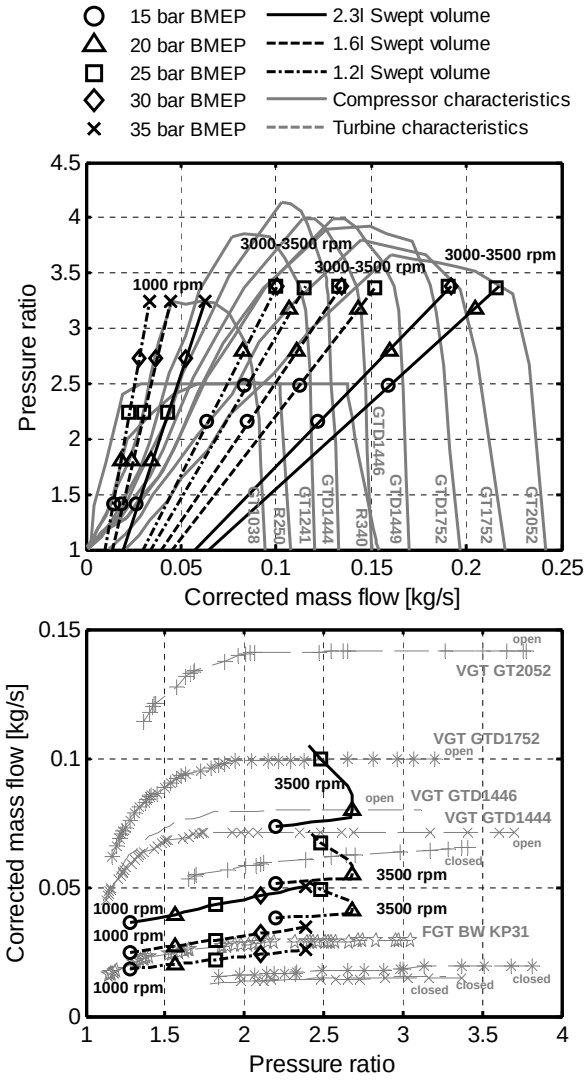

Figure 6.18: Comparison of current charger characteristic maps with downsized-downspeeded engines operating range requirements (top: compressor and supercharger, bottom: turbine).

The GTD1444 turbine (called T211(35) thereafter) is one of the smallest VGT present in the automotive market, while the GT1038 is equipped with

one of the smallest compressors. To represent the smallest available FGT, the KP31 FGT from BorgWarner has also been taken into consideration. This turbine drive a compressor similar to the GT1038 but its swallowing capacity is smaller than the GT1038. For the supercharger, the characteristic maps of the smallest Eaton designs (R250 and R340) have been retained. With this special emphasis on the smallest components, these maps allow to judge in terms of gas mass flows the lower technological limits of the current boosting systems.

In the same graphs, the operating conditions obtained at 1000 rpm and rated speeds with state-of-art efficiencies, reference pressure losses characteristics, advanced in-cylinder pressure limitations, 210°C maximum outlet compressor temperature and without EGR, have been plotted for the three engine displacements as a function of BMEP levels. At rated speeds, EGR operations have not been represented here because, on the one hand, the engine characteristics lines calculated with LP EGR are relatively closed to the ones obtained without EGR. Only small deviations toward higher corrected gas mass flows could be observed due to higher compressor inlet temperatures. On the other hand, the engine characteristics lines calculated with HP EGR are significantly moved towards lower gas mass flows but, as these operations allow to reduce charger size differences between both stages, they are normally less critical for the main turbocharger matching. In any case, it can be observed in figure 6.18 that the current characteristics maps have appropriate operating ranges to respond for each engine displacement to the main turbocharger requirements. Besides, a large number of turbocharger designs are available in these ranges. Therefore, there is an important margin to optimize for a particular application the main turbocharger matching according to the power level, rated speed, fuel consumption, EGR abilities, etc...

For the second charger, operating conditions at 1250 rpm with 30% HP EGR move also the engine characteristic lines towards lower gas mass flows, but generally full load a 1000 rpm stays the most critical running operation. For the 2.3l engine, it can be noticed in figure 6.18 the smallest compressors present significant surge margins to respond to the boost demands while, on the 1.6l engine, these surge margins are reduced to a minimum making the operating points coincide with the GT1038's surge line. As already mentioned, this surge line cannot obviously be considered as a strict limitation due to its strong dependence of the installation and measuring methods. Nonetheless, it can be concluded the 1.6l engine has a swept volume close to the current

technological limits to achieve high low-end boost pressures with state-of-art automotive centrifugal compressors. The development of smaller compressor designs is therefore necessary for further engine downsizing such as 1.2l engines. These conclusions are also valid for eBoosters which employ the same compressors.

In terms of turbines, the KP31 FGT has a swallowing capacity small enough to accommodate the 1.6l and 2.3l engine gas mass flows. However, while certain transient abilities can be expected when fitted on the 2.3l engine, KP31 characteristics are too close to the 1.6l engine operating conditions to show fast transient potential on this engine displacement. On the 1.2l engine, its swallowing capacity is directly too large to produce the required power. So, as for compressors, smaller FGT need to be developed for engine downsizing.

For superchargers, the R250 design can respond to the different boost demands but the operating conditions are relatively close to the minimum allowable gas mass flows where supercharger maps have poor efficiencies. Although gas mass flows are not so limited as with centrifugal compressors, the development of smaller superchargers is necessary for efficient engine downsizing. Due to tight operating clearances and high thermal sensitivity, current superchargers provide maximum compression ratio of 2.5. If low-end torque objectives are higher than approximately 25 bar BMEP, new supercharger designs able to work under high compression ratio will be thus also required.

6.4.2 Future Turbocharger Maps Requirements

In the following section, the transient performance of the different boosting architectures will be analyzed with the 0D engine model in actuator oriented configuration. To run the simulations and check these performances, new characteristic maps of smaller compressors and smaller turbines have to be defined to respond to the required boost pressure demands. For the supercharger, to avoid new map definition, the R250 design has been maintained on the three engine displacements despite its relatively poor matching.

The smaller turbocharger maps are scaled from the existing characteristics applying the dimensional analysis to compressible fluids through a turbomachine [97]. The functional relationships between non-dimensional variables are:

$$\Pi, \eta = f\left\{\frac{\dot{m}\sqrt{RT_{in}}}{D^2 P_{in}}\ , \frac{ND}{\sqrt{RT_{in}}}, \mathrm{Re}, \gamma\right\} \tag{6.1}$$

and, as explained in chapter 4 for a machine handling a specific gas, operating at high Reynolds number and considering corrected values, become:

$$\Pi, \eta = f \left\{ \frac{\dot{m}\sqrt{\frac{T_{in}}{T_{ref}}}}{D^2 \frac{P_{in}}{P_{ref}}} \ , \frac{ND}{\sqrt{\frac{T_{in}}{T_{ref}}}} \right\} \tag{6.2}$$

The turbomachines operate therefore with the same pressure ratios and efficiencies and the scaling relationships for gas mass flows and shaft speed are expressed as:

$$\frac{\dot{m}_{base}}{D^2_{base}} = \frac{\dot{m}_{scaled}}{D^2_{scaled}} \quad and \quad N_{base} D_{base} = N_{scaled} D_{scaled} \tag{6.3}$$

These relationships verify that blade tip speeds are maintained among scaled turbochargers since they are manufactured with the same material and have the same tensile strength. However in section 6.2.3, it has been reported how efficiencies vary with compressor and turbine sizes. So, identical efficiencies cannot be assumed between the different scaled characteristics and here only similar efficiency variations have been considered. Then, an efficiency offset calculated from the correlations showed in figure 6.5 has been applied to the whole map to approximate size influences.

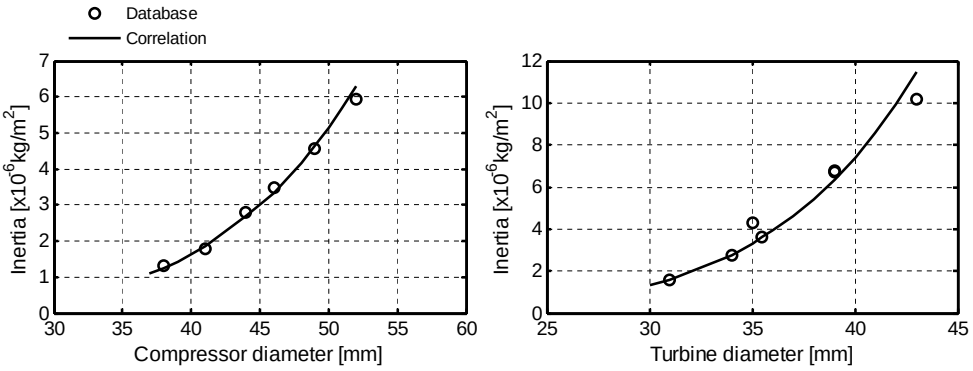

Figure 6.19: Compressor and turbine inertias as a function of wheel diameters.

Finally, to complete the scaling process, turbocharger inertias have to be defined according to the new compressor and turbine sizes. These inertias

are strongly dependant of turbocharger design and wheel materials but, analyzing turbochargers from the same family, correlations can generally be set as a function of wheel diameter. Here, considering the HTT family previously described, the obtained correlations are shown in figure 6.19 where the curves have been extrapolated to lower wheel diameters to estimate the new turbocharger inertias.

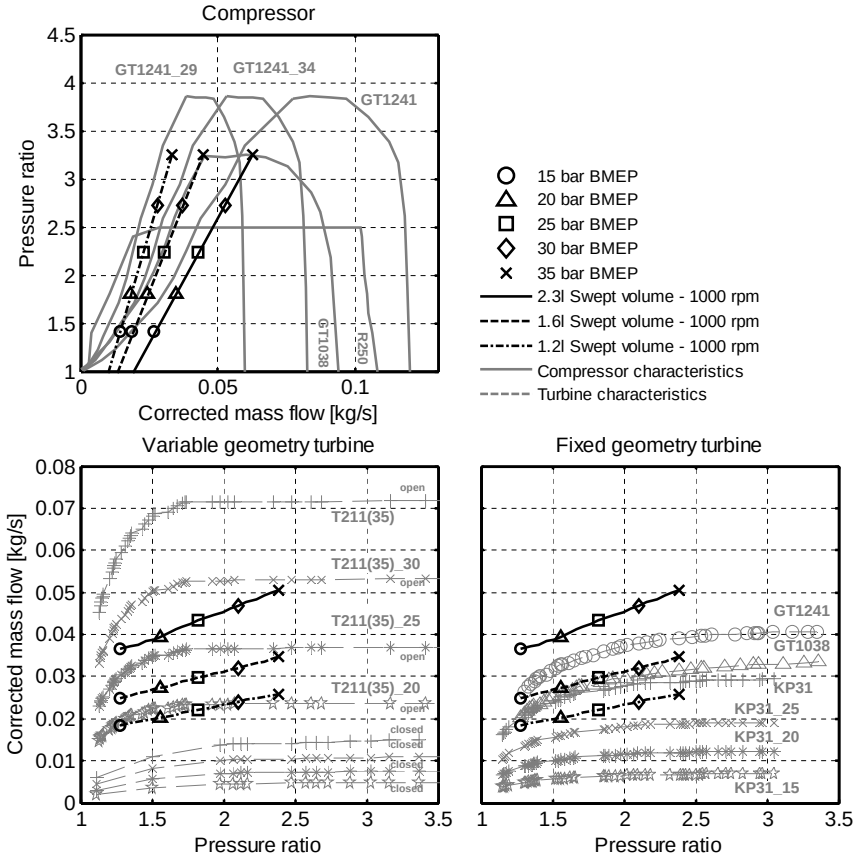

Figure 6.20: Turbocharger characteristics maps for downsized engines operating ranges requirements.

For the transient simulations, the GT1241 compressor has been selected to equip the second stage of the 2.3l engine and two compressors have been scaled from this design to fit the 1.6l and 1.2l engine requirements. These compressors are respectively called GT1241_34 and GT1241_29 and their wheel diameters have been reduced from the baseline until reaching safe surge margins under

full load operations at 1000 rpm. The result of this scaling process is shown in figure 6.20 and table 6.7.

Table 6.7: Compressors characteristics.

	Wheel diameter [mm]	Inertia $[10^{-6}kg/m^2]$	Peak efficiency [%]
GT1241	41	1.86	73.8
GT1241_34	34	0.71	72.8
GT1241_29	29	0.31	72.3

Table 6.8: Turbines characteristics.

	Type	Wheel diameter [mm]	Inertia $[10^{-6}kg/m^2]$	Peak efficiency [%]
T211(35)	VGT	35	4.32	65.5
T211(35)_30	VGT	30	1.29	63
T211(35)_25	VGT	25	0.43	60
T211(35)_20	VGT	20	0.11	56
GT1241	FGT	35.5	3.59	65.5
GT1038	FGT	34	2.76	64.5
KP31	FGT	31	1.58	63.5
KP31_25	FGT	25	0.43	60
KP31_20	FGT	20	0.11	56
KP31_15	FGT	15	0.02	51

On the exhaust side, at the difference of the compressor maps where steady operating conditions can be employed to evaluate the adequacy of possible compressor operating ranges, the transient aspect is too important to define required swallowing capacity directly from turbine characteristic maps. So, representative series of small FGT and VGT have rather been specified to evaluate on each engine displacement several turbine power abilities under low gas mass flow conditions. Although the considered 2T turbocharger architecture has been established with a FGT in the HP stage, VGT turbines have also been analyzed here. In fact, the swallowing capacities of the smallest VGT in closed position are smaller than the ones of the smallest FGT. When reduced swallowing capacities are required for the second charger, the use of VGT can therefore limit the need of small turbines development. The turbine series used in the simulations are composed of three FGT scaled from the KP31 design and three VGT scaled from the T211(35) design (GTD1444). Their characteristics are reported in table 6.8 and figure 6.20.

6.5 Transients Results

With the new turbocharger characteristic maps previously defined, cold transient tests at 1000 rpm have been simulated with the different boosting architectures for the three engine displacements. As described in chapter 5, these transient cycles are critical for the charging systems due to low gas mass flows and thermal inertias. Time responses obtained under these transient operations are therefore quite representative of the performance of both engine and boosting architectures. In modern engines development, it is generally assumed that one second represents a good time response to reach the maximum low-end torque starting from low load, while two seconds corresponds to poor transient abilities. Between both times, transient responses can be judged acceptable or not according to the specific application.

For the simulations, the pressure losses characteristics of Engine C components have been employed on the 2.3l engine and then scaled on the 1.6l and 1.2l engines to obtain the same pressure drops under the corresponding gas mass flows. Compressor outlet and exhaust manifold temperatures have not been restrained in the calculations but specific control strategies have been implemented on the turbines actuators to avoid excessive exhaust manifold pressure (limitation fixed at 4.5 bar). The smoke limiter has been calibrated with a maximum fuel to air ratio of 0.9 and advanced in-cylinder pressure limitations have been retained in the cylinders.

In this section, the results obtained in single stage operations will be first reported to characterize the turbo-lag of small turbochargers. Then, the results obtained in two-stage operations will be presented to determine the impacts of the main turbocharger on time responses and to analyze the transient behavior of eBooster and supercharger configurations.

6.5.1 Turbochargers Response

Turbo-lag phenomenon is influenced by three main factors which are the turbine swallowing capacity, both compressor and turbine efficiencies and turbocharger inertia. A sensitivity study has thus been carried out on these factors to quantify their influences on transient response.

For the impact of swallowing capacities, the different FGT described in table 6.8 have been coupled to the GT1241 compressor and then fitted on

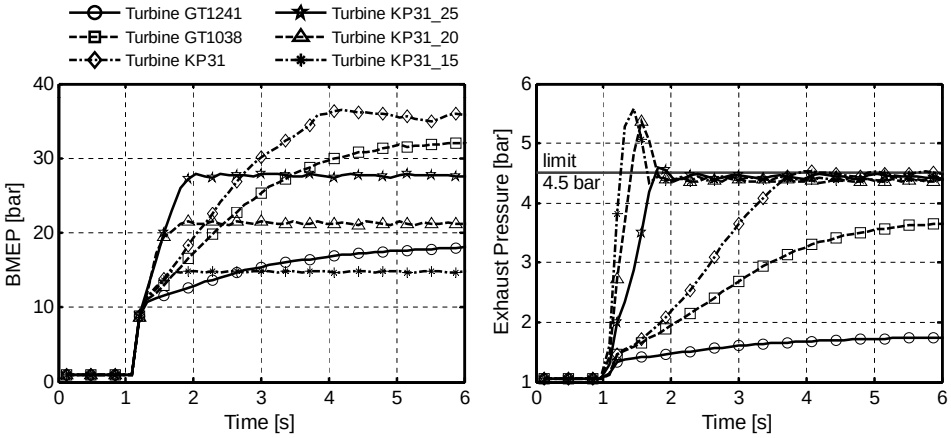

Figure 6.21: Influence of turbine swallowing capacity on transient performance during cold transient test cycles at 1000rpm on the 2.3l engine.

the 2.3l engine. The transient results obtained in single stage operations are shown in figure 6.21. Even though the GT1241 FGT is able to provide relatively high low-end torque in steady conditions, it can be observed how its power ability is too small under low gas mass flow and cold conditions to produce acceptable transient responses. Reducing the turbine effective section improves this situation and here a low end-torque objective of 30 bar BMEP can be reached in 3 seconds and 2 seconds with the GT1038 and KP31 FGT respectively. At 20 bar BMEP, the KP31 swallowing capacity represents a good match for the 2.3l engine achieving the torque objective in around 1 second. This time response can further be enhanced to 0.6 second using the KP31_25 FGT but its small effective section leads rapidly to choked conditions restricting the maximum reachable BMEP to 27 bar due to exhaust manifold pressure limitations. With the turbine almost chocked, reducing even more the swallowing capacity strongly decrease the maximum BMEP and does not improve the time response. In fact at the beginning of the transient, the benefits of smaller turbine section are offset by higher engine backpressures. For a given engine displacement, there is therefore a limit in turbine size reduction to maximize transient performance and here for the 2.3l engine an objective of 30 bar BMEP cannot be achieved in 1 second with small state-of-art turbine designs.

Regarding turbocharger efficiencies and inertias, variations of 10 points and 25% have been considered respectively. The simulations have been per-

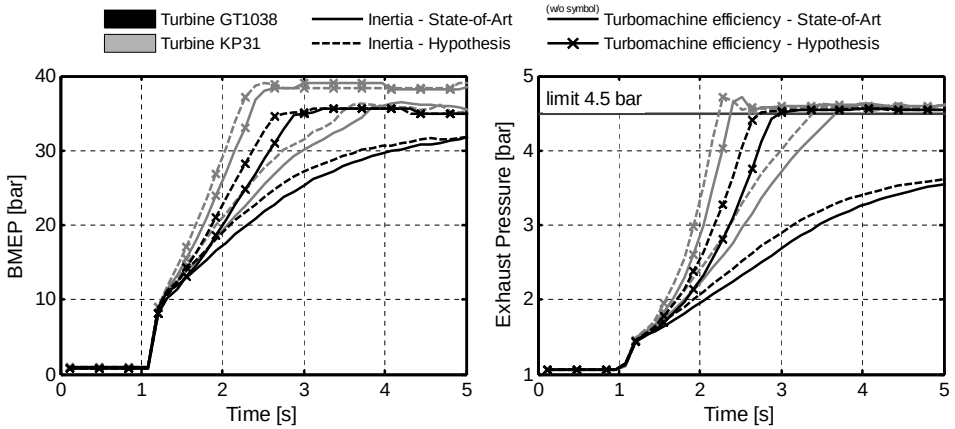

Figure 6.22: Influence of turbocharger efficiencies and inertia on transient performance during cold transient test cycles at 1000rpm on the 2.3l engine.

formed with the GT1038 and KP31 turbines fitted in the 2.3l engine. The results are shown in figure 6.22. As these turbines already have relatively low inertias, it can be noticed that the use of advanced material to significantly reduce their inertia has limited consequences on transient responses. Here, benefits of only 0.2-0.3 second have been obtained with 25% inertia reduction. However, the improvements in turbocharger efficiencies present important potential to enhance transient performance. In fact, increasing by 10 points the turbocharger efficiencies allow the time responses to be reduced by 50% and higher BMEP to be reached. With these efficiencies variations, the objective of 30 bar BMEP can now be achieved in 1 second using a turbine slightly smaller than the KP31 FGT. Small effective sections and efficient designs are therefore the fundamental combination to reduce turbo-lag phenomena.

Analyzing the turbine requirements for the different engine displacements, it can be observed in figure 6.23 for an objective of 20 bar BMEP that the KP31 FGT provides a good transient response on the 2.3l engine but its swallowing capacity is too large to have some power abilities on the 1.6l engine. The corresponding time response is thus extremely slow and a 20% smaller turbine (KP31_25) has to be developed to reach the torque objective within 1 second. On the 1.2l engine, the low gas mass flows are even more critical and a 35% smaller turbine (KP31_20) is required to reach the same performance. These scaling values can obviously be reduced if more efficient designs are developed in parallel to small swallowing capacities. For an objective of 30 bar BMEP,

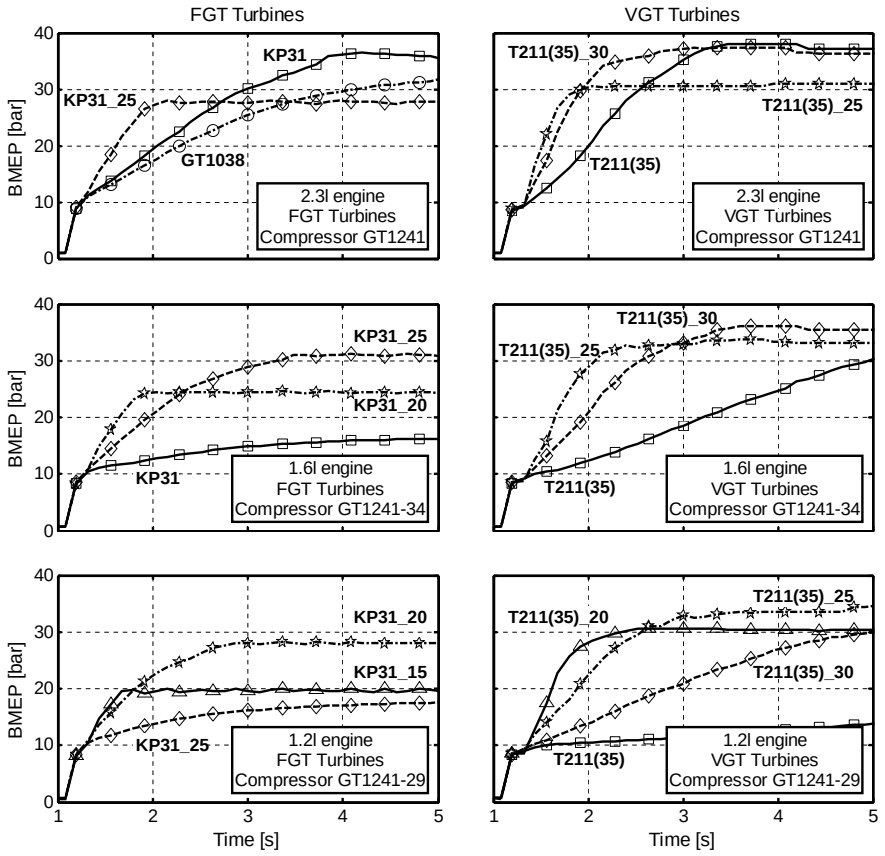

Figure 6.23: Turbine requirements to fulfill transient performance objectives in downsized-downspeeded engines during cold transient test cycles at 1000rpm.

efficiencies improvements are also essential and the trends underlined on the 2.3l engine can be generalized to the other engine displacements. So, turbines slightly smaller and significantly more efficient than the ones retained for the 20 bar BMEP objective need to be developed to reach this power level within 1 second.

With VGT turbines, it can be noticed for the 2.3l engine that the smallest VGT available in the automotive market takes the same time to reach 20 bar BMEP as the smallest FGT. In fact, the benefits of smaller swallowing capacity obtained in closed position are offset by lower efficiency and higher inertia. Applying to the VGT the scaling factors previously defined for the FGT, this

effect can also be verified for the 1.6l and 1.2l engines where the T211(35)_30 and T211(35)_25 produce similar time responses as the KP31_25 and KP31_20 respectively. At 20 bar BMEP, fitting a VGT in the HP stage presents thus little interest for the 2.3l engine but, for other engine displacements, the bigger wheel diameters involved can justify its use to reduce the efforts in small turbine designs development (wheel diameter differences of around 5mm). For higher BMEP, VGT are progressively open at the end of the transient to limit choked conditions adapting their swallowing capacity to the gas mass flows, so no power is lost through a wastegate. Transient performances are therefore enhanced with VGT and efficiencies improvements are less critical than for FGT. In that way, the objective of 30 bar BMEP within 1 second can be achieved with state-of-art turbine designs (T211(35)_30, T211(35)_25 and T211(35)_20 for the 2.3l, 1.6l and 1.2l engines respectively) or with the VGT defined at 20 bar BMEP increasing relatively their efficiencies. The use of VGT at this power level can thus reduce development efforts not only in small effective sections but also in highly efficient designs.

6.5.2 Two-Stage Performance

Two-stage turbocharging architecture:

In a two-stage turbocharging architecture, the main turbocharger can also have some abilities to produce boost at low engine speeds depending on its minimum swallowing capacity and VGT actuator strategies. This boost production has an impact on the second turbocharger operating conditions and on the whole transient performance. To illustrate these effects, simulations have been realized on the 2.3l engine with a FGT KP31 in the HP stage (wastegate closed) and a VGT GTD1752 in the LP stage. A relatively small turbocharger has especially been retained in the LP stage to increase boost abilities at low speeds and amplify the main turbocharger influences.

The results are shown in figure 6.24 where the transient responses obtained in two stage operations varying VGT position are compared to the response previously obtained in single stage operations with the same HP turbocharger. As it can be observed, the fastest transient is achieved in single stage operations when the small turbocharger works alone without any interactions from the LP stage. In two stage operations, even though 50% to 100% VGT openings produce here similar results, the time responses increase closing the VGT as more energy is recovered by the main turbocharger.

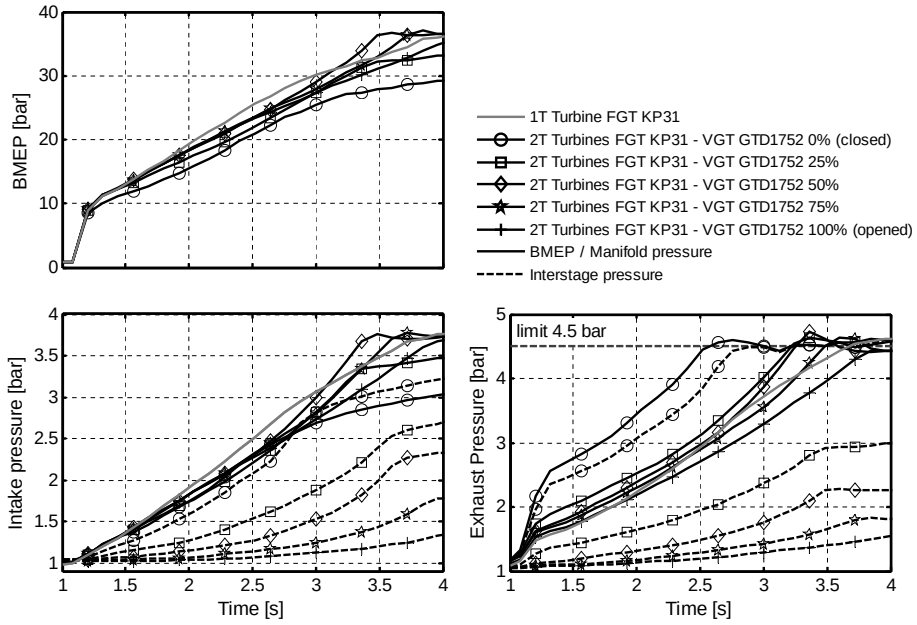

Figure 6.24: Effect of main turbocharger matching and VGT actuator strategies on transient performance (cold transient test cycles at 1000rpm on the 2.3l engine).

This behavior is explained in figure 6.25 with the different operating conditions plotted in the characteristics maps. Increasing the main turbocharger work increases the gas density in the HP stage. The adapted gas mass flows are therefore reduced in the second turbine and, having a given swallowing capacity, its power ability is lowered. This decrease of boost in the HP stage is more or less offset by the main turbocharger but, as the LP stage has a higher inertia, transient responses are deteriorated. So, the VGT has to be maintained in an open position to optimize the transient responses in a two-stage turbocharging configuration equipped with a VGT in the LP stage. Comparing the results obtained at 100% VGT opening with those obtained in single stage operations, slight differences exist here between both time responses because the main turbocharger has a relatively small matching and the VGT produced some work even in full open position. With a bigger matching more adapted to this engine displacement, theses differences would be insignificant. So, the conclusions found in the previous section are also valid in two-stage operations and the development of small high efficient turbines stay critical to fulfill the performance requirements of future downsized-downspeeded engines.

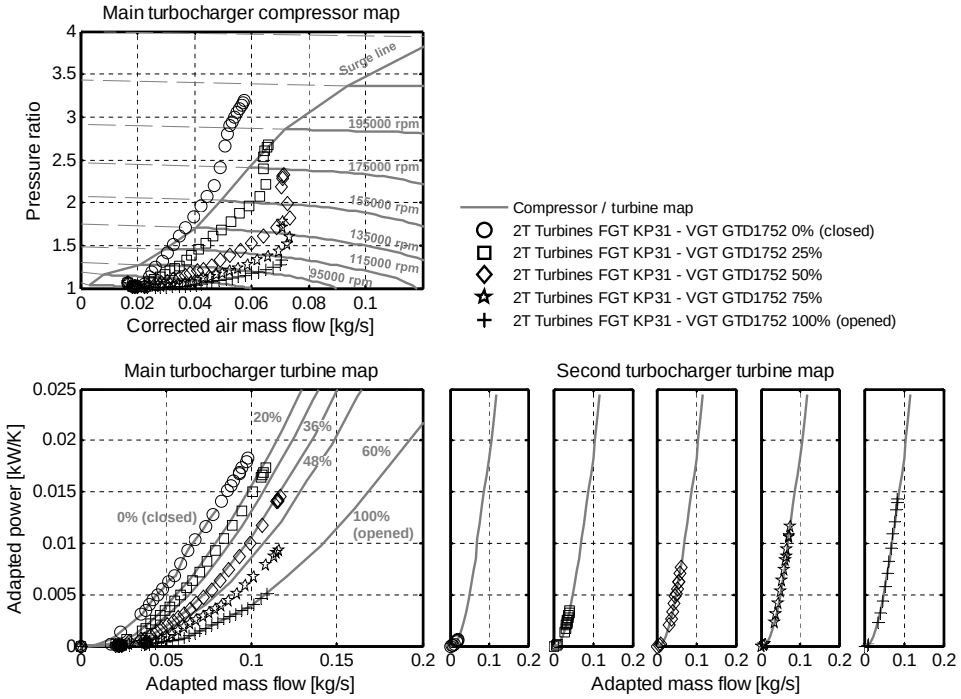

Figure 6.25: Interactions between HP and LP turbochargers during transient operations as a function of main turbocharger matching and VGT actuator strategies (cold transient test cycles at 1000rpm on the 2.3l engine).

Two-stage eBooster architecture:

In a 2T eBooster configuration, transient responses depend on the electric power supplied by the vehicle network and on the turbocharger boost abilities. As there is no interaction between the HP and LP stages in the exhaust side, the VGT is maintained in a closed position to optimize the turbine work production. According to the turbocharger matching, this position can be the closest VGT opening to generate the maximum power with the smallest turbine swallowing capacity, or the VGT opening that maximizes boost pressure preventing compressor surge.

To analyze the main characteristics of 2T eBooster architecture responses, calculations have been carried out on the 2.3l engine with a 4 kW eBooster (compressor GT1241) and a GTD1752 turbocharger. For the eBooster, the

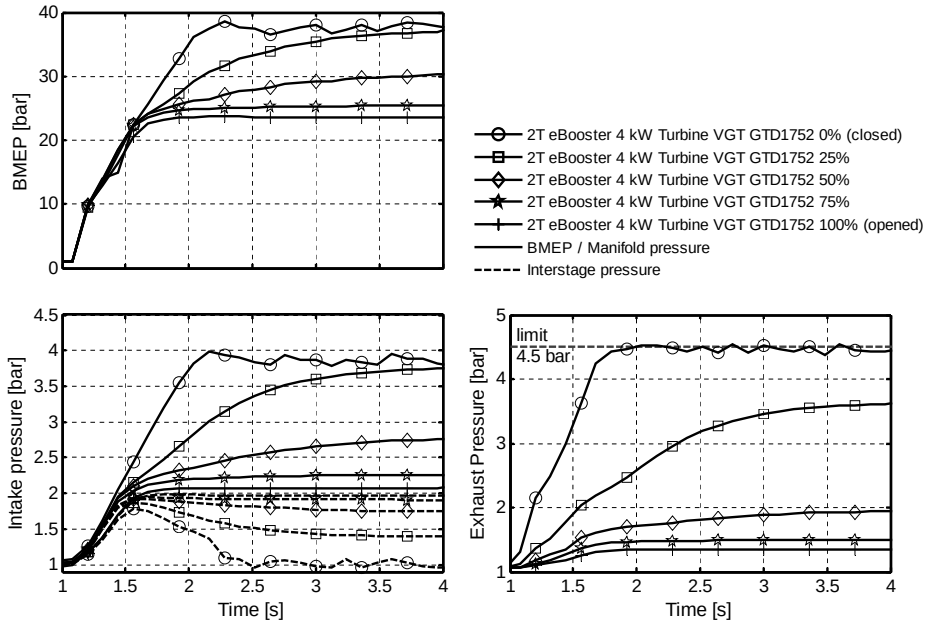

Figure 6.26: 2T eBooster architecture transient responses as a function of turbocharger boost abilities during cold transient test cycles at 1000rpm on the 2.3l engine.

compressor inertia has been doubled to simulate representative eBooster accelerations considering also a rough motor inertia [150, 247]. The results obtained under full eBooster electric power are shown in figure 6.26. The VGT position has been varied here to represent different turbocharger boost abilities at low speeds. Using a relatively small matching, it has to be noticed that the main compressor may get into surge for the closest VGT openings (see figure 6.27).

Regarding the intake pressure built-up, the transient response can be divided in two different parts. First, the eBooster provides the boost corresponding to the electric power in approximately 0.5 second. Then, if the turbine can produce some power under these low gas mass flows, the turbocharger will continue to accelerate according to its efficiencies, inertia and swallowing capacity. However, the resultant intake manifold pressure is not proportional to the turbocharger compression ratio. In fact due to electric power limitations, the operating conditions are moved in the eBooster compressor map along iso-power trajectories, see figure 6.27. On these trajectories, the compression

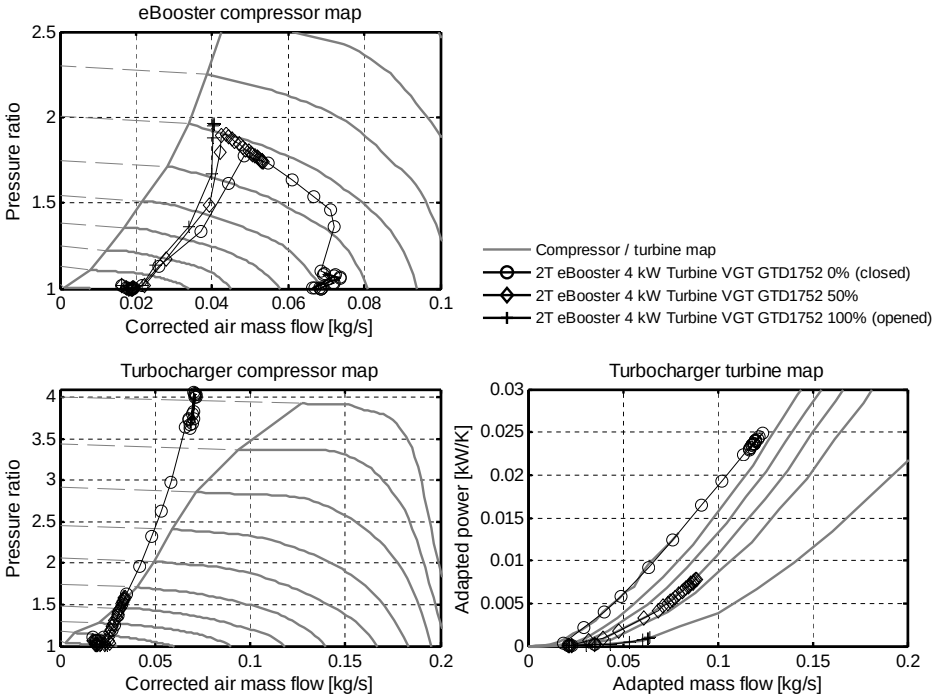

Figure 6.27: Transient operations plotted in the eBooster and turbocharger characteristics maps as a function of turbocharger boost abilities (cold transient test cycles at 1000rpm on the 2.3l engine).

ratio is reduced as the gas mass flow increases. The turbocharger has therefore to largely offset this boost decrease to elevate the intake pressure.

When 2T eBooster architecture is fitted in different engines displacement, the first part of the time response which is mainly controlled by the eBooster characteristics is not dependant of the engine swept volume, as shown in figure 6.28. Both 20 bar and 30 bar BMEP objectives can thus be reached in approximately 0.5 second on the different downsized engines if the eBooster and vehicle network are designed to the corresponding electric power levels. Otherwise, the eBooster will not produce the entire boost requirements and the time response will result slower according to the turbocharger matching and its abilities to provide the missing compression work.

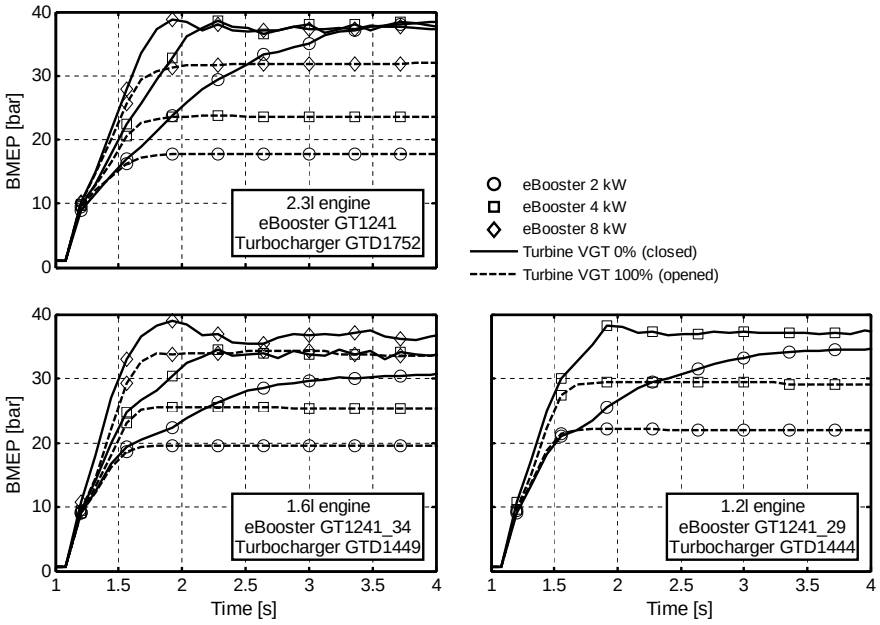

Figure 6.28: 2T eBooster architecture transient responses on different downsized-downspeeded engines as a function of turbocharger boost abilities and electric power levels (cold transient test cycles at 1000rpm).

Two-stage supercharger architecture:

In a 2T supercharger configuration, transient response depends on the transmission ratio, the clutch time delay characteristics and on the turbocharger boost abilities. Without interactions between the turbomachines in the exhaust side, the VGT is maintained in a closed position as for the 2T eBooster architecture. To analyze the main characteristics of 2T supercharger systems responses, simulations have been performed on the 2.3l engine with an Eaton R250 and a GTD1752 turbocharger. Two different transmission ratios have been selected for the calculations. The first one ($r_{gearbox} = 13$) corresponds to the transmission ratio which maximizes the compression ratio avoiding overshoots in the supercharger map (2.5 maximum compression ratio). While the second one ($r_{gearbox} = 10$) is relatively smaller to carry out a sensitivity analysis of the transmission ratio. In this second case, the supercharger runs at lower speeds with a maximum compression ratio of 2 during the transient. For supercharger engagement, a progressive activation time of 0.3 second has

been retained to reproduce the behavior of typical electromagnetic particle clutch or plate type friction clutch [146, 175]. The obtained results are shown in figures 6.29-6.30 where VGT positions have also been varied to represent different turbocharger boost abilities.

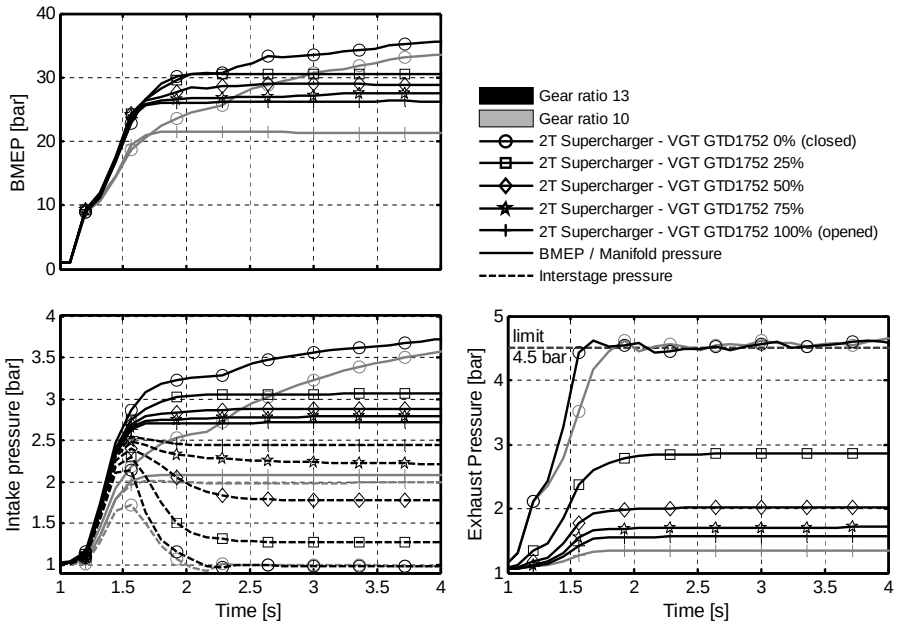

Figure 6.29: 2T supercharger architecture transient responses as a function of gear ratio and turbocharger boost abilities during cold transient test cycles at 1000rpm on the 2.3l engine.

In figure 6.29, it can be seen the supercharger provides directly at the end of its activation time the maximum boost corresponding to the transmission ratio. The first part of the transient is thus characterized by the clutch performance and the choice of the transmission ratio which is crucial to reach the low-end torque objectives. In the second part, as for the 2T eBooster configuration, the turbocharger can continue to accelerate according to its efficiencies, inertia and swallowing capacity. However, the intake pressure increase is much more limited here despite high reachable turbocharger compression ratios. In fact, the supercharger is a volumetric machine which runs during this transient test cycle at constant speed ($r_{gearbox}N_{mot}$). Being placed upstream the turbocharger, there is no significant air density variation at its inlet. The gas volumetric flows and the corresponding gas mass flows are thus relatively con-

stant. Only a slight increase can be observed in the supercharger map (figure 6.30) as the compression ratio decreases due to lower internal losses.

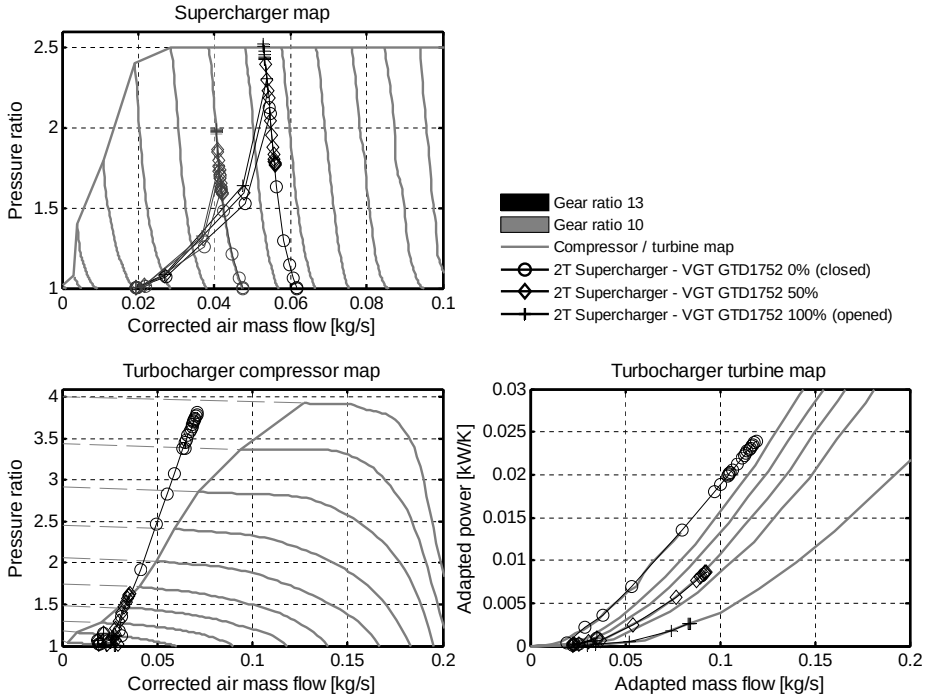

Figure 6.30: Transient operations plotted in the supercharger and turbocharger characteristics maps as a function of gear ratio and turbocharger boost abilities (cold transient test cycles at 1000rpm on the 2.3l engine).

So when the turbocharger accelerates and produces some boost, the gas mass flow is strongly restricted by the supercharger volumetric capacity and the supercharger compression ratio is reduced creating certain equilibrium between both chargers. Until completely offsetting this boost decrease to disengage the supercharger, the intake pressure can only suffer small variations and the BMEP increases noticed in figure 6.29 are the result of both slightly higher gas mass flows and lower supercharger brake power consumptions.

With the same Eaton supercharger, the time responses obtained for the other engine displacements are shown in figure 6.31. In each case, the transmission ratio has been optimized to maximize the supercharger compression ratio, while the VGT has been maintained fully open to reproduce typical matching (limited turbocharger boosting abilities at low speeds). As it can be

observed with this boosting architecture, an objective of 20 bar BMEP can be reached in approximately 0.5 second independently of the engine swept volume. Only the transmission ratio has to be reduced to adapt the supercharger speed to the low-end torque requirement. For an objective of 30 bar BMEP, as already explained, the current designs with maximum compression ratio of 2.5 do not allow this power level to be reached. But if new superchargers able to work under high compression ratios are developed, the same fast transient responses will be achieved.

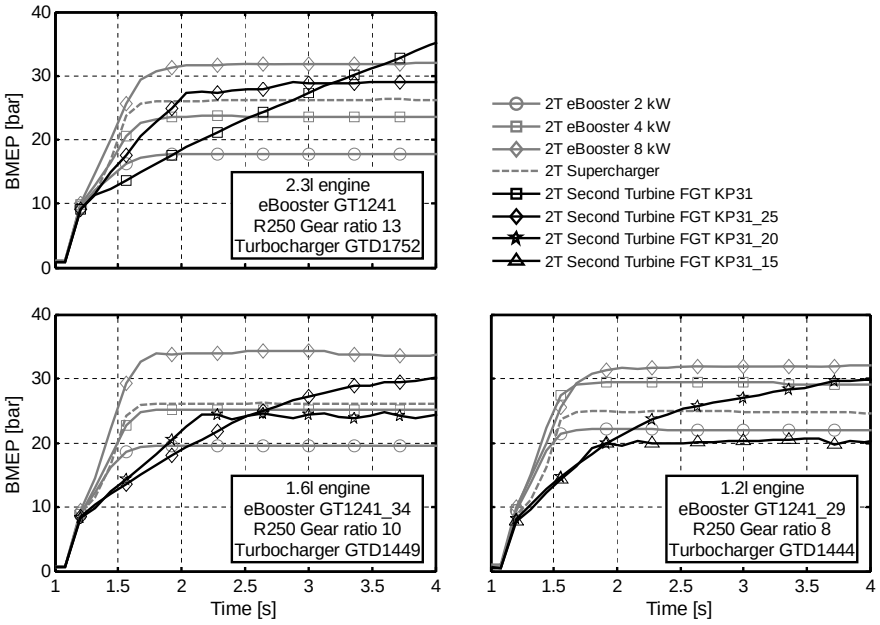

Figure 6.31: Synthesis of 2-Stage architecture transient performance on different downsized-downspeeded engines during cold transient test cycles at 1000rpm.

In figure 6.31, the results obtained with the other architectures have also been plotted to analyze the different systems. Having almost instantaneous time responses, the transient performance of 2T supercharger and 2T eBooster configurations are obviously quite similar. However the time responses of 2T turbocharging architectures are slower and turbo-lags make performance objectives of 1 second quite challenging on the smaller engine displacements. The final architecture selection will thus depend on the future development of small high efficient turbochargers and, if these turbochargers are not available, the choice between the 2T supercharger and 2T eBooster systems will depend on the evolution of vehicle architecture electrification.

6.6 Summary

A large parametric study has been carried out to characterize the limits and performance of the most promising boosting architecture on the same base engines. Simulations have been performed with the 0D engine model and a specific methodology has been defined to obtain general conclusions valid for most downsized-downspeeded engines. This methodology is based on the similarity theory to reproduce analogous behavior between the different downsized engines and, for the steady-state calculations, it is also based on an energetic approach to avoid influences of specific components designs (hypotheses on intake/exhaust line element characteristics, turbocharger maps, etc...).

With the energetic approach, several sensibilities studies have been conducted to determine the main factors that govern the architecture performance and to quantify their impacts on fuel consumption and maximum rated power. These factors regroup parameters such as turbocharger efficiencies, engine elements pressure losses characteristics, thermomechanical limitations (maximum in-cylinder pressure, exhaust manifold temperature, compressor outlet temperature, etc...), EGR rates and EGR system technology (HP and LP circuits). In two-stage operations, additional analyses have also been performed to compare the performance of the considered architectures characterizing the different systems interactions and evaluating possible inter-stage cooling benefits.

From these results, the required charger operating ranges have been confronted to state-of-art characteristic maps. Through a representative data base that allows the actual technological limits to be judged, new requirements have been defined for future turbocharger developments and new characteristic maps have been extrapolated to perform transient calculations.

In transient operations, the turbo-lag of small turbochargers has first been characterized with sensibility studies on turbine size, shaft inertia and turbocharger efficiencies. Then, the other specific factors affecting transient responses such as eBooster characteristics, supercharger transmission ratio, clutch delay time, etc... have been analyzed putting special emphasis on control strategies and main turbocharger boosting abilities at low speeds. Finally, an architecture comparison has been carried out on different downsized engines to determine the greatest transient performance that can be achieved with advanced charging systems.

In this chapter, most of the obtained conclusions play an integral part of the thesis contributions. So for the sake of brevity, only a summary of the performed analyses have been given here and all the corresponding conclusions have been directly reported in the following chapter specifically devoted to this purpose.

References

[36] R.V. Basshuysen and F. Schafer. *"Internal Combustion Engine Handbook: Basics, Components, Systems and Perspectives"*. SAE International, 2004. (Cit. on p. 239).

[37] C. Beatrice, G. Avolio, N. Del Giacomo, and C. Guido. *"Compression Ratio Influence on the Performance of an Advanced Single-Cylinder Diesel Engine Operating in Conventional and Low Temperature Combustion Mode"*. SAE Technical Paper 2008-01-1678, 2008. (Cit. on p. 228).

[46] A. Boretti and G. Cantore. *"Similarity Rules and Parametric Design of Race Engines"*. SAE Technical Paper 2000-01-0669, 2000. (Cit. on p. 228).

[61] E. Cacciatori, B. Bonnet, N.D. Vaughan, M. Burke, D. Price, and K. Wejrzanowski. *"Regenerative Braking Strategies for a Parallel Hybrid Powertrain with Torque Controlled IVT"*. SAE Technical Paper 2005-01-3826, 2005. (Cit. on p. 252).

[64] G. Cantore and E. Mattarelli. *"Similarity Rules and Parametric Design of Four Stroke Moto GP Engines"*. SAE Technical Paper 2004-01-3560, 2004. (Cit. on p. 228).

[84] G. Cipolla, A. Vassallo, A.E. Catania, E. Spessa, C. Stan, and L. Drischmann. *"Combined Application of CFD Modeling and Pressure-Based Combustion Diagnostics for the Development of a Low Compression Ratio High-Performance Diesel Engine"*. SAE Technical Paper 2007-24-0034, 2007. (Cit. on p. 228).

[97] S.L. Dixon. *"Fluid Mechanics and Thermodynamics of Turbomachinery"*. Pergamon Press Ltd, 1998. (Cit. on pp. 153, 261).

[103] B. Engels. *"Lifetime Prediction for Turbocharger Compressor Wheels - Why Use Titanium?"* Borg Warner Turbo Systems Knowledge Library, 2003. (Cit. on p. 250).

[120] J. Galindo, J.R. Serrano, C. Guardiola, and C. Cervello. *"Surge Limit Definition in a Specific Test Bench for the Characterization of Automotive Turbochargers"*. Experimental Thermal and Fluid Science, Vol. 30, pp. 449-462., 2006. (Cit. on pp. 148, 232).

[123] J. Galindo, A. Tiseira, F.J. Arnau, and R. Lang. *"On-Engine Measurement of Turbocharger Surge Limit. Experimental Techniques"*. Society for Experimental Mechanics, 2011. (Cit. on p. 232).

[146] H. Hiereth and P. Prenninger. *"Charging the Internal Combustion Engine"*. NewYork: Springer-Verlag Wien, ISBN 978-3-211-33033-3, 2003. (Cit. on pp. 20, 41, 42, 86, 87, 275).

[150] P. Hoecker, J.W. Jaisle, and S. Munz. *"The eBooster from BorgWarner Turbo Systems - The Key Component for a New Automobile Charging System"*. Borg Warner Turbo Systems Knowledge Library, 2000. (Cit. on pp. 54, 62, 63, 272).

[161] M.F. Howlett, W. Schnider, N. Ausserhofer, M. Weissbaeck, O. Soustelle, P. Ragot, P. Mallet, and J. Rozen. *"3-Cylinder Aggressive Downsized Diesel"*. Conference Internationale et Exposition Motorisation Diesel: Face au Defi de la Competitivite. Rouen, 2010. (Cit. on pp. 53, 239).

[175] R. Jorgensen and M. Sitar. *"System Performance and Control Requirements for a Sequentially Compounded Supercharged and Turbocharged Gasoline Engine"*. Eaton Corporation Publications, Engine Air Management Operations, 2004. (Cit. on pp. 45, 53, 275).

[208] R. Lang. *"Contribucion a la Mejora del Margen de Bombeo en Compressors Centrifugos de Sobrealimentacion"*. Tesis Doctoral, Universidad Politecnica de Valencia, Valencia, 2011. (Cit. on p. 232).

[247] S. Munz, M. Schier, H.P. Schmalzl, and T. Bertolini. *"eBooster - Design and Performance of an Innovative Electrically Driven Charging System"*. Borg Warner Turbo Systems Knowledge Library, 2000. (Cit. on pp. 57, 60, 61, 272).

[260] F Payri and J.M. Desantes. *"Motores de Combustion Interna Alternativos"*. Editorial Reverte, ISBN 978-84-8363-705-0, 2011. (Cit. on p. 228).

[306] V. Simon, G. Oberholz, and M. Mayer. *"Exhaust Gas Temperature 1050^{o}C - An Engineering Challenge"*. Borg Warner Turbo Systems Knowledge Library., 2000. (Cit. on p. 245).

[309] G. Sovran. *"The Impact of Regenerative Braking on the Powertrain Delivered Energy Required for Vehicle Propulsion"*. SAE Technical Paper 2011-01-0891, 2011. (Cit. on p. 252).

[345] E. Watel, A. Pagot, P. Pacaud, and J.C. Schmitt. *"Matching and Evaluating Methods for Euro 6 and Efficient Two-Stage Turbocharging Diesel Engine"*. SAE Technical Paper 2010-01-1229, 2010. (Cit. on pp. 34, 37, 39, 253).

Chapter 7

Conclusions

Contents

7.1 Introduction **282**
7.2 Boosting Technologies **282**
7.3 Modeling Tools **284**
7.4 Trends and Limits of Two-Stage Systems **287**

7.1 Introduction

In this doctoral thesis, the potential of advanced charging architectures performance has been investigated to establish the most efficient solutions for achieving the forthcoming CO_2 emissions standards with downsized - downspeeded Diesel engines.

Summarizing the results that have been presented, the main conclusions can be structured in different groups according to the various phases followed in the development of this thesis. First, the conclusions deduced from the literature review where a wide variety of systems have been described will be presented. Then in the third section, the conclusions relative to the methodology and the development of new modelling tools to perform efficient matching calculations will be reported. Finally, different analyses have been carried out to characterize the boosting architectures and to quantify the impacts of high EGR rates, thermo-mechanical limits and turbocharger sizes on their performance. The results obtained during these analyses will be presented in the fourth section.

7.2 Boosting Technologies

An exhaustive literature review has been performed to assess the current state-of-art in boosting technologies. From this study, the main conclusions are:

- The benefits obtained by each technology during their last development studies cannot be directly compared due to the large variety of engines considered in the literature. But, their potential to improve the main properties that characterize a boosting system have been analyzed and synthesized highlighting their pros and cons when compared to a conventional VGT turbocharger. All these conclusions are summarized in table 7.1 (identical to table 2.1 in section 2.8).

- Single-stage boosting technologies such as mechanical superchargers, electrically assisted turbochargers and mechanical or electrical turbocompounding systems do not present any potential to respond to the high

specific power and low-end torque demands of the downsized-downspeeded Diesel engines.

Technologies baseline : VGT turbocharger	Low end torque	Response	Max power	Range	Fuel consump-tion	Packaging	Comple-xity	EGR HP capabili-ties	Temp at catalyst entrance	Technolo-gical availabi-lity
Sequential parallel two-stage turbocharging system	++	++	0	++	-	-	--	+	0	++
Serial two-stage turbocharging system	+	+	++	+	+	--	-	++	--	++
Sequential serial two-stage turbocharging system	++	++	+	++	+	--	-	+	-	++
Single stage mechanical supercharger	++	++	0	0	--	-	0	--	++	++
Mechanical auxiliary supercharging	++	++	+	++	-	--	-	0	0	++
Electrically assisted turbocharger	0	+	0	0	0	0	--	+	0	--
Electric booster + turbocharger	++	++	+	++	+	-	-	0	0	-
Centrifugal compressor enhancement devices	+	+	0	+	0	0	-	0	0	-
Mechanical turbocompounding	0	-	+	0	++	--	-	+	-	++
Electric turbocompounding	0	-	+	0	++	--	--	+	-	--

Table 7.1: Left: Potential for improvements of the main boosting architectures.

- Centrifugal compressor enhancement devices present interesting potential to increase the low end torque maintaining typical rated power levels. They could therefore respond to light degrees of downsizing avoiding the complexity of multi-stage systems. But, as nowadays the current VGT cannot correctly drive the compressor in its entire extended operating range, their implication in advanced boosting architecture is extremely limited.

- Sequential parallel two-stage turbocharging systems allow to increase the low-end torque and present several advantages in terms of packaging and heat losses. However the small two turbochargers have lower global efficiency than a larger LP turbocharger and induce the need for complex transition management. In addition, the architecture evolution to very small displacement engines and higher boosting pressure is limited. That is why serial two-stage configurations are generally preferred when compared to parallel systems.

- Serial two-stage turbocharging systems provide high pressure ratios to increase both low-end torque and rated power. But, as both stages are

continuously working together, their operating ranges are relatively restricted. This technology which presents important performance potential for heavy-duty applications cannot thereby be applied to passenger cars Diesel engines, unless future engines are extremely downspeeded.

- Finally the most promising boosting systems to increase the performance of passenger cars downsized-downspeeded Diesel engines are the sequential serial two-stage turbocharging, mechanical auxiliary supercharging and electric booster. These architectures combine the advantages of a relatively large turbocharger to efficiently boost the engine in most operating conditions with the benefits of a small second charger to achieve high low-end torque and fast transient responses.

7.3 Modeling Tools

After evidencing the most promising charging architectures, different modeling tools have been developed as part of the methodology to reach the objectives of this thesis. First an analytical pre-design model has been developed to study the main parameters that govern the architecture behavior. Equations giving the relationship between total compression ratio and total expansion ratio as a function of basic engine parameters have been extended to two-stage systems. With this model, the main conclusions that have been remarked are:

- Influence of the LP and HP expansion ratios on the PMEP, total compression ratio and brake thermal efficiency were characterized for given operating conditions underlining the linear relations that exist between optimized turbochargers work distribution and total compression ratio.

- Best architecture performance is achieved with the highest intercooler cooling capacity but cooling fluid temperature has a stronger impact than intercooler efficiency.

- The highest exhaust temperature and the highest turbocharger efficiencies allow also to reach the best performance, but the architecture behavior is very sensitive to these parameters and overall system efficiency can significantly drop decreasing their values.

- Very fast simulations can be performed with this model to check the influences of different variables independently. So for a given application and given operating conditions, more conclusions could be easily obtained to pre-establish specific boosting components requirements.

Being mainly conceptual, this model cannot be employed for matching calculations where relevant parameters like volumetric efficiency, IMEP, exhaust temperature and heat transfers need to be predicted as a function of running conditions. In addition, transient aspects are also fundamental for the final turbocharger size selection. That is why more sophisticated models have been then developed with special emphasis on the matching issue. These models developments are firstly based on the definition of a new representation of turbine characteristics maps combined with a new matching procedure. The conclusions relative to the new turbine representation are:

- An alternative set of homogeneous parameters based on natural factors such as turbocharger power and turbine gas mass flow has been defined for characterizing the turbine behavior.
- These parameters are independent of the inlet turbine pressure and allow to perform direct matching calculations from boost pressure objectives without any iteration.
- Using conservative parameters which are mass and energy, the new turbine characteristics are particularly robust to speed variations and show lower sensitiveness to pulsating flow conditions and heat transfer phenomena.
- The characteristics are more compact and allow all the turbine performance data to be plotted in a single graph as a compressor map for easier interpretation.
- These curves are accurately fitted with quadratic polynomial functions which have the particularity to be continuously differentiable and without discontinuities.
- Interpolation methods applied to this representation are more compact to implement in a turbocharger submodel and more reliable in most operating conditions. The accuracy of the whole engine simulation is thus improved.

- Avoiding iterations and employing standard linear interpolation routines, computational times are significantly reduced.

With this new turbine representation, a straightforward matching procedure has been defined determining first the compressor requirements from boost pressure objectives and then, setting the turbine needs from the corresponding turbocharger powers. This matching procedure requires important input data and presents many variations depending on the considered boosting architecture. For that reason, both representation and procedure have been finally integrated in a whole engine model able to reproduce and match any boosting configuration. The main conclusions that have been obtained during the engine model development are:

- Nowadays, the best trade-off between maximum physical description and minimum computational cost to perform efficient matching calculations is a combination of 0D phenomenological combustion model, with a 0D filling & emptying model for the multi-cylinders and manifolds, and a MVEM for the other air path elements. Advantages of reasonable computational cost from the 0D and MVEM approaches are thus combined with the physical depth of detailed cycle resolved cylinder models.
- To reduce computational expenses, a new boost pressure oriented resolution algorithm has been defined to directly run the steady-state matching simulations in a natural sense from engine performance objectives to charging system configuration. The developed engine model integrates thereby two resolution approaches: a boost pressure oriented model for steady state conditions and a conventional actuators oriented model for transient operations.
- Compared to 1D approach, a 0D engine model allows to significantly reduce the number of specified parameters to keep a good control on the assumptions realized when model calibrations must be extrapolated to new base engines. With few tuned parameters, sensitivity studies are straightforward to estimate the impact of the calibration process on architecture matching.
- The predictive capabilities of the engine model have been demonstrated on three different base engines in both steady and transient conditions. With combustion model uncertainties lower than 2% and engine model

uncertainties not exceeding 2% in the intake path, 5% in the exhaust line, 5% for the BMEP and 15 mbar for the PMEP, the overall accuracy of 0D engine models has been judged more than sufficient to carry out matching calculations.

- 0D approach presents important limitations to reproduce gas dynamics phenomena in the manifolds. But it has been justified the corresponding uncertainties are generally acceptable in the low to middle engine speed range (up to 3500 - 4000 rpm), and some basic empirical correlations are sufficient to correct air mass flow estimations in the case of engines equipped with tuned intake line. Considering downspeeded engines, 0D models are thus valid to perform matching calculations in the whole engine operating range.

7.4 Trends and Limits of Two-Stage Systems

Following the development and validation of all modeling tools, a comprehensive study has been carried out with the 0D engine model to synthesize the performance and components requirements of the most promising boosting architectures. The conclusions obtained during this study have been regrouped in four categories according to their relation with the thermomechanical limitations, the engine components characteristics, the charger maps requirements and the architecture performance. Regarding the thermomechanical limitations, the main conclusions that have been drawn are:

- Considering typical compression ratio used in modern engine developments, there are no benefits to increase the current state-of-art in-cylinder pressure limits for moderate BMEP objectives (around 20 bar). For strong BMEP objectives (around 30 bar), significant fuel savings can be obtained at low speeds but the differences in BSFC observed at high speeds are too small to justify an increase of the current limits.
- The maximum allowable compressor outlet temperature always restricts cylinder charge densities before exceeding the maximum in-cylinder pressure at the end of the compression stroke. So, the in-cylinder pressure limits do not restrain the maximum engine performance. However at low speeds, as they forced to retard the injection timings, maximum reachable BMEP are reduced due to lower combustion efficiencies. Maximum

in-cylinder pressures can therefore be considered as indirect limiting factors.

- Without EGR requirements at full load, the maximum allowable exhaust temperature is the limiting factor to increase the engine performance. Exhaust temperature limitations have to be higher than 850°C at low speeds and higher than 950°C at rated speeds so that the maximum outlet compressor temperature becomes more restrictive. Materials and turbocharger technologies used on gasoline engines are thus necessary to develop highly-rated Diesel downsized-downspeeded engines.

- With EGR requirements at full load (imposed by the new emissions test cycles), the limiting factor is the maximum allowable compressor outlet temperature which restricts the engine performance before the exhaust constraints exceed 800°C. Titanium compressor wheel as advanced plastic materials in the intake piping are thus required in that case for the further development of highly-rated downsized-downspeeded engines.

- Extending the compressor outlet temperature limitations from 190°C to 210°C allows to increase the maximum BMEP of around 3 bar at rated speeds and between 1 bar and 3 bar at low speeds.

- In a sequential serial two-stage boosting configuration, an intermediate intercooler presents little potential to reduce the compressor thermal constraints due to the architecture matching and the type of operating modes.

- In a 2T eBooster configuration, the maximum electric power level defined by the eBooster motor or by the electric vehicle network is generally the limiting factor to reach high low-end torques. These power levels have to approximately exceed 10 kW, 8 kW and 6 kW on 2.3l, 1.6l and 1.2l engines respectively so that the maximum compressor outlet temperature becomes more restrictive.

Concerning the engine components characteristics, the main conclusions that have been highlighted are:

- Even though the main turbocharger has the ability to produce boost at low speeds, the maximum fuel savings that can be obtained with an

intermediate intercooler are too small to justify the cost and packaging constraints that involve its implementation.

- The minimization of the elements pressure drops is fundamental to improve in the medium to high speed range the fuel consumption of downsized-downspeeded engines. Optimizing the elements pressure losses characteristics (for example reducing by two the aftertreatment pressure drops) can bring the same BSFC benefits as increasing by 10 points the turbocharger efficiencies.

- Improving the turbocharger efficiencies increases the maximum BMEP in the whole engine speed range mainly due to lower compressor outlet temperature and achieves significant BSFC reductions at rated speeds. With efficiencies variations of 10 points, 3-4 bar higher BMEP has been obtained with fuel savings of around 5 g/kWh and 10 g/kWh at 3000 rpm and 3500 rpm respectively.

- Turbocharger efficiencies enhancements present also important potential to enhance transient performance. For example, increasing by 10 points the turbocharger efficiencies allows a reduction by 50% in the time responses.

- For the supercharger, an efficiency variation of 10 points does not reduce in a significant way the required mechanical power. So, supercharger design optimization does not show important potential to diminish fuel penalties generated by mechanical chargers.

- As the second turbocharger is relatively small, the use of advanced material to reduce its inertia has limited consequences on transient responses. Here benefits of only 0.2-0.3 second have been obtained with 25% inertia reduction.

- Decreasing the turbine effective section improves the turbo-lag but, for a given engine displacement, fastest transient responses are achieved when the benefits of smaller swallowing capacity start to be offset by higher engine backpressures. From this point, reducing even more the turbine section leads rapidly to chocked conditions restricting the maximum reachable BMEP without enhancing time responses.

With regard to the charger maps requirements, the main conclusions that have been mentioned are:

- In a two-stage architecture developed for highly-rated Diesel downsized-downspeeded engines, the compressors and turbines currently available in the automotive market have appropriate operating ranges to respond to the main turbocharger requirements. With a lot of design possibilities, there is therefore important flexibility to optimize for a particular application the main turbocharger matching according to the power level, rated speed, fuel consumption, EGR abilities, etc...

- For the second charger, 1.6l engine displacements are close to the current technological limits to achieve high low-end boost pressures with state-of-art automotive centrifugal compressors. The development of smaller compressor designs is therefore necessary for further engine downsizing such as 1.2l engines. These conclusions are also valid for eBoosters which employ centrifugal compressors.

- Volumetric superchargers can work under lower gas mass flow than current centrifugal compressors but their efficiencies are quite poor under these conditions. The development of smaller superchargers is thus necessary for efficient engine downsizing with 2T supercharger configuration.

- Current superchargers provide maximum compression ratio of about 2.5. If low-end torque objectives are higher than approximately 25 bar BMEP, new supercharger designs able to work under high compression ratio are required.

- The development of small efficient turbines is critical to fulfill the performance requirements of future downsized-downspeeded engines.

- For moderate BMEP objectives, the smallest FGT currently available can fulfill the performance requirements on a 2.3l engine. However the development of 20% and 30% smaller FGT are required to reach similar performance on a 1.6l and 1.2l engine respectively. For strong BMEP objectives, efficiencies improvements are also essential to avoid choked conditions induced by small swallowing capacities. FGT slightly smaller and significantly more efficient than those expressed for the 20 bar BMEP objective are thus necessary to achieve the desired performance.

- Considering VGT turbines in the HP stage, for moderate BMEP objectives, a VGT presents few interests on the 2.3l engine. However on the other engine displacements, the bigger wheel diameters involved can

justify its use to reduce the efforts in small turbine designs development (the VGT wheel diameter is about 5mm bigger than a FGT at iso-performance). For strong BMEP objectives, transient performances are enhanced with VGT and efficiencies improvements are less critical than with FGT. The use of VGT can thus reduce development efforts not only in small effective sections but also in highly efficient designs.

Finally with regard to the architecture performance, the main conclusions that have been made are:

- Under two-stage operations, the 2T turbocharger architecture is much more efficient than the 2T supercharger configuration (fuel benefits of around 15 g/kWh at 20 bar BMEP and 35 g/kWh at 35 bar BMEP), but less efficient than the 2T eBooster architecture when electric power is provided by an external source (fuel penalties or around 5 g/kWh).
- In terms of maximum performance, the 2T eBooster architecture allows to reach 1-2 bar higher maximum BMEP than the 2T turbocharger configuration due to free exhaust gas mass flows. Whereas, the 2T supercharger architecture reaches 2-5 bar lower maximum BMEP due to brake power consumption.
- Considering LP EGR, increasing by 15% the LP EGR rates generates in single-stage operations fuel consumption penalties from 5 g/kWh to 10 g/kWh and reduces the maximum reachable BMEP by 5-7 bar due to the maximum compressor outlet temperature. In two-stage operations, the LP EGR consequences are similar with the 2T turbocharger configuration while they are much more important with the 2T supercharger system because of higher brake power demands. With the 2T eBooster architecture, these influences are quite limited as the electric power is supplied externally.
- Considering HP EGR, the performance at low speeds are relatively close to those of the LP EGR circuit. In the medium to high speed range, if identical turbocharger efficiencies and pressure losses are assumed (engine elements matched for each EGR system), similar fuel consumptions are obtained between both circuits but, if the same engine components are employed (lower pressure drops in the gas path with HP EGR), important fuel savings are achieved with the HP EGR system. The gas

path pressure drops are therefore the most influential factors when both circuits are compared and the elements pressure losses characteristics are critical for the LP EGR system.

- For the architecture control in transient, the main VGT of a 2T turbocharger configuration has to be maintained in an open position to optimize the time responses, while in 2T supercharger and eBooster architectures, the main VGT must be kept closed to maximize the boost abilities of the main turbocharger.
- With 2T supercharger and 2T eBooster configurations, transient responses of any highly-rated Diesel downsized-downspeeded engine are very fast (about 0.5 second during cold transient test cycles at 1000 rpm). The power level reached at the end of the transient depends on the electric power for the eBooster and on the transmission ratio for the supercharger. With the 2T turbocharger architecture, the transient responses are slower and, even defining new small efficient turbine requirements, performance objective of 1 second during cold transient test cycles are quite challenging for the smaller engine displacements.

In light of these results, a wide overview of the main trends and limits in advanced boosting architecture for future passenger cars downsized-downspeeded Diesel engines has been given with this research work. In the end, several architectures present the desired potentials to enhance the engine performance. The final definition of the charging systems will thus depend not only on the specific objectives of each application but also on the future development of components such as titanium compressor wheels, small turbines, small superchargers, vehicle electric networks, etc...

Bibliography

[1] *" Council Directive 91/441/EEC of 26 June 1991 on the Approximation of the Laws of the Member States Relating to Measures to Be Taken Against Air Pollution by Emissions from Motor Vehicles"*. Official Journal of the European Union, 30/08/1991, pp. 1-106, 1991. (Cit. on p. 3).

[2] *" Council Directive 98/69/EEC of 13 October 1998 on the Approximation of the Laws of the Member States Relating to Measures to be Taken Against Air Pollution by Emissions from Motor Vehicles"*. Official Journal of the European Union, 28/12/1998, pp. 1-65, 1998. (Cit. on p. 3).

[3] *" Emission Standards for Model Year 2007 and Later Heavy-duty Highway Engines"*. US. Environmental Protection Agency (EPA), http://www.epa.gov, 2001. (Cit. on p. 125).

[4] *" JANAF Thermodynamical Tables"*. DOW Chemical Company, 1962, Addendum, 1966. (Cit. on p. 176).

[5] *" Regulation 443/2009 of the European Parliament and of the Council of 23 April 2009 Setting Emission Performance Standards for New Passenger Cars as Part of the Community's Integrated Approach to Reduce CO2 Emissions from Light-Duty Vehicles"*. Official Journal of the European Union, 05/06/2009, pp. L140/1-15, 2009. (Cit. on p. 5).

[6] *" Regulation 715/2007 of the European Parliament and of the Council of 20 June 2007 on Type Approval of Motor Vehicles with Respect to Emissions from Light Passenger and Commercial Vehicles (Euro 5 and Euro 6) and on Access to Vehicle Repair and Maintenance Information"*. Official Journal of the European Union, 29/06/2007, pp. L171/1-16, 2007. (Cit. on p. 3).

[7] *" Supercharger Testing Standard SAE J1723"*. Society of Automotive Technology, issued 1995, 1995. (Cit. on p. 148).

[8] *" Turbocharger Gas Stand Test Code SAE J1826"*. Society of Automotive Technology, issued 1989, reaffirmed 1995, 1995. (Cit. on p. 148).

[9] *" Turbocharging Efficiencies - Definition and Guidelines for Measurement and Calculations"*. CIMAC Working Group, The International Council on Combustion Engines, No. 27, 2007. (Cit. on p. 148).

[10] A.N. Abdel Hamid. *"A New Technique for Stabilizing the Flow and Improving the Performance of Vaneless Radial Diffusers"*. ASME Journal of Turbomachinery, Vol.109, No. 1, pp.36-40, 1987. (Cit. on p. 78).

[11] A.N. Abdel Hamid. *"Control of Self-Excited Flow Oscillations in Vaneless Diffuser of Centrifugal Compression Systems"*. ASME paper 82-GT-188, 1982. (Cit. on p. 78).

[12] A.N. Abdel Hamid. *"Effects of Vaneless Diffuser Geometry on Flow Stability in Centrifugal Compression Systems"*. ASME paper 81-GT-10, 1981. (Cit. on p. 78).

[13] T.G. Adams. *"Comparison of a Turbocharger to Supercharger on a Spark Ignited Engine"*. SAE Technical Paper 841285, 1984. (Cit. on p. 44).

[14] A. Albrecht, O. Grondin, F. Le Berr, and G. Le Soliec. *"Towards a Stronger Simulation Support for Engine Control Design: a Methodological Point of View"*. Oil & Gas Science and Technology, Revue IFP, Vol. 62, No. 4, pp. 437-456, 2007. (Cit. on p. 170).

[15] K. Aleklett, M. Hook, K. Jakobsson, M. Lardelli, S. Snowden, and B. Soderbergh. *"The Peak of the Oil Age - Analyzing the World Oil Production Reference Scenario in World Energy Outlook 2008"*. Energy Policy, Vol.38, Issue 3, pp. 1398-1414, 2010. (Cit. on p. 3).

[16] M. Algrain. *"Controlling an Electric Turbo Compound System for Exhaust Gas Energy Recovery in a Diesel Engine"*. IEEE International Conference on Electro Information Technology, Lincoln, 2005. (Cit. on pp. 58, 89).

[17] M. Algrain and U. Hopmann. *"Diesel Engine Waste Heat Recovery Utilizing Electric Turbocompound Technology"*. Diesel Engine Emissions Reduction Conference, Newport, 2003. (Cit. on pp. 58, 89).

[18] W.J.D. Annand. *"Heat Transfer in the Cylinders of Reciprocating Internal Combustion Engines"*. Proceedings of the Institution of Mechanical Engineers, Vol. 177, pp. 973-990, 1963. (Cit. on p. 191).

[19] R.F. Ansdale. *"A Reconnaissance of Supercharging Technology 1902-1980"*. SAE Technical Paper 810003, 1981. (Cit. on p. 40).

[20] C. Arcoumanis and M.S. Baniasad. *"Analysis of Consecutive Fuel Injection Rate Signal Obtained by the Zeus and Bosch Methods"*. SAE Technical Paper 930921, 1993. (Cit. on p. 145).

[21] C. Arcoumanis and M. Gavaises. *"Linking Nozzle Flow with Spray Characteritics in a Diesel Fuel Injection System"*. Atomization and Sprays, Vol. 8, pp. 307-347, 1998. (Cit. on p. 145).

[22] O. Armas. *"Diagnostico Experimental del Proceso de Combustion en Motores Diesel de Inyeccion Directa"*. Tesis Doctoral, Universidad Politecnica de Valencia, Valencia, 1999. (Cit. on pp. 150, 192, 193, 205).

[23] S. Arnold. *"Single Sequential Turbocharger: a New Boosting Concept for Ultra-Low Emission Diesel Engines"*. SAE Technical Paper 2008-01-0298, 2008. (Cit. on p. 92).

[24] S. Arnold. *"Turbocharging Technologies to Meet Critical Performance Demands of Ultra-Low Emissions Diesel Engines"*. SAE Technical Paper 2004-01-1359, 2004. (Cit. on pp. 59, 79, 81, 91).

[25] S. Arnold, D. Calta, K. Dullack, C. Judd, and G. Thompson. *"Development of an Ultra-High Pressure Ratio Turbocharger"*. SAE Technical Paper 2005-01-1546, 2005. (Cit. on pp. 91, 92).

[26] S. Arnold, M. Groskreutz, S. Shahed, and K. Slupski. *"Advanced Variable Geometry Turbocharger for Diesel Engine Applications"*. SAE Technical Paper 2002-01-0161, 2002. (Cit. on p. 18).

[27] S. Arnold, K. Slupski, M. Groskreutz, G. Vrbas, R. Cadle, and S.M. Shahed. *"Advanced Turbocharging Technologies for Heavy-Duty Diesel Engines"*. SAE Technical Paper 2001-01-3260, 2001. (Cit. on p. 91).

[28] J. Arregle, J.J. Lopez, J.M. Garcia, and C. Fenollosa. *"Development of a Zero-Dimensional Diesel Combustion Model - Part 1 Analysis of the Quasi-Steady Diffusion Combustion Phase"*. Applied Thermal Engineering, Vol. 23, pp. 1301-1317, 2003. (Cit. on pp. 194, 195).

[29] J. Arregle, J.J. Lopez, J.M. Garcia, and C. Fenollosa. *"Development of a Zero-Dimensional Diesel Combustion Model - Part 2 Analysis of the Transient Initial and Final Diffusion Combustion Phases"*. Applied Thermal Engineering, Vol. 23, pp. 1319-1331, 2003. (Cit. on p. 194).

[30] J. Arregle, J.J. Lopez, J. Martin, and E. Mocholi. *"Development of a Mixing and Combustion Zero-Dimensional Model for Diesel Engines"*. SAE Technical Paper 2006-01-1382, 2006. (Cit. on pp. 173, 194).

[31] W. Attard, H.C. Watson, S. Konidaris, and M.A. Khan. *"Comparing the Performance and Limitations of a Downsized Formula SAE Engine in Normally Aspirated, Supercharged and Turbocharged Modes"*. SAE Technical Paper 2006-32-0072, 2006. (Cit. on p. 44).

[32] B.H. Bae, S.K. Sul, J.H. Kwon, and J.S. Byeon. *"Implementation of Sensorless Vector Control for Super-High-Speed PMSM of Turbo-Compressor"*. IEEE Transactions on Industry Applications, Vol. 39, pp. 811-818, 2003. (Cit. on p. 58).

[33] N. Baines. *"Fundamentals of Turbocharging"*. Concepts NREC. ISBN 0-933283-14-8, 2005. (Cit. on pp. 18, 26).

[34] C. Barba, C. Burkhardt, K. Boulouchos, and M.A. Bargende. *"A Phenomenological Combustion Model for Heat Release Rate Prediction in High-Speed Di Diesel Engines with Common Rail Injection"*. SAE Technical Paper 2001-01-2933, 2001. (Cit. on p. 194).

[35] J.C. Bass, A.S. Kushch, and N.B. Elsner. *"Thermoelectric Generator (TEG) on Heavy Diesel Trucks"*. 10^{th} International Conference on Thermoelectrics, Beijing, 2001. (Cit. on p. 81).

[36] R.V. Basshuysen and F. Schafer. *"Internal Combustion Engine Handbook: Basics, Components, Systems and Perspectives"*. SAE International, 2004. (Cit. on p. 239).

[37] C. Beatrice, G. Avolio, N. Del Giacomo, and C. Guido. *"Compression Ratio Influence on the Performance of an Advanced Single-Cylinder Diesel Engine Operating in Conventional and Low Temperature Combustion Mode"*. SAE Technical Paper 2008-01-1678, 2008. (Cit. on p. 228).

[38] J. Benajes, E. Reyes, and J.M. Lujan. *"Modelling Study of the Scavenging Process in a Turbocharged Diesel Engine with Modified Valve Operation"*. Proceedings of the Institution of Mechanical Engineers Part C: Journal of Mechanical Engineering Science, Vol. 210, pp. 383-393, 1996. (Cit. on p. 192).

[39] R.S. Benson. *"The Thermodynamics and Gas Dynamics of Internal Combustion Engines"*. Oxford University Press, Vol. 1, 1982. (Cit. on p. 152).

[40] R.W. Bentley. *"Global Oil and Gas Depletion: An Overview"*. Energy Policy, Vol. 30, pp. 189-205, 2002. (Cit. on p. 3).

[41] G. Benvenuto and U. Campora. *"Dynamic Simulation of a High-Performance Sequentially Turbocharged Marine Diesel Engine"*. International Journal of Engine Research, Vol. 3, No. 3, pp. 115-125, 2001. (Cit. on pp. 23, 26).

[42] P.N. Blumberg, Lavoie G.A., and R.J. Tabaczynski. *"Phenomenological Models for Reciprocating Internal Combustion Engines"*. Progress in Energy and Combustion Science, Vol. 5, pp. 123-167, 1979. (Cit. on p. 192).

[43] T. Boger and A.K. Heibel. *"Heat Transfer in Conductive Monolith Structures"*. Chemical Engineering Science, Vol. 60, pp. 1823-1835, 2005. (Cit. on p. 180).

[44] J. Bohbot, A. Lafossas, A. Albrecht, M. Miche, M. Chraibi, and A. Menegazzi. *"A New Coupling Approach Using a 1D System Simulation Software and a 3D Combustion Code Applied to Transient Engine Operation"*. SAE Technical Paper 2004-01-3002, 2004. (Cit. on p. 170).

[45] M. Bonello, D.M. Caldwell, J.A. Pigott, G.P. Prior, and T.M. Schag. *"The Supercharged Northstar DOHC 4.4L V8 Engine for Cadillac"*. SAE Technical Paper 2005-01-1854, 2005. (Cit. on p. 44).

[46] A. Boretti and G. Cantore. *"Similarity Rules and Parametric Design of Race Engines"*. SAE Technical Paper 2000-01-0669, 2000. (Cit. on p. 228).

[47] Y. Borila. *"A Sequential Turbocharging Method for Highly Rated Truck Diesel Engines"*. SAE Technical Paper 860074, 1986. (Cit. on p. 23).

[48] W. Bosch. *"The Fuel Rate Indicator: A New Measuring Instrument for Display of the Characteristics of Individual Injection"*. SAE Technical Paper 660749, 1966. (Cit. on p. 144).

[49] M.C. Brands, J.R. Werner, J.L. Hoehne, and S. Kramer. *"Vehicle Testing of Cummins Turbocompound Diesel Engine"*. SAE Technical Paper 810073, 1981. (Cit. on p. 87).

[50] A.R. Brandt. *"Testing Hubbert"*. Energy Policy, Vol. 35, Issue 5, pp. 3074-3088, 2007. (Cit. on p. 3).

[51] S. Bremm, M. Pfeifer, J. Leyrer, W. Mueller, S. Kurze, M. Paule, B. Keppeler, and G. Vent. *"Bluetec Emissions Control System for the US Tier 2 Bin 5 Legislation"*. SAE Technical Paper 2008-01-1184, 2008. (Cit. on p. 7).

[52] C. Brockbank. *"Application of a Variable Drive to Supercharger & Turbo Compounder Applications"*. SAE Technical Paper 2009-01-1465, 2009. (Cit. on pp. 47, 48, 83).

[53] P. Brynych, J. Macek, L. Pohorelsky, P.Y. Vallaude, J.C. Ricaud, and P. Obernesser. *"Optimization of a Two-Stroke Diesel Engine Air System"*. XLII International Scientific Conference of Czech, Slovak University Departments, and Institutions Dealing with the Research of Combustion Engines, Zilina, 2011. (Cit. on p. 41).

[54] R. Buchwald, G. Lautrich, O. Maiwald, and A. Sommer. *"Boost and EGR System for the Highly Premixed Diesel Combustion"*. SAE Technical Paper 2006-01-0204, 2006. (Cit. on pp. 31, 37–39).

[55] J. Bumby, S. Crossland, and J. Carter. *"Electrically Assisted Turbochargers: their Potential for Energy Recovery"*. Hybrid Vehicle Conference, Institution of Engineering and Technology, Coventry, 2006. (Cit. on p. 90).

[56] J.R. Bumby, S. Crossland, E. Spooner, and J. Carter. *"The Development of Turbocharger Accelerator Motors and Drives and their Integration into Vehicle Electrical Systems"*. International Conference on Automotive Electronics, London, 2005. (Cit. on p. 59).

[57] J.R. Bumby, E. Spooner, and M. Jagelia. *"A Solid Rotor Induction Machine for Turbo-Assist Operations"*. International Conference on Electrical Machines, Crete, 2006. (Cit. on p. 58).

[58] J.R. Bumby, E. Spooner, and M. Jagelia. *"High Speed Solid Rotor Induction Motors"*. IEEE International Conference on Electrical Power Applications, Vol. 153, pp. 31-39, 2006. (Cit. on pp. 58, 59).

[59] J.R. Bumby, E.S. Spooner, J. Carter, H. Tennant, G. Ganio Mego, G. Dellora, H. Gstrein W.and Sutter, and J. Wagner. *"Electrical Machines for Use in Electrically Assisted Turbochargers"*. International Conference on Power Electronics, Machines and Drives, Vol. 1, pp. 344-349, 2004. (Cit. on p. 58).

[60] D.J. Burtt and A.P. Kolstrup. *"Introducing the Rotrak Variable Speed Traction Drive Centrifugal Supercharger to Fully Exploit Engine Downsizing"*. 15^{th} Supercharging conference, Dresden, 2010. (Cit. on p. 47).

[61] E. Cacciatori, B. Bonnet, N.D. Vaughan, M. Burke, D. Price, and K. Wejrzanowski. *"Regenerative Braking Strategies for a Parallel Hybrid Powertrain with Torque Controlled IVT"*. SAE Technical Paper 2005-01-3826, 2005. (Cit. on p. 252).

[62] M. Canova, F. Chiara, G. Rizzoni, and Y.Y. Wang. *"Model-Based Characterization and Analysis of Diesel Engines with Two-Stage Turbochargers"*. SAE Technical Paper 2010-01-1220, 2010. (Cit. on pp. 29, 33, 35).

[63] C. Cantemir. *"Twin Turbo Strategy Operation"*. SAE Technical Paper 2001-01-0666, 2001. (Cit. on pp. 21, 22, 25).

[64] G. Cantore and E. Mattarelli. *"Similarity Rules and Parametric Design of Four Stroke Moto GP Engines"*. SAE Technical Paper 2004-01-3560, 2004. (Cit. on p. 228).

[65] G. Cantore, E. Mattarelli, and S. Fontanesi. *"A New Concept of Supercharging Applied to High Speed DI Diesel Engines"*. SAE Technical Paper 2001-01-2485, 2001. (Cit. on pp. 51, 52).

[66] M. Capobianco, A. Gambarotta, and G. Cipolla. *"Influence of the Pulsating Flow Operation on the Turbine Characteristics of a Small Internal Combustion Engine Turbocharger"*. IMechE 4^{th} International Conference on Turbochargers and Turbocharging, pp. 63-69, 1989. (Cit. on p. 160).

[67] G. Capon and T. Morris. *"The Effect of Air Inlet System Features on Automotive Turbocharger Compressor Performance"*. Ford Motor Company Publications 2010, pp. 93-110, 2010. (Cit. on p. 67).

[68] J.A. Caton and J.B. Heywood. *"An Experimental and Analytical Study of Heat Transfer in an Engine Exhaust Port"*. International Journal of Heat and Mass Transfer, Vol. 24, pp. 581-895, 1981. (Cit. on p. 188).

[69] C.J Chadwell and M. Walls. *"Analysis of a Superturbocharged Downsized Engine Using 1-D CFD Simulation"*. SAE Technical Paper 2010-01-1231, 2010. (Cit. on pp. 47, 48, 82).

[70] B. Challen and R. Baranescu. *"Diesel Engine Reference Book"*. London: Butterworth Heinemann Ltd, Second edition, ISBN 978-0750621762, 1999. (Cit. on p. 7).

[71] C.C. Chan. *"The State of the Art of Electric and Hybrid Vehicles"*. Proceedings of the IEEE Transactions on Vehicular Technology, Vol. 90, pp. 247-275, 2002. (Cit. on p. 2).

[72] A.J. Chapman. *"Heat Transfer"*. Macmillan Publishing Company, New York, 1960. (Cit. on p. 182).

[73] D.C. Chapman. *"Model 250-C30/C288 Compressor Development"*. AGARD Conference on Centrifugal Compressors, Flow Phenomenon and Performance, Vol. 282, No. 20, 1982. (Cit. on p. 75).

[74] A. Chasse, A. Albrecht, P. Moulin, A. Gautier P., L. Fontvieille, A. Guinois, and L. Doléac. *"A New Simulation Step Towards Virtual Bench Through the Challenging Case of Two-Stage Turbocharger Diesel Engine Control Design"*. SAE Technical Paper 2008-01-0355, 2008. (Cit. on pp. 32, 116).

[75] A. Chasse, P. Moulin, P. Gautier, A. Albrecht, L. Fontvieille, A. Guinois, and L. Doléac. *"Double Stage Turbocharger Control Strategies Development"*. SAE Technical Paper 2008-01-0988, 2008. (Cit. on pp. 32, 33, 127).

[76] H. Chen, I. Hakeem, and R. Martinez-Botas. *"Modelling of a Turbocharger Turbine Under Pulsating Inlet Conditions"*. Proceedings of the Institution of Mechanichal Engineers, Part A: Journal of Power and Energy, Vol. 210, No. 5, pp. 397-408, 1996. (Cit. on p. 158).

[77] S.K. Chen and P. Flynn. *"Development of a Compression Ignition Research Engine"*. SAE Technical Paper 650733, 1965. (Cit. on p. 207).

[78] P. Chesse, J. Hetet, X. Tauzia, and J. Frayet. *"Influence des Circuits de Liaison Moteur/Compresseur sur le Fonctionnement des Moteurs Diesel à Suralimentation Bi-Etagée"*. Revue Generale de Thermique, No. 37, pp. 801-812, 1998. (Cit. on p. 23).

[79] P. Chesse, X. Tauzia, J. Hetet, and G. Grosshans. *"Simulation des Phases de Fonctionnement Transitoires d'un Moteur Diesel Semi-Rapide à Suralimentation Séquentielle"*. Comptes Rendus de l'Académie des Sciences - Mechanics-Physics-Astronomy, Vol. 328, No 3, pp. 193-198, 2000. (Cit. on p. 23).

[80] F. Chmela and G. Orthaber. *"Rate of Heat Release Prediction for Direct Injection Diesel Engines Based on Purely Mixing Controlled Combustion"*. SAE Technical Paper 1999-01-0186, 1999. (Cit. on p. 194).

[81] C. Choi, S. Kwon, and S. Cho. *"Development of Fuel Consumption of Passenger Diesel Engine with 2-Stage Turbocharger"*. SAE Technical Paper 2006-01-0021, 2006. (Cit. on p. 34).

[82] M. Choshi, K. Asanomi, H. Abe, S. Okamoto, and M. Shoji. *"Development of V6 Miller Cycle Engine"*. JSAE Review, Vol. 15, pp. 195-200, 1994. (Cit. on p. 43).

[83] A. Chow and M.L. Wyszynski. *"Thermodynamic Modelling of Complete Engine Systems - A Review"*. Proceedings of the Institution of Mechanical Engineers, Part D: Journal of Automobile Engineering, Vol. 213, No. 4, pp. 403-415, 1999. (Cit. on p. 170).

[84] G. Cipolla, A. Vassallo, A.E. Catania, E. Spessa, C. Stan, and L. Drischmann. *"Combined Application of CFD Modeling and Pressure-Based Combustion Diagnostics for the Development of a Low Compression Ratio High-Performance Diesel Engine"*. SAE Technical Paper 2007-24-0034, 2007. (Cit. on p. 228).

[85] G. Claussen and C. Suhocki. *"Clean Diesel System Boosting Solution: TVS Supercharger"*. Eaton Corporation Publications, Engine Air Management Operations, 2010. (Cit. on pp. 44, 45).

[86] M. Coppinger and E. Swain. *"Performance Prediction of an Industrial Centrifugal Compressor Inlet Guide Vane System"*. Proceedings of the Institution of Mechanical Engineers Part A: Journal of Power and Energy, Vol. 214, pp. 153-164, 2000. (Cit. on pp. 68, 69, 71).

[87] J.M. Corberan. *"Contribucion al Modelado del Proceso de Renovacion de la Carga en MCIA"*. Tesis Doctoral, Universidad Politecnica de Valencia, Valencia, 1984. (Cit. on p. 186).

[88] R. Dambach and H.P. Hodson. *"Tip Leakage Flow - A Comparison between Small Axial and Radial Turbines"*. Micro-Turbine Generators Conference, Professional Engineering Publishing, pp. 97-108, London, 2000. (Cit. on p. 151).

[89] R. Dambach, H.P. Hodson, and I. Huntsman. *"An Experimental Study of Tip Clearence Flow in a Radial Inflow Turbine"*. ASME Journal of Turbomachinery, Vol. 121, Issue 4, pp. 644-650, 1999. (Cit. on p. 151).

[90] A. Dauron. *"Model-Based Powertrain Control: Many Uses, no Abuse"*. Oil & Gas Science and technology, Vol. 62, pp. 427-435, 2007. (Cit. on p. 6).

[91] J.E. Dec. *"A Conceptual Model of DI Diesel Combustion Based on Lasersheet Imaging"*. SAE Technical Paper 970873, 1997. (Cit. on pp. 191, 194).

[92] B. Degraeuwe. *"Contribution to the Thermal Management of DI Diesel Engines"*. Tesis Doctoral, Universidad Politecnica de Valencia, Valencia, 2007. (Cit. on p. 190).

[93] C. Depcik and D. Assanis. *"A Universal Heat Transfer Correlation for Intake and Exhaust Flows in a Spark-Ignition Internal Combustion Engine"*. SAE Technical Paper 2002-01-0372, 2002. (Cit. on pp. 181, 188).

[94] J.M. Desantes, J.M. Lujan, B. Pla, and J.A. Soler. *"Potential of Using a Nozzle at the Compressor Inlet of a High Speed Direct Injection Diesel Engine"*. Proceedings of the Institution of Mechanical Engineers Part D: Journal of Automobile Engineering, Vol. 225, No. 2, pp. 178-189, 2011. (Cit. on p. 73).

[95] A. Dhand, J. Baekhyun C.and Villegas, K. Svencara, B. Gao, M. Wieltsch, W. Thornton, S. Etemad, J. Parra, and R. Taylor. *"Engine Downsizing Using Electrically Driven Supercharger"*. 13$^{\text{th}}$ EAEC European Automotive Congress, Valencia, 2011. (Cit. on pp. 63, 64).

[96] F.A. Dibella, L.R. Di Nanno, and M.D. Koplow. *"Laboratory and On-Highway Testing of Diesel Organic Rankine Compound Long-Haul Vehicle Engine"*. SAE Technical Paper 830122, 1983. (Cit. on p. 81).

[97] S.L. Dixon. *"Fluid Mechanics and Thermodynamics of Turbomachinery"*. Pergamon Press Ltd, 1998. (Cit. on pp. 153, 261).

[98] V. Dolz. *"Contribucion al Modelado de la Transmision de Calor en los MCIA y su Aplicacion en el Aprovechamiento Energetico de los Gases de Escape Durante los Transitorios de Carga"*. Tesis Doctoral, Universidad Politecnica de Valencia, Valencia, 2006. (Cit. on pp. 181, 188).

[99] E. Doyle, L. Di Nanno, and S. Kramer. *"Installation of a Diesel-Organic Rankine Compound Engine in a Class 8 truck for a single-vehicle test"*. SAE Technical Paper 790646, 1979. (Cit. on p. 81).

[100] H.J. Ecker, M. Schwaderlapp, and D.K. Gill. *"Downsizing of Diesel Engines: 3-Cylinder/4-Cylinder"*. SAE Technical Paper 2000-01-0990, 2000. (Cit. on p. 8).

[101] R. Egnell. *"Combustion Diagnostics by Means of Multizone Heat Release Analysis and NO Calculation"*. SAE Technical Paper 981424, 1998. (Cit. on p. 194).

[102] A. Emadi, K. Rajashekara, S.S. Williamson, and S.M. Lukic. *"Topological Overview of Hybrid Electric and Fuel Cell Vehicular Power System Architectures and Configurations"*. Proceedings of the IEEE Transactions on Vehicular Technology, Vol. 54, pp. 763-770, 2005. (Cit. on p. 2).

[103] B. Engels. *"Lifetime Prediction for Turbocharger Compressor Wheels - Why Use Titanium?"* Borg Warner Turbo Systems Knowledge Library, 2003. (Cit. on p. 250).

[104] L. Eriksson. *"Modeling and Control of Turbocharged SI and DI Engines"*. Oil & Gas Science and Technology - Revue IFP, Vol. 62, No. 4, pp. 523-538, 2007. (Cit. on p. 172).

[105] C. Fenollosa. *"Aportacion a la Descripcion Fenomenologica del Proceso de Combustion por Difusion Diesel"*. Tesis Doctoral, Universidad Politecnica de Valencia, Valencia, 2003. (Cit. on p. 194).

[106] K. Fieweger, H. Paffrath, and N. Schorn. *"Drivability Assessment of an HSDI Diesel Engine with Electrically Assisted Boosting Systems"*. IMechE 7$^{\text{th}}$ International Conference on Turbochargers and Turbocharging, C602/009/2002, pp. 283-293, 2002. (Cit. on pp. 55, 63).

[107] Z. Filipi, Y. Wang, and D. Assanis. *"Effect of Variable Geometry Turbine (VGT) on Diesel Engine and Vehicle System Transient Response"*. SAE Technical Paper 2001-01-1247, 2001. (Cit. on p. 18).

[108] F.B. Fisher. *"Application of Map Width Enhancement Devices to Turbocharger Compressor Stages"*. SAE Technical Paper 880794, 1988. (Cit. on p. 75).

[109] U. Flaig, W. Polach, and G. Ziegler. *"Common Rail System (CR-System) for Passenger Car DI Diesel Engines - Experiences with Applications for Series Production Projects"*. SAE Technical Paper 1999-01-0191, 1999. (Cit. on p. 6).

[110] J.W. Fox, W.K. Cheng, and J.B. Heywood. *"A Model for Predicting the Residual Gas Fraction in Spark-Ignition Engines"*. SAE Technical Paper 931025, 1993. (Cit. on p. 192).

[111] N. Fraser, J. Fleischer T.and Thornton, and J. Rueckauf. *"Development of a Fully Variable Compressor Map Enhancer for Automotive Application"*. SAE Technical Paper 2007-01-1558, 2007. (Cit. on pp. 65, 68, 70, 71).

[112] V. Fsik. *"2-Stage Turbocharger Matching for a Light Duty Diesel Engine"*. Josef Bozek Research Center Publications, 2004. (Cit. on p. 34).

[113] N.F. Gale. *"Accuracy of the Ricardo Steady Estate Flow Rig"*. Ricardo Engeneering Report, Vol. DP.20395, 1975. (Cit. on p. 143).

[114] J. Galindo, H. Climent, C. Guardiola, and J. Domenech. *"Strategies for Improving the Mode Transition in a Sequential Parallel Turbocharged Automotive Diesel Engine"*. International Journal of Automotive Technology, Vol. 10, No. 2, pp. 141-149, 2009. (Cit. on pp. 23, 25).

[115] J. Galindo, H. Climent, C. Guardiola, and A. Tisiera. *"Assessment of a Sequentially Turbocharged Diesel Engine on Real Life Driving Cycles"*. International Journal of Vehicle Design, Vol. 49, No. 1/2/3, 2009. (Cit. on pp. 23–25).

[116] J. Galindo, J. Lujan, H. Climent, and C. Guardiola. *"Turbocharging System Design of a Sequentially Turbocharged Diesel Engine by Means of a Wave Action Model"*. SAE Technical Paper 2007-01-1564, 2007. (Cit. on pp. 23, 24).

[117] J. Galindo, J.M. Lujan, J.R. Serrano, V. Dolz, and S. Guilain. *"Description of a Heat Transfer Model Suitable to Calculate Transient Processes of Turbocharged Diesel Engines with One-Dimensional Gas-Dynamic Codes"*. Applied Thermal Engineering, Vol. 26, pp.66-76, 2006. (Cit. on pp. 181, 188).

[118] J. Galindo, J.M. Lujan, J.R. Serrano, and L. Hernandez. *"Combustion Simulation of Turbocharged HSDI Diesel Engines During Transient Operation Using Neural Networks"*. Applied Thermal Engineering, Vol. 25, pp. 877-898, 2005. (Cit. on pp. 196, 197).

[119] J. Galindo, J.R. Serrano, F. Arnau, and P. Piqueras. *"Description and Analysis of a One-Dimensional Gas-Dynamic Model with Independent Time Discretization"*. Proceedings of the ASME Internal Combustion Engine Division, Spring Technical Conference, Chicago, 2008. (Cit. on pp. 10, 116, 171).

[120] J. Galindo, J.R. Serrano, C. Guardiola, and C. Cervello. *"Surge Limit Definition in a Specific Test Bench for the Characterization of Automotive Turbochargers"*. Experimental Thermal and Fluid Science, Vol. 30, pp. 449-462., 2006. (Cit. on pp. 148, 232).

[121] J. Galindo, J.R. Serrano, X. Margot, A. Tiseira, N. Schorn, and H. Kindl. *"Potential of Flow Pre-Whirl at the Compressor Inlet of Automotive Engine Turbochargers to Enlarge Surge Margin and Overcome Packaging Limitations"*. International Journal of Heat and Fluid Flow, Vol. 28, pp. 374-387, 2007. (Cit. on pp. 67, 68).

[122] J. Galindo, J.R. Serrano, F. Vera, C. Cervello, and M. Lejeune. *"Relevance of Valve Overlap for Meeting Euro 5 Soot Emissions Requirements during Load Transient Process in Heavy Duty Diesel Engines"*. International Journal of Vehicle Design, Vol. 41, No. 1/2/3/4, pp. 343-367, 2006. (Cit. on p. 125).

[123] J. Galindo, A. Tiseira, F.J. Arnau, and R. Lang. *"On-Engine Measurement of Turbocharger Surge Limit. Experimental Techniques"*. Society for Experimental Mechanics, 2011. (Cit. on p. 232).

[124] P. Gautier, A. Albrecht, A. Chasse, P. Moulin, A. Pagot, L. Fontvieille, and D. Issartel. *"A Simulation Study of the Impact of LP EGR on a Two-Stage Turbocharged Diesel Engine"*. Oil & Gas Science and Technology, Revue IFP, Vol. 64, No. 3, pp. 361-379, 2009. (Cit. on p. 37).

[125] P. Gautier, A. Albrecht, P. Moulin, A. Chasse, L. Fontvieille, A. Guinois, and L. Doleac. *"A New Simulation Step Towards Virtual Bench Through the Challenging Case of Two-Stage Turbocharger Diesel Engine Control Design"*. SAE Technical Paper 2008-01-0355, 2008. (Cit. on pp. 170, 171).

[126] S. George, G. Morris, J. Dixon, D. Pearce, and G. Heslop. *"Optimal Boost Control for an Electrical Supercharging Application"*. SAE Technical Paper 2004-01-0523, 2004. (Cit. on p. 62).

[127] B. Georgi, S. Hunkert, J. Liang, and M. Willmann. *"Realizing Future Trends in Diesel Engine Development"*. SAE Technical Paper 972686, 1997. (Cit. on p. 6).

[128] A. Gil. *"Caracterizacion del Flujo de Aire en el Cilindro de Motores Diesel DI Mediante Calculo Tridimensional"*. Tesis Doctoral, Universidad Politecnica de Valencia, Valencia, 2003. (Cit. on p. 144).

[129] B.C. Glenn, D. Upadhyay, and G.N. Washington. *"Control Design of Electrically Assisted Boosting Systems for Diesel Powertrain Applications"*. IEEE Transactions on Control Systems Technology, Vol. 18, pp. 769-778, 2010. (Cit. on pp. 55, 57).

[130] R. Glover, M. Pratley, and M. Marfatia. *"Gear Design for Low Whine Noise in a Supercharged Application"*. SAE Technical Paper 2007-01-2293, 2007. (Cit. on p. 44).

[131] A. Greszler. *"Diesel Turbo-Compound Technology"*. ICCT/NESCCAF workshop - Improving the fuel economy of heavy-duty fleets II, 2008. (Cit. on p. 87).

[132] R.C. Griffith. *"Series Turbocharging for the Caterpillar Heavy-Duty On-Highway Truck Engines with ACERT Technology"*. SAE Technical Paper 2007-01-1561, 2007. (Cit. on pp. 29, 36).

[133] O. Grondin, R. Stobart, H. Chafouk, and J. Maquet. *"Modelling the Compression Ignition Engine for Control - Review and Future Trends"*. SAE Technical Paper 2004-01-0423, 2004. (Cit. on pp. 6, 170).

[134] D. Gurney. *"The Design of Turbocharged Engines Using 1-D Simulation"*. SAE Technical Paper 2001-01-0576, 2001. (Cit. on p. 10).

[135] L. Guzzella and C.H. Onder. *"Introduction to Modeling and Control of Internal Combustion Engine Systems"*. Springer-Verlag Berlin Heidelberg, ISBN 970-3-642-10774-0, 2010. (Cit. on p. 172).

[136] J. Hawley, F. Wallace, A. Cox, R. Horrocks, and G. Bird. *"Variable Geometry Turbocharging for Lower Emissions and Improved Torque Characteristics"*. Proceedings of the Institution of Mechanical Engineers Part D: Journal of Automobile Engineering, Vol. 213, pp. 145-159, 1999. (Cit. on pp. 7, 18).

[137] Y. He and C.C. Lin. *"Development and Validation of a Mean Value Engine Model for Integrated Engine and Control System Simulation"*. SAE Technical Paper 2007-01-1304, 2007. (Cit. on p. 172).

[138] Y. He and C. Rutland. *"Application of Artificial Neural Networks for Integration of Advanced Engine Simulation Methods"*. ASME ICE Division Fall 2000 Technical Meeting, Peoria, Illinois, 2000. (Cit. on p. 172).

[139] Y. He and C.J. Rutland. *"Application of Artificial Neural Networks in Engine Modeling"*. International of Engine Research, Vol. 5, No. 4, pp. 281-296, 2004. (Cit. on p. 172).

[140] S. Heinz. *"Development of a Worldwide Harmonised Heavy-Duty Engine Emissions Test Cycle"*. United Nations GRPE 42nd session, TRANS-WP29-GRPE-2001-2, 2001. (Cit. on p. 9).

[141] A. Heinzerling. *"Global Carbon Dioxide Emissions Fall in 2009 - Past Decade Still Sees Rapid Emissions Growth"*. Earth Policy Institute, Eco-Economy Indicators, 2010. (Cit. on p. 4).

[142] E. Hendricks. *"The Analysis of Mean Value Engine Models"*. SAE Technical Paper 890563, 1989. (Cit. on p. 172).

[143] E. Hendricks, A. Chevalier, M. Jensen, S.C. Sorenson, D. Trumpy, and J. Asik. *"Modelling of the Intake Manifold Filling Dynamics"*. SAE Technical Paper 960037, 1996. (Cit. on p. 172).

[144] F. Herbst, C.P. Stöber-Schmidt, P. Eilts, T. Sextro, J. Kammeyer, C. Natkaniec, J. Seume, D. Porzig, and H. Schwarze. *"The Potential of Variable Compressor Geometry for Highly Boosted Gasoline Engines"*. SAE Technical Paper 2011-01-0376, 2011. (Cit. on pp. 68, 70, 72).

[145] J. Heywood. *"Internal Combustion Engine Fundamentals"*. New York: McGraw-Hill Inc., ISBN 978-0070286375, 1988. (Cit. on pp. 2, 191).

[146] H. Hiereth and P. Prenninger. *"Charging the Internal Combustion Engine"*. NewYork: Springer-Verlag Wien, ISBN 978-3-211-33033-3, 2003. (Cit. on pp. 20, 41, 42, 86, 87, 275).

[147] C. Hill, D. Miller, and R. Gardner. *"2005 Ford GT Powertrain - Supercharged Supercar"*. SAE Technical Paper 2004-01-1252, 2004. (Cit. on p. 44).

[148] R. Hilpert. *"Experimental Study of Heat Dissipation of Heated Wire and Pipe in Air Current"*. Forschungsarbeiten auf dem Gebiete des Ingenieur - Wesens - Ausgabe A, Vol.4, No.5, pp.215-224, 1933. (Cit. on p. 181).

[149] H. Hiroyasu, T. Kadota, and M. Arai. *"Development and Use of a Spray Combustion Modeling to Predict Diesel Engine Efficiency and Pollutant Emissions - Part 1 Combustion Modeling"*. Bulletin of the Japan Society Mechanical Engineering, Vol. 26, pp. 569-575, 1983. (Cit. on pp. 194, 195).

[150] P. Hoecker, J.W. Jaisle, and S. Munz. *"The eBooster from BorgWarner Turbo Systems - The Key Component for a New Automobile Charging System"*. Borg Warner Turbo Systems Knowledge Library, 2000. (Cit. on pp. 54, 62, 63, 272).

[151] P. Hoecker, F. Pflüger, J. Jaisle, and S. Münz. *"Modern Turbocharging Designs for Passenger Car Diesel Engines"*. Borg Warner Turbo Systems Knowledge Library, 2000. (Cit. on p. 18).

[152] G. Hohenberg. *"Definition und Eigenschaften des Thermodynamischen Verlustwinkels von Kolbenmaschinen"*. Automobil-Industrie, Vol. 4, pp. 15-21, 1976. (Cit. on p. 193).

[153] J.P. Holman. *"Heat Transfer"*. McGraw Hill Book Company, Sixth Edition, New York, 1986. (Cit. on pp. 177, 180, 181, 188).

[154] U. Hopmann. *"Diesel Engine Waste Heat Recovery Utilizing Electric Turbocompound Technology"*. Diesel Engine Emissions Reduction Conference, San Diego, 2002. (Cit. on pp. 58, 89).

[155] U. Hopmann. *"Diesel Engine Waste Heat Recovery Utilizing Electric Turbocompound Technology"*. Diesel Engine Emissions Reduction Conference, San Diego, 2004. (Cit. on pp. 58, 89).

[156] U. Hopmann and C. Algrain. *"Diesel Engine Electric Turbo Compound Technology"*. SAE Technical Paper 2003-01-2294, 2003. (Cit. on pp. 58, 88, 89).

[157] M. Hori, N. Ikeya, S. Takabe, and Y. Miyagi. *"Examinations of a Lysholm Compressor's Performance and the Engine Performance Supercharged by the Lysholm Compressor"*. IMechE 6$^{\text{th}}$ International Conference on Turbocharging and Air Management Systems, C554/019/98, London, 1998. (Cit. on pp. 50, 51).

[158] D.T. Hountalas, C.O. Katsanos, and D.A. Kouremenos. *"Study of Available Exhaust Gas Heat Recovery Technologies for HD Diesel Engine Applications"*. International Journal of Alternative Propulsion, Vol. 1, No. 2/3, 2007. (Cit. on pp. 85, 88, 89).

[159] D.T. Hountalas, C.O. Katsanos, and V.T. Lamaris. *"Recovering Energy from the Diesel Engine Exhaust Using Mechanical and Electrical Turbocompounding"*. SAE Technical Paper 2007-01-1563, 2007. (Cit. on pp. 85, 86, 89).

[160] D.T. Hountalas, D.A. Kouremenos, G.C. Mavropoulos, K.B. Binder, and Schwarz V. *"Multi-Zone Combustion Modelling as a Tool for DI Diesel Engine Development - Application for the Effect of Injection Pressure"*. SAE Technical Paper 2004-01-0115, 2004. (Cit. on p. 173).

[161] M.F. Howlett, W. Schnider, N. Ausserhofer, M. Weissbaeck, O. Soustelle, P. Ragot, P. Mallet, and J. Rozen. *"3-Cylinder Aggressive Downsized Diesel"*. Conference Internationale et Exposition Motorisation Diesel: Face au Defi de la Competitivite. Rouen, 2010. (Cit. on pp. 53, 239).

[162] X. Hu. *"An Advanced Turbocharger Model for the Internal Combustion Engine"*. Doctoral Thesis, Purdue University, 2000. (Cit. on p. 151).

[163] R. Hunziker, H.P. Dickmann, and R. Emmrich. *"Numerical and Experimental Investigation of a Centrifugal Compressor with an Inducer Casing Bleed System"*. Proceedings of the Institution of Mechanical Engineers Part A: Journal of Power and Energy, Vol. 215, pp 783-791, 2001. (Cit. on pp. 74, 75).

[164] S. Ibaraki, Y. Yamashita, K. Sumida, H. Ogita, and Y. Jinnai. *"Development of the Hybrid Turbo, an Electrically Assisted Turbocharger"*. Mitsubishi Heavy Industries Technical Review, Vol. 43, pp.1-5, 2006. (Cit. on pp. 55, 59, 60).

[165] M. Ishino, Y. Iwakiri, A. Bessho, and H. Uchida. *"Effects of Variable Inlet Guide Vanes on Centrifugal Compressor Performance"*. ASME paper 99-GT-157, 1999. (Cit. on pp. 68–70).

[166] Y. Iwakiri and H. Uchida. *"Numerical Fluid Analysis of a Variable Geometry Compressor for Use in a Turbocharger"*. Toyota R&D Review, Vol. 41, No. 3, pp.15-21, 2006. (Cit. on p. 77).

[167] M. Jankovic, M. Jankovik, and I. Kolmanovsky. *"Constructive Lyapunov Control Design for Turbocharged Diesel Engines"*. IEEE Transactions on Control Systems Technology, Vol. 8, No.2, pp.288-299, 2000. (Cit. on p. 172).

[168] W. Jansen, A.F. Carter, and M.C. Swarden. *"Improvements in Surge Margin for Centrifugal Compressors"*. AGARD Conference on Centrifugal Compressors, Flow Phenomenon and Performance, Vol. 282, No.19, 1980. (Cit. on p. 75).

[169] F. Jayat, A. Reck, and K.V.R. Babu. *"SCR and SCRi as After-Treatment Systems for Low CO2 and Low NOx Vehicles"*. SAE Technical Paper 2011-26-0038, 2011. (Cit. on p. 7).

[170] J.P. Jensen, A.F. Kristensen, S.C. Sorenson, and N. Houback. *"Mean Value Modelling of Small Turbocharged Diesel Engine"*. SAE Technical Paper 910070, 1991. (Cit. on pp. 151, 152, 172).

[171] N. Jeuland, X. Montagne, and P. Duret. *"New HCCI/CAI Combustion Process Development: Methodology for Determination of Relevant Fuel Parameters"*. Oil & Gas Science and Technology, Revue IFP, Vol. 59, No. 6, pp. 571-579, 2004. (Cit. on p. 7).

[172] Z. Jiang, K. Cheng, and D.K. Harrison. *"A Concurrent Engineering Approach to the Development of a Scroll Compressor"*. Journal of Materials Processing Technology, Vol. 107, pp. 194-200, 2000. (Cit. on p. 41).

[173] K. Jiao, X. Li, H. Sun, T. Schram, E. Krivitzky, and L.M. Larosiliere. *"Numerical Investigation of Advanced Compressor Technologies to Meet Future Diesel Emission Regulations"*. SAE Technical Paper 2009-01-1469, 2009. (Cit. on p. 80).

[174] K. Jiao, H. Sun, X. Li, H. Wu, E. Krivitzky, T. Schram, and L.M. Larosiliere. *"Numerical Simulation of Air Flow Through Turbocharger Compressors with Dual Volute Design"*. Applied Energy, Vol. 86, pp. 2494-2506, 2009. (Cit. on p. 80).

[175] R. Jorgensen and M. Sitar. *"System Performance and Control Requirements for a Sequentially Compounded Supercharged and Turbocharged Gasoline Engine"*. Eaton Corporation Publications, Engine Air Management Operations, 2004. (Cit. on pp. 45, 53, 275).

[176] R. Kamo. *"Higher BMEP Prospects for Vehicular Diesels"*. IMechE 1^{th} International Conference of Turbocharging and Turbochargers, C62/78, London, 1978. (Cit. on p. 87).

[177] H. Kanesaka, G. Ozawa, and H. Seiyama. *"Future Prospects for Supercharging"*. SAE Technical Paper 982045, 1998. (Cit. on p. 51).

[178] M. Kao and J.J. Moskwa. *"Nonlinear Cylinder and Intake Manifold Pressure Observer for Engine Control and Diagnostics"*. SAE Technical Paper 940375, 1994. (Cit. on p. 172).

[179] D.D. Kapich. *"High Speed Hydraulic Turbine Driven Supercharger System and Controls Optimization"*. SAE Technical Paper 972676, 1997. (Cit. on p. 93).

[180] D.D. Kapich. *"Sequential Hydro-Supercharging System for Turbodiesels"*. SAE Technical Paper 961744, 1996. (Cit. on p. 93).

[181] D.D. Kapich. *"Very High Speed, Hydraulic Turbine Driven Supercharging System"*. SAE Technical Paper 951882, 1995. (Cit. on p. 93).

[182] T. Kattwinkel, R. Weiss, and J.P. Boeschlin. *"Mechatronic Solution for Electronic Turbocharger"*. SAE Technical Paper 2003-01-0712, 2003. (Cit. on p. 62).

[183] W.M. Kays and A.L. London. *"Compact Heat Exchangers"*. McGraw Hill Book Company, Second Edition, New York, 1964. (Cit. on p. 177).

[184] J. Kech and H. Klotz. *"Model Based Sequential Turbocharging Optimization for Series 8000 M70/M90 Engines"*. SAE Technical Paper 2002-01-0378, 2002. (Cit. on p. 23).

[185] R.J. Kee, F.M. Rupley, and J.A. Miller. *"The Chemkin Thermodynamic Data Base"*. Sandia Report, SAND87-8215B, 1991. (Cit. on p. 176).

[186] R. Kemmler, H.G. Lehmann, and J. Schommers. *"Trends in Development of Supercharged Gasoline Internal Combustion Engines"*. 7^{th} Supercharging conference, Dresden, 2000. (Cit. on p. 45).

[187] M. Khair. *"A Review of Diesel Particulate Filter Technologies"*. SAE Technical Paper 2003-01-2303, 2003. (Cit. on p. 6).

[188] Y. Kim, A. Engeda, R. Aungier, and G. Direnzi. *"The Influence of Inlet Flow Distortion on the Performance of a Centrifugal Compressor and the Development of an Improved Inlet Using Numerical Simulations"*. Proceedings of the Institution of Mechanical Engineers Part A: Journal of Power and Energy, Vol. 215, pp 323-338, 2001. (Cit. on p. 67).

[189] S. Kimura, O. Aoki, Y. Kitahara, and E. Aiyoshizawa. *"Ultra-Clean Combustion Technology Combining a Low-Temperature and Premixed Combustion Concept for Meeting Future Emissions Standards"*. SAE Technical Paper 2001-01-0200, 2001. (Cit. on p. 7).

[190] H. Kindl, N. Schorn, H. Schulte, J.R. Serrano, X. Margot, and J.C. Donayre. *"Influence of Various Compressor Inlet Designs on Compressor Performance"*. THIESEL Conference on Thermo- and Fluid Dynamic Processes in Diesel Engines, Valencia, 2004. (Cit. on p. 67).

[191] C. Klarhoefer and G. Winkler. *"Compounding a Passenger Car Diesel with a Positive Displacement Expander"*. IMechE 3^{th} International Conference of Turbocharging and Turbochargers, pp. 123-127, London, 1986. (Cit. on p. 83).

[192] H. Kleeberg, D. Tomazic, O. Lang, and K. Habermann. *"Future Potential and Development Methods for High Output Turbocharged Direct Injected Gasoline Engines"*. SAE Technical Paper 2006-01-0046, 2006. (Cit. on p. 53).

[193] W. Knecht. *"Diesel Engine Development in View of Reduced Emission Standards"*. Energy, Vol. 33, pp. 264-271, 2008. (Cit. on p. 54).

[194] R. Kociba and M.D. Parr. *"The General Motors Supercharged 3800 Engine"*. SAE Technical Paper 910685, 1991. (Cit. on pp. 44, 46).

[195] I. Kolmanovsky and A.G. Stefanopoulou. *"Evaluation of Turbocharger Power Assist System Using Optimal Control Techniques"*. SAE Technical Paper 2000-01-0519, 2000. (Cit. on p. 56).

[196] I. Kolmanovsky and A.G. Stefanopoulou. *"Optimal Control Techniques for Assessing Feasibility and Defining Subsystem Level Requirements: an Automotive Case Study"*. IEEE Transactions on Control Systems Technology, Vol. 9, pp. 524-534, 2001. (Cit. on pp. 56, 116).

[197] I. Kolmanovsky, A.G. Stefanopoulou, and B.K. Powell. *"Improving Turbocharged Diesel Engine Operation with Turbo Power Assist System"*. IEEE International Conference on Control Applications, pp.454-459, Kohala Coast, 1999. (Cit. on p. 56).

[198] K. Konishi, H. Yoshiki, and S. Tashiro. *"Performances of Radial Inflow Turbines for Exhaust Gas Turbochargers under Nonsteady Flow Conditions"*. International Gas Turbines Congress, pp. 157-164, Yokohama, 1991. (Cit. on p. 160).

[199] A.G. Konstandopoulos, E.A. Kladopoulou, S.L. Yang, J.H. Johnson, and G.G. Parker. *"A Study Describing the Performance of Diesel Particulate Filters During Loading and Regeneration - A Lumped Parameter Model for Control Applications"*. SAE Technical Paper 2003-01-0842, 2003. (Cit. on p. 180).

[200] A.G. Konstandopoulos, M. Kostoglou, E. Skaperdas, E. Papaioannou, D. Zarvalis, and E. Kladopoulou. *"Fundamental Studies of Diesel Particulate Filters - Transient Loading, Regeneration and Aging"*. SAE Technical Paper 2000-01-1016, 2000. (Cit. on p. 180).

[201] P.A. Konstantinidis, G.C. Koltsakis, and A.M. Stamatelos. *"Transient Heat Transfer Modelling in Automotive Exhaust Systems"*. Proceedings of the Institution of Mechanical Engineers Part C: Journal of Mechanical Engineering Science, Vol. 211, No.1, pp. 1-15, 1997. (Cit. on p. 181).

[202] J.C. Koval, A.W. Fedewa, K.A Hollman, and D.G. Woolcott. *"An Automotive Supercharger Noise Test Rig Incorporating Torsional Excitation"*. SAE Technical Paper 2005-01-2440, 2005. (Cit. on p. 44).

[203] R. Krebs, H. Szengel R.and Middendorf, M. Fleib, A. Laumann, and S. Voeltz. *"The New Dual-Charged FSI Petrol Engine by Volkswagen - Part 1: Design"*. MTZ Worldwide Edition, Vol. 66, pp. 844-856, 2005. (Cit. on p. 52).

[204] R. Krebs, R. Szengel, H. Middendorf, H. Sperling, W. Siebert, J. Theobald, and K. Michels. *"The New Dual-Charged FSI Petrol Engine by Volkswagen - Part 2: Thermodynamics"*. MTZ Worldwide Edition, Vol. 66, pp. 979-986, 2005. (Cit. on pp. 49, 53).

[205] I.J. Kruithof and W.L. Sturm. *"Development of a Heavy-Duty Diesel Engine with Two-Stage Turbocharging"*. ATZ AutoTechnology, Vol. 5, 2005. (Cit. on p. 29).

[206] A.S. Kushch, J.C. Bass, S. Ghamaty, and N.B. Elsner. *"Thermoelectric Development at HI-Z Technology"*. 10^{th} International Conference on Thermoelectrics, pp. 422-430, Beijing, 2001. (Cit. on p. 81).

[207] N. Kyrtatos and N. Watson. *"Application of Aerodynamically Induced Prewhirl to Small Turbocharger Compressor"*. ASME Journal of Engineering for Power, Vol. 102, pp. 934-950, 1980. (Cit. on p. 65).

[208] R. Lang. *"Contribucion a la Mejora del Margen de Bombeo en Compressors Centrifugos de Sobrealimentacion"*. Tesis Doctoral, Universidad Politecnica de Valencia, Valencia, 2011. (Cit. on p. 232).

[209] S. Langridge and H. Fessier. *"Strategies for High EGR Rates in a Diesel Engine"*. SAE Technical Paper 2002-01-0961, 2002. (Cit. on p. 37).

[210] M. Lapuerta, O. Armas, and V. Bermudez. *"Sensitivity of Diesel Engine Thermodynamic Cycle Calculation to Measurement Errors and Estimated Parameters"*. Applied Thermal Engineering, Vol. 20, pp. 843-861, 2000. (Cit. on pp. 150, 204).

[211] M. Lapuerta, O. Armas, and J.J. Hernandez. *"Diagnostic of D.I. Diesel Combustion from In-Cylinder Pressure Signal by Estimation of Mean Thermodynamic Properties of the Gas"*. Applied Thermal Engineering, Vol. 19, pp. 513-529, 1999. (Cit. on pp. 150, 205).

[212] M. Lapuerta, O. Armas, and J.J. Hernandez. *"Effect to the Injection Parameters of a Common Rail Injection System on Diesel Combustion through Thermodynamic Diagnosis"*. SAE Technical Paper 1999-01-0194, 1999. (Cit. on p. 150).

[213] M. Lapuerta, O. Armas, and S. Molina. *"Study of the Compression Cycle of a Reciprocating Engine Through the Polytropic Coefficient"*. Applied Thermal Engineering, Vol. 23, No. 3, pp. 313-323, 2003. (Cit. on p. 204).

[214] M. Lapuerta, R. Ballesteros, and J.R. Agudelo. *"Effect of the Gas State Equation on the Thermodynamic Diagnostic of Diesel Combustion"*. Applied Thermal Engineering, Vol. 26, pp. 1492-1499, 2006. (Cit. on p. 185).

[215] J.D. Ledger, R.S. Benson, and H. Furukawa. *"Improvement in Transient Performance of a Turbocharged Diesel Engine by Air Injection into the Compressor"*. SAE Technical Paper 730665, 1973. (Cit. on p. 94).

[216] B. Lee, Z. Filipi, D. Assanis, and D. Jung. *"Simulation-Based Assessment of Various Dual-Stage Boosting Systems in Terms of Performance and Fuel Economy Improvements"*. SAE Technical Paper 2009-01-1471, 2009. (Cit. on pp. 29, 34, 39).

[217] A. Lefebvre and S. Guilain. *"Transient Response of a Turbocharged SI Engine with an Electrical Boost Pressure Supply"*. SAE Technical Paper 2003-01-1844, 2003. (Cit. on pp. 60, 61).

[218] C.J. Leising, G.P. Purohit, S.P. DeGrey, and J.G. Finegold. *"Waste Heat Recovery"*. SAE Technical Paper 780686, 1978. (Cit. on p. 81).

[219] J.L Leroy and G. Grosshaus. *"New Development of Turbo-Compound Diesel Engines"*. IMechE 3th International Conference of Turbocharging and Turbochargers, pp. 97-104, London, 1986. (Cit. on p. 84).

[220] K. Levenberg. *"A Method for the Solution of Certain Non-Linear Problems in Least Squares"*. The Quarterly of Applied Mathematics, Vol. 2, pp. 164-168, 1944. (Cit. on p. 197).

[221] N. Lindenkamp. *"Designing a Charging System for a Diesel Engine"*. European Users Conference, Frankfurt, 2007. (Cit. on p. 53).

[222] H. Loren, L.H. Uthoff, and J.W. Yakimow. *"Supercharger vs. Turbocharger in Vehicle Applications"*. SAE Technical Paper 870704, 1987. (Cit. on p. 44).

[223] J.M. Lujan, V. Bermudez, J. R. Serrano, and C. Cervello. *"Test Bench for Turbocharger Groups Characterization"*. SAE Technical Paper 2002-01-0163, 2002. (Cit. on p. 148).

[224] J.M. Lujan, J.R. Serrano, F. Arnau, and V. Dolz. *"Heat Transfer Model to Calculate Turbocharged HSDI Diesel Engines Performance"*. SAE Technical Paper 2003-01-1066, 2003. (Cit. on pp. 181, 188).

[225] G. Lumsden, D. OudeNijeweme, N. Fraser, and H. Blaxil. *"Development of a Turbocharged Direct Injection Downsizing Demonstrator Engine"*. SAE Technical Paper 2009-01-1503, 2009. (Cit. on p. 8).

[226] C. Luttermann and W. Mährle. *"BMW High Precision Fuel Injection in Conjunction with Twin-Turbo Technology: a Combination for Maximum Dynamic and High Fuel Efficiency"*. SAE Technical Paper 2007-01-1560, 2007. (Cit. on p. 21).

[227] I. Macdougal and R.L. Elder. *"The Improvement of Operating Range in a Small High Speed Centrifugal Compressor Using Casing Treatment"*. IMechE 2th International Conference of Turbocharging and Turbochargers, C32/82, London, 1982. (Cit. on p. 75).

[228] J. Macek and O. Vitek. *"Simulation of Pulsating Flow Unsteady Operations of a Turbocharger Radial Turbine"*. SAE Technical Paper 2008-01-0295, 2008. (Cit. on pp. 116, 151).

[229] M. Marcic. *"Measuring Method for Diesel Multihole Injection Nozzles"*. Sensor and Actuators, Vol. 107, pp.152-158, 2003. (Cit. on p. 145).

[230] D. Marquardt. *"An Algorithm for Least-Squares Estimation of Non-Linear Parameters"*. SIAM Journal of Applied Mathematics, Vol. 11, pp.431-441, 1963. (Cit. on p. 197).

[231] G. Martin, V. Talon, P. Higelin, A. Charlet, and C. Caillol. *"Implementing Turbomachinery Physics into Data Map-Based Turbocharger Models"*. SAE Technical Paper 2009-01-0310, 2009. (Cit. on pp. 153, 162, 178).

[232] E. Mattarelli, F. Perini, and A. Rinaldini. *"Optimization of a Supercharged Single Cylinder Engine for a Formula SAE Racing Car"*. SAE Technical Paper 2009-01-0309, 2009. (Cit. on p. 44).

[233] E. Mattarelli, C.A. Rinaldini, A. Mazza, and M. Oliva. *"Development of a 2-Stage Supercharging System for a HSDI Diesel Engine"*. SAE Technical Paper 2009-01-2757, 2009. (Cit. on pp. 31, 34, 53).

[234] K.P. Mayer. *"Swirl Measurement on the Stationary Flow Test Bench by Means of a Momentum Meter"*. AVL Report Memory No. 618, 1982. (Cit. on p. 143).

[235] S.M. Milburn. *"Introducing a High Efficiency Variable Positive Displacement Automotive Supercharger"*. SAE Technical Paper 940845, 1994. (Cit. on p. 40).

[236] F. Millo, F. Mallamo, and G. Ganio Mego. *"The Potential of Dual Stage Turbocharging and Miller Cycle for HD Diesel Engines"*. SAE Technical Paper 2005-01-0221, 2005. (Cit. on pp. 29, 39, 40).

[237] F. Millo, F. Mallamo, E. Pautasso, and G. Ganio Mego. *"The Potential of Electric Exhaust Gas Turbocharging for HD Diesel Engines"*. SAE Technical Paper 2006-01-0437, 2006. (Cit. on pp. 58, 59, 90).

[238] Y. Miyagi, S. Takabe, K. Miyashita, and N. Ikeya. *"Experimental Study of New Lysholm Supercharger with a Simple Unloading System"*. SAE Technical Paper 960952, 1996. (Cit. on pp. 45, 46).

[239] H. Mohtar, A. Chesse, A. Yammine, and F. Hetet. *"Variable Inlet Guide Vanes in a Turbocharger Centrifugal Compressor: Local and Global Study"*. SAE Technical Paper 2008-01-0301, 2008. (Cit. on p. 70).

[240] H. Mohtar, P. Chesse, and D. Chalet. *"Effect of a Map Width Enhancement System on Turbocharger Centrifugal Compressor Performance and Surge Margin"*. Proceedings of the Institution of Mechanical Engineers Part D: Journal of Automobile Engineering, Vol. 225, No. 3, pp. 395-405, 2011. (Cit. on p. 76).

[241] M.L. Monaghan and H.F. Pettifer. *"Air Motion and its Effect on Diesel Performance and Emission"*. SAE Technical Paper 810255, 1981. (Cit. on p. 143).

[242] P. Moraal and I. Kolmanovsky. *"Turbocharger Modeling for Automotive Control Applications"*. SAE Technical Paper 1999-01-0908, 1999. (Cit. on pp. 116, 151, 162).

[243] T. Morel and R. Keribar. *"Heat Radiation in DI Diesel Engines"*. SAE Technical Paper 860445, 1986. (Cit. on p. 191).

[244] P. Moulin, O. Grondin, and L. Fontvieille. *"Control of a Two-Stage Turbocharger on a Diesel Engine"*. 48th IEEE Conference on Decision and Control, Shanghai, 2009. (Cit. on p. 32).

[245] E. Mueller, T. Kollman, and T. Reid. *"Performance Development of the Supercharged Mercury Marine Outboard Engines"*. SAE Technical Paper 2006-01-0015, 2006. (Cit. on p. 43).

[246] M. Muller, E. Hendricks, and S.C. Sorenson. *"Mean Value Modelling of Turbocharged Spark Ignition Engines"*. SAE Technical Paper 980784, 1998. (Cit. on p. 151).

[247] S. Munz, M. Schier, H.P. Schmalzl, and T. Bertolini. *"eBooster - Design and Performance of an Innovative Electrically Driven Charging System"*. Borg Warner Turbo Systems Knowledge Library, 2000. (Cit. on pp. 57, 60, 61, 272).

[248] P. Nefischer, M. Grubbauer, J. Honeder, G. Pessl, and M. Prosi. *"Diesel Engine with 2-Stage Turbocharging and Variable Turbine Geometry in Passenger Cars"*. THIESEL Conference on Thermo- and Fluid Dynamic Processes in Diesel Engines, Valencia, 2010. (Cit. on pp. 35, 36).

[249] S.A. Nelson, Z.S. Filipi, and D.N. Assanis. *"The Use of Neural Nets for Matching Fixed or Variable Geometry Compressors with Diesel Engines"*. Journal of Engineering for Gas Turbines and Power, Vol. 125, pp. 572-579, 2003. (Cit. on p. 153).

[250] B. Nikpour. *"Turbocharger Compressor Flow Range Improvement for Future Heavy Duty Diesel Engines"*. THIESEL Conference on Thermo- and Fluid Dynamic Processes in Diesel Engines, Valencia, 2004. (Cit. on pp. 75–77).

[251] T. Noguchi, Y. Takata, Y. Yamashita, and S. Ibaraki. *"160000-r/tr 2.7-kW Electric Drive of Supercharger for Automobiles"*. International Conference on Power Electronics and drives Systems, Kuala Lumpur, 2005. (Cit. on p. 59).

[252] T. Noguchi, Y. Takata, Y. Yamashita, Y. Komatsu, and S. Ibaraki. *"200000-r/tr 2-kW PM Motor Drive for Turbocharger"*. Electrical Engineering in Japan, Vol. 161, pp. 854-861, 2007. (Cit. on pp. 60, 89).

[253] D.L. Page. *"Emission Reductions and Improved Engine Performance with the Turbodyne System"*. Diesel Engine Emissions Reduction Conference, San Diego, 1995. (Cit. on p. 54).

[254] D.L. Page. *"Optimization of the Air/Fuel Ratio for Improved Engine Performance and Reduced Emissions"*. SAE Technical Paper 961714, 1996. (Cit. on pp. 55, 61).

[255] P. Pallotti, E. Torella, J. New, M. Criddle, and J. Brown. *"Application of an Electric Boosting System to an Small, Four-Cylinder S.I. Engine"*. SAE Technical Paper 2003-32-0039, 2003. (Cit. on p. 62).

[256] J. Park, K.S. Lee, S. Song, and K.M. Chun. *"Numerical Study of a Light-Duty Diesel Engine with a Dual-Loop EGR System Under Frequent Engine Operating Conditions Using the DOE Method"*. International Journal of Automotive Technology, Vol. 11, No. 5, pp. 616-623, 2010. (Cit. on p. 173).

[257] A.T.C. Patterson, R.J. Tett, and J. McGuire. *"Exhaust Heat Recovery Using Electro-Turbogenerator"*. SAE Technical Paper 2009-01-1604, 2009. (Cit. on p. 91).

[258] F. Payri, J. Benajes, J. Galindo, and J.R. Serrano. *"Modelling of Turbocharged Diesel Engines in Transient Operation - Part 2 Wave Action Models for Calculating the Transient Operation in a High Speed Direct Injection Engine"*. Proceedings of the Institution of Mechanical Engineers Part D: Journal of Automobile Engineering, Vol. 216, No. 6, pp. 479-493, 2002. (Cit. on pp. 197, 207).

[259] F. Payri, J. Benajes, and M. Reyes. *"Modelling of Supercharger Turbines in Internal Combustion Engines"*. International Journal of Mechanical Science, Vol. 8-9, pp. 853-869, 1996. (Cit. on pp. 152, 210).

[260] F Payri and J.M. Desantes. *"Motores de Combustion Interna Alternativos"*. Editorial Reverte, ISBN 978-84-8363-705-0, 2011. (Cit. on p. 228).

[261] F. Payri, J. Galindo, J.R. Serrano, and F.J. Arnau. *"Analysis of Numerical Methods to Solve One Dimensional Fluid-Dynamic Governing Equations Under Impulsive Flow in Tapered Ducts"*. International Journal of Mechanical Science, Vol. 46, pp. 981-1004, 2004. (Cit. on p. 171).

[262] F. Payri, X Margot, A. Gil, and J. Martin. *"Computational Study of the Heat Transfer to the Walls of a DI Diesel Engine"*. SAE Technical Paper 2005-01-0210, 2005. (Cit. on p. 191).

[263] F. Payri, X. Margot, A. Gil, and J. Martin. *"Prediction of Heat Transfer to the Walls in DI Diesel Engines"*. Proceedings of the 2nd EACC International European Automotive CFD Conference, Frankfurt, 2005. (Cit. on p. 191).

[264] F. Payri, S. Molina, J. Martin, and O. Armas. *"Influence of Measurement Errors and Estimated Parameters on Combustion Diagnostic"*. Applied Thermal Engineering, Vol. 26, pp. 226-236, 2006. (Cit. on pp. 150, 189, 192).

[265] F. Payri, J.R. Serrano, P. Fajardo, M.A. Reyes-Belmonte, and R. Gozalbo. *"A Physically Based Methodology to Extrapolate Performance Maps of Radial Turbines"*. Energy Conversion and Management, Vol. 55, pp.149-163, 2012. (Cit. on pp. 153, 210).

[266] R. Payri, V. Bermudez, F.J. Salvador, and A.H. Plazas. *"Study of the Influence of Nozzle Seat Type on Injection Rate and Spray Behavior"*. Proceedings of the Institution of Mechanical Engineers Part D: Journal of Automotive Engineering, Vol. 219, pp.667-689, 2005. (Cit. on p. 145).

[267] R Payri, J.M. Garcia, J. Salvador, and J. Gimeno. *"Using Spray Momentum Flux Measurements to Understand the Influence of Diesel Nozzle Geometry on Spray Characteristics"*. Fuel, Vol. 84, pp. 551-561, 2005. (Cit. on pp. 144, 145).

[268] R. Payri, S. Molina, F.J. Salvador, and J. Gimeno. *"A Study of the Relation Between Nozzle Geometry, Internal Flow and Sprays Characteristics in Diesel Injections Systems"*. Korean Society of Mechanical Engineers, Vol. 18, pp. 1222-1235, 2004. (Cit. on p. 145).

[269] F. Pfluger. *"Regulated Two-Stage Turbocharging - KKK's New Charging System for Commercial Diesel Engines"*. IMechE 6^{th} International Conference on Turbocharging and Air Management Systems, C554/035/98, London, 1998. (Cit. on pp. 27, 29, 30).

[270] P.R. Phillips, G.R. Chandler, D.M. Jolie, A.J.J. Wilkins, and M.V. Twigg. *"Development of Advanced Diesel Oxidation Catalysts"*. SAE Technical Paper 1999-01-3075, 1999. (Cit. on p. 6).

[271] S. Pischinger, S. Schernus, G. Lutkenmeyer, H.J. Theuerkauf, T. Winsel, and M. Ayeb. *"Investigation of Predictive Models for Application in Engine Cold-Start Behavior"*. SAE Technical Paper 2004-01-0994, 2004. (Cit. on p. 172).

[272] B. Pla. *"Análisis del Proceso de la Recirculación de los Gases de Escape de Baja Presión en Motores Diesel Sobrealimentados"*. Tesis Doctoral, Universidad Politecnica de Valencia, Valencia, 2009. (Cit. on p. 7).

[273] A. Plianos and R. Stobart. *"Modeling and Control of Diesel Engines Equipped with a Two-Stage Turbo-System"*. SAE Technical Paper 2008-01-1018, 2008. (Cit. on pp. 29, 35, 127).

[274] P. Podevin and M. Toussaint. *"Techniques Avancée de Suralimentation: le Turbocompresseur"*. 5ème Cycle de Conférence Utilisation Rationnelle de l'Energie dans les Moteurs, Paris, 2004. (Cit. on p. 57).

[275] J. Portalier, J. Blanc, F. Garnier, N. Hoffmann, N. Schorn, H. Kindl, J. Galindo, D. Jeckel, P. Uhl, and J. Laissus. *"Twin Turbo Boosting System Design for the New Generation of PSA 2.2-liter HDI Diesel Engines"*. THIESEL Conference on Thermo-and Fluid Dynamic Processes in Diesel Engines, Valencia, 2006. (Cit. on pp. 23, 24).

[276] C.D. Rakopoulos and E.G. Giakoumis. *"Review of Thermodynamic Diesel Engine Simulations under Transient Operating Conditions"*. SAE Technical Paper 2006-01-0884, 2006. (Cit. on p. 170).

[277] C.D. Rakopoulos, D.C. Rakopoulos, E.G. Giacoumis, and D.C. Kyritsis. *"Validation and Sensitivity Analysis of a Two Zone Diesel Engine Model for Combustion and Emissions Prediction"*. Energy Conversion and Management, Vol. 45, pp. 1471-1495, 2004. (Cit. on p. 194).

[278] Z. Ren, T. Campbell, and J. Yang. *"Theoretical and Experimental Study on the Performance of a Sequentially Turbocharged Diesel Engine"*. IMechE 6th International Conference on Turbocharging and Air Management Systems, C554/010/98, London, 1998. (Cit. on p. 23).

[279] M. Reyes. *"Modelo de Transferencia de Calor Para Colectores de Escape de Motores Alternativos"*. Tesis Doctoral, Universidad Politecnica de Valencia, Valencia, 1994. (Cit. on p. 188).

[280] B.J. Roback, M.R. Holl, M.L. Eble, and D. Thornton. *"Supercharging Ford's 4.6L for Affordable Performance"*. SAE Technical Paper 2003-01-3209, 2003. (Cit. on p. 44).

[281] C. Rodgers. *"Centrifugal Compressor Inlet Guide Vanes for Increased Surge Margin"*. ASME Journal of Turbomachinery, Vol. 113, No. 4, pp. 696-702, 1991. (Cit. on pp. 65, 68).

[282] C. Rodgers. *"Impeller Stalling as Influenced by Diffusion Limitations"*. ASME Journal of Fluids Engineering, Vol. 99, No. 1, pp. 84-94, 1977. (Cit. on pp. 65, 68).

[283] C. Romero. *"Contribucion al Conocimiento del Comportamiento Termico y la Gestion Termica de los Motores de Combustion Interna Alternativos"*. Tesis Doctoral, Universidad Politecnica de Valencia, Valencia, 2009. (Cit. on p. 213).

[284] O. Ryder, H. Sutter, and L. Jaeger. *"The Design and Testing of an Electrically Assisted Turbocharger for Heavy Duty Diesel Engines"*. IMechE 8th International Conference on Turbochargers and Turbocharging, pp. 157-166, London, 2006. (Cit. on pp. 59, 90).

[285] H. Sammons and E. Chatterton. *"The Napier Nomad Aircraft Diesel Engine"*. SAE Transactions, Vol. 63, No. 107, 1955. (Cit. on p. 82).

[286] M. Sandford, G. Page, and P. Crawford. *"The All New AJV8"*. SAE Technical Paper 2009-01-1060, 2009. (Cit. on p. 43).

[287] R. Sauerstein, R. Dabrowski, M. Becker, and W. Bullmer. *"Regulated Two-Stage Turbocharging for Gasoline Engines"*. Borg Warner Turbo Systems Knowledge Library, 2010. (Cit. on pp. 31, 32, 34).

[288] S. Saulnier and S. Guilain. *"Computational Study of Diesel Engine Downsizing Using Two-Stage Turbocharging"*. SAE Technical Paper 2004-01-0929, 2004. (Cit. on pp. 30, 136).

[289] K.P. Schindler. *"Why Do We Need the Diesel?"*. SAE Technical Paper 972684, 1997. (Cit. on p. 5).

[290] F. Schmitt and B. Engels. *"Regulated 2-Stage (R2S) Charging System for High Specific Power Engines"*. Congres Le Diesel: aujourd'hui et demain, Ecole Centrale, Lyon, 2004. (Cit. on pp. 28, 30, 34, 36).

[291] T.N. Schmitz, K.D. Holloh, R. Juergens, and G. Fleckenstein. *"Potential of Additional Mechanical Supercharging for Commercial Vehicle Engines"*. SAE Technical Paper 942268, 1994. (Cit. on pp. 42, 49–51).

[292] N. Schorn, E. Karvounis, U. Späder, H. Schulte, D. Jeckel, P. Barthelet, P. Cancalon, O. Salvat, J. Portalier, and J. Minichetti. *"Boosting Systems for Next Generation Passenger Car Diesel Engines - What Systems Will Complement VNT Technology?"* Aufladetechnische Konferenz, Dresden, 2004. (Cit. on pp. 18, 20, 21).

[293] M. Schwaderlapp, K. Habermann, and K. Yapici. *"Variable Compression Ratio - A Design Solution for Fuel Economy Concepts"*. SAE Technical Paper 2002-01-1103, 2002. (Cit. on p. 55).

[294] P.K. Senecal, J. Xin, and R.D. Reitz. *"Predictions of Residual Gas Fraction in IC Engines"*. SAE Technical Paper 962052, 1996. (Cit. on p. 192).

[295] J.R. Serrano, F.J. Arnau, V. Dolz, and P. Piqueras. *"Methodology for Characterization and Simulation of Turbocharged Diesel Engines Combustion during Transient Operation - Part 1: Data Acquisition and Post-Processing"*. Applied Thermal Engineering, Vol. 29, pp. 142-149, 2009. (Cit. on p. 151).

[296] J.R. Serrano, F.J. Arnau, V. Dolz, A. Tiseira, and C. Cervello. *"A Model of Turbocharger Radial Turbines Appropriate to be Used in Zero- and One-Dimensional Gas Dynamics Codes for Internal Combustion Engines Modelling"*. Energy Conversion and Management, Vol. 49, pp. 3729-3745, 2008. (Cit. on pp. 152, 210).

[297] J.R. Serrano, F.J. Arnau, V. Dolz, A. Tisiera, M. Lejeune, and N. Auffret. *"Analysis of the Capabilities of a Two-Stage Turbocharging System to Fulfill the US2007 Anti-Pollution Directive for Heavy Duty Diesel Engines"*. International Journal of Automobile Technology, Vol. 9, No. 3, pp. 227-288, 2008. (Cit. on pp. 28, 37, 39, 125).

[298] J.R. Serrano, H. Climent, C. Guardiola, and P. Piqueras. *"Methodology for Characterisation and Simulation of Turbocharged Diesel Engines Combustion During Transient Operation - Part 2: Phenomenological Combustion Simulation"*. Applied Thermal Engineering, Vol. 29, pp. 150-158, 2009. (Cit. on p. 197).

[299] J.R. Serrano, V. Dolz, A. Tiseira, and A. Paez. *"Influence of Environmental Conditions and Thermodynamic Considerations in the Calculations of Turbochargers Efficiency"*. SAE Technical Paper 2009-01-1468, 2009. (Cit. on p. 148).

[300] J.R. Serrano, B. Pla, R. Gozalbo, and D. Ospina. *"Estimation of the Extended Turbine Maps for a Radial Inflow Turbine"*. SAE Technical Paper 2010-01-1234, 2010. (Cit. on pp. 152, 210).

[301] S. Shaaban and J. Seume. *"Analysis of Turbocharger Non-Adiabatic Performance"*. IMechE 8^{th} International Conference on Turbocharging and Air Management Systems, C647/027, London, 2006. (Cit. on p. 158).

[302] S.M. Shahed. *"An Analysis of Assisted Turbocharging with Light Hybrid Powertrain"*. SAE Technical Paper 2006-01-0019, 2006. (Cit. on p. 56).

[303] S.M. Shahed. *"Smart Boosting Systems e-Turbo and e-Charger: New Frontier?"*. Diesel Engine Emissions Reduction Conference, Pasadena, 2001. (Cit. on p. 57).

[304] S.M. Shahed, C. Middlemass, and C. Balis. *"Design & Development of e-Turbo for SUV and Light Truck Applications"*. Diesel Engine Emissions Reduction Conference, Newport, 2003. (Cit. on pp. 59, 89).

[305] H. Simon, T. Wallmann, and T. Monk. *"Improvements in Performance Characteristics of Single-Stage and Multi-Stage Centrifugal Compressors by Simultaneous Adjustments of Inlet Guide Vanes and Diffuser Vanes"*. ASME Journal of Turbomachinery, Vol. 109, No. 1, pp. 41-47, 1987. (Cit. on pp. 65, 68).

[306] V. Simon, G. Oberholz, and M. Mayer. *"Exhaust Gas Temperature 1050^{o}C - An Engineering Challenge"*. Borg Warner Turbo Systems Knowledge Library., 2000. (Cit. on p. 245).

[307] D.A. Singer. *"Comparison of a Supercharger vs. a Turbocharger in a Small Displacement Gasoline Engine Application"*. SAE Technical Paper 850244, 1985. (Cit. on p. 44).

[308] W.L. Soong, G.B. Kliman, R.N. Johnson, R.A. White, and J.E. Miller. *"Novel High-Speed Induction Motor for a Commercial Centrifugal Compressor"*. IEEE Transactions on Industry Applications, Vol. 36, pp. 706-713., 2000. (Cit. on p. 58).

[309] G. Sovran. *"The Impact of Regenerative Braking on the Powertrain Delivered Energy Required for Vehicle Propulsion"*. SAE Technical Paper 2011-01-0891, 2011. (Cit. on p. 252).

[310] E. Spooner and J.R. Bumby. *"Solid-Rotor Axial-Flux Motors for Very High Speed Drives"*. International Conference on Electrical Machines, Vol. 12, Cracow, 2005. (Cit. on p. 58).

[311] A. Stanciu, C. Stan, and J. Beier. *"Adaptation of a Compact High Speed SI Engine for Supercharging in Base of Numerical Simulation"*. SAE Technical Paper 2006-01-1005, 2006. (Cit. on p. 44).

[312] J.H. Stang. *"Designing Adiabatic Components for Diesel Engine"*. SAE Technical Paper 780069, 1978. (Cit. on p. 87).

[313] N. Stosic, I.K. Smith, and A. Kovacevic. *"Optimisation of Screw Compressors"*. Applied Thermal Engineering, Vol. 23, pp. 1177-1195, 2003. (Cit. on p. 42).

[314] N. Stosic, I.K. Smith, A. Kovacevic, and E. Mujic. *"Geometry of Screw Compressor Rotors and their Tools"*. Centre for Positive Displacement Compressors, City University London, 2006. (Cit. on p. 42).

[315] P. Sweetlang and F. Schmitt. *"Regulated 2-Stage (R2S) Charging Systems for Future Diesel Applications"*. Borg Warner Turbo Systems Knowledge Library, 2004. (Cit. on pp. 30, 34).

[316] S. Takabe. *"Second Generation Lysholm Compressor"*. SAE Technical Paper 980774, 1998. (Cit. on pp. 42, 43, 50, 51).

[317] S. Takabe, K. Hatamura, H. Kanesaka, H. Kurata, Y. Iguchi, and H. Matsubara. *"Development of the High Performance Lysholm Compressor for Automotive Use"*. SAE Technical Paper 940843, 1994. (Cit. on p. 43).

[318] T. Taketomi, K. Kotani, M. Aoki, Y. Ogawa, and K. Hasegawa. *"Development of High-Performance TRE Turbo-Compressor"*. IHI Engineering Review, Vol. 36, No. 3, 2003. (Cit. on p. 68).

[319] H. Tange, N. Ikeya, M. Takanashi, and T. Hokari. *"Variable Geometry Diffuser of Turbocharger Compressor for Passenger Vehicles"*. SAE Technical Paper 2003-01-0051, 2003. (Cit. on pp. 78, 79, 81).

[320] X. Tauzia, J. Hetet, P. Chesse, G. Grosshans, and L. Mouillard. *"Computer Aided Study of the Transient Performances of a Highly Rated Sequentially Turbo-Charged Marine Diesel Engine"*. Proceedings of the Institution of Mechanical Engineers Part A: Journal of Power and Energy, Vol. 212, pp. 185-196, 1998. (Cit. on p. 23).

[321] D.H.W. Tennant and B.E. Walsham. *"The Turbocompound Diesel Engine"*. SAE Technical Paper 890647, 1989. (Cit. on pp. 85, 87).

[322] D.W.H. Tennant. *"A Compact Two-Stage Turbocharger Module"*. IMechE 4^{th} International Conference on Turbocharging and Air Management Systems, C405/042/90, London, 1990. (Cit. on p. 26).

[323] G.E. Thien. *"Derivation of the Formulas for the Evaluation of Stationary Flow Measurements of Intake and Exhaust Ports"*. AVL-FA-Report, No. 463/Gen./072, 1978. (Cit. on p. 143).

[324] G. Tippelmann. *"A New Method of Investigation of Swirl Ports"*. SAE Technical Paper 770404, 1977. (Cit. on p. 143).

[325] T. Tomita, N. Ikeya, D. Ishihara, N. Kondoh, and A. Ohkita. *"Hybrid Charging System for Heavy Duty Diesel Engines"*. SAE Technical Paper 910419, 1991. (Cit. on p. 49).

[326] A. Torregrosa, P. Olmeda, B. Degraeuwe, and M. Reyes. *"A Concise Wall Temperature Model for DI Diesel Engines"*. Applied Thermal Engineering, Vol. 26, pp.1320-1327, 2006. (Cit. on pp. 190, 191).

[327] A.J. Torregrosa, J. Galindo, C. Guardiola, and O. Varnier. *"Combined Experimental and Modeling Methodology for Intake Line Evaluation in Turbocharged Diesel Engines"*. International Journal of Automotive Technology, Vol. 12, No. 3, pp. 359-367, 2011. (Cit. on p. 173).

[328] A.J. Torregrosa, P. Olmeda, J. Martin, and C. Romero. *"A Tool for Predicting the Thermal Performance of a Diesel Engine"*. Heat Transfer Engineering, Vol. 32, pp. 891-904, 2011. (Cit. on pp. 190, 213).

[329] M. Toussaint and P. Podevin. *"Guide-Vanes Upstream the Impeller of Centrifugal Compressor"*. Conservatoire National des arts et Métiers, Chaire de turbomachines, 2005. (Cit. on pp. 65, 68, 73).

[330] H. Uchida. *"Transient Performance Prediction for Turbocharging Systems Incorporating Variable Geometry Turbochargers"*. Toyota R&D Review, Vol. 41, No. 3, pp. 22-28, 2006. (Cit. on p. 77).

[331] H. Uchida. *"Trend of Turbocharging Technologies"*. Toyota R&D Review, Vol. 41, No. 3, pp.1-8, 2006. (Cit. on pp. 55, 81).

[332] H. Uchida, A. Kashimoto, and Y. Iwakiri. *"Development of Wide Flow Range Compressor with Variable Inlet Guide Vane"*. Toyota R&D Review, Vol. 41, No. 3, pp. 9-14, 2006. (Cit. on pp. 74, 77).

[333] N. Ueda, N. Matsuda, M. Kamata, H. Sakai, and H. Kanesaka. *"Proposal of New Supercharging System for Heavy Duty Vehicular Diesel and Simulation Results of Transient Characteristics"*. SAE Technical Paper 2001-01-0277, 2001. (Cit. on p. 51).

[334] L.H. Uthoff and J.W. Yakimow. *"A Development of the Eaton Supercharger"*. SAE Technical Paper 870355, 1987. (Cit. on p. 44).

[335] J. Vetrovec. *"Fluid-Dynamic Supercharger"*. SAE Technical Paper 2008-01-0299, 2008. (Cit. on pp. 93, 94).

[336] J. Villegas, B. Gao, K. Svancara, W. Thornton, and J. Parra. *"Real-Time Engine Modelling for Engine Downsizing Using an Electric Supercharger"*. 13^{th} EAEC European Automotive Congress, Valencia, 2011. (Cit. on p. 63).

[337] O. Vitek, J. Macek, and M. Polasek. *"New Approach to Turbocharger Optimization Using 1-D Simulation Tools"*. SAE Technical Paper 2006-01-0438, 2006. (Cit. on p. 116).

[338] C.T. Vuk. *"Electric Turbo Compounding... A Technology Who's Time Has Come"*. Diesel Engine Emissions Reduction Conference, Chicago, 2005. (Cit. on pp. 90, 91).

[339] C.T. Vuk. *"Electric Turbo Compounding... A Technology Who's Time Has Come"*. Diesel Engine Emissions Reduction Conference, Detroit, 2006. (Cit. on p. 91).

[340] F.J. Wallace. *"The Ultimate Performance Potential of Compounded Diesel Engines for Heavy Vehicles"*. IMechE 4th International Conference of Turbocharging and Turbochargers, pp. 253-270, London, 1990. (Cit. on pp. 84, 85).

[341] F.J. Wallace and G.P. Blair. *"The Pulsating Flow Performance of Inward Radial Flow Turbines"*. ASME Gas Turbine Conference, Paper 65-GTP-21, Washinghton, 1965. (Cit. on p. 160).

[342] R. Walling. *"Eaton TVS Supercharged for Downsizing"*. Engine Expo, Stuttgart, 2009. (Cit. on p. 43).

[343] B.E. Walsham. *"Alternative Turbocharger Systems for the Automotive Diesel Engine"*. IMechE 4th International Conference of Turbocharging and Turbochargers, pp. 39-50, London, 1990. (Cit. on pp. 84, 85).

[344] H. Wang, R. Glover, and J. Koval. *"Analytical and Experimental Study on Gear Rattle in Supercharger"*. SAE Technical Paper 2005-01-2369, 2005. (Cit. on pp. 43, 44).

[345] E. Watel, A. Pagot, P. Pacaud, and J.C. Schmitt. *"Matching and Evaluating Methods for Euro 6 and Efficient Two-Stage Turbocharging Diesel Engine"*. SAE Technical Paper 2010-01-1229, 2010. (Cit. on pp. 34, 37, 39, 253).

[346] N. Watson. *"Transient Performance Simulation and Analysis of Turbocharged Diesel Engines"*. SAE Technical Paper 810338, 1981. (Cit. on p. 171).

[347] N. Watson and K. Banisoleiman. *"Performance of the Highly Rated Diesel Engine with a Variable Geometry Turbocharger"*. IMechE 3th International Conference on Turbocharging and Turbochargers, C121/86, London, 1986. (Cit. on p. 18).

[348] N. Watson and S. Janota. *"Turbocharging the Internal Combustion Engine"*. London: McMillan Publishers Ltd. ISBN 0-333-24290-4, 1982. (Cit. on pp. 10, 18, 55, 117, 153, 158).

[349] N. Watson, N.P. Kyrtatos, and K. Holmes. *"The Performance Potential of Limited Cooled Diesel Engines"*. Proceedings of the Institution of Mechanical Engineers Part A: Journal of Power and Energy, Vol. 197, No.3, pp. 197-207, 1983. (Cit. on p. 86).

[350] N. Watson and M. Marzouk. *"A Non-Linear Digital Simulation and Analysis of Turbocharged Diesel Engines under Transient Conditions"*. SAE Technical Paper 770123, 1977. (Cit. on p. 171).

[351] N. Watson, A.D. Pilley, and M.A. Marzouk. *"Combustion Correlation for Diesel Engine Simulation"*. SAE Technical Paper 800029, 1980. (Cit. on p. 196).

[352] S. Wedowski, S. Glück, R. Sauerstein, F. Schmitt, M. Westermaier, D. Oh, C. Schernus, and M. Subramaniam. *"Vehicle Demonstrator with 2-Stage Turbo SI engine - Simulation Based Layout of the GT2 Engine"*. GT-SUITE Conferences, Frankfurt, 2009. (Cit. on pp. 30–34, 36).

[353] W.M.S.R. Weerasinghe, R.K. Stobart, and S.M. Hounsham. *"Thermal Efficiency Improvement in High Output Diesel Engines a Comparison of a Rankine Cycle with Turbo-Compounding"*. Applied Thermal Engineering, Vol. 30, pp. 2253-2256, 2010. (Cit. on p. 81).

[354] F. Westin and R. Burenius. *"Measurement of Interstage Losses of a Two-Stage Turbocharger System in a Turbocharger Test Rig"*. SAE Technical Paper 2010-01-1221, 2010. (Cit. on p. 36).

[355] A. Whitfield and A.H. Abdullah. *"The Performance of a Centrifugal Compressor with High Inlet Prewhirl"*. ASME Journal of turbomachinery, Vol. 120, pp. 487-493, 1998. (Cit. on pp. 66–68).

[356] A. Whitfield, M.D.C. Doyle, and M.R. Firth. *"Design and Performance of a High Pressure Ratio Turbocharger Compressor: Part 1 Design Considerations"*. Proceedings of the Institution of Mechanical Engineers Part A: Journal of Power and Energy, Vol. 207, No. 2, pp. 115-124, 1993. (Cit. on pp. 65, 68).

[357] A. Whitfield, M.D.C. Doyle, and M.R. Firth. *"Design and Performance of a High Pressure Ratio Turbocharger Compressor: Part 2 Experimental Performance"*. Proceedings of the Institution of Mechanical Engineers Part A: Journal of Power and Energy, Vol. 207, No. 2, pp. 125-131, 1993. (Cit. on pp. 65, 68).

[358] A. Whitfield and A.J. Sutton. *"The Effect of Vaneless Diffuser Geometry on the Surge Margin of Turbocharger Compressors"*. Proceedings of the Institution of Mechanical Engineers Part D: Journal of Automobile Engineering, Vol. 203, No. 2, pp. 91-98, 1989. (Cit. on p. 78).

[359] A. Whitfield, A.J. Sutton, and H.J. Leonard. *"The Development of Turbocharger Compressors with Improved Surge Margin"*. IMechE 4^{th} International Conference on Turbocharging and Air Management Systems, C433/063/90, London, 1990. (Cit. on pp. 66, 78, 79).

[360] A. Whitfield, F.J. Wallace, and R.C. Atkey. *"Experimental and Theoretical Performance of a Radial Flow Turbocharger Compressor with Inlet Prewhirl"*. Proceedings of the Institution of Mechanical Engineers, Vol. 189, No. 1, pp. 177-186, 1975. (Cit. on pp. 65, 68).

[361] A. Whitfield, F.J. Wallace, and R.C. Atkey. *"The Effect of Variable Geometry on the Operating Range and Surge Margin of a Centrifugal Compressor"*. ASME paper 76-GT-98, 1976. (Cit. on p. 78).

[362] I. Wiebe. *"Halbempirische Formel fur die Verbrennungs-Geschwindigkeit"*. Verlag der Akadimie der Wissenschaften der Vd SSR, Moscow, 1956. (Cit. on p. 196).

[363] P.R. Williams. *"An Examination of the Methods Used to Vary the Output of Centrifugal Compressors with Particular Reference to Part-Load Efficiency"*. IMechE European Conference on Developments in Industrial Compressors, London, 1989. (Cit. on pp. 65, 68).

[364] D.E. Wilson. *"The design of a Low Specific Fuel Consumption Turbocompound Engine"*. SAE Technical Paper 860072, 1986. (Cit. on p. 87).

[365] N. Winkler and H.E. Angström. *"Simulations and Measurements of a Two-Stage Turbocharged Heavy-Duty Diesel Engine Including EGR in Transient Operation"*. SAE Technical Paper 2008-01-0539, 2008. (Cit. on pp. 28, 29, 33, 37, 39, 116).

[366] D.E. Winterbone and R.J. Pearson. *"Turbocharger Turbine Performance Under Unsteady Flow - A Review of Experimental Results and Proposed Models"*. IMechE 6^{th} International Conference on Turbocharging and Air Management Systems, C554/031/98, pp.193-206, London, 1998. (Cit. on p. 160).

[367] D.E. Winterbone, C. Thiruarooran, and A. Wellstead. *"A Wholly Dynamical Model of a Turbocharged Diesel Engine for Transfer Function Evaluation"*. SAE Technical Paper 770124, 1977. (Cit. on p. 171).

[368] D.E. Winterbone and M. Yoshitomi. *"The Accuracy of Calculating Wave Action in Engine Intake Manifolds"*. SAE Technical Paper 900677, 1990. (Cit. on p. 171).

[369] G. Woschni. *"A Universally Applicable Equation for the Instanatenous Heat Transfer Coefficient in the Internal Combustion Engine"*. SAE Technical Paper 670931, 1967. (Cit. on p. 190).

[370] G. Woschni. *"Die Berechnung der Wandverluste und der Thermischen Belastung der Bauteile von Dieselmotoren"*. MTZ 31/12, pp. 491-499, 1970. (Cit. on p. 190).

[371] Y.R. Wu and Z.H. Fong. *"Improved Rotor Profiling Based on the Arbitrary Sealing Line for Twin Screw Compressors"*. Mechanism and Machine Theory, Vol. 43, pp. 695-711, 2008. (Cit. on p. 42).

[372] Y.R. Wu and Z.H. Fong. *"Optimization Design of an Explicitly Defined Rack for the Generation of Rotors for Twin Screw Compressors"*. Mechanism and Machine Theory, Vol. 44, pp. 66-82, 2009. (Cit. on p. 42).

[373] J.C. Wurzenberger, P. Bartsch, and T. Katrasnik. *"Crank-Angle Resolved Real-Time Capable Engine and Vehicle Simulation - Fuel Consumption and Driving Performance"*. SAE Technical Paper 2010-01-0784, 2010. (Cit. on p. 116).

[374] J. Xiao, C. Gu, X. Shu, and C. Gao. *"Performance Analysis of a Centrifugal Compressor with Variable Inlet Guide Vanes"*. Frontiers of Energy and Power Engineering in China, Vol. 1, No. 4, pp. 473-476, 2007. (Cit. on pp. 68, 70).

[375] Y. Yamashita, S. Ibaraki, and H. Ogita. *"Development of Electrically Assisted Turbocharger for Diesel Engine"*. IMechE 8th International Conference on Turbochargers and Turbocharging, pp. 147-155, London, 2006. (Cit. on p. 60).

[376] H. Zhang and M. Bailey. *"Electrically Assisted Turbo-Charger Development for Performance and Emissions"*. Diesel Engine Emissions Reduction Conference, San Diego, 2000. (Cit. on p. 58).

[377] M. Zheng, G.T. Reader, and J.G. Hawley. *"Diesel Engine Exhaust Gas Recirculation - a Review on Advanced and Novel Concepts"*. Energy Conversion and Management, Vol. 45, pp. 883-900, 2004. (Cit. on p. 6).

[378] K. Zinner. *"Supercharging of Internal Combustion Engines"*. Berlin, Heidelberg, New York Springer-Verlag, 1978. (Cit. on p. 116).

[379] Y.H. Zweiri, J.F. Winterbone, and L.D. Seneviratne. *"Detailed Analytical Model of a Single-Cylinder Diesel Engine in the Crank-Angle Domain"*. Proceedings of the Institution of Mechanical Engineers Part D: Journal of Automobile Engineering, Vol. 215, pp. 1197-1216, 2001. (Cit. on p. 172).